DISSERTATION

PROTEOMIC PROFILING OF THE RAT RENAL PROXIMAL CONVOLUTED TUBULE IN RESPONSE TO CHRONIC METABOLIC ACIDOSIS

Submitted by

Dana Marie Freund

Department of Biochemistry and Molecular Biology

In partial fulfillment of the requirements

For the Degree of Doctor of Philosophy

Colorado State University

Fort Collins, Colorado

Spring 2013

Doctoral Committee:

Advisor: Norman Curthoys
Co-Advisor: Jessica Prenni

Jennifer Nyborg
Olve Peersen
Karen Dobos

ABSTRACT

PROTEOMIC PROFILING OF THE RAT RENAL PROXIMAL CONVOLUTED TUBULE IN RESPONSE TO CHRONIC METABOLIC ACIDOSIS

The human kidneys contain more than one million glomeruli which filter nearly 200 liters of plasma per day. The proximal tubule is the segment of the nephron that immediately follows the glomeruli. This portion of the nephron contributes to fluid, electrolyte and nutrient homeostasis by reabsorbing 60-70% of the filtered water and NaCl and an even greater proportion of $NaHCO_3$. The initial or convoluted portion of the proximal tubule reabsorbs nearly all of the nutrients in the glomerular filtrate and is the site of active secretion and many of the metabolic functions of the kidney. For example, the proximal convoluted tubule is the primary site of renal ammoniagenesis and gluconeogenesis, processes that are significantly activated during metabolic acidosis.

Metabolic acidosis is a common clinical condition that is characterized by a decrease in blood pH and bicarbonate concentration. Metabolic acidosis also occurs frequently as a secondary complication, which adversely affects the outcome of patients with various life-threatening conditions. This type of acidosis can occur acutely, lasting for a few hours to a day, or as a chronic condition where acid-base balance is not fully restored. Chronic metabolic acidosis, where the decrease in blood pH and bicarbonate last for 7 days, was the main focus of these studies. Acid-base homeostasis is achieved, in part, by the reabsorption of bicarbonate and excretion of ammonium ions and acids by the proximal convoluted tubule. Metabolic acidosis is partially compensated by an adaptive increase in renal ammoniagenesis and bicarbonate synthesis. During acidosis, there is increased extraction and mitochondrial catabolism of plasma glutamine within the renal proximal convoluted tubule. This process generates ammonium and

bicarbonate ions that facilitate the excretion of acid and partially restore acid-base balance. This response is mediated by a pronounced remodeling of the proteome of the proximal convoluted tubule that also produces an extensive hypertrophy.

Previous studies identified only a few mitochondrial proteins, including two key enzymes of glutamine metabolism, which are increased during chronic acidosis. Here, a workflow was developed to globally characterize the mitochondrial proteome of the proximal convoluted tubule. Two-dimensional liquid chromatography coupled with mass spectrometry (2D/LC-MS/MS) was utilized to compare mitochondrial enriched samples from control and chronic acidotic rats. Label-free quantitative strategies are commonly used in shot-gun proteomics to detect differences in protein abundance between biological sample groups. In this study we employed a combination of two such approaches, spectral counting (SpC) and average MS/MS total ion current (MS^2 TIC). In total, forty nine proteins were observed to be significantly altered in response to metabolic acidosis (p-value < 0.05). Of these, 32 proteins were uniquely observed as significantly different by SpC, 14 by MS^2 TIC, and only 3 by both approaches. Western blot analysis was used to validate the fold changes of eight of the proteins that showed an increase upon acidosis. Furthermore, using an antibody specific to acetylated lysine modifications indicated that chronic acidosis causes a 2.5 fold increase in this modification specifically in mitochondria. Western blot analysis established that the observed alterations in both protein abundance and lysine acetylation are not due to the associated hypertrophy. This study represents the first comprehensive analysis of whole mitochondrial proteome of the rat renal proximal convoluted tubule and its response to metabolic acidosis. Additionally, our analysis demonstrates an innovative dual approach for protein quantitation.

To further our understanding of the impact of acidosis on the mitochondrial proteome, mitochondrial inner membranes were isolated from control and acidotic rat proximal convoluted tubules. Additional LC-MS/MS analysis was performed, representing the first proteomic characterization of the mitochondrial inner membrane proteome of the rat renal proximal convoluted tubule. Specific sites of lysine acetylation were identified both in the inner membrane and whole mitochondria, the majority of which are novel sites. The results presented here showed successful enrichment of mitochondrial inner membranes and described the proteins and the known biological processes of this compartment of the mitochondria.

Previous proteomic analysis was performed on brush-border membrane vesicles isolated from proximal convoluted tubules from control, 1 d and 7 d acidotic rats. To validate the observed protein alterations, western blot analysis was performed on freshly isolated apical membrane. Additionally, the results from three independent proteomic studies focused on the apical membrane, mitochondrial, and soluble cytosolic fractions of the proximal convoluted tubules were compiled. Bioinformatics analysis was performed to describe predominate cellular processes and pathways that respond to chronic metabolic acidosis. The results of these studies demonstrate that the physiological response to the onset of metabolic acidosis requires pronounced changes in the renal proteome. The observed proteomic adaptations within the proximal convoluted tubule support the increased extraction of plasma glutamine and the increased synthesis and transport of glucose and of NH_4^+ and HCO_3^- ions. Overall, this dissertation describes the profiling of the proximal convoluted tubule proteome in response to chronic metabolic acidosis and provides the framework for future studies.

ACKNOWLEDGEMENTS

I consider myself incredibly fortunate to have had the help and support of many people, which allowed me to complete my dissertation. I appreciate the opportunity to be a member of the Department of Biochemistry and Molecular Biology for the past few years. I have been very lucky to have two wonderful advisors; Dr. Norman Curthoys and Dr. Jessica Prenni. They have taught me so much and encouraged my development as a scientist. I am grateful for the skills and confidence I have gained in their labs which allowed me to transition from a young graduate student into an independent scientist. I cannot imagine what graduate school would have been like without both of them to guide me. I would also like to thank my committee members Dr. Jennifer Nyborg, Dr. Olve Peersen, and Dr. Karen Dobos for their input and encouragement. I would like to acknowledge all current and past lab members from the Curthoys lab and *Proteomics and Metabolomics Facility* for assisting me in my training and for any contribution to my project. Huge thanks to my husband who has been at my side through my entire graduate school journey. I could not have done it without the constant support and encouragement from him. I would like to thank my parents for their unquestionable belief in my success with everything I pursue.

This research was supported in part by National Institute of Diabetes and Digestive and Kidney Diseases Grants DK-37124 and DK-75517 awarded to N. P. Curthoys. The apical membrane mass spectrometry including the spectral counting analysis, accurate mass and time tag analyses and data interpretation was performed by Scott J. Walmsley. The mass spectrometry for the apical membrane was performed at the Genomics and Proteomics Core facility of the Rocky Mountain Regional Center of Excellence for Biodefense and Emerging Infectious

Diseases Research (http://www.rmrce.colostate.edu). Kevin L. Schauer performed the mass spectrometry and data interpretation for the soluble cytosolic samples. Mass spectrometry for all mitochondrial and soluble cytosolic samples was performed in the Proteomics and Metabolomics Facility at Colorado State University (www.pmf.colostate.edu).

TABLE OF CONTENTS

CHAPTER 1

Introduction

1.1 Metabolic acidosis

Metabolic acidosis is a common clinical condition that is characterized by a decrease in blood pH and bicarbonate.[1] An overproduction of acid can be caused by a high protein diet or prolonged fasting due to an increased catabolism of endogenous proteins. Alterations in metabolism, such as diabetic ketoacidosis, lactic acidosis, renal failure, and acquired or genetic defects in metabolism, can also lead to metabolic acidosis. Excessive loss of base from diarrhea or renal defects in bicarbonate reabsorption can also result in metabolic acidosis.[2] Metabolic acidosis is the most common form of acid-base imbalance and it has adverse effects on patients with conditions such as cachexia, sepsis, trauma, uremia, renal disease, and HIV infection.

Maintaining an acid-base balance in the blood is physiologically essential for the wellbeing of an individual. Acid-base homeostasis is achieved by the renal reabsorption of bicarbonate and the excretion of acids and ammonium ions. When metabolic acidosis occurs, the physiological consequence is an adaptive response in the proximal convoluted tubules of the kidney.[3] The kidneys are complex organs composed of different types of tissue and made up of millions of nephrons. The nephron is the macroscopic functional unit of the kidney which filters the blood to retain nutrients and expel waste. The filtrate enters the nephron at the glomerulus and the segment immediately follow is the proximal convoluted tubule (Fig. 1.1). The proximal convoluted tubule is imperative to acid-base homeostasis and the response to metabolic acidosis.

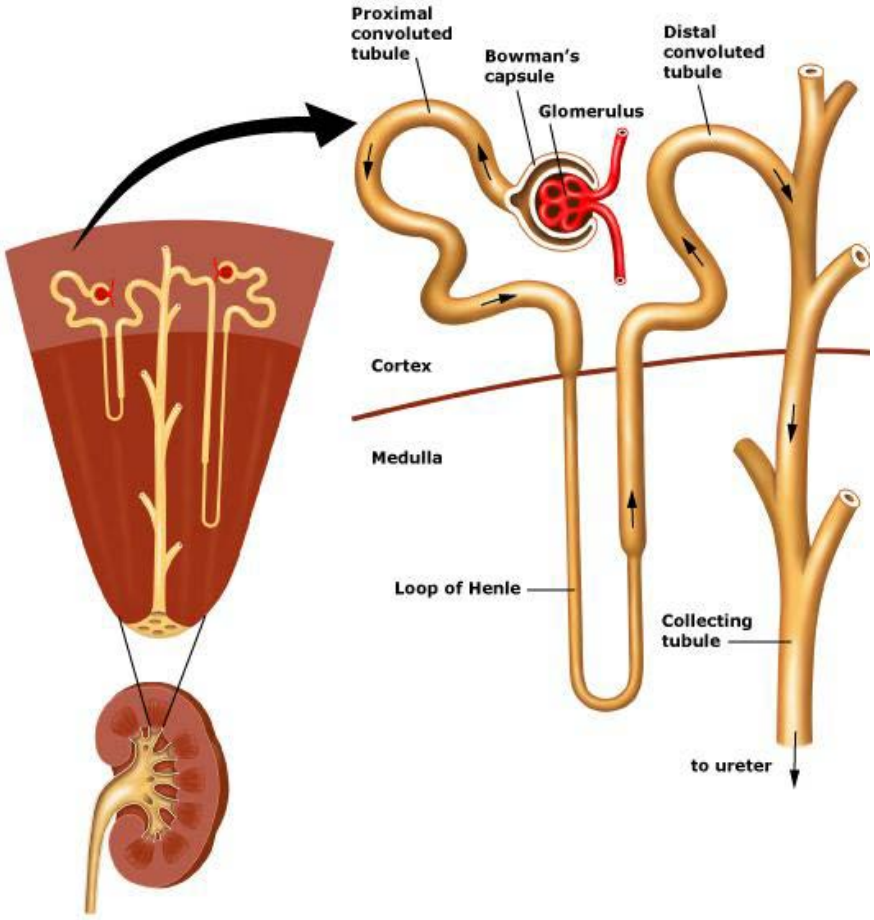

Fig. 1.1. The Anatomy of the Nephron. Blood enters the nephron and is filtered by the glomerulus and Bowman's capsule. The blood filtrate flows through the proximal convoluted tubule, loop of Henley, distal tubule, and finally to the collecting duct. The cells of the proximal convoluted tubule are involved in responding to metabolic acidosis. (Figure from Waltham et al. 2009.[4])

1.2 The proximal convoluted tubule

The kidney is comprised of nephrons, each of which consists of multiple segments with distinct morphologic and functional characteristics. The proximal convoluted tubule (PCT) is the first segment of the nephron to encounter the glomerular filtrate. As a result, it has a central role in maintaining fluid, electrolyte and nutrient homeostasis. The proximal convoluted tubule is responsible for the reabsorption of 60-70% of the water, NaCl and an even more of the $NaHCO_3$ from the filtrate. The proximal convoluted tubule is comprised of polarized epithelia cells. These cells contain an apical brush border membrane which is involved in the reabsorption of nutrients from the filtrate and a basolateral membrane located at the interface with the blood. The initial or convoluted portion of the proximal tubule reabsorbs nearly all of the nutrients in the glomerular filtrate and is the site of active secretion and many of the metabolic functions of the kidney. For example, the proximal convoluted tubule is the primary site of renal ammoniagenesis and gluconeogenesis, processes that are significantly up-regulated during metabolic acidosis. The proximal convoluted tubule is the main focus of these studies because of its significant role in metabolic acidosis and its proximity to the entrance of filtrate from the glomeruli.

1.3 Glutamine metabolism during metabolic acidosis

During metabolic acidosis, acid-base balance is partially restored by increased ammoniagenesis and gluconeogenesis from the plasma glutamine.[5] This process begins with catabolism of glutamine in the renal proximal convoluted tubule.[6] At the onset of metabolic acidosis, glutamine secretion from muscle tissue into the blood is increased two-fold.[7] The extraction of glutamine from the blood into proximal convoluted tubule cells of the kidney is increased by more than 35%.[8] Glutamine enters the PCT cell by the basolateral glutamine transporter (SN1) and from the luminal side. Once transported into the cell, glutamine actively

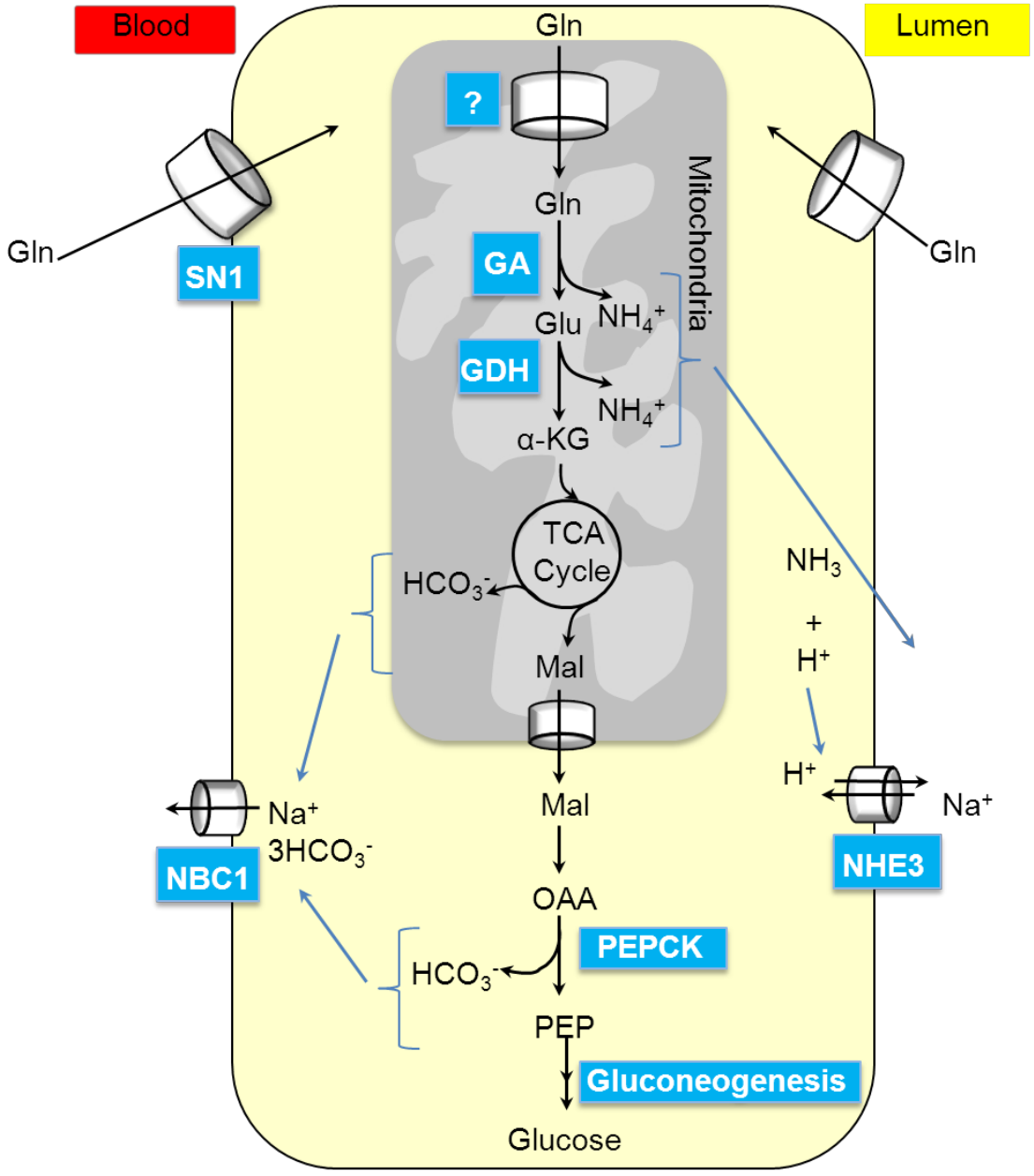

Fig. 1.2. Glutamine Catabolism Pathway in Renal Proximal Convoluted Tubule Cell During Chronic Metabolic Acidosis. The basolateral glutamine transporter (SN1), glutaminase (GA), glutamate dehydrogenase (GDH), phosphoenolpyruvate carboxykinase (PEPCK), and Na+/H+ exchanger (NHE3) are up-regulated proteins involved in the response to metabolic acidosis. Blue boxes are proteins, transporters, and processes that are known to increase during metabolic acidosis. (Modified from Curthoys et al. 2007).[12]

enters the mitochondrial matrix where it is catabolized by glutaminase (GA) (Fig. 1.2).[9] An unknown transporter, most likely a member of the SLC25 gene family, is responsible for the transport of glutamine through the mitochondrial inner membrane to the matrix.[10, 11] Inside the mitochondrial matrix, GA converts glutamine to glutamate and glutamate dehydrogenase (GDH) oxidizes glutamate to α-ketoglutarate (α-KG).[11] The cytosolic phospho*enol*pyruvate carboxykinase (PEPCK) channels intermediates of the citric acid cycle to phosphoenolpyruvate (PEP) and produces bicarbonate.[13] Activation of the apical Na^+/H^+ exchanger (NHE3) acidifies the urine and facilitates the removal of cellular ammonium ions.[11] Additionally, NHE3 is responsible for bicarbonate reabsorption predominantly by means of hydrogen ion secretion on the luminal side.[14] The reabsorbed and synthesized bicarbonate are then transported out the basolateral membrane by the Na^+/HCO_3^- co-transporter (NBC1) into the blood.[15]

1.4 Acute and chronic metabolic acidosis

Metabolic acidosis can be either acute, lasting a few hours, or chronic if the acid-base balance is not restored. If untreated, chronic metabolic acidosis can lead to mental retardation in infants or bone softening, greater calcium deposits in the kidneys, and the formation of urinary system stones in adults. During chronic metabolic acidosis, renal catabolism of glutamine is maintained by increased expression of genes that encode transporters and key enzymes. Many proteins including PEPCK and GA are up-regulated in response to metabolic acidosis within the proximal convoluted tubule.[16,17] The initial increase in PEPCK results from increased transcription of the respective gene, which has more than a dozen regulatory elements that control its expression.[16] The p38 mitogen-activated protein kinase (MAPK) signaling pathway may mediate the increased transcription of PEPCK mRNA during metabolic acidosis.[18] The increased amount of GA protein is due solely to selective stabilization of the respective mRNA.[19]

There are multiple isoforms of GA mRNA, however, it is the kidney type glutaminase (KGA) that is highly expressed in rat renal PCT cells and is the pH responsive variant.[20]

During chronic metabolic acidosis (CMA) the abundance and/or activity of the basolateral glutamine transporter (SN1), mitochondrial inner membrane glutamine transporter, GDH, NHE3, and NBC1 all increase to facilitate the restoration of acid-base balance.[21] These combined adaptations occur to increase bicarbonate ion reabsorption, production of bicarbonate and ammonium ions, and their apical and basolateral membrane transport. These adaptations restore acid-base balance and have been well characterized, but the cellular pathways involved in sensing the variation in pH have not been characterized.

1.5 Preliminary studies of a systems biology understanding of metabolic acidosis

1.5a The first proteomic study of the proximal convoluted tubular response during metabolic acidosis

Proteomics investigation was the next most logical step in our understanding the global biological processes and proteins that may also contribute to the proximal convoluted tubular response to metabolic acidosis. Proteomics takes a global and comprehensive view of a system at a specific cellular state, in this case the PCT cell during metabolic acidosis. Mass spectrometry (MS) is a powerful tool that can be used to analyze peptides and proteins based on their mass to charge (m/z) ratio. The field of MS-based proteomics has advanced greatly and allowed for wide range of experimentation.

A proteomics study was previously conducted by Curthoys et al. as a first step to a better understanding of the proteins and possible pathways that respond to metabolic acidosis.[21] In this study, difference in-gel electrophoresis (DIGE) analysis was applied on control and 7-d chronic

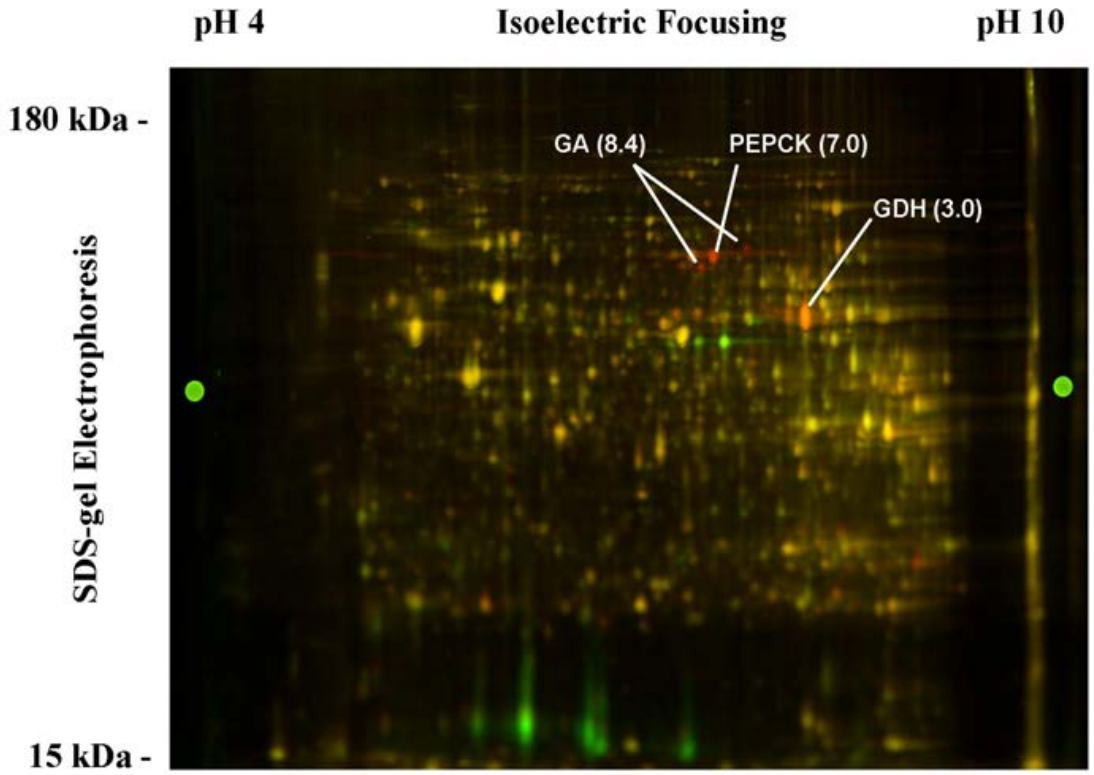

Fig. 1.3. Difference In-Gel Electrophoresis (DIGE) analysis of proximal convoluted tubules isolated from control and 7 d acidotic rats. Control and 7 d acidotic tubules were labeled and separated by 2-dimensional gel electrophoresis. Yellow spots are unchanged proteins, red or green spots represent proteins that are increased or decreased in abundance, respectively. (Figure from Curthoys et al. 2007)[22]

acidotic rat PCT whole cell lysates to characterize the proteome remodeling that occurs during metabolic acidosis. Over 120 protein spots were observed to be changing and picked for further mass spectrometry analysis by MALDI/TOF/TOF to identify the proteins (Fig. 1.3). This analysis confirmed the adaptive responses of the already well characterized GA, GDH, and PEPCK, which were observed to have the greatest fold induction. Furthermore, previously unrecognized proteins were observed to have abundance changes during metabolic acidosis. Overall, 21 proteins increased 1.5 to 5.6 fold and 16 proteins decreased with fold changes from 0.67 to 0.03 in the proximal convoluted tubule during CMA. Of the 37 proteins that are altered in acidosis 13 are known mitochondrial proteins. A few proteins were confirmed with Western blot analysis but not all proteins were shown to have altered abundance. This may be due to modifications such as phosphorylation that can alter the expression patterns observed with DIGE analysis without changes in protein abundance.

Further information on function and known phosphorylation sites of the proteins identified in this study was obtained from UniProtKB (www.uniprot.org/) protein knowledgebase and PhosphositePlus (www.phosphosite.org). These resources listed 16 of the 21 proteins that increase in expression during metabolic acidosis as known phosphoproteins. Additionally, 7 of the 16 proteins decreasing in expression are also known to be phosphoproteins. These and other phosphoproteins may play an important role in the renal response to metabolic acidosis as suggested by their molecular function. The DIGE analysis is not specific for phosphorylation and the limited amount of protein in spots extracted for identification from the DIGE gels was insufficient for phosphopeptide detection. Therefore, direct evidence of protein phosphorylation was not observed in this study. The DIGE analysis was performed on 7-d acidotic rats which causes chronic metabolic acidosis. During chronic

metabolic acidosis the renal proximal tubule undergoes hypertrophy.[23] Some of the proteins identified in the DIGE analysis, such as cathepsin B which participates in protein turnover, may contribute to renal hypertrophy and not specifically the change in pH during CMA. Subsequent studies will need to be conducted to explain the contribution hypertrophy has to proteome remodeling during metabolic acidosis.

In summary, this initial proteomic study established that the isolation of proximal convoluted tubules from renal cortex by collagenase digestion and Percoll density gradient centrifugation yields a highly enriched sample that consists primarily of the S1 and S2 segments of the proximal tubule which constitute the convoluted portion. This study indicated a remodeling of the proteome that occurs in this segment of the nephron in response to metabolic acidosis. This study also suggests protein phosphorylation as well as mitochondrial proteins may be important for the renal response to metabolic acidosis.

1.5b The kidney transcriptome during metabolic acidosis

A genome-wide microarray mRNA profiling study characterized transcriptional changes in the kidney during metabolic acidosis.[24] The mRNAs from whole kidneys were isolated from control and 2 or 7-d acidotic mice. The microarray analysis detected 13,000 genes, approximately 40% of the genes on the mouse genomic array. In both 2 and 7 day acidosis 333 mRNAs were up-regulated and 342 down-regulated. Only 15 genes were quantified with qRT-PCR and all but one showed the expected change in expression observed from the microarray analysis. Gene expression changes of the aquaporin 2 water channel, basolateral glutamine transporter (SN1), and the Cl^-/HCO_3^- exchanger pendrin were confirmed at the protein level with Western blot analysis. Gene clustering revealed many genes encoding proteins involved in solute

transport, cell growth, water homeostasis, apoptosis, and energy metabolism. Pathway analysis indicated that ammoniagenesis, glycolysis/gluconeogenesis, ATP synthesis, arginine metabolism, and sodium reabsorption all played a significant role in the response to metabolic acidosis.

The proteomics and genomics studies detected corresponding mRNAs and proteins involved in the renal response to metabolic acidosis. For example, 10 of the 21 increased proteins based on DIGE analysis showed increases at the transcript level. There were three down-regulated proteins that showed complimentary expression at the transcript level as well. Collectively, these studies suggest mechanisms and pathways that may be significant in the response to acidosis. The largest concern with this analysis is that the study was of whole kidney and it is uncertain which segment of the nephron or cell type is producing the changes in gene expression. Additionally, transcript level changes do not always translate to protein level changes therefore it is important to also investigate protein changes.

1.5c Two-dimensional gel electrophoresis to determine phosphoproteins and total protein abundance changes in WKPT cells during acute metabolic acidosis

In the work presented in this section, two-dimensional (2D) gel electrophoresis and mass spectrometry were used to characterize the global changes of phosphoproteins in a cell culture system that models the renal response to metabolic acidosis (Unpublished data D.M. Freund). The Wistar-Kyoto rat proximal tubule (WKPT) cell line was treated for 24 hours with an acidic medium (pH 6.9) to model acute metabolic acidosis, while control cells were kept in pH 7.4 media. The WKPT cell line was established from microdissection of rat renal proximal tubular epithelial cells that express the SV40 T-antigen.[25] Three biological replicates of pH 6.9-treated

cells and three replicates of pH 7.4 control cells were acquired. After sample preparation, proteins were separated on 2D gels. The gels were fixed, stained with ProQ Diamond (ProQ D) phosphoprotein fluorescent gel stain (Invitrogen), and imaged. ProQ D is selective to phosphate moieties, which allows for quantitative analysis of protein phosphorylation. After each gel is imaged for phosphoproteins, they were post-stained with Sypro Ruby, a total protein gel stain (Invitrogen) and a second image was collected. A total of twelve gel images were compared in this analysis: three biological replicates of control and three of acutely acidotic stained with ProQ D (6 ProQ D images) and Sypro Ruby (6 Sypro Ruby images). Significantly changing protein spots were excised from gels, subjected to tryptic digestion, and analyzed by LC-MS/MS.

There were 13 protein spots observed to increase or decrease in the level of phosphorylation (Table 1.1). Of these, 10 proteins exhibited an increase in phosphorylation ranging from 5.4 to 1.6 fold and 3 proteins exhibited a decrease in phosphorylation ranging from 0.4-0.2 fold. Fold changes correlate to a protein spot that was quantified, however multiple proteins were often identified in one spot. Additionally, there were 13 protein spots changing in total abundance during metabolic acidosis (Table 1.2). Of these, 10 proteins were observed to increase with fold changes ranging from 5.8 to 1.9 and 3 proteins were observed to decrease with fold changes ranging from 0.4-0.3. The cellular location and function of proteins obtained from UniprotKB are included in the tables.

A wide range isoelectric focusing strip, pH 3-10, was used to separate proteins in the first dimension followed by a second dimension separation by molecular weight. In most cases this should result in discrete spots containing a single protein, however, in some cases, proteins with similar size and/or isoelectric point will co-migrate. Thus, in a few spots more than one protein was identified, leading to difficulty in accurate interpretation of the results. This co-migration

Table 1.1. Proteins with Phosphorylation Changes in WKPT Cells during Metabolic Acidosis

Fold Change	Protein Identified	Cellular Location	Unique Peptides	Function
5.4	hnRPD-like protein	Cytosol/ Nucleus	2	Transcription regulation
3.0	BiP	ER	17	Chaperone
3.0	hnRNP H	Nucleus	5	mRNA processing
2.6	Enolase	Cytosol	14	Glycolysis
2.4	PDI-A3	ER	15	Chaperone
2.3*	60 S ribosomal protein p2	Cytosol	5	Protein synthesis
	Myosin light chain 6	Cytosol	6	Motor protein
2.1*	HSP60	Mitochondrial	17	Chaperone
	Hnrpk	Cytosol/ Nucleus	3	mRNA processing
2.1*	Actin	Cytosol	6	Cytoskeleton
	Enolase	Cytosol	3	Glycolysis
2.0*	Tubulin beta-5 chain	Cytosol	3	Microtubule
	Endoplasmin	ER	4	Chaperone
	PDI	ER	3	Chaperone
1.6*	HSP 60	Mitochondrial	13	Chaperone
	BiP	ER	10	Chaperone
	Hnrpk	Cytosol/ Nucleus	9	mRNA processing
0.4	Suclg2 protein	Mitochondria	4	TCA cycle
0.3*	PDI- A3	ER	11	Chaperone
	GAPDH	Cytosol	5	Glycolysis
0.2	Heat shock cognate 71	Cytosol	3	Chaperone

* More than one protein may be listed for a spot with an indicated fold change because of co-migration effects.

Table 1.2. Proteins Identified with Abundance Changes in WKPT Cells during Metabolic Acidosis

Fold Change	Protein Identified	Cellular Location	Unique Peptides	Function
5.8	Tropomyosin-4	Cytosol	11	Cytoskeleton
4.4*	Actin	Cytosol	2	Cytoskeleton
	EIF3F	Cytosol	2	Protein Synthesis
4.3	HSP 60	Mitochondrial	11	Chaperone
3.7*	Actin	Cytosol	4	Cytoskeleton
	NudC	Cytosol	2	Dynactin Complex
3.4	RKIP	Cytosol	4	Raf-1 inhibitor
2.9	Actin	Cytosol	7	Cytoskeleton
2.2	Tropomyosin-4	Cytosol	2	Cytoskeleton
2.0*	Heat shock 70 kDa protein 1L	Mitochondrial	2	Chaperone
	Heat shock cognate 71	Cytosol	2	Chaperone
2.0	Heat shock cognate 71	Cytosol	11	Chaperone
1.9	EF-1-beta	Cytosol	5	Protein Synthesis
0.4*	HSP 60	Mitochondrial	13	Chaperone
	PDI-A3	ER	4	Chaperone
0.4	Stress-induced phosphoprotein 1	Cytosol/ Nucleus	7	Mediates HSC70 and HSP90
0.3*	PDI- A3	ER	11	Isomerase
	GAPDH	Cytosol	5	Glycolysis

* More than one protein may be listed for a spot with an indicated fold change because of co-migration effects.

effect represents one of the major challenges in analyzing a complex sample such as a whole cell lysate with a gel based method. Improved separation by liquid chromatography allows for more confident detection of quantitative changes in protein abundance and phosphorylation.

This preliminary study suggests that a remodeling of the rat proximal convoluted tubule proteome as well as the phosphoproteome occurs in response to pH changes during metabolic acidosis. The increased amount of total protein and changes in phosphorylation of proteins involved in protein folding and degradation indicates cells are undergoing major changes in order to respond to the decrease in pH. Unfortunately, the use of gel-based methods to analyze very complex cellular lysates was determined to limit the protein identifications and ability to confidently quantify changes. Moreover, the WKPT cell line is not clonal which likely contributed to the lack of validation of protein changes by Western blot analysis (Data not shown.).

While collectively these preliminary studies demonstrate significant changes in a rat kidney cell line that models metabolic acidosis, studies using freshly isolated rat renal proximal convoluted tubules will provide a more physiologically relevant characterization of the response to acidosis. Therefore, subsequent proteomics studies utilized male Sprague-Dawley rats, which are made acutely acidotic by loading the stomach with 20 mmol NH_4Cl and providing 0.28 M NH_4Cl as the only available drinking water for 24 hours or chronically acidotic by providing only the NH_4Cl solution for 7 days. The proximal convoluted tubules were isolated from rat kidneys by Percoll density gradient centrifugation.[26] This procedure yields 3-5 mg of protein from the kidneys of one rat. This amount of protein is sufficient for subsequent fractionation and proteomic analysis. The complexity of a whole cell extract must be reduced to obtain deep coverage of proteins in a proteomics experiment. To achieve comprehensive coverage and

quantitative data, cells should preferably be separated into subcellular fractions before protein analysis. Therefore, the proteome changes of the proximal convoluted tubule during metabolic acidosis were examined in three separate fractions: apical membrane, [27] mitochondria, [28] and soluble cytosolic fraction. (Unpublished data of Schauer, K.L., Freund, D.M., Prenni, J.E. and Curthoys, N.P.).

1.6 Liquid chromatography mass spectrometry-based quantitative proteomics

Discovery-based proteomics involves protein profiling at a global level, allowing for detection of quantitative differences in protein abundance, and biomarker discovery.[29] This type of experiment focuses on the identification of proteins and the detection of changes rather than the accuracy of quantitation. The bottom-up proteomics approach identifies proteins based on detection and identification of their proteolytic peptides. The analytical proteomic approaches employed for protein quantitation can be grouped into two major categories, labeling and label-free.[30]

1.6a Labeling methods

Examples of labeling approaches include stable isotope labeling by amino acids in cell culture (SILAC)[31], isotope coded affinity tags (ICAT)[32], tandem mass tags (TMT)[33] and isobaric tag for relative and absolute quantitation (iTRAQ).[34] Labeling can be metabolic, chemical or enzymatic using either isotopic or isobaric labels that alter the mass of a peptide.[35] Many of the methods for relative quantitation label with natural occurring stable heavy isotopes of ^{13}C, ^{15}N, ^{18}O, and ^{2}H. The incorporation of heavy isotopes in a peptide produces a mass shift in the mass spectrum. The labeled and unlabeled peptides differ only in their isotopic composition and have identical physical and chemical properties. This can be utilized of to

compare the intensities of mass-shifted peaks within the same mass spectrum for relative quantitation. SILAC is the most commonly used labeling method for cell culture in which proteins are labeled metabolically. For example, proteins can be labeled in vivo during protein synthesis by using growth medium that contains ^{13}C-lysine and/or ^{13}C-arginine.

For samples not derived from culture, such as tissues, ICAT is an alternative labeling method. ICAT chemically labels peptides by coupling a sulfhydryl-reactive group to cysteine residues. The ICAT label consists of the sulfhydryl-reactive group, an affinity group for isolation of the tagged peptides, and a linker in light and heavy form. The linker is made of either deuterium atoms or ^{13}C substitutions to make the tag heavy. In both SILAC and ICAT the two samples to be compared are labeled light or heavy and subsequently mixed. After LC-MS/MS analysis, the peak intensities of identical peptides with heavy or light labels are compared, and their ratio is calculated for quantitation. ICAT has the disadvantage of side reactivity of the tag and the limitation of only cysteine residues can be labeled with this tag. Therefore, this method does not produce global labeling and is biased towards peptides with cysteine residues.

TMT and iTRAQ are chemical labeling methods that use isobaric reagent mass tags that allow for multiplexing. Multiplexing capabilities are due to the availability of eight different tags for iTRAQ (or six for TMT) that can be analyzed within a single experiment. Both are chemical labels, and consequently, can be applied to many sample types and are not limited to cell culture as in metabolic labeling like SILAC. The mass tags contain an amine-reactive group, a balance group, and a reporter group. Tags contain different distributions of heavy isotopes between the balance and reporter groups. The tags label samples by the crosslinking of the reactive moiety to primary amines or cysteine residues of peptides. These tags are then cleaved upon fragmentation in the collision cell of the mass spectrometer. The labels are designed so that upon fragmentation

the different tags produce reporter ions with identical chemical composition but different molecular weights because of their different isotope compositions. The intensities of these ions are proportional to the relative abundances of the labeled peptide. A significant advantage of this method is identical peptides from the different labeled samples co-elute and are detected as a single precursor ion.

Enzymatic labeling of peptides can be performed with the incorporation of heavy stable isotopes during enzymatic proteolysis.[36] The proteolysis can be performed in the presence of heavy (H_2 ^{18}O) or light (H_2 ^{16}O) water that incorporates either two ^{18}O or ^{16}O atoms at the C-terminus of peptides. There will then be a mass shift of 4 Da between the heavy and light labeled peptides. Incomplete labeling and back exchange are the main pitfalls of this chemical labeling technique. However, it is less biased as it is not dependent on specific residues and all peptides have the option to be labeled. Overall, labeling methods are highly accurate, however, they require complex sample preparation, are limited in sampling size, have issues with incomplete labeling, are expensive, and involve time consuming data analysis.[37]

1.6b Label-free methods

Label-free approaches have become widely employed for the detection of relative protein abundance differences due to their ease of use in diverse applications.[38] Label-free quantitative strategies are commonly used and ideally suited for large scale discovery experiments with the goal of detecting significant differences between biological states to drive follow up studies. Additionally, they have been shown to enable relative quantitation over a larger dynamic range as compared to stable isotope labeling approaches.[38] There are two widely used strategies for label free quantitative measurements. One strategy is a simple counting approach, which

compares the number of tandem mass spectra detected for identified peptides of a given protein.[39] The other approach is based on total ion current of either the peptide precursor ion or the peptide fragment ions for each peptide assigned to a given protein.

There is a strong correlation between the amount of protein in a sample and the number of tandem mass spectra assigned to peptides from the protein.[40] The use of this correlation to determine relative quantitation in proteomics experiments is called spectral counting (SpC). SpC analysis has been shown to be highly sensitive for the detection of subtle changes in protein abundance.[41] However, when only a few spectra are identified for a protein it can lead to highly inaccurate representation of the abundance.[41] Thus, while SpC can suffer from inaccuracy in the quantitative measurement, it is extremely reproducible in detecting significant differences and is very easy to implement.

Another example of label-free approach is the use of ion intensity as a quantitative measure. The signal intensities of ions have been shown to directly correlate with ion concentrations.[42] Therefore, extracted peak areas from extracted ion chromatograms in LC-MS measurements can be used to determine relative quantitation of peptides and proteins between different samples. The mostly commonly employed use of this approach is based on the quantitative value from the ion current of the parent ion which requires high resolution measurements to ensure neighboring peaks are distinguished.[43] An alternative strategy is instead based on the average or sum of the total ion current of the MS/MS spectra (MS^2 TIC). This strategy is particularly useful for experiments utilizing low resolution instruments such as linear ion traps. MS^2 TIC methods have also been shown to provide improved sensitivity (as compared with SpC) for the detection of relative changes in low abundance proteins.[44] However, MS^2 TIC is not as reproducible as SpC due to inherent variation in sampling across a chromatographic

peak over all samples within an experiment. Taken together, label-free approaches have wider dynamic range and broader proteome coverage, whereas labeling approaches offer higher quantitative accuracy.

1.7 Overview

Multiple investigators have contributed to the current understanding of the physiological response to metabolic acidosis. These studies have identified specific cellular responses that occur during metabolic acidosis such as increased glutamine catabolism. However, other possible important proteins and the cellular pathways that mediate this essential adaptive response have not been determined. Proteomics studies help explain physiological processes at the cellular and molecular level. The studies described in this dissertation will further our understanding of the response of the proximal convoluted tubule to pH changes. Decreases in blood pH and bicarbonate concentration during metabolic acidosis produce an equivalent decrease in the intracellular pH.[45] Therefore, changes in the proteome that are observed may be due to the slight decrease in the intracellular pH. The work presented in this dissertation was focused on the overall goal of generating novel hypotheses regarding the cellular processes and pathways that respond to metabolic acidosis. Additionally, increased glutamine catabolism not only occurs in metabolic acidosis, but also in cancer cells. Therefore this work may also contribute to a better understand of glutamine metabolism in cancer.

REFERENCES

1. Wagner, C. A., Metabolic acidosis: new insights from mouse models. Curr Opin Nephrol Hypertens 2007, 16 (5), 471-6.

2. Curthoys, N. P., zeta-Crystallin: a tale of two cells. Kidney Int 2009, 76 (7), 691-693.

3. Karinch, A. M.; Lin, C. M.; Wolfgang, C. L.; Pan, M.; Souba, W. W., Regulation of expression of the SN1 transporter during renal adaptation to chronic metabolic acidosis in rats. Am J Physiol Renal Physiol 2002, 283 (5), F1011-9.

4. Waltham, M., Anatomy of the Nephron. UpToDate, I. 2009.

5. Curthoys, N. P.; Gstraunthaler, G., Mechanism of increased renal gene expression during metabolic acidosis. Am J Physiol-Renal 2001, 281 (3), F381-F390.

6. P. Vinay, e. a., Effects of fatty acids on renal ammoniagenesis in in vivo and in vitro studies. Am J Physiol 1976, 231 (3), 880-7.

7. Hughey, R. P.; Rankin, B. B.; Curthoys, N. P., Acute Acidosis and Renal Arteriovenous Differences of Glutamine in Normal and Adrenalectomized Rats. Am J Physiol 1980, 238 (3), F199-F204.

8. Curthoys, N. P.; Gstraunthaler, G., Mechanism of increased renal gene expression during metabolic acidosis. Am J Physiol Renal Physiol 2001, 281 (3), F381-90.

9. Sastrasinh, M.; Sastrasinh, S., Effect of acute pH change on mitochondrial glutamine transport. Am J Physiol 1990, 259 (6 Pt 2), F863-6.

10. Palmieri, F., The mitochondrial transporter family (SLC25): physiological and pathological implications. Pflugers Arch 2004, 447 (5), 689-709.

11. Lowry, M.; Ross, B. D., Activation of oxoglutarate dehydrogenase in the kidney in response to acute acidosis. Biochem J 1980, 190 (3), 771-80.

12. Curthoys, N. P., Renal ammonium ion production and excretion. 2007; Vol. 4th Edition, p 1601-1619.

13. Taylor, L.; Curthoys, N. P., Glutamine Metabolism: Role in acid-base balance. Biochem. Molec Biol. Ed. 2004, 32, 291-304.

14. Reilly, R. F.; Perazella, M. A., Acid-base, fluids, and electrolytes. McGraw-Hill Medical: New York, 2007; p xii, 483 p.

15. Soriano, J. R., Renal Tubular Acidosis: The Clinical Entity. J Am Soc Nephrol 2002, 13, 2160-2170.

16. Hanson, R. W.; Reshef, L., Regulation of phosphoenolpyruvate carboxykinase (GTP) gene expression. Annu Rev Biochem 1997, 66, 581-611.

17. Hwang, J. J.; Perera, S.; Shapiro, R. A.; Curthoys, N. P., Mechanism of altered renal glutaminase gene expression in response to chronic acidosis. Biochemistry 1991, 30 (30), 7522-6.

18. Feifel, E.; Obexer, P.; Andratsch, M.; Euler, S.; Taylor, L.; Tang, A. M.; Wei, Y.; Schramek, H.; Curthoys, N. P.; Gstraunthaler, G., p38 MAPK mediates acid-induced transcription of PEPCK in LLC-PK1-FBPase(+) cells. Am J Physiol-Renal 2002, 283 (4), F678-F688.

19. Laterza, O. F.; Curthoys, N. P., Specificity and functional analysis of the pH-responsive element within renal glutaminase mRNA. Am J Physiol-Renal 2000, 278 (6), F970-F977.

20. Porter, L. D.; Ibrahim, H.; Taylor, L.; Curthoys, N. P., Complexity and species variation of the kidney-type glutaminase gene. Physiol. Genomics 2002, 9, 157-166.

21. Curthoys, N. P.; Taylor, L.; Hoffert, J. D.; Knepper, M. A., Proteomic analysis of the adaptive response of rat renal proximal tubules to metabolic acidosis. Am J Physiol-Renal 2007, 292 (1), F140-F147.

22. Curthoys, N. P.; Taylor, L.; Hoffert, J. D.; Knepper, M. A., Proteomic analysis of the adaptive response of rat renal proximal tubules to metabolic acidosis. Am J Physiol Renal Physiol 2007, 292 (1), F140-7.

23. Lotspeich, W. D., Renal Hypertrophy in Metabolic Acidosis and Its Relation to Ammonia Excretion. Am J Physiol 1965, 208, 1135-42.

24. Nowik, M.; Lecca, M. R.; Velic, A.; Rehrauer, H.; Brandli, A. W.; Wagner, C. A., Genome-wide gene expression profiling reveals renal genes regulated during metabolic acidosis. Physiol Genomics 2008, 32 (3), 322-34.

25. Woost, P. G.; Orosz, D. E.; Jin, W.; Frisa, P. S.; Jacobberger, J. W.; Douglas, J. G.; Hopfer, U., Immortalization and characterization of proximal tubule cells derived from kidneys of spontaneously hypertensive and normotensive rats. Kidney Int 1996, 50 (1), 125-34.

26. Curthoys, N. P.; Taylor, L.; Hoffert, J. D.; Knepper, M. A., Proteomic analysis of the adaptive response of rat renal proximal tubules to metabolic acidosis. American Journal of Physiology - Renal Physiology 2007, 292 (1), F140-F147.

27. Walmsley, S. J.; Freund, D. M.; Curthoys, N. P., Proteomic profiling of the effect of metabolic acidosis on the apical membrane of the proximal convoluted tubule. Am J Physiol Renal Physiol 2012, 302 (11), F1465-77.

28. Freund D.M., P. J. E., Curthoys N.P., Response of the Mitochondrial Proteome of Rat Renal Proximal Convoluted Tubules to Chronic Metabolic Acidosis. Am J Physiol Renal Physiol 2013, 304(2) F145-F155.

29. Mallick, P.; Kuster, B., Proteomics: a pragmatic perspective. Nat Biotechnol 2010, 28 (7), 695-709.

30. Xie, F.; Liu, T.; Qian, W. J.; Petyuk, V. A.; Smith, R. D., Liquid chromatography-mass spectrometry-based quantitative proteomics. The Journal of biological chemistry 2011, 286 (29), 25443-9.

31. Ong, S. E.; Blagoev, B.; Kratchmarova, I.; Kristensen, D. B.; Steen, H.; Pandey, A.; Mann, M., Stable isotope labeling by amino acids in cell culture, SILAC, as a simple and accurate approach to expression proteomics. Mol Cell Proteomics 2002, 1 (5), 376-86.

32. Gygi, S. P.; Rist, B.; Gerber, S. A.; Turecek, F.; Gelb, M. H.; Aebersold, R., Quantitative analysis of complex protein mixtures using isotope-coded affinity tags. Nature biotechnology 1999, 17 (10), 994-9.

33. Thompson, A.; Schäfer, J.; Kuhn, K.; Kienle, S.; Schwarz, J.; Schmidt, G.; Neumann, T.; Hamon, C., Tandem Mass Tags: A Novel Quantification Strategy for Comparative Analysis of Complex Protein Mixtures by MS/MS. Analytical Chemistry 2003, 75 (8), 1895-1904.

34. Ross, P. L.; Huang, Y. N.; Marchese, J. N.; Williamson, B.; Parker, K.; Hattan, S.; Khainovski, N.; Pillai, S.; Dey, S.; Daniels, S.; Purkayastha, S.; Juhasz, P.; Martin, S.; Bartlet-Jones, M.; He, F.; Jacobson, A.; Pappin, D. J., Multiplexed protein quantitation in Saccharomyces cerevisiae using amine-reactive isobaric tagging reagents. Mol Cell Proteomics 2004, 3 (12), 1154-69.

35. Nikolov, M.; Schmidt, C.; Urlaub, H., Quantitative mass spectrometry-based proteomics: an overview. Methods Mol Biol 2012, 893, 85-100.

36. Mirgorodskaya, O. A.; Kozmin, Y. P.; Titov, M. I.; Korner, R.; Sonksen, C. P.; Roepstorff, P., Quantitation of peptides and proteins by matrix-assisted laser desorption/ionization mass spectrometry using (18)O-labeled internal standards. Rapid Commun Mass Spectrom 2000, 14 (14), 1226-32.

37. Panchaud, A.; Affolter, M.; Moreillon, P.; Kussmann, M., Experimental and computational approaches to quantitative proteomics: status quo and outlook. Journal of proteomics 2008, 71 (1), 19-33.

38. Bantscheff, M.; Schirle, M.; Sweetman, G.; Rick, J.; Kuster, B., Quantitative mass spectrometry in proteomics: a critical review. Analytical and bioanalytical chemistry 2007, 389 (4), 1017-31.

39. Bantscheff, M.; Schirle, M.; Sweetman, G.; Rick, J.; Kuster, B., Quantitative mass spectrometry in proteomics: a critical review. Anal Bioanal Chem 2007, 389 (4), 1017-31.

40. Liu, H.; Sadygov, R. G.; Yates, J. R., 3rd, A model for random sampling and estimation of relative protein abundance in shotgun proteomics. Anal Chem 2004, 76 (14), 4193-201.

41. Old, W. M.; Meyer-Arendt, K.; Aveline-Wolf, L.; Pierce, K. G.; Mendoza, A.; Sevinsky, J. R.; Resing, K. A.; Ahn, N. G., Comparison of label-free methods for quantifying human proteins by shotgun proteomics. Mol Cell Proteomics 2005, 4 (10), 1487-502.

42. Voyksner, R. D.; Lee, H., Investigating the use of an octupole ion guide for ion storage and high-pass mass filtering to improve the quantitative performance of electrospray ion trap mass spectrometry. Rapid Commun Mass Spectrom 1999, 13 (14), 1427-37.

43. Zhu, W.; Smith, J. W.; Huang, C. M., Mass spectrometry-based label-free quantitative proteomics. Journal of biomedicine & biotechnology 2010, 2010, 840518.

44. Wu, Q.; Zhao, Q.; Liang, Z.; Qu, Y.; Zhang, L.; Zhang, Y., NSI and NSMT: usages of MS/MS fragment ion intensity for sensitive differential proteome detection and accurate protein fold change calculation in relative label-free proteome quantification. The Analyst 2012, 137 (13), 3146-53.

45. Sahai, A.; Laughrey, E.; Tannen, R. L., Relationship between intracellular pH and ammonia metabolism in LLC-PK1 cells. Am J Physiol 1990, 258 (1 Pt 2), F103-8.

CHAPTER 2

Response of the Mitochondrial Proteome of Rat Renal Proximal Convoluted Tubules to Chronic Metabolic Acidosis [1]

2.1 Summary

Metabolic acidosis is a common clinical condition that is caused by a decrease in blood pH and bicarbonate concentration. Increased extraction and mitochondrial catabolism of plasma glutamine within the renal proximal convoluted tubule generates ammonium and bicarbonate ions that facilitate the excretion of acid and partially restore acid-base balance. Previous studies identified only a few mitochondrial proteins, including two key enzymes of glutamine metabolism, which are increased during chronic acidosis. A workflow was developed to characterize the mitochondrial proteome of the proximal convoluted tubule. Based upon the increase in specific activity of cytochrome c oxidase, the isolated mitochondria were enriched 8-fold. Two-dimensional liquid chromatography coupled with mass spectrometry was utilized to compare mitochondrial enriched samples from control and chronic acidotic rats. Proteomic analysis identified 901 proteins in the control and acidotic samples. Further analysis identified 37 peptides that contain an N-ε-acetyl-lysine; of these, 22 are novel sites. Spectral counting analysis revealed 33 proteins that are significantly altered in abundance in response to chronic metabolic acidosis. Western blot analysis was performed to validate the calculated changes in abundance. Thus, the current study represents the first comprehensive analysis of the mitochondrial proteome of the rat renal proximal convoluted tubule and its response to metabolic acidosis.

2.2 Introduction

Metabolic acidosis is a common clinical condition that results from a decrease in blood pH and the concentration of bicarbonate ions.[1, 2] This type of acidosis can occur acutely, lasting for a few hours to a day, or as a chronic condition where acid-base balance is not fully restored. Metabolic acidosis also occurs frequently as a secondary complication, which adversely affects the outcome of patients with various life-threatening conditions. Acid-base homeostasis is achieved, in part, by the renal reabsorption and net synthesis of bicarbonate ions and by the excretion of acids and ammonium ions.[3]

The various segments of the nephron exhibit rapid and sustained adaptive responses during the onset of metabolic acidosis.[4] For example, the proximal convoluted tubule exhibits a pronounced increase in ammoniagenesis and gluconeogenesis.[5] To support this adaptation, the renal proximal convoluted tubule extracts and catabolizes large amounts of plasma glutamine.[6] The extracted glutamine is transported into the mitochondrial matrix where it is deamidated by the kidney-type glutaminase (KGA) to yield glutamate and an ammonium ion. Subsequently, glutamate dehydrogenase (GDH) oxidizes the glutamate to α-ketoglutarate and yields a second ammonium ion. Further oxidation by α-ketoglutarate dehydrogenase generates an initial bicarbonate ion.[7] The cytosolic phosphoenolpyruvate carboxykinase (PEPCK) channels intermediates of the citric acid cycle to the gluconeogenic precursor, phosphoenolpyruvate, and produces a second bicarbonate ion.[8] Activation of the apical Na^+/H^+ exchanger (NHE3) acidifies the glomerular filtrate and facilitates the removal of cellular ammonium ions.[9] The increased secretion of hydrogen ions also promotes bicarbonate reabsorption from the lumen.[10] The reabsorbed and newly synthesized bicarbonate ions are then transported across the basolateral membrane by the $Na^+/3HCO_3^-$ co-transporter (NBC1).[9]

Increased expression of the key transporters and enzymes of this pathway sustains the increased renal catabolism of glutamine during chronic metabolic acidosis.[5] Various proteins, including KGA[11, 12], are up-regulated within the proximal convoluted tubule in response to metabolic acidosis. Increased expression of the mitochondrial KGA is due to selective stabilization of the KGA mRNA.[13, 14] This process is mediated by two 8-base AU-sequences that function as pH-response elements (pH-RE).[15] During chronic acidosis, the protein levels of the basolateral glutamine transporter (SN1), an unidentified mitochondrial glutamine transporter, GDH, PEPCK, and NHE3 are all increased to facilitate the restoration of acid-base balance.[4] The combined adaptations sustain the increased synthesis of ammonium ions, the increased reabsorption and production of bicarbonate ions, and their vectorial transport across the apical and basolateral membranes, respectively. However, recent transcriptome[16] and proteomic analyses[17, 18] indicate that the renal expression of a large number of additional mRNA transcripts and proteins are also altered in response to acidosis.

The sensitivity of proteomic profiling can be significantly enhanced by reducing the focus to highly enriched subcellular fractions. Mitochondria are essential organelles that transduce metabolic energy by electron transport and ATP synthesis. They are also involved in other functions such as apoptosis, ionic homeostasis, carbohydrate and amino acid metabolism, and the β-oxidation of fatty acids. In the current study, mitochondria were purified from proximal convoluted tubules that were isolated from normal and chronically acidotic rats. The mitochondrial proteins were digested with trypsin, fractionated by two-dimensional liquid chromatography, and analyzed by mass spectrometry. Many of the observed changes in protein abundance were subsequently validated by Western blot analysis.

2.3 Materials and methods

2.3a Animals

All experiments were performed using male Sprague-Dawley rats (~200 g) obtained from Charles River Laboratories (Kingston, NY). The rats were fed rodent chow (Harlan-Teklad, Madison, WI). Arterial blood pH and HCO_3^- concentrations were measured with an i-STAT 1 VetScan (Abaxis). The control rats were provided with tap water for drinking and had an arterial blood pH of 7.37 ± 0.03 and HCO_3^- concentration of 23.9 ± 2.4 mM. Acute metabolic acidosis was induced by stomach loading rats with 20 mmol NH_4Cl/kg body wt and providing 0.28 M NH_4Cl as their drinking water for 1 day (1 d). This protocol produced pronounced decreases in blood pH (7.11 ± 0.04) and HCO_3^- concentration (8.8 ± 1.1 mM). Rats that were made acidotic for 3 d or 7 d were provided with 0.28 M NH_4Cl as their sole source of drinking water. After 7 d of chronic acidosis, blood pH (7.34 ± 0.03) and HCO_3^- concentration (15.6 ± 0.9 mM) were partially compensated. On average the control rats consumed 34.3 ± 1.9 ml/day of water and the acidotic rats consumed a 36.4 ± 2.5 ml/day of the NH_4Cl solution. All of the procedures were approved by the Institutional Animal Care and Use Committee at Colorado State University.

2.3b Isolation of proximal convoluted tubules and mitochondrial fractions

Rat renal proximal convoluted tubules were isolated as described previously.[19] Briefly, freshly isolated renal cortex was digested with collagenase and the proximal convoluted tubules were purified by Percoll gradient centrifugation. The isolated proximal convoluted tubules were pelleted by centrifuging for 10 min at 1000xg at 4°C and resuspended in homogenization buffer containing 300 mM sucrose, 1 mM EDTA, 12 mM HEPES, and 1 mM phenylmethylsulfonylfluoride (PMSF). The resuspended tubules were homogenized with 20

passes in a 5 ml Teflon homogenizer. The homogenate was centrifuged twice at 700xg for 10 min at 4°C to pellet nuclei and cellular debris. The supernatant was centrifuged twice at 7000xg for 10 min at 4°C to pellet mitochondria and remove soluble cytosolic proteins and smaller organelles. The pellet was resuspended in 400 µl of homogenization buffer and washed twice by centrifugation at 7000xg for 10 min at 4°C. The final pellet containing mitochondria was resuspended in 1.0 ml of homogenization buffer and layered onto two sucrose step gradients each containing 750 µl of 1.0 M, 1.0 ml of 1.3 M, 1.0 ml of 1.6 M, and 250 µl of 2.0 M sucrose. The sucrose step gradients were centrifuged for 60 min at 134,000xg at 4°C. The mitochondrial fraction was recovered as a dense reddish-brown band, divided into four tubes, and washed three times by centrifugation for 20 min at 74,000xg at 4°C. Three of the pellets were combined and resuspended in 100 µl of 6 M urea with 1 mM PMSF and stored at -80°C. The fourth mitochondrial pellet was resuspended in 40 µl of homogenization buffer and used immediately to assay for cytochrome c oxidase activity.[20] Bradford[21] and bicinchoninic acid[22] (Pierce) protein assays were performed to determine protein concentrations.

2.3c Cytochrome c oxidase assay

Mitochondrial enrichment was calculated as the increase in specific activity of cytochrome c oxidase. This activity was determined by measuring the oxidation of reduced cytochrome c at 550 nm. The reaction mixture contained 0.3 mg/ml of cytochrome c dissolved in 30 mM potassium phosphate, pH 7.4.[20] The cytochrome c was reduced by addition of sodium hydrosulfite. The initial rates of oxidation were measured in crude homogenates of proximal convoluted tubules and the purified mitochondrial fractions. The specific activity for each

sample was calculated relative to the protein concentration and used to estimate the fold purification.

2.3d Proteomic sample preparation

The study compared mitochondrial fractions of proximal convoluted tubules isolated from control rats (n=3) and 7 d chronic acidotic rats (n=3). For proteomic analysis, 50 µg of protein in 6 M urea were bath sonicated for 5 min and vortexed to lyse the organelles. An acetone precipitation was performed prior to in-solution protein digestion. Briefly, the proteins were resuspended in 8 M urea and 0.2% ProteaseMAX surfactant (Promega), reduced with dithiothreitol, and alkylated with idoacetamide. The samples were digested with trypsin for 3 h at 37°C and then stopped with 0.5% trifluoroacetic acid. The peptides were dried in a speed-vac and purified using a reverse phase C18 TopTip (Glygen). The purified peptides were dried in a speed-vac and reconstituted in 50 µl of 0.1% formic acid/3% acetonitrile.

2.3e Mass spectrometry

Fractionation by two-dimensional liquid chromatography (2D-LC) was performed to increase the number of peptides identified in the samples. A 10-ug aliquot of each sample was injected onto a strong cation exchange (SCX) column (ZORBAX BioSCX Series II, 300 µm × 35 mm, 3.5 µm column, Agilent). Peptides were eluted from the SCX column using 20 µl salt bumps of 10, 15, 25, 35, 50, 75, 150, and 500 mM NaCl. The eluted peptides were further fractionated on a reverse phase column (1100 nanoHPLC, Zorbax C18, 5µm, 75 µm ID x 150mm column, Agilent) using a linear gradient from 25%-55% of 90% acetonitrile and 0.1% formic acid at a flow rate of 300 nl/min. Peptides were eluted from the reverse phase column

directly into the mass spectrometer (LTQ linear ion trap, Thermo Scientific) and spectra were collected over a m/z range of 200-2000 Da using a dynamic exclusion limit of 3 tandem mass spectra (MS/MS) of a given peptide mass for 30 sec and an exclusion duration of 90 sec. Compound lists of the resulting spectra were generated using Xcalibar 2.2 software (Thermo Scientific) with an intensity threshold of 5,000 and 1 scan/group. Duplicate 2D-LC injections were performed for each biological sample. All chromatograms were manually checked for consistency in retention time between injections and replicates. A tryptic digest of bovine serum albumin was injected between samples for quality control.

2.3f Bioinformatics

The MS/MS spectra were searched against the Uniprot-KB Rattus norvegicus protein sequence database (74,140 sequence entries) concatenated with a reverse database using both the Mascot (version 2.3.02, Matrix Science) and SEQUEST (version v.27, rev. 11, Sorcerer, Sage-N Research) database search engines. The search parameters were: average mass, peptide mass tolerance of 2.5 Da, fragment ion mass tolerance of 1.0 Da, complete tryptic digestion allowing two missed cleavages, variable modifications of methionine oxidation and lysine acetylation, and a fixed modification of cysteine carbamidomethylation. Peptide identifications from both search engine results were combined using protein identification algorithms in Scaffold 3 (Version 3.6.0, Proteome Software). Peptide and protein probability thresholds of 90% and 99%, respectively, were applied with Peptide and Protein Prophet algorithms in Scaffold 3.[23, 24] Proteins containing shared peptides were grouped by Scaffold 3 to satisfy the laws of parsimony. A peptide false discovery rate (FDR) of 0.2% was determined by the target decoy approach of searching the reversed database.[25] Only proteins that were identified by a minimum of 2 unique

peptides in at least 2 biological replicates were considered confidently identified. Gene Ontology (GO) terms for cellular locations and processes were extracted from Scaffold 3. Additional functional information on the identified proteins was manually determined from Uniprot-KB database (www.uniprot.org).

2.3g Spectral counting

Spectral counting analysis was performed to determine the relative protein abundance changes between control and chronic metabolic acidosis. Spectral counts (SpC) correspond to the sum of all MS/MS spectra identified for all of the peptides assigned to an individual protein. The number of spectral counts has been shown to highly correlate to the abundance of a protein in a sample.[26] Total spectral counts for all peptides identified for each protein were determined by summing the spectra identified using both the Mascot and SEQUEST database search engines for the analysis of each raw file from each biological replicate. The MS/MS data was normalized between samples in Scaffold 3 by using the sum of spectral counts for each sample to determine a scaling factor that was then applied to each protein in the sample. A pseudo value of 1 was added to all normalized values to eliminate zero values and fold changes were calculated using the mean normalized spectral counts for the three biological replicates for each condition. The following analyses were performed to assess data quality: principal components analysis, box plots, density plots, and scatter plots. Variance in the raw data was assessed by analyzing the number of proteins identified per sample, the total spectra identified, and the total peptides identified. Correlation of sample replicates was tested using Pearson's correlation and Spearman's rank sum correlation tests. All of the statistical analysis was performed using the R v2.13 statistics package (http://r-project.org). To test for significant changes in protein abundance, the Student's T-test was performed on the normalized spectral count values using

Scaffold 3. Fold changes ≥ 1.5 with a p-value ≤ 0.05 were considered significant. Manual validation of MS/MS spectra was performed for protein identifications above the thresholds that were based on two unique peptides for proteins with significant p-values and for acetylated peptides. Criteria for manual validation included the following: 1) a minimum of at least 3 theoretical y or b ions in consecutive order that are peaks greater than 5% of the maximum intensity; 2) an absence of prominent unassigned peaks greater than 5% of the maximum intensity; and 3) indicative residue specific fragmentation, such as intense ions N-terminal to proline and immediately C-terminal to aspartate and glutamate.

2.3h Western blot analyses

Additional mitochondrial fractions of isolated proximal convoluted tubules were prepared to validate the SpC data. The samples included control, 1-d acute acidotic, 3-d acidotic and 7-d chronic acidotic rats. For Western blotting, samples containing 10 μg of protein were separated by 8 or 10% SDS-PAGE. Proteins were transferred to polyvinylidenedifluoride membranes (Immobilon-FL, Millipore) and the blots were incubated overnight with the primary antibodies. The following rabbit polyclonal antibodies were used to validate changes identified by SpC: kidney-type glutaminase (KGA)[27], glutamate dehydrogenase (GDH) (Rockland); carbonic anhydrase 5B (CA5B) (Acris); UDP-glucuronosyltransferase 1A1 (UGT1A1) (Millipore); Catalase (CAT) (Abcam); and acetyl-Coenzyme A acyltransferase 1, (ACAA1), enoyl-coenzyme A hydratase/3-hydroxyacyl-coenzyme A dehydrogenase (EHHADH), and 17-β-hydroxysteroid dehydrogenase 4 (HSD17B4) (GeneTex). Peroxisomal enrichment was determined using a rabbit anti-peroxisomal biogenesis factor 3 (PEX3) antibody (GeneTex). A rabbit anti-acetylated-lysine (K-Ac^2-100) antibody (Cell Signaling) was used to quantify changes

in total acetylation. The mouse monoclonal antibody for glyceraldehyde-3-phosohoate dehydrogenase (GAPDH) (GeneTex) was the loading control for proximal convoluted tubule homogenates and soluble cytosolic fractions. Rabbit antibodies to malate dehydrogenase 2 and aconitase 2 (Aviva Systems Biology) and a mouse monoclonal antibody to the 70 kDa subunit of mitochondrial succinate dehydrogenase (SDH) (MitoSciences) were used as loading controls for all mitochondrial samples. Either 680 Dylight-conjugated goat anti-mouse IgG or 800 Dylight-conjugated goat anti-rabbit IgG (Pierce) was used as a secondary antibody. The resulting bands were visualized and quantified using an Odyssey Infrared Imager (LI-COR Biosciences).

2.3i Renal hypertrophy

Sham operated (n=3) and left side unilateral nephrectomized rats (UNX) (n=3) were purchased from Charles River Laboratories (Kingston, NY). To achieve maximal compensatory hypertrophy, the rats were sacrificed 21-d post-operation.[28] The average wet weights of the right kidneys of the sham operated and UNX rats were 1.35 ± 0.05 g and 1.82 ± 0.11 g, respectively. Therefore, unilateral nephrectomy resulted in a 36% increase in the wet weight of the right kidney.

2.4 Results

2.4a Isolation of mitochondria and peroxisomes from proximal convoluted tubules

Proximal convoluted tubules were isolated from rat renal cortex by Percoll density gradient centrifugation.[29] This preparation was previously shown to be essentially free of other nephron segments and to contain ~95% proximal convoluted tubules.[17, 18] Mitochondria were purified using differential and sucrose density centrifugation procedures similar to the protocol

of Reifschneider, et al.[30] Cytochrome c oxidase and protein assays were performed to determine the enrichment of mitochondria (Fig. 2.1 A). This analysis indicated that the mitochondria were enriched approximately 8-fold compared to homogenates of the corresponding proximal convoluted tubules. Because of their similar densities, it was not possible to obtain mitochondria that are free of peroxisomes. Therefore, peroxisomal biogenesis factor 3 (PEX3), which is an integral membrane protein that participates in peroxisomal biogenesis[31], was used as a marker to assess the enrichment of peroxisomes in the mitochondrial fractions. Western blot analysis indicated PEX3 was enriched approximately 4-fold when compared to the homogenates of the proximal convoluted tubules (Fig. 2.1 B). These data confirm that this protocol enriches predominantly for intact mitochondria and to a lesser extent for peroxisomes. Importantly, there was no significant difference in enrichment of control versus chronic metabolic acidotic samples.

2.4b Proteomic profiling of mitochondrial fractions from control and 7-d acidotic rats

A proteomic approach was utilized to profile the proteins that are expressed in the mitochondria of the proximal convoluted tubule and to identify those that exhibit altered abundance in response to chronic metabolic acidosis (Fig. 2.2). The digestion was deemed complete because there is only staining present below the 17 kDa marker indicating the sample contains only peptides (Fig. 2.3). Initially, triplicate biological samples of mitochondrial fractions were isolated from proximal convoluted tubules of control and 7-d chronic acidotic rats. Duplicate injections of each sample were analyzed by online two-dimensional LC/MS/MS, employing strong cation exchange and C18-reverse phase chromatography for peptide separation. Extensive fractionation of the samples was necessary to identify proteins because of

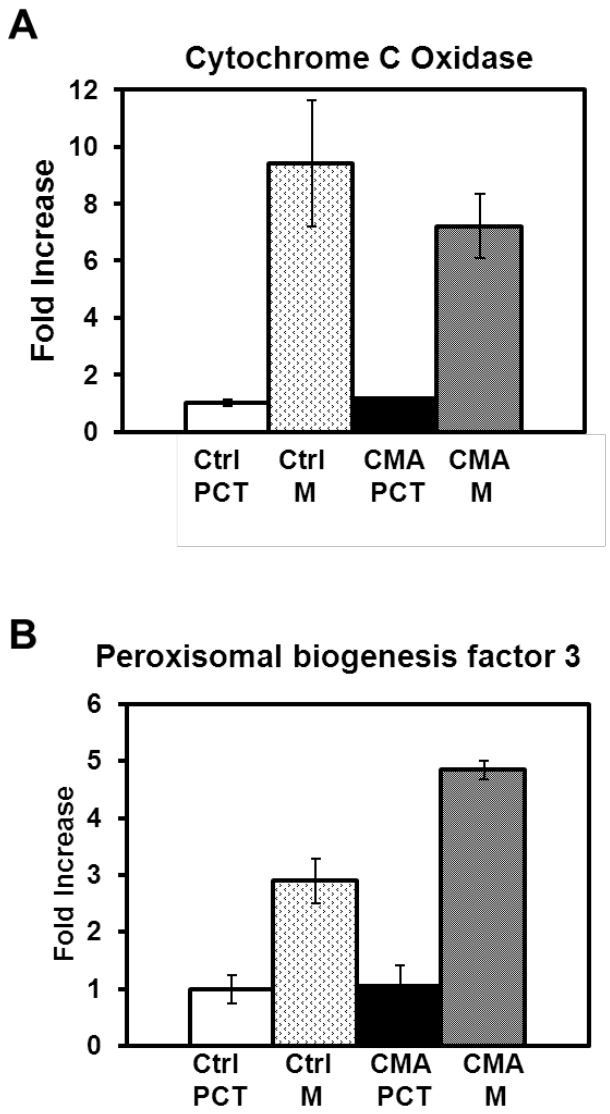

Fig. 2.1. Enrichment of cytochrome c oxidase and peroxisomal biogenesis factor 3 in isolated mitochondrial samples. A. Homogenates of proximal convoluted tubules (PCT) and the mitochondrial fractions (M) isolated from three control (Ctrl) and three 7-d chronic acidotic (CMA) rats were assayed for cytochrome c oxidase activity and protein concentration. The reported data are the mean ± S.E. of the fold increase in specific activities of the triplicate acidotic PCT or M samples, normalized to the control PCT samples. B. The corresponding increases in peroxisomal biogenesis factor 3 were quantified by Western blot analysis. The reported data are the mean ± the range of the fold increases measured in duplicate biological samples.

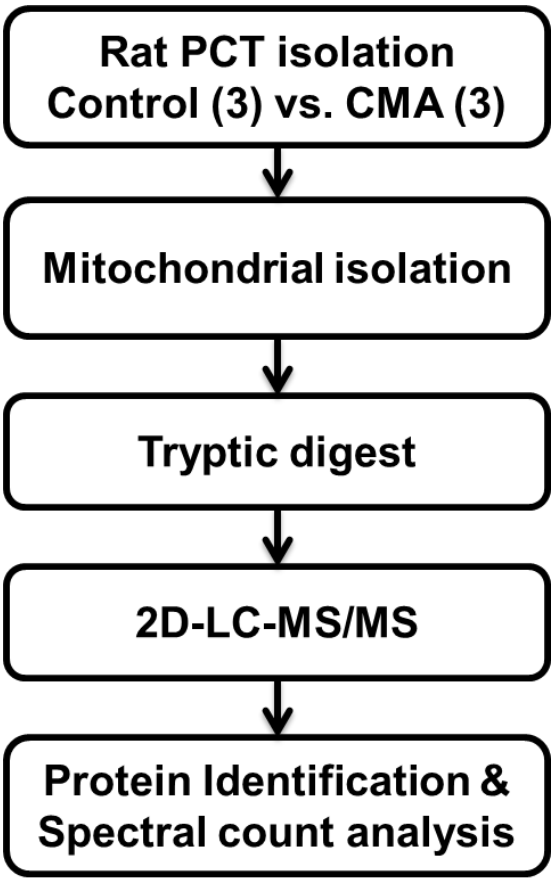

Fig. 2.2. Proteomics workflow - Proximal convoluted tubules (PCT) were isolated from three control and three 7-d chronic acidotic rats (CMA). The tubules were homogenized and the mitochondria were isolated by differential and sucrose gradient centrifugations. Following tryptic digestion, duplicate injections of the resulting peptides were analyzed by two-dimensional liquid chromatography (2D-LC) coupled directly with tandem mass spectrometry (MS/MS). Proteins were identified by searching the mass spectra versus the Uniprot-KB Rat protein sequence database. Spectral counting was performed to determine significant changes in protein abundance.

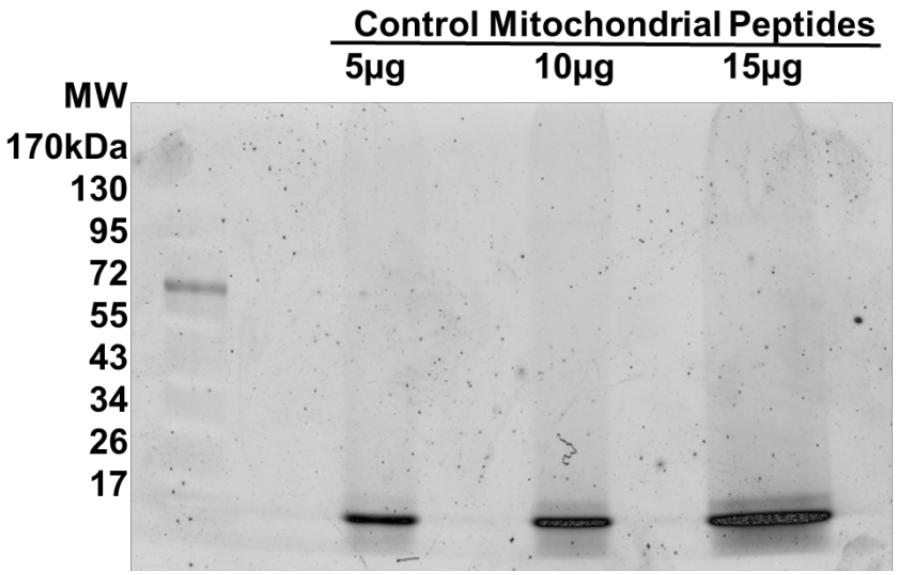

Fig. 2.3. Complete tryptic digestion of mitochondrial proteins. Peptides were separated by SDS-PAGE and stained with Sypro Ruby total protein stain (Molecular Probes). No proteins are present in peptide digestion.

the complex nature of the protein mixture (Fig. 2.4). Mass spectra were searched using both Mascot and SEQUEST search engines and the protein identifications were compiled and validated using Scaffold 3. The two-dimensional LC/MS/MS analyses of the mitochondrial fractions identified a total of 901 proteins in all samples with a peptide FDR of 0.2% calculated based on hits to a decoy database. A complete list of the identified proteins along with their mean spectral counts and transmembrane domain predictions are available at http://helixweb.nih.gov/ESBL/Database/PCT/ (Table 2.1). There are 183 proteins or, 20% of the total identified proteins, which contain at least one predicted transmembrane helix.[33] The presence of predicted transmembrane domains indicates that the mitochondrial isolation and digestion protocols were conducive to retaining and solubilizing membrane proteins.

Of the 901 proteins identified, 11 were unique to the control samples, 12 were unique to the chronic acidotic samples, and 878 were common to both based on presence in at least one biological sample (Fig. 2.5 A). The current version of the MitoProteome Database (http://www.mitoproteome.org/data/proteome/index.html) lists 780 proteins that pass stringent criteria and are well-characterized mitochondrial proteins. 272 of the proteins identified in this study (35%) are listed in the MitoProteome Database. Information on the cellular location and function of the identified proteins was also derived from the Gene Ontology (GO) terms in Scaffold 3. Cellular locations are represented as a percent of the 625 proteins that were annotated with a cellular location GO term (Fig. 2.5 B). As expected, the majority of the proteins (325 or 52%) were identified as mitochondrial. The next most prominent localization was cytosolic proteins (22%), followed by endoplasmic reticulum (9%), which has an interface with the mitochondrial membrane.[34] There were 8% plasma membrane proteins, which is not surprising because the mitochondria of the proximal convoluted tubule are positioned adjacent to the apical

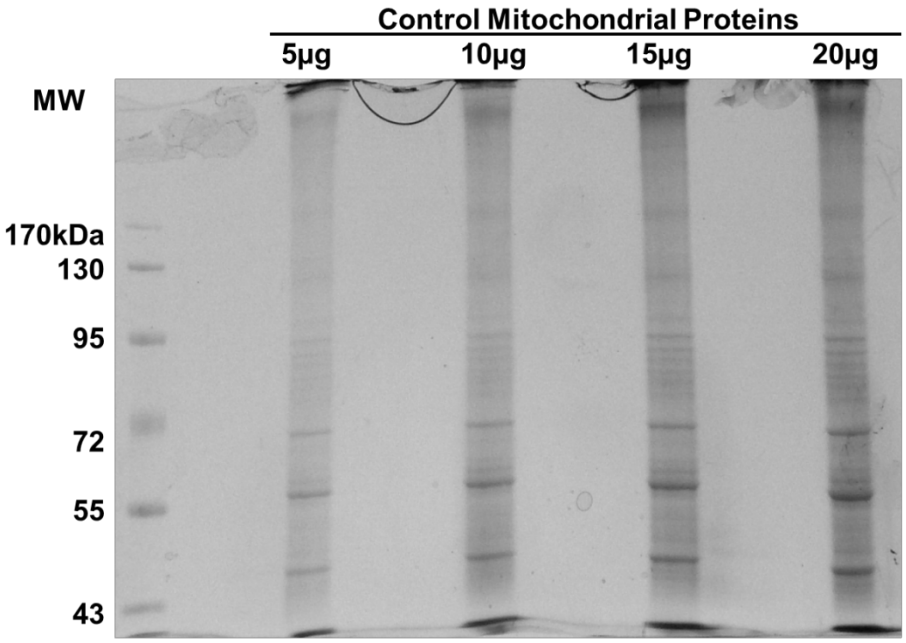

Fig. 2.4. Complexity of proximal convoluted tubule mitochondrial protein samples. Proteins were separated by SDS-PAGE and stained with Sypro Ruby total protein stain (Molecular Probes).

Table 2.1. Control and Acidotic Rat Proximal Convoluted Tubule Proteome

				Normalized mean spectral counts				Predicted
Proteins identified (901)	**Gene Name**	**Accession #**	**P-value**	**Ctrl**	**Ctrl S.E.**	**CMA**	**CMA S.E.**	**TMD**
[3-methyl-2-oxobutanoate dehydrogenase [lipoamide]] kinase, mitochondrial	Bckdk	Q00972	0.87	3.1	1.0	3.3	0.3	
[Pyruvate dehydrogenase [lipoamide]] kinase isozyme 2, mitochondrial	Pdk2	Q64536	0.08	9.4	2.9	20.5	3.8	
10 kDa heat shock protein, mitochondrial	Hspe1	P26772	0.44	129.2	24.2	154.0	16.4	
14-3-3 protein beta/alpha	Ywhab	P35213	0.47	13.7	6.8	7.0	4.8	
14-3-3 protein epsilon	Ywhae	P62260	0.36	27.3	10.8	14.5	6.0	
14-3-3 protein zeta/delta	Ywhaz	P63102	0.20	31.7	10.0	15.0	4.6	
2,4-dienoyl-CoA reductase, mitochondrial	Decr1	Q64591	0.08	66.7	11.5	95.4	4.5	
28S ribosomal protein S31, mitochondrial	Mrps31	B0BN56	0.61	0.4	0.4	0.9	0.9	
2-amino-3-carboxymuconate-6-semialdehyde decarboxylase	Acmsd	Q8R5M5	0.18	6.6	3.3	1.2	0.3	
2-hydroxyacyl-CoA lyase 1	Hacl1	Q8CHM7	0.32	1.9	1.9	4.1	0.7	
2-methoxy-6-polyprenyl-1,4-benzoquinol methylase, mitochondrial	Coq5	Q4G064	0.87	0.7	0.7	0.6	0.3	
2-oxoglutarate dehydrogenase, mitochondrial	Ogdh	Q5XI78	0.97	235.5	22.8	236.4	10.5	
2-oxoisovalerate dehydrogenase subunit alpha, mitochondrial (Fragment)	Bckdha	P11960	0.97	36.8	6.7	37.2	8.1	
2-oxoisovalerate dehydrogenase subunit beta, mitochondrial	Bckdhb	P35738	0.57	23.1	5.9	18.8	3.6	
39S ribosomal protein L10, mitochondrial	Mrpl10	P0C2C4	0.74	1.4	1.4	0.9	0.5	
39S ribosomal protein L17, mitochondrial	Mrpl17	Q6PDW6	0.32	1.1	0.6	0.3	0.3	
3-hydroxyisobutyrate dehydrogenase, mitochondrial	Hibadh	P29266	0.16	117.4	19.5	150.9	2.7	
3-hydroxyisobutyryl-CoA hydrolase, mitochondrial	Hibch	Q5XIE6	0.44	1.1	1.1	2.7	1.6	
3-mercaptopyruvate sulfurtransferase	Mpst	P97532	0.68	72.6	5.6	79.1	13.2	
3-oxoacyl-[acyl-carrier-protein] synthase, mitochondrial	Oxsm	G3V6R7	0.98	3.3	1.7	3.3	0.7	
40S ribosomal protein S15	Rps15	P62845	0.19	1.9	1.0	0.3	0.3	
40S ribosomal protein S19	Rps19	P17074	0.16	2.7	1.4	0.3	0.3	
4-aminobutyrate aminotransferase, mitochondrial	Abat	P50554	0.75	142.8	18.8	150.7	13.7	
4F2 cell-surface antigen heavy chain	Slc3a2	Q794F9	0.02	105.6	13.0	50.5	6.8	1
4-hydroxyphenylpyruvate dioxygenase	Hpd	P32755	0.62	10.4	4.3	7.8	2.2	
5,10-methenyltetrahydrofolate synthetase (5-formyltetrahydrofolate cyclo-ligase)	Mthfs	Q5M9F6	0.89	2.2	1.7	2.6	1.8	
5'-nucleotidase	Nt5e	P21588	0.56	2.3	1.7	1.2	0.3	1
60 kDa heat shock protein, mitochondrial	Hspd1	P63039	0.41	834.0	196.0	1039.3	103.5	
60S acidic ribosomal protein P0	Rplp0	P19945	0.82	5.9	2.7	5.1	2.0	
60S acidic ribosomal protein P2	Rplp2	P02401	0.06	2.6	0.7	0.6	0.3	
60S ribosomal protein L12	Rpl12	P23358	0.12	11.3	4.4	2.1	1.3	
60S ribosomal protein L15	Rpl15	P61314	0.37	7.0	2.3	4.0	2.0	
60S ribosomal protein L7	Rpl7	P05426	0.16	3.4	1.0	1.2	0.7	
78 kDa glucose-regulated protein	Hspa5	P06761	0.54	98.3	14.8	113.0	16.2	
Acad9 protein	Acad9	B1WC61	0.76	9.2	4.1	7.3	4.1	
Acetyl-CoA acetyltransferase, mitochondrial	Acat1	P17764	0.52	181.7	16.9	201.3	22.1	
Acetyl-Coenzyme A acyltransferase 2 , isoform CRA_f	Acaa2	G3V9U2	0.35	225.8	47.4	290.6	39.9	
Acid ceramidase	Asah1	Q6P7S1	0.41	0.4	0.4	1.2	0.8	
Aconitate hydratase, mitochondrial	Aco2	Q9ER34	0.22	455.8	27.6	508.0	23.4	
Actin, alpha cardiac muscle 1	Actc1	P68035	0.40	276.0	47.5	230.7	8.4	
Actin, cytoplasmic 2	Actg1	P63259	0.52	311.2	30.0	286.8	17.3	
Actin-related protein 3	Actr3	Q4V7C7	0.29	4.0	2.5	0.9	0.5	
Acyl carrier protein	LOC683884	D3ZF13	0.95	30.0	2.6	29.2	11.9	
Acyl-CoA dehydrogenase family member 11	Acad11	B3DMA2	0.59	1.5	1.5	0.6	0.6	
Acyl-CoA synthetase family member 2, mitochondrial	Acsf2	Q499N5	0.33	63.2	13.9	44.5	9.5	
Acyl-CoA thioesterase 9	Acot9	Q5U2X8	0.30	3.2	2.2	0.6	0.3	
Acyl-CoA-binding protein	Dbi	P11030	0.24	23.5	7.5	13.1	1.2	
Acyl-Coenzyme A dehydrogenase, very long chain	Acadvl	Q5M9H2	0.25	90.1	19.6	118.4	8.1	
Acyl-coenzyme A synthetase ACSM2, mitochondrial	Acsm2	O70490	0.63	233.2	25.4	248.1	13.6	
Acyl-coenzyme A synthetase ACSM3, mitochondrial	Acsm3	Q6SKG1	0.35	27.4	9.3	41.5	9.6	
Acyl-coenzyme A synthetase ACSM5, mitochondrial	Acsm5	Q6AYT9	0.30	0.7	0.7	5.4	3.8	
Acyl-coenzyme A thioesterase 2, mitochondrial	Acot2	O55171	0.36	86.7	13.4	70.7	8.0	
Acyl-protein thioesterase 1	Lypla1	P70470	0.86	15.5	6.0	16.6	0.2	
Acylpyruvase FAHD1, mitochondrial	Fahd1	Q6AYQ8	0.11	30.8	9.8	56.5	8.2	
Adaptor protein complex AP-1, beta 1 subunit, isoform CRA_a	Ap1b1	G3V9N8	0.59	17.8	4.6	14.1	4.3	
Adenosylhomocysteinase	Ahcy	P10760	0.68	3.1	2.0	2.1	0.8	
Adenylate kinase 3	Ak3	Q6P2A5	0.60	14.2	3.9	16.8	2.7	
Adenylate kinase isoenzyme 4, mitochondrial	Ak4	Q9WUS0	0.13	140.6	13.0	181.8	16.9	
Adenylyl cyclase-associated protein 1	Cap1	Q08163	0.38	4.1	3.5	0.6	0.3	
Adipocyte plasma membrane-associated protein	Apmap	Q7TP48	0.69	17.6	6.7	13.8	5.7	
ADP/ATP translocase 1	Slc25a4	Q05962	0.84	99.2	32.8	106.8	10.6	4
ADP/ATP translocase 2	Slc25a5	Q09073	0.72	265.7	54.0	286.6	12.7	2
ADP-ribosylation factor 3	Arf3	P61206	0.47	5.1	2.6	3.0	0.6	
ADP-ribosylation factor-like protein 8B	Arl8b	Q66HA6	0.37	5.8	2.4	3.2	0.7	
Aflatoxin B1 aldehyde reductase member 2	Akr7a2	Q8CG45	0.98	19.3	3.0	19.2	3.7	
Aflatoxin B1 aldehyde reductase member 3	Akr7a3	P38918	0.33	3.8	0.8	5.9	1.7	
Agmatinase, mitochondrial	Agmat	Q0D2L3	0.22	16.2	2.2	21.5	2.9	
A-kinase anchor protein 2	Akap2	Q5U301	0.60	11.1	7.3	15.7	3.4	

Alanine--glyoxylate aminotransferase 2, mitochondrial	Agxt2	Q64565	0.38	426.8	51.9	486.4	29.8	
Alanyl (Membrane) aminopeptidase	Anpep	G3V7W7	0.12	146.6	28.7	63.5	31.8	1
Alcohol dehydrogenase [NADP+]	Akr1a1	P51635	0.25	102.9	27.6	64.4	6.0	
Aldehyde dehydrogenase family 6, subfamily A1, isoform CRA_b	Aldh6a1	G3V7J0	0.94	314.7	67.5	320.7	16.8	1
Aldehyde dehydrogenase family 9, subfamily A1	Aldh9a1	G3V6J0	0.30	45.1	6.7	36.7	2.6	
Aldehyde dehydrogenase, mitochondrial	Aldh2	P11884	0.76	206.3	22.5	214.2	9.0	
Aldo-keto reductase family 1, member B10 (Aldose reductase)	Akr1b10	Q6AY99	0.20	8.5	5.6	22.0	6.7	
Aldo-keto reductase family 1, member C1	Akr1c1	Q3MHS3	0.76	5.8	2.0	7.2	3.6	
Alkaline phosphatase, tissue-nonspecific isozyme	Alpl	P08289	0.79	23.7	8.6	21.0	4.2	
All-trans-13,14-dihydroretinol saturase, isoform CRA_b	Retsat	G3V7V6	0.04	0.7	0.4	7.5	2.3	1
Alpha-2-HS-glycoprotein	Ahsg	P24090	0.61	16.9	6.9	20.9	2.5	
Alpha-2-macroglobulin receptor-associated protein	Lrpap1	Q99068	0.12	25.4	5.7	36.5	0.4	
Alpha-2u globulin PGCL2	LOC298116	Q8K1Q6	0.31	592.2	156.2	829.6	133.7	
Alpha-actinin-4	Actn4	Q9QXQ0	0.44	81.4	40.1	44.5	14.4	
Alpha-aminoadipic semialdehyde dehydrogenase	Aldh7a1	Q64057	0.62	166.5	17.1	155.2	11.7	
Alpha-aminoadipic semialdehyde synthase, mitochondrial	Aass	A2VCW9	0.19	56.3	16.2	116.3	34.0	
Alpha-crystallin B chain	Cryab	P23928	0.37	1.4	1.4	0.0	0.0	
Alpha-enolase	Eno1	P04764	0.25	107.0	35.7	56.2	12.5	
Alpha-methylacyl-CoA racemase	Amacr	G3V8F9	0.40	11.0	5.6	5.6	1.0	
Alpha-N-acetylgalactosaminidase	Naga	Q66H12	0.26	0.4	0.4	4.3	3.0	
Aminoacylase-1A	Acy1a	Q6AYS7	0.22	18.4	8.8	5.3	1.4	
Aminopeptidase N	Anpep	P15684	0.12	145.0	27.9	90.6	1.0	1
Amnionless (Predicted)	Amn	D3ZFK9	0.35	0.8	0.8	2.7	1.6	1
Anamorsin	Ciapin1	Q5XID1	0.52	2.2	2.2	0.6	0.6	
Angiotensinogen	Agt	P01015	0.76	5.8	0.9	6.5	2.1	
Anionic trypsin-1	Prss1	P00762	0.19	77.5	9.7	62.1	0.6	
AP-2 complex subunit alpha-2	Ap2a2	P18484	0.48	20.0	7.9	12.2	6.2	
AP-2 complex subunit mu	Ap2m1	P84092	0.76	5.3	0.9	4.8	1.3	
Apoa1bp protein	Apoa1bp	B0BNM1	0.72	5.1	2.9	7.0	4.0	
Apolipoprotein A-I	Apoa1	P04639	0.19	5.4	1.6	2.1	1.3	
Apolipoprotein A-IV	Apoa4	P02651	0.04	46.3	10.0	83.6	7.6	
Apolipoprotein E	Apoe	P02650	0.57	36.9	13.4	48.0	12.2	
Apolipoprotein H	Apoh	Q5I0M1	0.07	8.8	5.4	23.2	2.1	
Apoptosis-inducing factor 1, mitochondrial	Aifm1	Q9JM53	0.83	56.2	12.7	59.3	4.4	
Aquaporin-1	Aqp1	P29975	0.20	65.5	7.6	46.4	9.9	6
Argininosuccinate lyase	Asl	P20673	0.13	23.6	6.9	9.6	3.0	
Argininosuccinate synthase	Ass1	P09034	0.07	125.9	31.6	47.3	6.7	
Armadillo repeat-containing X-linked protein 1	Armcx1	Q5U310	0.50	1.2	1.2	0.3	0.3	1
ARP1 actin-related protein 1 homolog B (Yeast)	Actr1b	B2RYJ7	0.57	1.8	1.0	2.7	1.1	
Aspartate aminotransferase, cytoplasmic	Got1	P13221	0.25	4.0	2.5	0.6	0.3	
Aspartate aminotransferase, mitochondrial	Got2	P00507	0.43	160.2	14.5	182.7	21.1	
Aspartoacylase-2	Acy3	Q5M876	0.74	1.2	1.2	1.7	0.8	
Aspartyl aminopeptidase	Dnpep	Q4V8H5	0.26	12.2	4.3	6.3	1.5	
ATP synthase gamma chain	LOC100360100	Q6QI09	0.28	103.1	5.1	93.6	5.8	
ATP synthase subunit alpha, mitochondrial	Atp5a1	P15999	0.38	928.2	109.0	797.2	74.2	
ATP synthase subunit b, mitochondrial	Atp5f1	P19511	0.42	139.4	19.8	121.2	4.2	
ATP synthase subunit beta, mitochondrial	Atp5b	P10719	0.33	2271.5	189.5	2056.3	48.5	
ATP synthase subunit d, mitochondrial	Atp5h	P31399	0.29	228.5	20.3	197.3	15.8	
ATP synthase subunit e, mitochondrial	Atp5i	P29419	0.28	26.9	2.6	41.7	11.4	
ATP synthase subunit O, mitochondrial	Atp5o	Q06647	0.50	138.4	22.8	157.0	10.9	
ATP synthase, H+ transporting, mitochondrial F1 complex, delta, CRA_b	Atp5d	G3V7Y3	0.09	20.2	2.5	13.2	2.0	
ATP synthase-coupling factor 6, mitochondrial	Atp5j	P21571	0.03	115.6	4.4	96.9	3.3	
ATPase family AAA domain-containing protein 1	Atad1	Q505J9	0.09	0.4	0.4	1.8	0.5	
ATPase family AAA domain-containing protein 3	Atad3	Q3KRE0	0.61	2.2	1.6	3.5	1.9	
ATPase inhibitor, mitochondrial	Atpif1	Q03344	1.00	7.7	3.3	7.7	0.7	
ATPase, H transporting, lysosomal V1 subunit G1	Atp6v1g1	B2GUV5	0.24	12.5	4.3	6.3	1.0	
ATPase, H+ transporting, lysosomal 38kDa, V0 subunit d1	Atp6v0d1	Q5M7T6	0.70	22.3	5.8	18.6	6.7	
ATPase, H+ transporting, V1 subunit D, isoform CRA_c	Atp6v1d	Q6P503	0.46	8.9	2.8	6.3	1.4	
ATPase, H+ transporting, V1 subunit E isoform 1, isoform CRA_a	Atp6v1e1	G3V7L8	0.77	92.4	34.2	103.5	11.2	
ATP-binding cassette sub-family B member 7, mitochondrial	Abcb7	Q704E8	0.57	7.3	3.8	4.7	1.9	5
ATP-binding cassette sub-family B member 8, mitochondrial	Abcb8	Q5RKI8	0.53	1.1	1.1	0.3	0.3	4
ATP-binding cassette sub-family D member 3	Abcd3	P16970	0.04	29.3	6.3	52.5	4.0	3
ATP-binding cassette sub-family G member 2	Abcg2	Q80W57	0.47	13.3	3.5	9.9	2.5	6
ATP-dependent Clp protease ATP-binding subunit clpX-like, mitochondrial	Clpx	Q5U2U0	0.60	2.2	0.6	2.7	0.6	
Beta-2-microglobulin	B2m	P07151	0.39	4.3	1.2	7.2	2.8	1
Beta-hexosaminidase subunit alpha	Hexa	Q641X3	0.20	3.9	2.1	0.6	0.3	1
Beta-lactamase-like protein 2	Lactb2	Q561R9	0.37	12.3	4.1	8.0	0.9	
Bifunctional ATP-dependent dihydroxyacetone kinase/FAD-AMP lyase (cyclizing)	Dak	Q4KLZ6	0.19	17.6	7.9	4.2	2.9	
Biphenyl hydrolase-like (Serine hydrolase)	Bphl	Q3B8N9	0.62	42.9	7.9	47.2	1.3	
Brain protein 44-like protein	Brp44l	P63031	0.50	48.3	3.2	42.9	6.6	
Branched-chain-amino-acid aminotransferase, mitochondrial	Bcat2	O35854	0.48	14.1	6.5	8.6	2.5	
CaiB/baiF CoA-transferase family protein C7orf10 homolog	NA	Q68FU4	0.41	5.1	2.8	2.1	1.7	
Calbindin	Calb1	P07171	0.14	16.1	8.4	0.9	0.0	
Calmodulin	Calm1	P62161	0.76	33.6	7.7	30.8	4.1	
Calnexin	Canx	P35565	0.01	35.1	3.6	14.8	1.5	1

Calreticulin	Calr	P18418	0.86	40.2	4.5	38.9	5.3	
Canopy 2 homolog (Zebrafish)	Cnpy2	A0JN30	0.82	1.1	0.0	0.9	0.9	
Carbonic anhydrase 2	Ca2	P27139	0.45	18.6	8.3	11.1	3.4	
Carbonic anhydrase 5B, mitochondrial	Ca5b	Q66HG6	0.07	0.0	0.0	4.7	1.9	
Carbonyl reductase family member 4	Cbr4	Q7TS56	0.11	1.5	0.7	6.9	2.5	
Carnitine O-acetyltransferase	Crat	Q704S8	0.81	10.8	3.0	12.0	3.8	1
Carnitine O-palmitoyltransferase 1, liver isoform	Cpt1a	P32198	0.50	15.9	8.9	9.2	1.8	
Carnitine O-palmitoyltransferase 2, mitochondrial	Cpt2	P18886	0.42	23.0	1.7	20.1	2.7	
Catalase	Cat	P04762	0.01	55.1	12.0	123.1	8.3	
Catechol-O-methyltransferase domain containing 1 (Predicted), isoform CRA_a	Comtd1	D3ZM21	0.64	5.9	3.0	4.1	2.1	1
Catenin (Cadherin associated protein), alpha 1	Ctnna1	Q5U302	0.11	37.2	5.1	25.9	2.2	
Cathepsin B	Ctsb	P00787	0.26	17.3	3.8	10.9	3.1	
Cathepsin D	Ctsd	P24268	0.50	3.0	2.4	6.7	4.3	
Cathepsin L1	Ctsl1	P07154	0.46	13.9	5.6	8.9	2.6	
Cationic trypsin-3	Try3	P08426	0.21	1.5	0.8	0.3	0.3	
CDGSH iron-sulfur domain-containing protein 1	Cisd1	B0K020	0.57	148.8	9.2	142.1	5.5	1
Cell division control protein 42 homolog	Cdc42	Q8CFN2	0.84	3.0	2.5	2.4	0.8	
Chloride intracellular channel 4, isoform CRA_b	Clic4	G3V8C4	0.59	48.9	11.0	40.2	10.0	
Chloride intracellular channel protein 1	Clic1	Q6MG61	0.65	6.0	3.5	4.0	2.0	
Choline dehydrogenase	Chdh	Q6UPE0	0.32	67.3	13.5	90.0	15.0	
Citrate lyase subunit beta-like protein, mitochondrial	Clybl	Q5I0K3	0.08	21.3	3.9	10.0	2.8	
Citrate synthase	Cs	G3V936	0.29	99.6	8.8	82.6	11.0	
Clathrin heavy chain 1	Cltc	P11442	0.20	94.7	20.0	62.2	5.9	
Coenzyme A synthase	Coasy	Q5XIA5	0.21	9.9	2.2	6.5	0.6	
Coenzyme Q6 homolog (Yeast)	Coq6	Q68FU7	0.60	5.3	1.9	4.1	0.7	
Cofilin-1	Cfl1	P45592	0.25	27.4	7.8	15.9	3.6	
Coiled-coil domain-containing protein 51	Ccdc51	Q5PPN7	0.12	0.0	0.0	2.1	1.0	1
Coiled-coil-helix-coiled-coil-helix domain containing 3 (Predicted), CRA_a	Chchd3	D3ZUX5	0.21	6.6	3.1	11.3	0.7	
Collagen alpha-1(I) chain	Col1a1	P02454	0.16	1.2	0.7	2.7	0.5	
Collectrin	Tmem27	Q9ESG3	0.81	65.2	5.1	69.2	14.7	1
Complement component 1 Q subcomponent-binding protein, mitochondrial	C1qbp	O35796	0.30	76.2	14.4	59.0	2.6	
Corticosteroid 11-beta-dehydrogenase isozyme 2	Hsd11b2	P50233	0.33	3.9	2.1	1.5	0.8	
Creatine kinase U-type, mitochondrial	Ckmt1	P25809	0.86	5.5	3.4	6.2	0.9	
Cubilin	Cubn	O70244	0.26	71.0	16.3	48.7	5.2	
Cystathionine gamma-lyase	Cth	P18757	0.37	2.3	1.3	3.9	0.9	
Cytochrome b5	Cyb5a	P00173	0.01	37.5	5.8	64.7	2.8	1
Cytochrome b-c1 complex subunit 1, mitochondrial	Uqcrc1	Q68FY0	0.31	306.9	43.9	255.0	9.7	
Cytochrome b-c1 complex subunit 2, mitochondrial	Uqcrc2	P32551	0.35	182.4	7.0	196.8	11.5	
Cytochrome b-c1 complex subunit 6, mitochondrial	Uqcrh	Q5M9I5	0.22	24.0	2.5	16.7	4.3	
Cytochrome b-c1 complex subunit 8	Uqcrq	Q7TQ16	0.59	42.6	12.5	34.8	4.5	1
Cytochrome b-c1 complex subunit Rieske, mitochondrial	Uqcrfs1	P20788	0.28	29.9	6.3	21.3	2.9	
Cytochrome c oxidase subunit 2	Mt-co2	Q8SEZ5	0.37	72.5	16.0	90.6	8.4	2
Cytochrome c oxidase subunit 4 isoform 1, mitochondrial	Cox4i1	P10888	0.49	78.5	7.0	71.1	6.8	1
Cytochrome c oxidase subunit 5A, mitochondrial	Cox5a	P11240	0.12	179.2	11.4	154.6	4.7	
Cytochrome c oxidase subunit 5B, mitochondrial	Cox5b	P12075	0.58	30.1	5.0	33.6	3.1	
Cytochrome c oxidase subunit 6A1, mitochondrial	Cox6a1	P10818	0.31	5.0	1.2	3.2	1.0	
Cytochrome c oxidase subunit 6C-2	Cox6c2	P11951	0.77	58.9	6.1	62.2	8.5	1
Cytochrome c oxidase subunit 7A2, mitochondrial	Cox7a2	P35171	0.25	28.9	2.2	36.3	5.1	1
Cytochrome c, somatic	Cycs	P62898	0.63	177.8	8.3	170.2	12.1	
Cytochrome c-1 (Predicted), isoform CRA_c	Cyc1	D3ZFQ8	0.52	147.3	19.2	133.5	4.2	
Cytochrome P450 2C23	Cyp2c23	P24470	0.20	70.1	5.3	82.1	5.6	1
Cytochrome P450 2D26	Cyp2d26	P10634	0.56	1.5	0.4	0.9	0.9	1
Cytochrome P450 4A12	Cyp4a12	P24464	0.79	21.3	5.4	18.1	9.9	2
Cytochrome P450 4A14	Cyp4a14	P20817	0.91	92.6	20.7	98.7	49.5	2
Cytochrome P450 4A2	Cyp4a2	P20816	0.02	91.2	22.0	175.1	7.7	1
Cytoplasmic dynein 1 heavy chain 1	Dync1h1	P38650	0.18	13.2	5.6	3.9	1.2	
Cytosol aminopeptidase	Lap3	Q68FS4	0.84	10.4	3.8	11.3	1.1	
Cytosolic 10-formyltetrahydrofolate dehydrogenase	Aldh1l1	P28037	0.25	12.0	4.4	5.9	0.9	
Cytosolic non-specific dipeptidase	Cndp2	Q6Q0N1	0.27	12.7	6.5	4.2	1.1	
D-2-hydroxyglutarate dehydrogenase, mitochondrial	D2hgdh	P84850	0.99	4.5	2.3	4.4	2.1	
D-3-phosphoglycerate dehydrogenase	Phgdh	O08651	0.16	4.3	1.6	1.2	0.8	
D-amino-acid oxidase	Dao	O35078	0.09	141.2	12.3	174.2	8.6	
D-beta-hydroxybutyrate dehydrogenase, mitochondrial	Bdh1	P29147	0.57	9.4	4.9	6.3	1.0	
D-dopachrome decarboxylase	Ddt	P80254	0.63	8.6	3.1	6.3	2.9	
Dehydrogenase/reductase (SDR family) member 1	Dhrs1	Q6AXY8	0.13	1.8	1.0	0.0	0.0	
Dehydrogenase/reductase SDR family member 4	Dhrs4	Q8VID1	0.44	10.1	5.7	5.0	1.8	
Delta-1-pyrroline-5-carboxylate dehydrogenase, mitochondrial	Aldh4a1	P0C2X9	0.48	173.1	24.8	195.8	14.9	
Delta-aminolevulinic acid dehydratase	Alad	P06214	0.73	13.5	4.6	11.6	2.4	
Deoxyguanosine kinase (Predicted), isoform CRA_a	Dguok	D3ZDE4	0.18	5.3	0.5	6.2	0.1	
Dihydrolipoamide branched chain transacylase E2	Dbt	B2GV15	0.77	44.1	4.4	42.6	2.1	
Dihydrolipoamide S-succinyltransferase (E2 of 2-oxo-glutarate), CRA_a	Dlst	G3V6P2	0.95	50.0	6.6	50.5	0.4	
Dihydrolipoyl dehydrogenase, mitochondrial	Dld	Q6P6R2	0.48	151.2	18.4	168.1	12.0	
Dihydrolipoyllysine-residue acetyltransferase of pyruvate dehydrogenase	Dlat	P08461	0.93	40.7	14.1	42.1	7.6	
Dihydropteridine reductase	Qdpr	P11348	0.75	1.5	1.5	2.1	1.1	
Dimethylaniline monooxygenase [N-oxide-forming] 1	Fmo1	P36365	0.11	72.9	6.0	57.2	5.0	1

Dimethylaniline monooxygenase [N-oxide-forming] 3	Fmo3	Q9EQ76	0.09	4.4	2.6	15.1	3.9	
Dimethylaniline monooxygenase [N-oxide-forming] 4	Fmo4	Q8K4B7	0.62	2.2	1.3	3.0	0.6	
Dimethylglycine dehydrogenase	Dmgdh	Q5RKL4	0.06	47.4	7.6	68.3	2.5	
Dimethylglycine dehydrogenase, mitochondrial	Dmgdh	Q63342	0.00	40.9	1.8	75.0	4.7	
Dipeptidase 1	Dpep1	P31430	0.93	12.3	4.7	11.9	2.3	
Dipeptidyl peptidase 2	Dpp7	Q9EPB1	0.99	2.4	1.9	2.4	1.3	
DnaJ (Hsp40) homolog, subfamily C, member 11	Dnajc11	B1WBY5	0.32	2.2	1.6	0.3	0.3	
DnaJ homolog subfamily A member 1	Dnaja1	P63036	0.33	5.7	2.3	3.0	0.8	
Dolichyl-diphosphooligosaccharide--protein glycosyltransferase 48 kDa subunit	Ddost	Q641Y0	0.37	2.4	1.4	5.5	2.8	2
Dolichyl-diphosphooligosaccharide--protein glycosyltransferase subunit 1	Rpn1	P07153	0.07	47.0	3.8	35.5	2.6	1
Dolichyl-diphosphooligosaccharide--protein glycosyltransferase subunit 2	Rpn2	P25235	0.08	25.2	5.0	12.8	1.8	3
Dynein light chain 2, cytoplasmic	Dynll2	Q78P75	0.12	1.6	0.8	0.0	0.0	
Ectonucleoside triphosphate diphosphohydrolase 5	Entpd5	Q6P6S9	0.02	8.0	0.8	18.2	2.5	2
Ectonucleotide pyrophosphatase/phosphodiesterase family member 3	Enpp3	P97675	0.62	1.9	1.3	1.2	0.3	1
Ectonucleotide pyrophosphatase/phosphodiesterase family member 6	Enpp6	B0BND0	0.35	13.4	6.3	6.6	1.7	
EH domain-containing protein 1	Ehd1	Q641Z6	0.44	57.3	19.6	40.4	2.1	
ElaC homolog 2 (E. coli)	Elac2	G3V6F5	0.90	2.6	1.6	2.4	0.3	
Electron transfer flavoprotein subunit alpha, mitochondrial	Etfa	P13803	0.56	124.4	43.8	160.1	36.2	
Electron transfer flavoprotein subunit beta	Etfb	Q68FU3	0.05	93.0	9.3	125.5	6.5	
Electron transfer flavoprotein-ubiquinone oxidoreductase, mitochondrial	Etfdh	Q6UPE1	0.87	23.8	1.8	24.7	5.4	
Elongation factor 1-alpha 1	Eef1a1	P62630	0.38	57.8	11.2	45.2	6.2	
Elongation factor 2	Eef2	P05197	0.63	2.7	1.6	1.8	0.5	
Elongation factor G, mitochondrial	Gfm1	Q07803	0.58	9.5	5.3	6.2	0.1	
Elongation factor Ts, mitochondrial	Tsfm	Q9QYU2	0.68	4.4	2.3	3.3	0.8	
Elongation factor Tu, mitochondrial	Tufm	P85834	0.96	75.2	10.1	75.8	6.9	
Endoplasmic reticulum resident protein 29	Erp29	P52555	0.78	1.5	1.0	1.2	0.7	1
Endoplasmin	Hsp90b1	Q66HD0	0.62	64.2	7.8	59.3	4.8	
Enolase (Fragment)	NA	F1LZ68	0.60	0.7	0.7	0.3	0.3	
Enoyl Coenzyme A hydratase domain containing 2 (Predicted), isoform CRA_a	Echdc2	D3ZIL6	0.69	4.1	1.2	4.8	0.8	
Enoyl-CoA delta isomerase 1, mitochondrial	Eci1	P23965	0.04	76.7	6.5	116.2	10.8	
Enoyl-CoA delta isomerase 2, mitochondrial	Eci2	Q5XIC0	0.19	18.2	5.6	28.7	3.7	
Enoyl-CoA hydratase domain-containing protein 3, mitochondrial	Echdc3	Q3MIE0	0.01	0.4	0.4	3.8	0.6	
Enoyl-CoA hydratase, mitochondrial	Echs1	P14604	0.06	29.6	5.6	45.6	2.8	
Envoplakin (Predicted)	Evpl	G3V765	0.09	0.4	0.4	3.0	1.1	
Epithelial cell adhesion molecule	Epcam	O55159	0.80	5.1	2.4	6.4	4.2	1
Epoxide hydrolase 1	Ephx1	P07687	0.01	11.1	3.3	36.3	4.9	
Equilibrative nucleoside transporter 3	Slc29a3	Q80WK7	0.24	7.1	3.3	1.8	1.8	
Erlin-2	Erlin2	B5DEH2	0.55	0.4	0.4	1.2	1.2	
Erythrocyte protein band 4.1-like 3	Epb4.1l3	A3E0T0	0.39	61.7	20.7	40.7	6.6	
ES1 protein homolog, mitochondrial	NA	P56571	0.58	19.0	9.3	24.7	1.0	
Ester hydrolase C11orf54 homolog	NA	Q5U2Q3	0.17	17.6	8.9	2.1	2.1	
Ethylmalonic encephalopathy 1	Ethe1	B0BNJ4	0.46	47.2	8.1	55.7	6.4	
Eukaryotic translation initiation factor 4A1	Eif4a1	Q6P3V8	0.13	13.2	4.0	5.7	0.4	
Eukaryotic translation initiation factor 5A-1	Eif5a	Q3T1J1	0.45	3.9	1.2	2.4	1.3	
Evolutionarily conserved signaling intermediate in Toll pathway, mitochondrial	Ecsit	Q5XIC2	0.53	4.5	1.2	5.3	0.5	
Extracellular superoxide dismutase [Cu-Zn]	Sod3	Q08420	0.08	0.4	0.4	2.7	0.9	
Ezrin	Ezr	P31977	0.38	110.9	17.1	88.0	15.6	
F-actin-capping protein subunit beta	Capzb	Q5XI32	0.18	5.5	3.2	0.3	0.3	
Folate receptor 1 (Adult), isoform CRA_b	Folr1	G3V8M6	0.71	6.6	2.2	5.2	2.7	
Frataxin, mitochondrial	Fxn	D3ZYW7	0.92	10.8	3.4	11.3	3.1	
Fructose-1,6-bisphosphatase 1	Fbp1	P19112	0.28	122.8	34.5	79.0	8.3	
Fructose-bisphosphate aldolase	Aldob	Q66HT1	0.97	7.9	1.0	5.3	0.8	
Fructose-bisphosphate aldolase A	Aldoa	P05065	0.12	131.2	25.9	132.5	14.0	
Fumarate hydratase 1	Fh1	Q5M964	0.98	124.4	63.2	122.5	5.5	
Fumarylacetoacetase	Fah	P25093	0.79	5.8	3.2	4.5	2.8	
Fumarylacetoacetate hydrolase domain-containing protein 2	Fahd2	B2RYW9	0.01	29.6	5.9	61.1	3.8	
Gamma-glutamyltranspeptidase 1	Ggt1	P07314	0.12	9.1	4.6	22.4	4.8	1
GDNF-inducible zinc finger protein 1	Gzf1	D3ZUU2	0.76	1.2	0.7	0.9	0.5	
Gelsolin	Gsn	Q68FP1	0.21	13.3	5.2	21.4	1.5	
Glucose-6-phosphatase	G6pc	P43428	0.28	3.0	1.3	4.7	0.2	9
Glucose-6-phosphate isomerase	Gpi	Q6P6V0	0.34	31.4	11.9	17.4	4.9	
Glutamate carboxypeptidase 2	Folh1	P70627	0.23	9.2	1.9	17.6	5.7	1
Glutamate dehydrogenase 1, mitochondrial	Glud1	P10860	0.00	431.5	45.2	715.7	7.9	
Glutamate--cysteine ligase catalytic subunit	Gclc	P19468	1.00	1.2	1.2	1.2	0.8	
Glutaminase kidney isoform, mitochondrial	Gls	P13264	0.02	17.7	2.1	59.3	10.7	
Glutamyl aminopeptidase	Enpep	P50123	0.24	38.8	10.4	20.8	8.0	1
Glutaryl-Coenzyme A dehydrogenase (Predicted)	Gcdh	D3ZT90	0.69	51.9	11.9	57.5	5.5	
Glutathione peroxidase 1	Gpx1	P04041	0.29	98.4	12.1	119.7	12.5	
Glutathione S-transferase alpha-1	Gsta1	P00502	0.74	28.9	5.7	31.0	1.9	
Glutathione S-transferase alpha-3	Gsta3	P04904	0.56	119.1	34.3	96.1	10.7	
Glutathione S-transferase kappa 1	Gstk1	P24473	0.36	6.5	3.3	11.6	3.8	
Glutathione S-transferase mu 4	Gstm4	Q5BK56	0.54	1.9	1.3	3.3	1.7	
Glutathione S-transferase P	Gstp1	P04906	0.81	8.9	7.8	6.8	1.3	
Glyceraldehyde-3-phosphate dehydrogenase	Gapdh	P04797	0.34	162.2	43.8	112.8	10.8	
Glycerate kinase	Glyctk	Q0VGK3	0.96	22.9	9.6	22.3	1.2	

Glycerol-3-phosphate dehydrogenase [NAD+], cytoplasmic	Gpd1	O35077	0.96	13.2	5.2	12.9	3.6	
Glycine amidinotransferase, mitochondrial	Gatm	P50442	0.12	393.7	36.0	299.0	32.8	
Glycine C-acetyltransferase, CRA_b	Gcat	G3V7E4	0.96	15.9	5.4	15.6	3.3	
Glycine cleavage system H protein, mitochondrial	Gcsh	Q5I0P2	0.85	37.9	6.8	36.5	1.7	
Glycine N-acyltransferase	Glyat	Q5PQT3	0.13	160.5	22.3	212.5	15.4	
Glycine N-acyltransferase-like protein Keg1	Keg1	Q9Z2Y0	0.25	3.3	2.1	6.6	1.2	
G-protein coupled receptor family C group 5 member C	Gprc5c	Q3KRC4	0.91	1.9	1.9	2.1	0.3	8
Granulins	Grn	P23785	0.54	7.5	3.6	10.5	2.6	
GrpE protein homolog 1, mitochondrial	Grpel1	P97576	0.04	10.2	0.9	16.3	1.8	
Guanine nucleotide binding protein (G protein), gamma 12, isoform CRA_a	Gng12	G3V6P8	0.15	1.5	1.0	4.5	1.4	
Guanine nucleotide-binding protein G(i) subunit alpha-1	Gnai1	P10824	0.99	2.4	1.9	2.4	1.2	
Guanine nucleotide-binding protein G(s) subunit alpha isoforms XLas	Gnas	Q63803	0.48	9.8	3.7	6.6	1.6	
Guanine nucleotide-binding protein subunit alpha-11	Gna11	Q9JID2	0.57	4.3	2.1	3.0	0.2	
Haloacid dehalogenase-like hydrolase domain containing 3	Hdhd3	B2RYT7	0.56	7.0	3.8	4.5	1.1	
Heat shock cognate 71 kDa protein	Hspa8	P63018	0.45	94.3	25.0	73.1	3.8	
Heat shock protein 75 kDa, mitochondrial	Trap1	Q5XHZ0	0.32	21.8	2.7	18.7	0.3	
Heat shock protein HSP 90-alpha	Hsp90aa1	P82995	0.19	30.7	11.2	12.0	3.7	
Heat shock protein HSP 90-beta	Hsp90ab1	P34058	0.52	51.3	21.5	35.6	5.9	
Hemopexin	Hpx	P20059	0.18	7.8	2.3	14.7	3.6	1
Hepatitis B virus x interacting protein (Predicted), isoform CRA_a	Hbxip	D3ZF11	0.99	3.9	2.0	3.9	2.0	
Heterogeneous nuclear ribonucleoprotein K	Hnrnpk	P61980	0.46	3.0	2.5	0.9	0.5	
Histidine triad nucleotide binding protein 2 (Predicted), isoform CRA_a	Hint2	D4AB01	0.11	24.8	3.7	33.7	2.2	
Histidine triad nucleotide-binding protein 1	Hint1	P62959	0.55	1.2	1.2	2.7	1.9	
Histone cell cycle regulation defective interacting protein 5 (Predicted), CRA_a	Nfu1	D3ZA85	0.84	4.2	1.0	3.8	1.5	
Histone H2A	LOC680322	D3ZZ29	0.83	21.5	4.0	20.4	2.2	
Histone H2B	Hist1h2bf	D3Z8U0	0.35	6.5	3.3	2.3	2.3	
Histone H4	Hist1h4b	P62804	0.31	6.6	2.2	9.5	1.2	
Hsc70-interacting protein	St13	P50503	0.37	3.7	3.7	0.0	0.0	
HtrA serine peptidase 2	Htra2	B0BNB9	0.45	3.0	2.0	4.8	0.9	1
Hydroxyacid oxidase 2	Hao2	Q07523	0.16	256.5	57.5	361.1	19.9	
Hydroxyacid-oxoacid transhydrogenase, mitochondrial	Adhfe1	Q4QQW3	0.53	12.3	2.5	15.3	3.4	
Hydroxyacyl-coenzyme A dehydrogenase, mitochondrial	Hadh	Q9WVK7	0.59	163.2	15.1	154.3	3.1	
Hydroxymethylglutaryl-CoA lyase, mitochondrial	Hmgcl	P97519	0.82	20.4	6.6	18.7	2.3	
Hydroxymethylglutaryl-CoA synthase, mitochondrial	Hmgcs2	P22791	0.06	0.0	0.0	2.7	1.1	
Hydroxysteroid dehydrogenase-like protein 2	Hsdl2	Q4V8F9	0.29	14.7	4.3	19.9	0.2	
Hypothetical LOC304650 (Predicted), isoform CRA_b	RGD1310262	D4A1K4	0.89	4.8	2.2	5.3	2.4	
Hypoxanthine-guanine phosphoribosyltransferase	Hprt1	P27605	0.96	1.2	0.6	1.2	0.8	
Hypoxia up-regulated protein 1	Hyou1	Q63617	0.15	1.5	1.5	5.4	1.6	1
Inosine triphosphate pyrophosphatase	Itpa	D3ZW55	0.09	5.4	1.1	2.7	0.6	
Integrator complex subunit 11	Cpsf3l	Q3MHC2	0.94	2.6	1.4	2.7	0.6	
Integrin beta-1	Itgb1	P49134	0.23	9.0	3.3	3.8	1.5	1
Integrin, alpha 6, isoform CRA_a	Itga6	G3V667	0.98	2.0	2.0	2.1	0.8	1
Inter-alpha trypsin inhibitor, heavy chain 1 (Predicted), isoform CRA_a	Itih1	B2RYM3	0.19	0.0	0.0	2.4	1.5	
Inter-alpha-trypsin inhibitor heavy chain H3	Itih3	Q63416	0.33	5.7	2.0	8.0	0.5	
Iodotyrosine dehalogenase 1	Iyd	Q5BK17	0.12	1.1	1.1	3.9	0.8	1
IQ motif containing GTPase activating protein 1 (Predicted), isoform CRA_b	Iqgap1	G3V7Q7	0.21	2.3	1.3	0.3	0.3	
Isochorismatase domain-containing protein 2, mitochondrial	Isoc2	Q5U3Z3	0.85	4.4	2.5	3.8	1.5	
Isocitrate dehydrogenase [NAD] subunit beta, mitochondrial	Idh3B	Q68FX0	0.97	42.1	12.0	42.7	7.4	
Isocitrate dehydrogenase [NADP] cytoplasmic	Idh1	P41562	0.20	86.7	43.0	20.7	5.3	
Isocitrate dehydrogenase [NADP], mitochondrial	Idh2	P56574	0.82	371.4	42.9	382.5	12.5	
Isocitrate dehydrogenase 3 (NAD), gamma	Idh3g	Q5XIJ3	0.16	42.5	7.1	27.8	4.7	
Isoform 1 of Ectonucleotide pyrophosphatase/phosphodiesterase, member 1	Enpp1	Q924C3	0.49	4.5	2.5	2.4	1.1	1
Isoform 11-HSD1B of Corticosteroid 11-beta-dehydrogenase isozyme 1	Hsd11b1	P16232	0.37	0.0	0.0	0.9	0.9	
Isoform 2 of Adenylate kinase 2, mitochondrial	Ak2	P29410	0.13	62.3	7.8	91.1	13.3	
Isoform 2 of Alpha-adducin	Add1	Q63028	0.61	7.9	4.1	5.4	1.8	
Isoform 2 of AP-2 complex subunit beta	Ap2b1	P62944	0.47	13.1	3.3	10.1	1.7	
Isoform 2 of Basigin	Bsg	P26453	0.10	65.0	11.6	36.5	6.5	1
Isoform 2 of Brain-specific angiogenesis inhibitor 1-associated protein 2	Baiap2	Q6GMN2	0.23	3.1	1.0	5.7	1.6	
Isoform 2 of Cadherin-related family member 5	Cdhr5	Q9JIK1	0.69	20.5	5.8	17.9	2.2	1
Isoform 2 of Catechol O-methyltransferase	Comt	P22734	0.94	8.4	2.7	8.6	1.4	1
Isoform 2 of Dynamin-like 120 kDa protein, mitochondrial	Opa1	Q2TA68	0.65	25.6	12.5	19.4	1.7	
Isoform 2 of Electrogenic sodium bicarbonate cotransporter 1	Slc4a4	Q9JI66	0.22	124.2	12.9	95.1	15.3	9
Isoform 2 of Fibrinogen alpha chain	Fga	P06399	0.31	2.3	0.1	4.2	1.7	
Isoform 2 of Protein transport protein Sec31A	Sec31a	Q9Z2Q1	0.67	1.1	1.1	1.8	1.1	
Isoform 2 of Sodium/potassium-transporting ATPase subunit gamma	Fxyd2	Q04679	0.30	17.1	6.9	8.7	1.6	1
Isoform 2 of Solute carrier family 22 member 1	Slc22a1	Q63089	0.22	5.9	3.5	0.6	0.6	12
Isoform 2 of Trimethyllysine dioxygenase, mitochondrial	Tmlhe	Q91ZW6	0.36	21.2	14.8	42.3	14.3	
Isoform 2 of Voltage-dependent anion-selective channel protein 3	Vdac3	Q9R1Z0	0.42	13.3	7.2	20.3	3.4	
Isoform Cytoplasmic of Cysteine desulfurase, mitochondrial	Nfs1	Q99P39	0.45	8.6	1.9	11.1	2.3	
Isoform Cytoplasmic of Fumarate hydratase, mitochondrial	Fh	P14408	0.41	167.8	34.9	134.9	7.6	
Isoform Cytoplasmic+peroxisomal of Peroxiredoxin-5, mitochondrial	Prdx5	Q9R063	0.60	38.3	6.0	33.4	6.1	
Gamma-2 of Serine/threonine-protein phosphatase PP1-gamma catalytic	Ppp1cc	P63088	0.77	1.9	1.4	2.4	1.2	
Isoform II of V-type proton ATPase 116 kDa subunit a isoform 1	Atp6v0a1	P25286	0.09	7.4	2.5	1.5	1.1	6
Isoform III of Cystathionine beta-synthase	Cbs	P32232	0.09	5.8	1.9	1.2	0.8	
Isoform Long of Annexin A2	Anxa2	Q07936	0.30	0.8	0.4	2.4	1.3	

Isoform M2 of Pyruvate kinase isozymes M1/M2	Pkm2	P11980	0.06	1.5	0.4	0.3	0.3	
Isoform Non-brain of Clathrin light chain A	Clta	P08081	0.44	2.8	1.8	1.2	0.3	
Isoform p59 of Disabled homolog 2	Dab2	O88797	0.81	27.5	10.0	24.8	3.4	
Isoform SERCA2A of Sarcoplasmic/endoplasmic reticulum calcium ATPase 2	Atp2a2	P11507	0.49	5.6	1.2	7.1	1.6	8
Isoform Short of Brain protein 44	Brp44	P38718	0.40	18.4	7.4	28.6	8.0	
Isovaleryl-CoA dehydrogenase, mitochondrial	Ivd	P12007	0.79	43.0	9.8	45.9	2.9	
Junction plakoglobin	Jup	Q6P0K8	0.64	1.9	1.9	0.9	0.5	
Kynurenine 3-monooxygenase	Kmo	O88867	0.62	11.5	4.3	8.9	2.2	2
Kynurenine/alpha-aminoadipate aminotransferase, mitochondrial	Aadat	Q64602	0.13	6.8	2.2	16.2	4.5	
Kynurenine--oxoglutarate transaminase 1, mitochondrial	Ccbl1	Q08415	0.78	33.2	4.3	34.8	3.1	
Kynurenine--oxoglutarate transaminase 3	Ccbl2	Q58FK9	0.93	1.1	1.1	1.2	0.3	
Lactamase, beta (Predicted)	Lactb	D3ZFJ6	0.11	8.7	1.8	3.8	1.5	
Laminin, alpha 1	Lama1	D4A409	0.93	2.2	1.1	2.3	1.2	1
Legumain	Lgmn	Q9R0J8	0.74	7.5	0.7	6.6	2.6	
LETM1 and EF-hand domain-containing protein 1, mitochondrial	Letm1	Q5XIN6	0.49	50.2	8.2	39.0	12.4	1
Leucine-rich PPR motif-containing protein, mitochondrial	Lrpprc	Q5SGE0	0.89	64.2	22.1	60.6	7.4	
Leucine-rich repeat-containing protein 59	Lrrc59	Q5RJR8	0.33	11.5	1.8	16.8	4.5	1
Liver carboxylesterase 3	Ces1	Q63108	0.72	3.7	3.7	2.1	2.1	
Liver carboxylesterase 4	NA	Q64573	0.23	156.8	39.3	215.8	14.2	
Liver carboxylesterase B-1	NA	Q63010	0.26	105.2	28.2	148.8	18.4	
L-lactate dehydrogenase A chain	Ldha	P04642	0.59	0.7	0.7	1.5	1.1	
L-lactate dehydrogenase B chain	Ldhb	P42123	0.33	60.2	24.4	31.6	8.3	
Lman2 protein	Lman2	B0BNG3	0.81	2.6	1.0	2.4	0.3	1
Lon protease homolog 2, peroxisomal	Lonp2	Q3MIB4	0.45	1.1	1.1	2.1	0.2	
Lon protease homolog, mitochondrial	Lonp1	Q924S5	0.05	86.5	10.1	57.5	2.7	
Long-chain specific acyl-CoA dehydrogenase, mitochondrial	Acadl	P15650	0.18	90.2	6.0	100.9	2.7	
Long-chain-fatty-acid--CoA ligase 1	Acsl1	P18163	0.07	10.4	5.1	23.8	1.7	1
Low-density lipoprotein receptor-related protein 2	Lrp2	P98158	0.25	639.2	130.9	455.7	40.7	1
LRRGT00043	Nme4	Q6TXF6	0.20	4.1	0.9	7.4	2.0	
L-xylulose reductase	Dcxr	Q920P0	0.30	3.4	1.3	1.8	0.5	
Lysine-specific demethylase 3A	Kdm3a	Q63679	0.19	8.9	2.0	5.6	0.6	
Lysosome-associated membrane glycoprotein 1	Lamp1	P14562	0.49	3.8	2.3	2.1	0.3	1
Lysozyme C-1	Lyz1	P00697	0.94	74.7	24.8	71.9	28.5	
MACRO domain-containing protein 1 (Fragment)	Macrod1	Q8K4G6	0.58	3.7	1.4	5.0	1.6	
Macrophage migration inhibitory factor	Mif	P30904	0.70	3.6	2.1	2.7	0.5	
Major vault protein	Mvp	Q62667	0.61	0.7	0.7	0.3	0.3	
Malate dehydrogenase, cytoplasmic	Mdh1	O88989	0.60	37.8	18.9	26.4	6.2	
Malate dehydrogenase, mitochondrial	Mdh2	P04636	0.21	158.5	32.8	215.5	19.2	
Maleylacetoacetate isomerase	Gstz1	P57113	0.92	28.4	10.5	27.3	1.3	
Mannosyl-oligosaccharide glucosidase	Mogs	O88941	0.92	4.5	2.3	4.2	1.1	1
Medium-chain specific acyl-CoA dehydrogenase, mitochondrial	Acadm	P08503	0.47	60.4	4.5	54.2	6.3	
Membrane-associated progesterone receptor component 1	Pgrmc1	P70580	0.41	23.1	4.5	29.6	5.5	1
Membrane-bound aminopeptidase P	Xpnpep2	Q99MA2	0.33	29.6	6.2	22.5	1.2	
Membrane-bound carbonic anhydrase 12	Car12	A2IBE2	0.10	58.7	10.4	35.9	2.7	1
Metaxin 2	Mtx2	Q5U1Z9	0.30	13.6	4.5	8.0	1.4	
Methylcrotonoyl-CoA carboxylase beta chain, mitochondrial	Mccc2	Q5XIT9	0.76	64.4	14.4	58.3	11.3	
Methylmalonyl CoA epimerase (Predicted), isoform CRA_d	Mcee	D4A197	0.70	17.1	6.6	19.9	1.3	
Mitochondrial antiviral-signaling protein	Mavs	Q66HG9	0.96	2.0	1.5	2.1	1.2	
Mitochondrial carnitine/acylcarnitine carrier protein	Slc25a20	P97521	0.97	5.8	3.1	5.7	1.2	3
Mitochondrial carrier homolog 2 (C. elegans)	Mtch2	B0BN52	0.75	21.0	6.7	24.2	6.5	
Mitochondrial dicarboxylate carrier	Slc25a10	O89035	0.64	57.7	15.1	66.6	8.5	
Mitochondrial import inner membrane translocase subunit Tim10	Timm10	P62074	0.74	0.4	0.4	0.6	0.6	
Mitochondrial import inner membrane translocase subunit Tim13	Timm13	P62076	0.70	4.2	0.7	5.0	1.8	
Mitochondrial import inner membrane translocase subunit Tim8 A	Timm8a	Q9WVA1	0.93	4.4	1.7	4.7	1.9	
Mitochondrial import inner membrane translocase subunit Tim9	Timm9	Q9WV97	0.46	4.8	1.8	7.2	2.4	
Mitochondrial import receptor subunit TOM20 homolog	Tomm20	Q62760	0.67	4.5	1.6	3.3	2.1	1
Mitochondrial import receptor subunit TOM40 homolog	Tomm40	Q75Q40	0.45	12.0	4.0	8.6	0.9	
Mitochondrial peptide methionine sulfoxide reductase	Msra	Q923M1	0.91	24.8	3.2	25.5	4.9	
Mitochondrial Rho GTPase	Rnf135	A1L1L6	0.34	0.7	0.4	1.5	0.6	1
Mitochondrial ribosomal protein L20	Mrpl20	B2GV62	0.40	0.4	0.4	1.2	0.8	
Mitochondrial ribosomal protein L45 (Predicted)	Mrpl45	D4A104	0.64	1.1	1.1	1.8	0.9	
Mitochondrial ribosomal protein L50 (Predicted)	Mrpl50	D3ZYL4	0.89	1.4	1.4	1.2	0.6	
Mitochondrial ribosomal protein L53	Mrpl53	B2RYW4	0.18	3.7	1.8	0.6	0.3	
Mitochondrial ribosomal protein S27 (Predicted), isoform CRA_b	Mrps27	D4A3E8	0.19	0.8	0.4	1.8	0.5	
Mitochondrial ribosomal protein S35 (Predicted)	Mrps35	D4A9Z6	0.53	2.2	2.2	0.6	0.6	
Mitochondrial-processing peptidase subunit beta	Pmpcb	Q03346	0.95	9.2	3.4	9.0	2.2	
Mitofusin-1	Mfn1	Q8R4Z9	0.39	0.4	0.4	1.2	0.8	
Mitofusin-2	Mfn2	Q8R500	0.42	4.0	2.1	2.1	0.6	1
Monoglyceride lipase	Mgll	Q8R431	0.15	3.7	2.0	9.3	2.5	
MOSC domain-containing protein 2, mitochondrial	Mosc2	O88994	0.58	24.1	8.5	17.7	6.5	1
Mtch1 protein	Mtch1	B0BN30	0.70	3.3	1.9	4.2	0.6	2
Myosin light polypeptide 6	Myl6	Q64119	0.97	56.9	15.5	56.2	8.1	
Myosin regulatory light chain 12B	Myl12b	P18666	0.54	10.5	8.3	4.8	1.6	
Myosin, heavy polypeptide 9, non-muscle	Myh9	G3V6P7	0.09	180.4	22.2	127.7	8.3	
Myosin-Ic	Myo1c	Q63355	0.61	0.7	0.7	0.3	0.3	

N(G),N(G)-dimethylarginine dimethylaminohydrolase 1	Ddah1	O08557	0.19	20.1	10.7	3.0	1.4	
Na(+)/H(+) exchange regulatory cofactor NHE-RF1	Slc9a3r1	Q9JJ19	0.84	51.4	13.1	48.6	3.4	
Na(+)/H(+) exchange regulatory cofactor NHE-RF3	Pdzk1	Q9JJ40	0.59	200.2	54.9	165.8	22.3	
N-acetyltransferase 8	Nat8	Q9QXT3	0.58	8.6	3.3	6.3	1.9	2
NADH dehydrogenase (Ubiquinone) 1 alpha subcomplex, 8	Ndufa8	D4A311	0.56	41.9	10.3	49.1	4.4	
NADH dehydrogenase (Ubiquinone) 1 beta subcomplex 8	Ndufb8	B2RYS8	0.47	23.6	5.5	17.4	5.3	
NADH dehydrogenase (Ubiquinone) 1 beta subcomplex, 11 (Predicted)	Ndufb11	D4A7L4	0.27	18.0	2.9	13.9	1.5	1
NADH dehydrogenase (Ubiquinone) 1 beta subcomplex, 5 (Predicted), CRA_b	Ndufb5	D4A565	0.42	29.4	8.1	22.0	1.7	1
NADH dehydrogenase (Ubiquinone) 1 beta subcomplex, 6 (Predicted)	Ndufb6	D3ZZ21	0.38	21.6	2.0	18.4	2.6	1
NADH dehydrogenase (Ubiquinone) 1 beta subcomplex, 7 (Predicted)	Ndufb7	D3ZLT1	0.27	33.6	5.7	23.3	5.7	
NADH dehydrogenase (Ubiquinone) 1 beta subcomplex, 9	Ndufb9	B2RYW3	0.40	26.3	5.3	20.8	2.5	
NADH dehydrogenase (Ubiquinone) Fe-S protein 3 (Predicted), isoform CRA_c	Ndufs3	D3ZG43	0.39	98.1	10.9	109.8	5.4	
NADH dehydrogenase (Ubiquinone) Fe-S protein 5	LOC100361505	B5DEL8	0.85	33.0	5.0	34.3	4.3	
NADH dehydrogenase (Ubiquinone) Fe-S protein 7	Ndufs7	Q5RJN0	0.47	41.3	11.5	50.6	2.7	
NADH dehydrogenase (Ubiquinone) Fe-S protein 8 (Predicted), isoform CRA_a	Ndufs8	B0BNE6	0.50	29.5	6.0	24.9	0.5	
NADH dehydrogenase (Ubiquinone) flavoprotein 1	Ndufv1	Q5XIH3	0.56	69.4	4.9	65.8	3.1	
NADH dehydrogenase (Ubiquinone) flavoprotein 3-like, isoform CRA_a	Ndufv3	G3V644	0.80	21.7	5.0	23.2	3.1	
NADH dehydrogenase [ubiquinone] 1 alpha subcomplex assembly factor 4	Ndufaf4	Q9NQR8	0.67	3.7	2.5	5.1	1.9	
NADH dehydrogenase [ubiquinone] 1 alpha subcomplex subunit 10, mitochondria	Ndufa10	Q561S0	0.69	45.2	17.2	52.6	1.8	
NADH dehydrogenase [ubiquinone] 1 alpha subcomplex subunit 11	Ndufa11	Q80W89	0.99	24.3	5.1	24.4	6.5	2
NADH dehydrogenase [ubiquinone] 1 alpha subcomplex subunit 2	Ndufa2	D3ZS58	0.64	21.5	2.8	23.9	3.8	
NADH dehydrogenase [ubiquinone] 1 alpha subcomplex subunit 5	Ndufa5	Q63362	0.58	43.0	8.7	36.7	6.0	
NADH dehydrogenase [ubiquinone] 1 alpha subcomplex subunit 6	Ndufa6	D4A3V2	0.17	5.6	4.1	13.3	2.2	
NADH dehydrogenase [ubiquinone] 1 alpha subcomplex subunit 9, mitochondrial	Ndufa9	Q5BK63	0.59	71.5	16.7	84.7	14.8	
NADH dehydrogenase [ubiquinone] 1 subunit C2	Ndufc2	Q5PQZ9	0.85	33.1	6.8	31.7	1.7	1
NADH dehydrogenase [ubiquinone] flavoprotein 2, mitochondrial	Ndufv2	P19234	0.55	30.8	4.7	27.6	1.8	
NADH dehydrogenase [ubiquinone] iron-sulfur protein 2, mitochondrial	Ndufs2	Q641Y2	0.08	75.2	10.3	49.9	2.7	
NADH dehydrogenase [ubiquinone] iron-sulfur protein 4, mitochondrial	Ndufs4	Q5XIF3	0.40	69.5	8.9	60.5	3.5	
NADH-cytochrome b5 reductase 3	Cyb5r3	P20070	0.09	15.5	2.0	25.7	4.1	
NADH-ubiquinone oxidoreductase 75 kDa subunit, mitochondrial	Ndufs1	Q66HF1	0.81	112.9	10.9	108.6	11.9	
NADH-ubiquinone oxidoreductase chain 4	Mtnd4	P05508	0.71	13.0	4.6	10.5	4.1	13
NADH-ubiquinone oxidoreductase chain 5	Mt-nd5	Q8SEZ0	0.51	12.1	6.3	16.9	1.6	15
NADPH--cytochrome P450 reductase	Por	P00388	0.04	13.2	1.4	21.6	2.6	1
Napsin	Napsa	Q9QX71	0.97	34.7	8.0	35.1	6.7	
Ndufa4 protein	Ndufa4	B2RZD6	0.86	13.0	3.2	11.6	7.0	1
Ndufa7 protein	Ndufa7	A9UMV9	0.21	12.3	3.7	20.3	3.8	
Neutral and basic amino acid transport protein rBAT	Slc3a1	Q64319	0.20	73.2	20.1	38.1	10.8	1
Nicalin	Ncln	Q5XIA1	0.57	1.2	0.6	2.4	2.0	2
Nicotinamide nucleotide transhydrogenase	Nnt	Q5BJZ3	0.93	101.5	32.1	104.8	9.8	12
Nit1 protein	Nit1	Q5PQK6	0.91	13.1	2.1	12.7	2.2	
NLR family member X1	Nlrx1	Q5FVQ8	0.46	2.2	1.1	1.2	0.6	
Non-specific lipid-transfer protein	Scp2	P11915	0.74	10.8	4.3	9.2	0.6	
Nucleobindin-1	Nucb1	Q63083	0.42	14.4	5.2	23.1	8.2	
Nucleoside diphosphate kinase B	Nme2	P19804	0.32	17.1	7.5	8.6	0.9	
Obp3 protein	Obp3	Q78E14	0.98	19.2	19.2	18.4	18.4	
OCIA domain-containing protein 1	Ociad1	Q5XIG4	0.26	8.6	3.9	13.9	1.5	
Omega-amidase NIT2	Nit2	Q497B0	0.29	49.1	8.6	37.6	3.6	
Ornithine aminotransferase, mitochondrial	Oat	P04182	0.79	74.5	10.6	78.0	6.2	
Oxoglutarate dehydrogenase-like (Predicted), isoform CRA_a	Ogdhl	D3ZQD3	0.56	11.3	5.8	6.0	6.0	
Oxysterol-binding protein (Fragment)	Osbpl8	F1M0B9	0.24	2.7	0.4	5.4	2.0	1
Palmitoyl-protein thioesterase 1	Ppt1	P45479	0.44	3.2	2.7	0.9	0.5	
Paraplegin	Spg7	Q7TT47	0.57	3.3	1.9	2.1	0.3	2
PDZK1-interacting protein 1	Pdzk1ip1	Q923S2	0.60	18.7	6.6	14.9	1.4	1
Peptidase (Mitochondrial processing) alpha	Pmpca	Q68FX8	0.94	18.8	9.2	19.6	4.2	
Peptidyl-prolyl cis-trans isomerase A	Ppia	P10111	0.56	41.0	20.6	27.3	7.1	
Peptidyl-prolyl cis-trans isomerase B	Ppib	P24368	0.07	14.3	4.0	31.7	5.7	1
Peptidyl-prolyl cis-trans isomerase F, mitochondrial	Ppif	P29117	0.18	2.9	1.6	0.3	0.3	
Peroxiredoxin-1	Prdx1	Q63716	0.94	28.8	11.8	29.9	8.6	
Peroxiredoxin-2	Prdx2	P35704	0.57	1.2	0.6	2.4	2.0	
Peroxiredoxin-6	Prdx6	O35244	0.22	21.1	5.2	13.1	1.7	
Peroxisomal acyl-coenzyme A oxidase 1	Acox1	P07872	0.02	26.2	6.8	51.4	0.5	
Peroxisomal bifunctional enzyme	Ehhadh	P07896	0.01	14.3	3.5	31.5	2.0	
Peroxisomal multifunctional enzyme type 2	Hsd17b4	P97852	0.00	48.1	3.6	95.3	5.3	
Peroxisomal trans-2-enoyl-CoA reductase	Pecr	Q9WVK3	0.56	21.1	3.5	25.3	5.6	
Peroxisome assembly factor 2	Pex6	P54777	0.89	0.7	0.7	0.6	0.6	
Phenazine biosynthesis-like domain-containing protein	Pbld	Q68G31	0.51	2.3	0.7	1.5	0.8	
Phenylalanine-4-hydroxylase	Pah	P04176	0.32	19.7	10.6	7.2	3.4	
Phosphatidylethanolamine-binding protein 1	Pebp1	P31044	0.42	24.1	11.0	14.0	2.6	
Phosphatidylinositide phosphatase SAC1	Sacm1l	Q9ES21	0.85	6.6	2.2	7.1	1.3	2
Phosphoenolpyruvate carboxykinase, cytosolic [GTP]	Pck1	P07379	0.09	15.0	8.2	33.9	2.8	
Phosphoglucomutase-1	Pgm1	P38652	0.40	5.1	2.0	2.7	1.4	
Phosphoglycerate kinase 1	Pgk1	P16617	0.39	28.6	12.7	15.1	5.9	
Phosphoglycerate mutase 1	Pgam1	P25113	0.20	15.1	4.9	6.1	3.2	
Phosphoserine aminotransferase	Psat1	D3ZHJ1	0.51	1.1	0.0	1.8	0.9	
Phosphotriesterase-related protein	Pter	Q63530	0.35	5.7	0.7	4.8	0.6	

Plasma glutamate carboxypeptidase	Pgcp	Q6IRK9	0.44	15.5	4.5	11.6	0.8	
Plasma protease C1 inhibitor	Serping1	Q6P734	0.22	0.4	0.4	1.8	0.9	
Plasmolipin	Pllp	P47987	0.16	0.7	0.7	3.0	1.1	4
Plexin B2	Plxnb2	D3ZQ57	0.18	2.2	1.1	4.8	1.2	
Polyadenylate-binding protein 1	Pabpc1	Q9EPH8	0.38	5.1	2.8	1.8	1.8	
Polypyrimidine tract binding protein 1, isoform CRA_c	Ptbp1	D3ZB30	0.54	3.0	0.3	2.1	1.3	
Polyribonucleotide nucleotidyltransferase 1	Pnpt1	G3V6G7	0.99	8.0	5.7	8.0	2.2	
Potassium-transporting ATPase alpha chain 1	Atp4a	P09626	0.85	30.1	7.7	28.5	1.6	8
PRA1 family protein 3	Arl6ip5	Q9ES40	0.96	3.7	2.6	3.5	1.8	4
Probable 2-oxoglutarate dehydrogenase E1 component DHKTD1, mitochondrial	Dhtkd1	Q4KLP0	0.91	106.0	29.7	109.7	6.3	
Probable N-acetyltransferase CML1	Cml1	Q9QXT4	0.89	2.2	2.2	1.8	1.8	1
Pro-cathepsin H	Ctsh	P00786	0.09	8.5	2.0	3.8	0.7	
Prodh2 protein	Prodh2	B0BNG1	0.45	37.5	13.2	26.4	2.8	
Profilin-1	Pfn1	P62963	0.82	6.3	3.3	7.2	1.9	
Programmed cell death 6-interacting protein	Pdcd6ip	Q9QZA2	0.14	4.6	1.8	1.2	0.6	
Prohibitin	Phb	P67779	0.47	84.0	9.6	75.7	4.2	
Prohibitin-2	Phb2	Q5XIH7	0.56	95.7	35.4	73.2	6.3	
Proliferation-associated 2G4	Pa2g4	Q6AYD3	0.55	0.4	0.4	1.2	1.2	
Proline synthetase co-transcribed (Predicted)	Prosc	D3ZCA0	0.88	33.5	2.3	32.9	3.2	
Propionyl coenzyme A carboxylase, beta polypeptide	Pccb	Q68FZ8	0.64	65.0	11.3	71.3	5.3	
Propionyl-CoA carboxylase alpha chain, mitochondrial	Pcca	P14882	0.42	23.0	7.6	31.3	5.3	
Propionyl-CoA carboxylase beta chain, mitochondrial	Pccb	P07633	0.85	68.5	11.9	65.9	5.6	
Prostaglandin E synthase 2 (Predicted), isoform CRA_b	Ptges2	D4AE56	0.42	10.0	3.2	6.9	1.4	
Prostaglandin reductase 2	Ptgr2	Q5BK81	0.54	3.7	3.7	1.2	0.6	
Proteasome activator complex subunit 1	Psme1	Q63797	0.86	0.8	0.4	0.9	0.5	
Proteasome subunit alpha type-2	Psma2	P17220	0.29	5.8	3.0	2.1	0.6	
Protein AMBP	Ambp	Q64240	0.02	2.0	0.9	13.8	3.2	
Protein disulfide-isomerase	P4hb	P04785	0.24	59.9	15.5	61.4	3.8	
Protein disulfide-isomerase A3	Pdia3	P11598	0.93	15.7	3.1	14.3	3.1	
Protein disulfide-isomerase A6	Pdia6	Q63081	0.76	35.5	8.3	49.0	5.4	
Protein DJ-1	Park7	O88767	0.80	9.6	3.6	8.4	2.5	
Protein FAM151A	Fam151a	Q642A7	0.04	32.8	6.3	11.7	2.5	1
Protein FAM162A	Fam162a	Q4QQV3	0.45	0.4	0.4	0.9	0.5	1
Protein Mpv17	Mpv17	Q5BK62	0.15	0.4	0.4	1.2	0.3	2
Protein NDRG1	Ndrg1	Q6JE36	0.54	22.9	4.3	26.1	2.1	
Protein phosphatase 2 , regulatory subunit A (PR 65), alpha, CRA_a	Ppp2r1a	Q5XI34	0.81	2.6	2.1	2.1	0.6	
Protein TBRG4	Tbrg4	Q5M9G9	0.52	1.1	1.1	0.3	0.3	
Protein transport protein Sec61 subunit alpha isoform 1	Sec61a1	P61621	0.85	1.8	1.3	2.1	0.3	10
Protoporphyrinogen oxidase (Predicted)	Ppox	D3ZVN7	0.76	2.9	2.3	2.1	0.8	
Putative ATP-dependent RNA helicase DHX30	Dhx30	Q5BJS0	0.46	0.4	0.4	0.9	0.5	
Putative uncharacterized protein RGD1307051_predicted	RGD1307051	D3ZDV3	0.26	81.6	15.6	107.0	11.3	
Pyridine nucleotide-disulfide oxidoreductase domain-containing protein 2	Pyroxd2	Q68FT3	0.41	82.0	20.9	107.5	18.1	
Pyridoxal kinase	Pdxk	O35331	0.18	11.1	6.4	0.6	0.6	
Pyruvate carboxylase, mitochondrial	Pc	P52873	0.58	514.5	127.2	434.8	41.6	
Pyruvate dehydrogenase E1 component subunit beta, mitochondrial	Pdhb	P49432	0.80	119.0	24.0	112.3	8.7	
Quinone oxidoreductase	Cryz	Q6AYT0	0.45	22.4	11.4	45.0	24.3	
Quinone oxidoreductase-like protein 2	NA	B0BNC9	0.71	32.9	10.3	37.2	2.3	
Rab GDP dissociation inhibitor alpha	Gdi1	P50398	0.56	3.5	1.8	2.1	1.3	
Rab GDP dissociation inhibitor beta	Gdi2	P50399	0.22	22.4	6.3	12.6	2.3	
Ragulator complex protein LAMTOR1	Lamtor1	Q6P791	0.71	1.1	1.1	0.6	0.6	
Ras-related C3 botulinum toxin substrate 1	Rac1	Q6RUV5	0.37	3.0	2.0	0.9	0.5	
Ras-related protein Rab-11B	Rab11b	O35509	0.60	6.0	4.3	3.3	2.0	
Ras-related protein Rab-14	Rab14	P61107	0.35	22.0	0.2	20.0	1.9	
Ras-related protein Rab-1B	Rab1b	P10536	0.25	5.5	3.1	11.1	2.8	
Ras-related protein Rab-21	Rab21	Q6AXT5	0.01	1.5	0.8	9.5	1.6	
Ras-related protein Rab-2A	Rab2a	P05712	0.42	4.3	2.2	6.5	1.0	
Ras-related protein Rab-7a	Rab7a	P09527	0.19	10.1	3.5	16.4	1.8	
Ras-related protein Ral-B	Ralb	P36860	0.47	2.3	1.2	1.2	0.8	
Ras-related protein Rap-1A	Rap1a	P62836	0.87	28.7	8.3	27.0	4.7	
RCG20978, isoform CRA_e	RGD1563216	D4A4L5	0.64	5.5	2.5	6.8	0.7	
RCG32401, isoform CRA_a	Ctsa	D3ZPA9	0.10	11.5	3.3	4.4	0.4	
RCG32615, isoform CRA_a	Rab5c	B0BNK1	0.77	9.3	2.4	8.3	2.3	
RCG32945	Ndufb10	D4A0T0	0.91	49.9	6.0	49.0	3.7	
RCG33185	Ccdc56	D3Z9I1	0.83	7.4	2.9	8.1	1.0	1
RCG34610, isoform CRA_c	Srsf1	D4A9L2	0.20	1.5	0.9	0.0	0.0	
RCG34648	LOC100363222	D4ADG2	0.42	3.3	2.3	5.6	1.0	
RCG35999, isoform CRA_a	Smtn	D4ABA5	0.37	0.0	0.0	0.6	0.6	
RCG37494	Acss1	D3ZZN3	0.17	56.1	12.0	35.2	3.5	
RCG38845, isoform CRA_b	rCG_38845	D3ZE15	0.52	31.5	9.4	39.5	6.6	1
RCG39036, isoform CRA_a	Cdh16	G3V7L4	0.18	16.2	8.2	2.7	0.6	1
RCG40097	Rras2	Q5BJU0	0.47	2.3	0.8	1.2	1.2	
RCG41911	Mrps16	D4A7X1	0.44	6.4	2.2	4.4	0.8	
RCG41951, isoform CRA_a	LOC679739	D3ZCZ9	0.31	15.2	5.1	21.3	1.3	
RCG43751	LOC100361295	D3ZKG1	0.25	8.9	2.3	13.7	2.8	
RCG44002, isoform CRA_a	Tmem14c	B0BNJ9	0.09	0.4	0.4	1.8	0.5	4

RCG46430	Mgst3	D4ADS4	0.31	63.5	6.1	51.8	8.0	4
RCG49810, isoform CRA_a	Magmas	D3ZZV1	0.49	4.0	2.5	2.1	0.3	
RCG52629	Atp6v1a	D4A133	0.39	196.5	25.0	165.3	20.5	
RCG52860, isoform CRA_b	Hgd	G3V6C2	0.11	6.9	2.4	1.5	1.1	
RCG55135, isoform CRA_b	Tln1	G3V852	0.57	3.3	1.1	4.2	0.8	
RCG55602	Man2a1	G3V7Y9	0.64	3.0	3.0	1.5	0.3	1
RCG57079, isoform CRA_a	LOC100361733	D4A4Q4	0.42	6.8	2.5	4.2	1.6	
RCG57686	LOC100363253	D3ZMY7	0.72	6.5	5.9	4.2	1.3	
RCG58071, isoform CRA_a	Rpl4	Q6P3V9	0.37	1.5	1.5	0.0	0.0	
RCG58449, isoform CRA_a	Atp5l	G3V9A9	0.16	74.1	7.2	59.0	5.1	
RCG60159	Uqcrb	B2RYS2	0.69	147.2	27.6	135.3	2.7	
Regulator of microtubule dynamics protein 1	Fam82b	Q4G069	0.15	17.0	3.8	8.9	2.4	
Retinal dehydrogenase 1	Aldh1a1	P51647	0.09	21.8	7.1	5.1	2.4	
Retinoid-inducible serine carboxypeptidase	Scpep1	Q920A6	0.20	3.7	1.3	5.9	0.7	1
Retinol-binding protein 1	Rbp1	P02696	0.75	6.1	5.5	4.1	1.5	
Retinol-binding protein 4	Rbp4	P04916	0.07	15.5	4.5	29.9	3.4	
RGD1564894 protein	RGD1564894	B1H250	0.88	4.1	3.1	3.6	0.9	
Ribonuclease 4	Rnase4	O55004	0.04	7.5	1.4	17.7	3.2	1
Ribonuclease UK114	Hrsp12	P52759	0.61	17.3	2.7	14.7	3.9	
Ribosomal protein, mitochondrial, L15	Mrpl19	D4A4A9	0.96	1.8	1.0	1.8	0.0	
Rngtt protein	Rngtt	B5DFA8	0.47	1.2	0.7	0.6	0.3	
Saccharopine dehydrogenase-like oxidoreductase	Sccpdh	Q6AY30	0.47	25.1	9.4	17.6	1.4	1
Selenium-binding protein 1	Selenbp1	Q8VIF7	0.64	7.5	3.3	5.7	1.2	
Selenocysteine lyase	Scly	Q68FT9	0.90	1.1	1.1	0.9	0.9	
Sepiapterin reductase	Spr	P18297	0.87	4.8	3.8	4.2	0.3	
Serine (Or cysteine) proteinase inhibitor, clade H, member 1, isoform CRA_b	Serpinh1	Q5RJR9	0.79	23.9	5.6	26.3	6.2	
Serine hydroxymethyltransferase	Shmt2	Q5U3Z7	0.85	54.1	18.1	57.8	5.0	
Serine/threonine-protein kinase TNNI3K	Tnni3k	Q7TQP6	0.70	2.0	1.5	1.2	1.2	
Serum albumin	Alb	P02770	0.89	51.8	8.0	49.9	10.1	
Short/branched chain specific acyl-CoA dehydrogenase, mitochondrial	Acadsb	P70584	0.94	13.7	3.5	14.1	3.6	
Short-chain specific acyl-CoA dehydrogenase, mitochondrial	Acads	P15651	0.21	32.6	1.7	40.0	4.7	
Sideroflexin 2, isoform CRA_a	Sfxn2	G3V8N0	0.77	1.8	1.3	2.3	1.0	4
Sideroflexin-1	Sfxn1	Q63965	0.41	50.6	11.0	63.5	8.9	2
Similar to 2210023G05Rik protein (Predicted)	Ces2g	D3ZXQ0	0.18	5.2	2.9	14.9	5.2	1
Similar to C50H11.1, isoform CRA_a	Acsf3	D3ZUX7	0.22	14.1	5.8	24.2	3.9	
Similar to cytoplasmic beta-actin (Predicted)	Actbl2	D3ZRN3	0.65	66.2	9.3	60.9	5.7	
Similar to Glutathione S-transferase, theta 3 (Predicted)	Gstt1	D3Z8I7	0.79	21.8	8.1	25.4	9.7	
Similar to intracellular membrane Ca^{+2} -independent phospholipase A2 gamma	RGD1311444	D3ZRC4	0.61	2.9	2.9	1.2	0.8	
Similar to ionized calcium binding adapter molecule 2 (Iba2) (Predicted)	Aif1l	D3ZRD9	0.30	5.6	3.6	1.1	1.1	
Similar to KIAA1749 protein (Predicted), isoform CRA_a	Cgnl1	D4A3V5	0.06	0.0	0.0	2.1	0.8	
Similar to Neuropilin-and tolloid-like protein 1 (Predicted)	Neto1	D4AAD6	0.58	2.7	1.3	1.8	0.5	1
Similar to pM5 protein; DNA segment, Chr 7, ERATO Doi 156, (Predicted)	Nomo1	D3ZSA9	0.99	4.4	3.0	4.5	1.8	
Similar to Protein C8orf1 (HT41) (Predicted), isoform CRA_b	Osgin2	D3ZB49	0.37	0.0	0.0	0.6	0.6	
Similar to putative lipid kinase (Predicted), isoform CRA_c	Agk	D3Z9L0	0.23	1.8	1.0	4.4	1.6	
Similar to RIKEN cDNA 0610010D20 (Predicted)	Hoga1	D4A2K1	0.21	67.3	5.2	77.4	4.3	
Similar to RIKEN cDNA 1810022C23	Eci3	Q5M884	0.16	2.6	2.1	8.5	2.7	
Similar to RIKEN cDNA 2810055F11 (Predicted)	RGD1305721	D3ZV91	0.40	6.1	3.9	2.4	0.5	
Similar to RIKEN cDNA 5730502D15 gene (Predicted)	Trabd	D3ZML4	0.37	1.1	1.1	0.0	0.0	
Similar to RIKEN cDNA C630028N24 gene (Predicted), isoform CRA_b	Agphd1	D3ZUX1	0.83	0.8	0.4	0.6	0.6	
Similar to serine hydolase like protein, isoforms Serhl-2 (Predicted)	Serhl2	D4A071	0.31	3.3	1.9	6.6	2.2	
Similar to SNF2/RAD54 family protein (Predicted)	Ercc6l	D4A0G9	0.37	0.7	0.7	0.0	0.0	
Sodium- and chloride-dependent creatine transporter 1	Slc6a8	P28570	0.79	3.8	3.2	2.7	1.9	12
Sodium/glucose cotransporter 2	Slc5a2	P53792	0.69	73.0	34.5	57.8	9.2	14
Sodium/hydrogen exchanger 3	Slc9a3	P26433	0.52	11.4	0.4	13.4	2.8	12
Sodium/potassium-transporting ATPase subunit alpha-1	Atp1a1	P06685	0.56	307.6	45.7	272.2	32.7	10
Sodium/potassium-transporting ATPase subunit beta-1	Atp1b1	P07340	0.46	58.5	17.5	43.9	3.1	1
Sodium-dependent glucose transporter 1	Naglt1	Q80T22	0.35	3.7	3.7	8.4	2.2	11
Sodium-dependent neutral amino acid transporter B(0)AT1	Slc6a19	Q2A865	0.33	14.6	7.6	5.9	2.1	12
Sodium-dependent phosphate transport protein 2A	Slc34a1	Q06496	0.41	36.8	5.8	31.3	1.7	11
Sodium-dependent phosphate transport protein 2C	Slc34a3	Q8K4R8	0.30	6.3	2.9	2.7	0.9	11
Solute carrier family 12 member 3	Slc12a3	P55018	0.21	1.6	0.8	0.3	0.3	11
Solute carrier family 2, facilitated glucose transporter member 2	Slc2a2	P12336	0.48	4.8	3.7	1.8	1.1	11
Solute carrier family 22 member 12	Slc22a12	Q3ZAV1	0.40	0.4	0.4	1.2	0.8	10
Solute carrier family 22 member 5	Slc22a5	O70594	0.20	4.2	1.3	2.1	0.2	11
Solute carrier family 22 member 6	Slc22a6	O35956	0.28	3.8	0.7	7.0	2.5	8
Solute carrier family 22 member 8	Slc22a8	Q9R1U7	0.25	5.3	0.6	3.0	1.6	9
Mitochondrial carrier; adenine nucleotide translocator, 3, CRA_c	Slc25a3	G3V741	0.36	164.4	17.3	137.4	19.5	2
Solute carrier family 25 (Mitochondrial carrier; ornithine transporter) 15	Slc25a15	D4A575	0.46	12.1	8.5	5.0	1.7	
Solute carrier family 25 (Mitochondrial carrier; oxoglutarate carrier), 11, CRA_b	Slc25a11	G3V6H5	0.94	28.1	12.1	29.3	7.0	
Solute carrier family 25 member 42	Slc25a42	P0C546	0.29	1.5	0.7	4.1	2.1	1
Solute carrier family 43, member 2 (Predicted), isoform CRA_a	Slc43a2	D3ZDC2	0.63	10.3	6.9	6.6	1.8	12
Sorbitol dehydrogenase	Sord	P27867	0.26	27.8	13.1	10.2	3.3	
Sorting and assembly machinery component 50 homolog	Samm50	Q6AXV4	0.80	39.6	8.2	42.7	7.4	
Sorting nexin-3	Snx3	Q5U211	0.26	9.8	5.0	3.0	1.3	
Spectrin alpha chain, brain	Sptan1	P16086	0.19	162.2	47.4	87.2	6.9	

Spectrin beta 2, isoform CRA_a	Sptbn1	G3V6S0	0.33	93.9	18.3	71.2	9.0	
Sphingosine-1-phosphate lyase 1	Sgpl1	Q8CHN6	0.48	1.4	1.4	0.3	0.3	
Stomatin-like protein 2	Stoml2	Q4FZT0	0.19	17.2	3.4	11.6	1.0	
Succinate dehydrogenase [ubiquinone] flavoprotein subunit, mitochondrial	Sdha	Q920L2	0.10	244.1	16.1	290.7	15.0	
Succinate dehydrogenase [ubiquinone] iron-sulfur subunit, mitochondrial	Sdhb	P21913	0.18	14.1	4.1	23.8	4.4	
Succinate dehydrogenase complex, subunit C, integral membrane protein	Sdhc	Q641Z9	0.97	33.4	6.1	33.6	1.1	3
Succinyl-CoA ligase [ADP/GDP-forming] subunit alpha, mitochondrial	Suclg1	P13086	0.46	30.4	10.3	38.9	0.7	1
Succinyl-CoA:3-ketoacid-coenzyme A transferase 1, mitochondrial	Oxct1	B2GV06	0.72	129.7	39.1	114.1	9.9	
Sulfate anion transporter 1	Slc26a1	P45380	0.12	6.8	0.9	3.9	1.1	9
Sulfite oxidase, mitochondrial	Suox	Q07116	0.57	40.0	8.5	34.0	4.5	
Sulfotransferase 1C2A	Sult1c2a	Q9WUW9	0.14	69.7	27.4	19.4	4.1	
Superoxide dismutase [Cu-Zn]	Sod1	P07632	0.81	31.4	9.0	33.9	3.3	
Superoxide dismutase [Mn], mitochondrial	Sod2	P07895	0.91	67.8	13.3	69.5	2.6	
Sushi domain containing 2 (Predicted), isoform CRA_a	Susd2	D3ZEV8	0.33	48.2	10.2	35.9	4.7	
Synaptojanin-2-binding protein	Synj2bp	Q9WVJ4	0.80	20.4	9.3	23.2	4.1	1
Synaptosomal-associated protein 23	Snap23	O70377	0.42	1.5	1.0	0.6	0.3	
Syntaxin-binding protein 2	Stxbp2	Q62753	0.45	3.7	3.7	0.6	0.3	
T-complex protein 1 subunit alpha	Tcp1	P28480	0.11	2.3	1.1	0.0	0.0	
T-complex protein 1 subunit beta	Cct2	Q5XIM9	0.08	4.2	1.1	1.5	0.3	
T-complex protein 1 subunit gamma	Cct3	Q6P502	0.21	2.3	1.3	0.3	0.3	
Tektin-1	Tekt1	Q99JD2	0.58	0.4	0.4	1.1	1.1	
Testis expressed 264	Tex264	Q5XIF0	0.14	3.3	1.2	0.9	0.5	1
Thiomorpholine-carboxylate dehydrogenase	Crym	Q9QYU4	0.68	6.9	4.6	4.6	2.3	
Thioredoxin domain containing 13	Tmx4	G3V912	0.30	0.4	0.4	1.2	0.6	1
Thioredoxin reductase 1, cytoplasmic	Txnrd1	O89049	0.17	1.2	0.7	2.7	0.5	
Thioredoxin, mitochondrial	Txn2	P97615	0.39	5.1	2.2	3.0	0.3	
Thioredoxin-dependent peroxide reductase, mitochondrial	Prdx3	Q9Z0V6	0.19	63.7	6.6	76.2	4.2	
Thiosulfate sulfurtransferase	Tst	P24329	0.70	134.4	5.1	137.8	6.2	
Threonine synthase-like 2	Thnsl2	Q5M7T9	0.42	2.7	1.6	1.2	0.3	
Tissue alpha-L-fucosidase	Fuca1	P17164	0.27	1.6	0.8	3.5	1.3	1
Tissue-type transglutaminase	Tgm2	Q9WVJ6	0.19	5.6	3.6	0.0	0.0	
Transcobalamin-2	Tcn2	Q9R0D6	0.73	1.9	1.9	2.7	1.4	
Transcription factor A, mitochondrial	Tfam	Q91ZW1	0.16	7.1	1.9	3.2	1.2	
Transforming protein RhoA	Rhoa	P61589	0.67	20.4	4.5	17.1	5.7	
Transgelin-2	Tagln2	Q5XFX0	0.97	3.7	2.7	3.6	0.9	
Transient receptor potential cation channel subfamily V member 4	Trpv4	Q9ERZ8	0.29	12.2	3.7	7.5	1.2	6
Transitional endoplasmic reticulum ATPase	Vcp	P46462	0.71	14.5	7.7	10.9	4.7	
Transketolase, isoform CRA_a	Tkt	G3V826	0.20	49.7	21.1	17.0	3.9	
Translocator of inner mitochondrial membrane 44, isoform CRA_b	Timm44	G3V640	0.92	33.5	8.0	32.5	4.8	
Translocon-associated protein subunit delta	Ssr4	Q07984	0.37	3.1	1.1	6.0	2.7	1
Transmembrane 9 superfamily member 4	Tm9sf4	Q4KLL4	0.37	1.1	1.1	0.0	0.0	9
Transmembrane emp24 domain-containing protein 10	Tmed10	Q63584	0.67	11.0	1.4	10.1	1.5	2
Transmembrane emp24 domain-containing protein 2	Tmed2	Q63524	0.82	1.9	1.3	1.5	1.1	2
Transmembrane protein 126A	Tmem126a	Q5HZA9	0.42	5.9	2.8	3.3	0.8	3
Transthyretin	Ttr	P02767	0.35	0.8	0.4	2.0	1.1	
Tricarboxylate transport protein, mitochondrial	Slc25a1	P32089	0.14	48.6	5.3	72.1	11.5	
Trifunctional enzyme subunit alpha, mitochondrial	Hadha	Q64428	0.19	139.5	18.4	186.9	24.1	
Trifunctional enzyme subunit beta, mitochondrial	Hadhb	Q60587	0.97	43.0	2.2	43.5	9.7	
Triosephosphate isomerase	Tpi1	P48500	0.09	54.7	9.6	32.1	2.9	
tRNA modification GTPase GTPBP3, mitochondrial	Gtpbp3	Q5PQQ1	0.27	1.1	0.6	2.4	0.8	
Tubulin alpha-1B chain	Tuba1b	Q6P9V9	0.58	64.3	18.3	53.1	3.1	
Tubulin beta-2A chain	Tubb2a	P85108	0.57	105.7	30.6	85.8	10.1	
Tubulin beta-4B chain	Tubb4b	Q6P9T8	0.68	104.8	31.7	90.3	7.1	
Tubulin beta-5 chain	Tubb5	P69897	0.62	106.4	30.0	89.7	8.5	
Ube2l3 protein	Ube2l3	B2RZA9	0.96	3.5	1.9	3.6	0.5	
Ubiquinone biosynthesis protein COQ9, mitochondrial	Coq9	Q68FT1	0.40	11.0	5.0	15.7	0.5	
UDP-glucose 6-dehydrogenase	Ugdh	O70199	0.43	4.6	3.4	1.5	0.8	
UDP-glucose:glycoprotein glucosyltransferase 1	Uggt1	Q9JLA3	0.79	3.0	2.0	3.6	1.0	1
UDP-glucuronosyltransferase 1-1	Ugt1a1	Q64550	0.00	11.0	1.8	54.1	4.5	2
UDP-glucuronosyltransferase 1-6	Ugt1	P08430	0.30	19.4	9.2	34.1	8.3	1
UDP-glucuronosyltransferase 2B15	Ugt2b15	P36511	0.00	1.8	1.0	17.0	0.7	1
UMP-CMP kinase	Cmpk1	Q4KM73	0.58	4.6	1.8	7.6	4.7	
Uncharacterized protein	Abca2	D3ZD68	0.97	1.5	1.5	1.4	1.4	9
Uncharacterized protein	Acaa1b	F1LPD6	0.00	11.3	1.1	28.4	2.8	
Uncharacterized protein	Aco1	D4ACL3	0.85	11.4	8.0	13.2	4.2	1
Uncharacterized protein	Add3	D4A3Q7	0.91	1.9	1.9	2.1	0.8	
Uncharacterized protein	Aldh8a1	D3ZXY4	0.75	20.7	8.5	23.7	2.2	
Uncharacterized protein	Apool	D3Z9T6	0.53	9.8	2.1	8.0	1.4	
Uncharacterized protein	Arhgef19	D4ACS5	0.56	2.7	1.1	1.8	0.9	
Uncharacterized protein	Atp5j2	D3ZAF6	0.64	33.4	6.6	28.9	6.2	1
Uncharacterized protein	Atp6v0a4	D3ZY90	0.56	17.6	7.9	12.5	1.8	6
Uncharacterized protein	Atp6v1h	D3ZW96	0.84	36.4	18.4	32.5	3.1	
Uncharacterized protein	Basp1	F1LNN9	0.55	18.3	7.0	13.5	2.9	
Uncharacterized protein	Ccdc88c	D4A9W1	0.88	1.4	1.4	1.1	1.1	
Uncharacterized protein	Cep290	D4A5F2	0.82	1.2	1.2	0.9	0.5	

Uncharacterized protein	Cfb	D4A0Y1	0.01	1.2	0.7	7.7	1.4	
Uncharacterized protein	Chd5	D3ZD32	0.83	0.8	0.4	0.6	0.6	
Uncharacterized protein	Cisd3	D4AA84	0.79	1.5	0.9	1.2	0.3	
Uncharacterized protein	Ckap4	D3ZH41	0.98	4.9	3.7	4.8	0.6	1
Uncharacterized protein	Col6a3	D4A115	0.28	0.8	0.4	3.3	2.0	1
Uncharacterized protein	Cox6b1	D3ZD09	0.38	72.3	2.0	58.8	13.6	
Uncharacterized protein	Cyp4f39	D4A1H9	0.54	1.2	0.7	1.8	0.5	1
Uncharacterized protein	Dnah8	F1MAM6	0.10	0.7	0.7	2.7	0.5	
Uncharacterized protein	Dnaja3	E9PSW5	0.69	11.3	6.0	8.6	2.1	
Uncharacterized protein	Dnm3	D4AAL9	0.64	3.0	3.0	1.5	0.3	
Uncharacterized protein	Dpp4	F1M7X5	0.69	132.3	19.0	123.3	9.2	1
Uncharacterized protein	Eprs	F1LMJ9	0.57	1.2	0.6	0.6	0.6	
Uncharacterized protein	Flnb	D3ZD13	0.02	4.2	0.5	2.1	0.3	
Uncharacterized protein	Ganab	D4A0W9	0.35	16.3	1.4	21.0	4.2	1
Uncharacterized protein	Gldc	D3ZJJ9	0.17	101.8	23.8	167.3	30.9	
Uncharacterized protein	Gm2a	D3ZR01	0.28	20.5	5.9	32.2	7.2	
Uncharacterized protein	Grhpr	D4A6S1	0.77	5.0	2.3	4.2	1.1	
Uncharacterized protein	Grsf1	F1LMB8	0.28	1.5	0.9	4.4	2.1	
Uncharacterized protein	Gstt1	D3ZUM0	0.65	16.0	6.2	19.2	2.2	
Uncharacterized protein	Hagh	F1LQI1	0.28	13.2	1.7	11.0	0.5	
Uncharacterized protein	Hccs	D3ZL85	0.50	6.3	1.4	5.1	0.9	
Uncharacterized protein	Hectd1	D3ZLS5	0.47	0.8	0.8	1.8	0.9	
Uncharacterized protein	Hsd17b10	F1LNT4	0.70	138.1	25.0	148.3	1.1	
Uncharacterized protein	Hspa9	F1M953	0.36	123.7	32.3	162.0	19.1	
Uncharacterized protein	Idh3a	F1LNF7	0.76	62.1	7.7	57.1	13.0	
Uncharacterized protein	Immt	D3ZSD1	0.53	112.5	20.0	128.5	11.8	
Uncharacterized protein	Irf9	D3ZV47	0.21	1.5	0.7	0.3	0.3	
Uncharacterized protein	Krt10	D3ZBV7	0.18	27.3	3.7	20.8	1.7	
Uncharacterized protein	Ktn1	D4ADW6	0.22	0.4	0.4	1.8	0.9	1
Uncharacterized protein	Lama5	F1MAN8	0.59	4.5	3.4	2.4	0.8	
Uncharacterized protein	Lamc1	F1MAA7	0.16	3.7	2.0	0.3	0.3	1
Uncharacterized protein	LOC100359876	F8WFR8	0.17	0.7	0.7	2.4	0.6	
Uncharacterized protein	LOC100365958	F1LM78	0.96	1.8	1.3	1.7	1.3	
Uncharacterized protein	LOC100366131	D4A5M0	0.69	4.2	0.9	4.8	0.9	
Uncharacterized protein	LOC259245	E9PT15	0.19	71.9	7.1	92.0	10.5	
Uncharacterized protein	LOC317516	F1MAP2	0.56	3.5	1.8	2.1	1.2	
Uncharacterized protein	LOC685778	D4A5G8	0.76	89.4	4.3	92.9	10.0	
Uncharacterized protein	LOC686139	D3ZXK4	0.27	9.0	2.5	5.4	1.1	
Uncharacterized protein	LOC688963	F1LPG5	0.87	42.8	1.4	42.3	2.5	
Uncharacterized protein	Maoa	D3ZFS8	0.95	2.5	2.5	2.3	1.2	
Uncharacterized protein	Maob	F1LPM4	0.21	8.7	3.3	2.6	2.6	1
Uncharacterized protein	Map7d2	D4A1J8	0.26	2.7	1.1	4.7	1.0	
Uncharacterized protein	Mars	D3Z941	0.24	0.4	0.4	1.8	0.9	
Uncharacterized protein	Mccc1	F1LP30	0.94	44.3	7.1	43.8	3.0	
Uncharacterized protein	Mecr	F1LPY7	0.95	6.3	5.3	6.0	0.4	
Uncharacterized protein	Mipep	D3ZAI9	0.89	0.0	0.0	0.9	0.9	
Uncharacterized protein	Mrpl12	D3ZXF9	0.54	1.5	1.5	1.8	1.0	
Uncharacterized protein	Mrps36	D3Z8T2	0.96	7.1	2.5	5.4	0.6	
Uncharacterized protein	Myh10	F1LQ02	0.24	2.6	1.3	2.4	2.4	
Uncharacterized protein	Myh4	F1LMU0	1.00	28.2	6.2	17.9	4.2	
Uncharacterized protein	Myo18a	D3ZFD0	0.71	1.2	0.7	1.2	0.6	
Uncharacterized protein	Myo1d	D3ZKZ9	0.39	2.2	2.2	4.4	0.4	
Uncharacterized protein	Myo6	D4A5I9	0.38	74.5	13.1	56.9	11.9	
Uncharacterized protein	Myof	D4AB02	0.82	1.1	0.6	1.5	1.5	1
Uncharacterized protein	NA	D3ZNI6	0.29	6.5	1.7	4.2	0.8	
Uncharacterized protein	NA	D4A5V2	0.30	1.1	0.6	0.3	0.3	
Uncharacterized protein	NA	D3ZJ63	0.35	0.7	0.7	2.0	1.0	
Uncharacterized protein	NA	D3ZE29	0.40	79.9	9.2	66.9	10.2	2
Uncharacterized protein	NA	D4ABH6	0.44	712.3	193.7	897.7	94.7	
Uncharacterized protein	NA	D3ZSD6	0.45	81.6	25.6	59.3	6.2	
Uncharacterized protein	NA	D4A8P9	0.50	11.6	5.2	15.5	1.0	
Uncharacterized protein	NA	D3ZJD0	0.56	3.6	2.1	2.1	0.8	
Uncharacterized protein	NA	D3ZX87	0.57	1.1	0.6	2.4	2.0	
Uncharacterized protein	NA	E9PT51	0.59	0.7	0.7	0.3	0.3	
Uncharacterized protein	NA	D3ZTX4	0.68	119.5	37.2	102.2	12.0	1
Uncharacterized protein	NA	D4A3J6	0.69	118.7	40.7	100.7	10.3	1
Uncharacterized protein	NA	D4AD84	0.70	24.2	6.6	21.1	3.8	
Uncharacterized protein	NA	D4A5T2	0.75	1.4	1.4	0.9	0.5	
Uncharacterized protein	NA	D3ZCN7	0.77	1.2	0.7	0.9	0.5	
Uncharacterized protein	NA	D3ZJX5	0.79	2.2	2.2	2.9	1.5	1
Uncharacterized protein	NA	D4A774	0.82	55.6	2.9	59.1	13.8	
Uncharacterized protein	NA	D4A9J5	0.83	1.1	0.6	0.9	0.9	
Uncharacterized protein	NA	D3ZEA8	0.84	0.8	0.4	0.9	0.5	
Uncharacterized protein	NA	D4ADA8	0.84	0.8	0.8	0.6	0.6	
Uncharacterized protein	NA	F1M7S9	0.91	0.7	0.7	0.6	0.6	

Uncharacterized protein	Nars2	F1LNQ5	0.24	0.0	0.0	1.5	1.1	
Uncharacterized protein	Nipsnap1	D4A867	0.55	82.5	10.5	74.3	7.0	
Uncharacterized protein	Obp3	F1LQM1	0.29	512.1	130.0	711.7	101.6	
Uncharacterized protein	Pdhx	F1LQ44	0.70	11.3	6.0	8.7	1.9	
Uncharacterized protein	Picalm	F1LR19	0.48	21.8	7.3	15.6	3.1	
Uncharacterized protein	Pitrm1	D3ZKD5	0.44	11.2	2.0	7.9	3.4	
Uncharacterized protein	Pls1	F1LQQ6	0.21	17.6	7.0	6.0	3.2	
Uncharacterized protein	Ppa2	D4A830	0.97	45.2	4.7	44.6	13.5	
Uncharacterized protein	Prodh	F1MAR6	0.56	5.4	4.8	2.4	0.8	
Uncharacterized protein	Rab1	E9PU16	0.34	6.3	3.4	11.1	3.0	
Uncharacterized protein	Rdx	E9PT65	1.00	25.5	3.2	25.6	5.5	
Uncharacterized protein	RGD1308772	D3ZIN5	0.30	5.5	2.8	9.8	2.2	
Uncharacterized protein	RGD1310427	D3ZFJ7	0.36	4.9	1.3	3.3	0.8	
Uncharacterized protein	RGD1311756	D4A9W3	0.68	25.4	3.6	27.8	4.1	
Uncharacterized protein	RGD1563398	D3ZUC6	0.27	2.7	1.6	0.6	0.3	
Uncharacterized protein	Rmnd1	E9PU34	0.32	1.1	0.6	0.3	0.3	
Uncharacterized protein	Sardh	D4A9I9	0.88	28.2	9.2	29.7	1.2	
Uncharacterized protein	Sec63	D3ZBN7	0.25	1.9	0.7	0.6	0.6	3
Uncharacterized protein	Slc25a25	F8WFM9	0.37	0.0	0.0	0.6	0.6	
Uncharacterized protein	Slc25a45	D3ZL04	0.26	2.2	1.6	0.0	0.0	
Uncharacterized protein	Slc30a9	D3ZQY3	0.77	3.5	1.3	2.9	1.1	5
Uncharacterized protein	Stt3b	E9PTQ6	0.61	0.4	0.4	0.9	0.9	10
Uncharacterized protein	Sucla2	F1LM47	0.78	45.1	8.6	48.2	5.5	
Uncharacterized protein	Sult1c2	F1LNK1	0.11	55.5	19.4	15.5	2.7	
Uncharacterized protein	Tln2	D3ZA84	0.29	1.8	1.0	0.6	0.3	
Uncharacterized protein	Tomm7	D3ZMR1	0.92	3.7	1.8	3.9	1.3	1
Uncharacterized protein	Tpm3	F1LRP5	0.12	17.7	8.9	0.3	0.3	
Uncharacterized protein	Ubc	F1LML2	0.67	22.3	8.5	17.5	6.1	
Uncharacterized protein	Upf3b	D3ZBE8	0.60	1.9	1.4	2.7	0.5	
Uncharacterized protein	Vat1	Q3MIE4	0.73	3.1	1.6	2.3	1.5	
Uncharacterized protein	Vil1	B5DFA0	0.35	50.2	19.0	29.5	3.7	
Uncharacterized protein	Vill	D3Z8F1	0.68	4.2	1.3	6.0	3.8	
Uncharacterized protein	Vnn1	Q4KLZ0	0.87	3.3	2.8	3.9	1.7	
Uncharacterized protein	Vps13a	D3Z8N6	0.61	2.3	0.6	3.6	2.3	
Uncharacterized protein	Vps35	G3V8A5	0.26	4.7	2.4	1.5	0.8	
Uncharacterized protein (Fragment)	Abcc4	F1LR52	0.05	2.6	1.0	0.0	0.0	3
Uncharacterized protein (Fragment)	Abhd14b	F1M5R3	0.23	5.1	2.6	1.2	0.8	
Uncharacterized protein (Fragment)	Ank3	F1LM13	0.69	7.9	1.6	9.2	2.6	
Uncharacterized protein (Fragment)	Auh	F1LU71	0.51	9.1	1.2	8.0	0.9	
Uncharacterized protein (Fragment)	Bucs1	F1M1W1	0.56	8.8	6.5	4.0	4.0	
Uncharacterized protein (Fragment)	Erp44	F1M396	0.17	3.4	1.1	1.5	0.3	
Uncharacterized protein (Fragment)	Gsr	F1LQY0	0.97	21.7	5.5	21.9	2.7	
Uncharacterized protein (Fragment)	Ldhd	F1LVD7	0.04	27.0	4.0	45.7	4.5	
Uncharacterized protein (Fragment)	LOC100360623	F1LW74	0.50	4.3	2.2	2.4	1.3	
Uncharacterized protein (Fragment)	LOC100360985	F1LX07	0.57	7.1	1.8	8.9	2.3	
Uncharacterized protein (Fragment)	LOC684509	F1LY36	0.65	10.9	2.2	12.4	2.1	1
Uncharacterized protein (Fragment)	Msn	F1LP60	0.80	86.2	16.7	92.3	14.4	
Uncharacterized protein (Fragment)	Mthfd1	F1LW12	0.98	14.1	6.2	14.3	2.4	
Uncharacterized protein (Fragment)	Myo5b	F1LUM1	0.30	1.5	0.9	0.3	0.3	
Uncharacterized protein (Fragment)	Myo7b	F1M885	0.82	7.0	2.1	6.2	2.4	
Uncharacterized protein (Fragment)	NA	F1LSP2	0.29	14.6	6.2	6.9	1.2	
Uncharacterized protein (Fragment)	NA	F1M566	0.42	5.4	5.4	0.6	0.6	
Uncharacterized protein (Fragment)	NA	F1M2K6	0.61	0.7	0.7	0.3	0.3	
Uncharacterized protein (Fragment)	NA	F1M3J4	0.72	5.5	2.3	4.5	1.0	2
Uncharacterized protein (Fragment)	NA	F1LVH4	0.75	4.1	0.9	4.5	0.5	
Uncharacterized protein (Fragment)	Ndufa12	F1LXA0	0.72	16.9	4.6	14.9	2.2	
Uncharacterized protein (Fragment)	Nln	F1LW44	0.88	2.9	2.4	2.4	1.6	
Uncharacterized protein (Fragment)	Nmnat3	F1LTJ2	1.00	1.8	1.0	0.0	0.0	
Uncharacterized protein (Fragment)	Pcca	F1M8L5	0.70	5.3	1.0	5.3	1.8	
Uncharacterized protein (Fragment)	Pck2	F1LQJ7	0.61	4.7	2.5	6.5	3.3	
Uncharacterized protein (Fragment)	Pm20d1	F1M0Q9	0.81	6.0	3.4	8.1	1.5	
Uncharacterized protein (Fragment)	RGD1564651	F1LUA8	0.76	15.2	0.3	16.5	5.1	
Uncharacterized protein (Fragment)	Slc25a13	F1LZW6	0.93	0.4	0.4	0.6	0.6	
Uncharacterized protein (Fragment)	Slc5a12	F1LW51	0.76	133.3	32.2	130.2	12.9	10
Uncharacterized protein (Fragment)	Suclg2	F1LPV8	0.93	17.1	4.9	15.4	1.0	
Uncharacterized protein (Fragment)	Tf	F1LMP2	0.28	56.3	10.2	55.3	5.7	1
Uncharacterized protein (Fragment)	Tns1	F1LN42	0.30	9.6	4.9	20.1	7.0	
Uncharacterized protein (Fragment)	Txnrd2	F1M6X5	0.77	4.5	1.2	5.1	1.1	
UPF0598 protein C8orf82 homolog	NA	Q642A4	0.13	1.8	1.0	0.0	0.0	
Up-regulated during skeletal muscle growth protein 5	Usmg5	Q9JJW3	0.32	3.6	3.1	8.0	2.3	1
Very long-chain acyl-CoA synthetase	Slc27a2	P97524	0.52	50.3	4.0	54.2	3.8	2
Vesicle-associated membrane protein-associated protein A	Vapa	Q9Z270	0.27	4.0	2.3	0.9	0.5	1
Vesicle-associated membrane protein-associated protein B	Vapb	Q9Z269	0.86	1.5	1.5	1.2	0.3	1
Vimentin	Vim	P31000	0.46	6.5	6.5	1.2	0.8	
Vinculin	Vcl	P85972	0.54	1.5	0.4	1.2	0.3	

Vitamin D-binding protein	Gc	P04276	0.01	15.0	4.4	40.2	1.9
Voltage-dependent anion-selective channel protein 1	Vdac1	Q9Z2L0	0.18	236.5	24.8	293.3	24.3
Voltage-dependent anion-selective channel protein 2	Vdac2	P81155	0.88	28.8	11.3	30.6	1.0
V-type proton ATPase subunit B, brain isoform	Atp6v1b2	P62815	0.61	145.6	22.4	129.2	19.3
V-type proton ATPase subunit C 1	Atp6v1c1	Q5FVI6	0.62	19.1	2.5	16.3	4.7
V-type proton ATPase subunit F	Atp6v1f	P50408	0.56	10.8	2.0	8.5	3.1
Xaa-Pro aminopeptidase 1	Xpnpep1	O54975	0.83	6.9	2.3	7.9	3.8
Xanthine dehydrogenase/oxidase	Xdh	P22985	0.95	3.4	2.8	3.6	1.1

Ctrl = Control, S.E. = Standard Error, CMA = Chronic Metabolic Acidosis, TMD= transmembrane domains

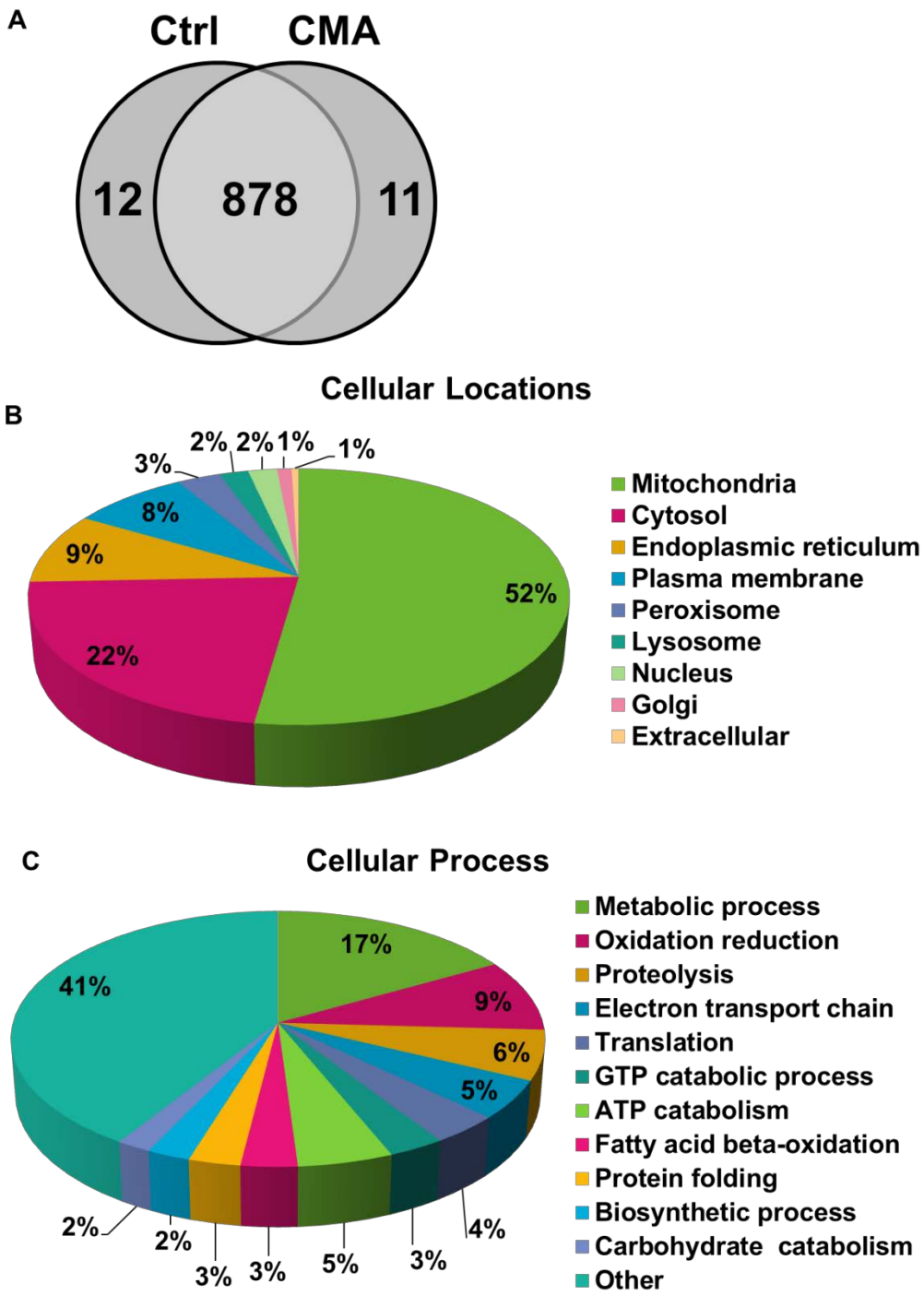

Fig. 2.5. Proteomic analysis- A. Venn diagram of total proteins identified in the mitochondria prepared from proximal convoluted tubules isolated from control (Ctrl) and 7-d chronic acidotic (CMA) rats. A total of 901 proteins were identified; 878 were common in both samples, while 12 and 11 were unique to the control and acidotic samples, respectively. Pie charts of the cellular locations (Panel B) and cellular processes (Panel C) as determined by Gene Ontology (GO) analysis of the identified proteins.

membrane.[35] Thus far only 105 peroxisomal proteins have been identified in rat.[36] As a result, even though peroxisomes were enriched in the mitochondrial fraction, only 16 proteins or 3% of the total were annotated as peroxisomal. Cellular processes were annotated for 455 of the proteins, which were classified into 131 different processes (Fig. 2.5 C). The general annotation of metabolic process (17%) contained the largest cluster of proteins. Major mitochondrial processes such as oxidation/reduction (9%), electron transport chain (5%), and fatty acid β-oxidation (3%) clustered a large portion of the proteins. Many clusters of central cellular processes contained 5 or fewer proteins. Collectively, they accounted for 41% of the annotated proteins and they were categorized as other in Fig. 2.5 C. Overall, mitochondrial proteins were the most frequently annotated location and mitochondrial processes were the most prominent clusters.

2.4c Mitochondrial protein lysine acetylation

Recently, lysine acetylation has been identified as an important mechanism that regulates cellular metabolism.[37] Western blot analysis of the mitochondrial samples obtained from triplicate preparations of control, 1-d acute, 3-d, and 7-d chronic acidotic rat proximal convoluted tubules were performed using an anti-acetyl-lysine antibody (Fig. 2.6 A). This analysis indicated that a large number of proteins are acetylated. The signal for all of the acetylated proteins was quantified and normalized to the control samples. The resulting data demonstrate that the level of mitochondrial protein acetylation increased with the progression of acidosis (Fig. 2.6 B). In the 7-d chronic acidotic samples, lysine acetylation was increased 2.5-fold relative to the control mitochondria. Western blot analysis of proximal convoluted tubule homogenates and soluble cytosolic fractions exhibit no change in protein acetylation (Fig. 2.6 C-E), which indicates that

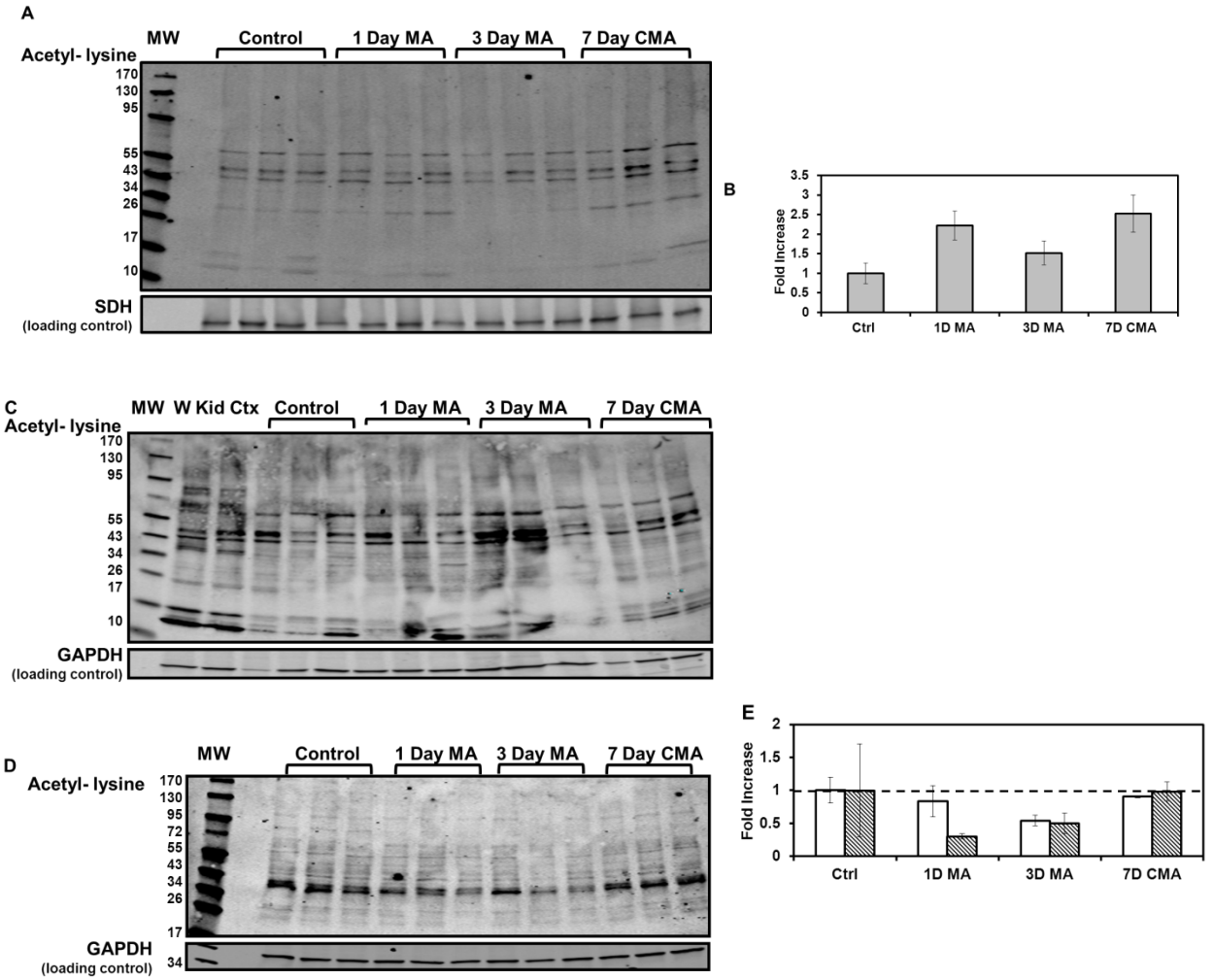

Fig. 2.6. Western blot analysis of the temporal changes in lysine acetylation of total proteins during development of acidosis. A. Mitochondrial samples were isolated from proximal convoluted tubules of three control (Ctrl), three 1-d acidotic (MA), three 3-d acidotic (MA) and three 7-d chronic acidotic (CMA) rats. Western blot analysis was performed using an anti-N-ε-acetyl-lysine antibody. The bands were imaged and quantified with an Odyssey Infrared Imager. B. The acetylation of mitochondrial proteins increased during the onset of acidosis. The combined intensities of each lane in Panel A were normalized to the level of succinate dehydrogenase (SDH), which served as a loading control. The reported data are the mean ± the S.E. of triplicate samples. C. Western blot analysis of control whole kidney (W Kid) and cortex (Ctx) and time course of MA proximal convoluted tubule homogenates with an anti-N-ε-acetyl-lysine antibody. D. Western blot analysis of soluble cytosolic fractions from proximal convoluted tubule with an anti-N-ε-acetyl-lysine antibody. E. The combined intensities of each lane in Panel C (homogenates in white) or D (soluble cytosolic in lines) were normalized to the level of glyceraldehyde 3-phosphate dehydrogenase (GAPDH), which served as a loading control. The reported data are the mean ± the S.E. of triplicate samples.

Table 2.2. Identification of Acetylated Peptides

Protein name	Accession #	Gene	# of Modified Spectra		Peptide Sequence	Site *	Novel
			Control	7 Day CMA			
ATP synthase subunit beta	P10719	Atp5b	13		KGSITSVQAIYVPADDLTDPAPATTFAHLDAR	K351	Yes
ATP synthase subunit alpha	P15999	Atp5a1	1		LKEIVTNFLAGFEP	K541	No
Glutamate dehydrogenase 1	P10860	Glud1	1		KGFIGPGIDVPAPDMSTGER	K212	Yes
				1	ISGASEKDIVHSGLAYTMER	K503	No
ADP/ATP translocase 2	Q09073	Slc25a5	16	29	TDAAVSFAKDFLAGGVAAAISK	K10	No
			22	38	TDAAVSFAKDFLAGGVAAAISKTAVAPIER	K10 or K23	No
			6		KGTDIMYTGTLDCWR	K245	Yes
Malate dehydrogenase	P04636	Mdh2	1		VNVPVIGGHAGKTIIPLISQCTPK	K203	No
10 kDa heat shock protein	P26772	Hspe1	2		AGQAFRKFLPLFDR	K8	No
Cytochrome c oxidase subunit 5A	P11240	Cox5a	2		KGMNTLVGYDLVPEPK	K68	Yes
Myosin, heavy polypeptide 9	G3V6P7	Myh9	9	10	AQQAADKYLYVDKNFINNPLAQADWAAK	K8 or K14	K8-Yes, K14-No
3-hydroxyacyl-CoA dehydrogenase 2	F1LNT4	Hsd17b10	4	1	AAACRSVKGLVAVITGGASGLGLSTAK	K9	No
78 kDa glucose-regulated protein	P06761	Hspa5	3	4	LGGKLSPEDKETMEK	K585	No
Fructose-1,6-bisphosphatase 1	P19112	Fbp1	2		KGNIYSINEGYAK	K206	Yes
4F2 cell-surface antigen heavy chain	Q794F9	Slc3a2	8		SQDTEVDMKDVELNELEPEKQPMNAADGAAAGEK	K10 or K21	Yes
Protein Myo6	D4A5I9	Myo6	13	5	MEDGKPVWAPHPTDGFQMGNIVDIGPDSLTIEPLNQK	K5	Yes
Medium-chain specific acyl-CoA dehydrogenase	P08503	Acadm	3		KGDEYVINGQK	K179	No
ADP/ATP translocase 1	Q05962	Slc25a4	18	39	GDQALSFLKDFLAGGIAAAVSK	K10	No
			8	8	GDQALSFLKDFLAGGIAAAVSKTAVAPIER	K10 or K23	K10-No, K23-Yes
NADH dehydrogenase1 alpha subcomplex 5	Q63362	Ndufa5	1		ILDLLK	K36	No
ATP-binding cassette sub-family D member 3	P16970	Abcd3	2		LSGGEKQR	K6	Yes
Sorbitol dehydrogenase	P27867	Sord	13	7	AAPAKGENLSLVVHGPGDIR	K6	No
Uncharacterized protein	D3ZE29	unknown	2		TDAAVSFAKDFLAGGVAAANSKTAVAPIER	K10 or K23	Yes
Ndufa7 protein	A9UMV9	Ndufa7		5	ALVSGKTAESSAVAATK	K80 or K91	Yes
Glutathione S-transferase alpha	P00502	Gsta1	5	9	SGKPVLHYFNAR	K4	Yes
Uncharacterized protein	D4A5M0	unknown	3	4	LGEHNINVLEGDEQFVNAAK	K92	Yes
Protein Map7d2	D4A1J8	Map7d2	6	16	KSSENLSLDDCNK	K563 or K575	Yes
Uncharacterized protein	F1M7S9	unknown		1	NLSSTANLKVLEADPYFTVK	K5306	Yes
				1	ELPLIFITPLSDVK	K5124	Yes
Uncharacterized protein	D4A5F2	Cep290	1	2	MKAQEVELALEEVEK	K62	Yes
				1	EVELKVEVSK	K1150 K 1155	Yes
Testis- and ovary-specific PAZ domain-containing 1	D3ZUC6	Topaz1	1		AMKKAELPLIPEGNPK	K93, K94, or K106 (2 sites)	Yes
IQ motif containing GTPase activating protein	G3V7Q7	Iqgap1	1		KNKEQLSDMMMINK	K940, K942 (2 sites)	Yes
Serine/threonine-protein kinase TNNI3K	Q7TQP6	Tnni3k	2		ILDLQSKLIIAVDVAK	K563 or K572	Yes
Uncharacterized protein	D4A5V2	unknown	2		MGYKLQDLTDVQIMAR	K265	Yes
Tektin-1	Q99JD2	Tekt1	1	3	IRLERSLESYK	K106	Yes
Enolase (Fragment)	F1LZ68	unknown	1		MLNNGSHAGNKLAMK	K86 or K90	No
RCG35999, isoform CRA_a	D4ABA5	Smtn		1	KAMIEKLEK	K771	No

* Site determing ion for the acetyl-lysine was not always present and the acetyl peptide may have more than one possible lysine that could be modified.

this hyperacetylation is specific to the mitochondria. To further investigate protein acetylation in metabolic acidosis, all MS/MS spectra were searched with the variable modification of lysine acetylation to identify acetylated peptides and the specific lysines that are modified. The mitochondrial data set contained 37 acetylated peptides from 31 different proteins (Table 2.2). This analysis identified 39 total sites of lysine acetylation, of which 22 were novel sites not previously curated on PhosphoSitePlus (www.phosphosite.org). The identified acetylated proteins are involved in transport, ATP synthesis, and lipid and carbohydrate metabolism. Five acetylated proteins are components of the oxidative phosphorylation pathway; two proteins are contained in complex I, one in complex IV, and two in complex V. Acetylation of lysines has been proposed to prevent protein degradation by blocking sites of ubiquitination.[38] Interestingly, eight of the identified acetylation sites were previously identified as sites of ubiquitination (www.phosphosite.org).

2.4d Spectral count analysis

Spectral counting is not reliable for quantifying differences in proteins with low SpC values.[39] Therefore, only proteins with a total of > 10 SpC from all three biological replicates were included in the analysis to determine changes in relative protein abundance. Additionally, at least 2 unique spectra had to be identified in at least two biological replicates for a protein to be considered for analysis. Using this cut-off, spectral counting identified 33 proteins that exhibit a significant fold change (fold change ≥ 1.5, p-value ≤ 0.05) in the control versus 7-d acidotic samples (Table 2.3). Two of the identified mitochondrial proteins were KGA and GDH, which are key enzymes of glutamine catabolism. Both KGA[11, 12] and GDH[40] were previously established to be up-regulated during metabolic acidosis. UDP-glucuronosyltransferase-1A1

(UGT1A1) was significantly increased (4.6 fold). Catalase (CAT) has been localized to both the mitochondria and peroxisomes. By spectral counting, catalase was increased 2.2-fold during chronic metabolic acidosis. Additional proteins that are localized to both the mitochondria and peroxisomes that were increased during acidosis include acetyl coenzyme A acyltransferase 1B (ACAA1), 17-beta-hydroxysteroid dehydrogenase 4 (HSD17B4), and enoyl-coenzyme A hydratase/3-hydroxyacyl-coenzyme A dehydrogenase (EHHADH). Another novel protein of interest, carbonic anhydrase 5B (CA5B), was also found to increase 5.7-fold, but with a borderline significant p-value of 0.068. This isoform of carbonic anhydrase contains a cleavable mitochondrial targeting signal and immunofluorescence analysis established that the mature CA5B protein is localized in mitochondria.[41, 42]

2.4e Validation of proteins altered in metabolic acidosis by Western blotting

The increased expression of eight of the proteins identified by spectral counting was analyzed by Western blotting (Fig. 2.7 A). The fold increases calculated by spectral counting and Western blot analyses for six proteins, KGA, GDH, CA5B, CAT, ACAA1, and HSD17B4, were statistically equivalent (Fig. 2.7 B). UGT1a1 exhibited a 4.6–fold increase in SpC, but only a 1.6-fold increase by Western blotting. UGT1a1 is a protein of the UGT1 gene family, which has nine alternatively spliced variants. There is significant sequence homology among the variants, which is indistinguishable in the mass spectrometry analysis. The detection of shared peptides can lead to artificial inflation of the SpC due to contributions from the various isoforms. In contrast, the antibody used in Western blotting is specific to the UGT1a1 isoform and should represent a more accurate measurement of abundance of this variant. Based upon SpC, EHHADH was increased 2.1-fold. However, this change was not validated by Western blot

Table 2.3. Significant Changes in Protein Abundance during Chronic Metabolic Acidosis

Protein name	Uniprot		Mass, kDa	P-value	Mean Spectral Counts ± S.E.		Fold Change	Potential pH-RE	Location	TMD
	Accession #	Gene			Control	7 Day CMA				
UDP-glucuronosyltransferase 2B15	P36511	Ugt2b15	61	0.00022	1.8 ± 1.0	17.0 ± 0.7	6.4	Yes	ER	1
Carbonic anhydrase 5B, mitochondrial	Q66HG6	Ca5b	37	0.068*	0.0 ± 0.0	4.7 ± 1.9	5.7	Yes	M	
Protein AMBP	Q64240	Ambp	39	0.024	2.0 ± 0.9	13.8 ± 3.2	5.0	No	membrane	
UDP-glucuronosyltransferase 1-1	Q64550	Ugt1a1	60	0.00086	11.0 ± 1.8	54.1 ± 4.5	4.6	Yes	ER	2
All-trans-13,14-dihydroretinol saturase, CRA_b	G3V7V6	Retsat	67	0.043	0.7 ± 0.4	7.5 ± 2.3	4.9	No	unknown	1
Ras-related protein Rab-21	Q6AXT5	Rab21	24	0.011	1.5 ± 0.8	9.5 ± 1.6	4.1	Yes	membrane	
Uncharacterized protein	D4A0Y1	Cfb	141	0.014	1.2 ± 0.7	7.7 ± 1.4	4.0	NA	extracellular	
Glutaminase kidney isoform, mitochondrial	P13264	Gls	74	0.019	17.7 ± 2.1	59.3 ± 10.7	3.2	Yes	M	
Enoyl-CoA hydratase domain-containing protein 3	Q3MIE0	Echdc3	32	0.0061	0.4 ± 0.4	3.8 ± 0.6	3.6	Yes	M	
Epoxide hydrolase 1	P07687	Ephx1	53	0.013	11.1 ± 3.3	36.3 ± 4.9	3.1	No	ER	
Vitamin D-binding protein	P04276	Gc	54	0.0062	15.0 ± 4.4	40.2 ± 1.9	2.6	No	extracellular	
Acetyl-Coenzyme A acyltransferase 1B	F1LPD6	Acaa1b	44	0.0049	11.3 ± 1.1	28.4 ± 2.8	2.4	No	M & P	
Catalase	P04762	Cat	60	0.0095	55.1 ± 12.0	123.1 ± 8.3	2.2	Yes	M & P	
Ribonuclease 4	O55004	Rnase4	17	0.044	7.5 ± 1.4	17.7 ± 3.2	2.2	Yes	extracellular	1
Ectonucleoside triphosphate diphosphohydrolase 5	Q6P6S9	Entpd5	47	0.018	8.0 ± 0.8	18.2 ± 2.5	2.1	No	ER	2
Enoyl-coenzyme A hydratase/3-hydroxyacyl-coenzyme A	P07896	Ehhadh	79	0.014	14.3 ± 3.5	31.5 ± 2.0	2.1	Yes	M & P	
Fumarylacetoacetate hydrolase domain-containing 2	B2RYW9	Fahd2	35	0.011	29.6 ± 5.9	61.1 ± 3.8	2.0	Yes	M	
17-beta-hydroxysteroid dehydrogenase 4	P97852	Hsd17b4	79	0.0018	48.1 ± 3.6	95.3 ± 5.3	2.0	No	M & P	
Cytochrome P450 4A2	P20816	Cyp4a2	58	0.023	91.2 ± 22.0	175.1 ± 7.7	1.9	Yes	ER	1
Peroxisomal acyl-coenzyme A oxidase 1	P07872	Acox1	75	0.021	26.2 ± 6.8	51.4 ± 0.5	1.9	No	ER & M	
Dimethylglycine dehydrogenase, mitochondrial	Q63342	Dmgdh	96	0.0024	47.4 ± 7.6	68.3 ± 2.5	1.5	Yes	M	
Apolipoprotein A-IV	P02651	Apoa4	44	0.041	46.3 ± 10.0	83.6 ± 7.6	1.8	No	ER	
ATP-binding cassette sub-family D member 3	P16970	Abcd3	75	0.037	29.3 ± 6.3	52.5 ± 4.0	1.8	Yes	M & P	3
Cytochrome b5	P00173	Cyb5a	15	0.014	37.5 ± 5.8	64.7 ± 4.8	1.7	Yes	ER & M	1
Glutamate dehydrogenase 1, mitochondrial	P10860	Glud1	61	0.0035	431.5 ± 45.2	715.7 ± 7.9	1.7	Yes	M	
Probable D-lactate dehydrogenase, mitochondrial	F1LVD7	Ldhd	52	0.037	27.0 ± 4.0	45.7 ± 4.5	1.7	NA	M	
NADPH--cytochrome P450 reductase	P00388	Por	77	0.044	13.2 ± 1.4	21.6 ± 2.6	1.6	Yes	ER & M	1
GrpE protein homolog 1, mitochondrial	P97576	Grpel1	24	0.04	10.2 ± 0.9	16.3 ± 1.8	1.5	No	M	
Enoyl-CoA delta isomerase 1, mitochondrial	P23965	Eci1	32	0.035	76.7 ± 6.5	116.2 ± 10.8	1.5	No	M	
Filamin-B	D3ZD13	Flnb	278	0.023	4.2 ± 0.5	2.1 ± 0.3	0.6	NA	cytsol	
4F2 cell-surface antigen heavy chain	Q794F9	Slc3a2	58	0.02	105.6 ± 13.0	50.5 ± 6.8	0.5	NA	membrane	1
Calnexin	P35565	Canx	67	0.0069	35.1 ± 3.6	14.8 ± 1.5	0.4	NA	ER	1
Protein FAM151A	Q642A7	Fam151a	67	0.036	29.0 ± 6.1	13.0 ± 2.6	0.4	NA	membrane	1

Proteins in italics were previously shown to be induced during acidosis. * Greater than 0.05 p-value. Potential pH response element (pH-RE), NA if 3' UTR not sequenced or fold decrease. Location mitochondria (M), peroxisome (P), endoplasmic reticulum (ER). Number of transmembrane domains predicted (TMD).

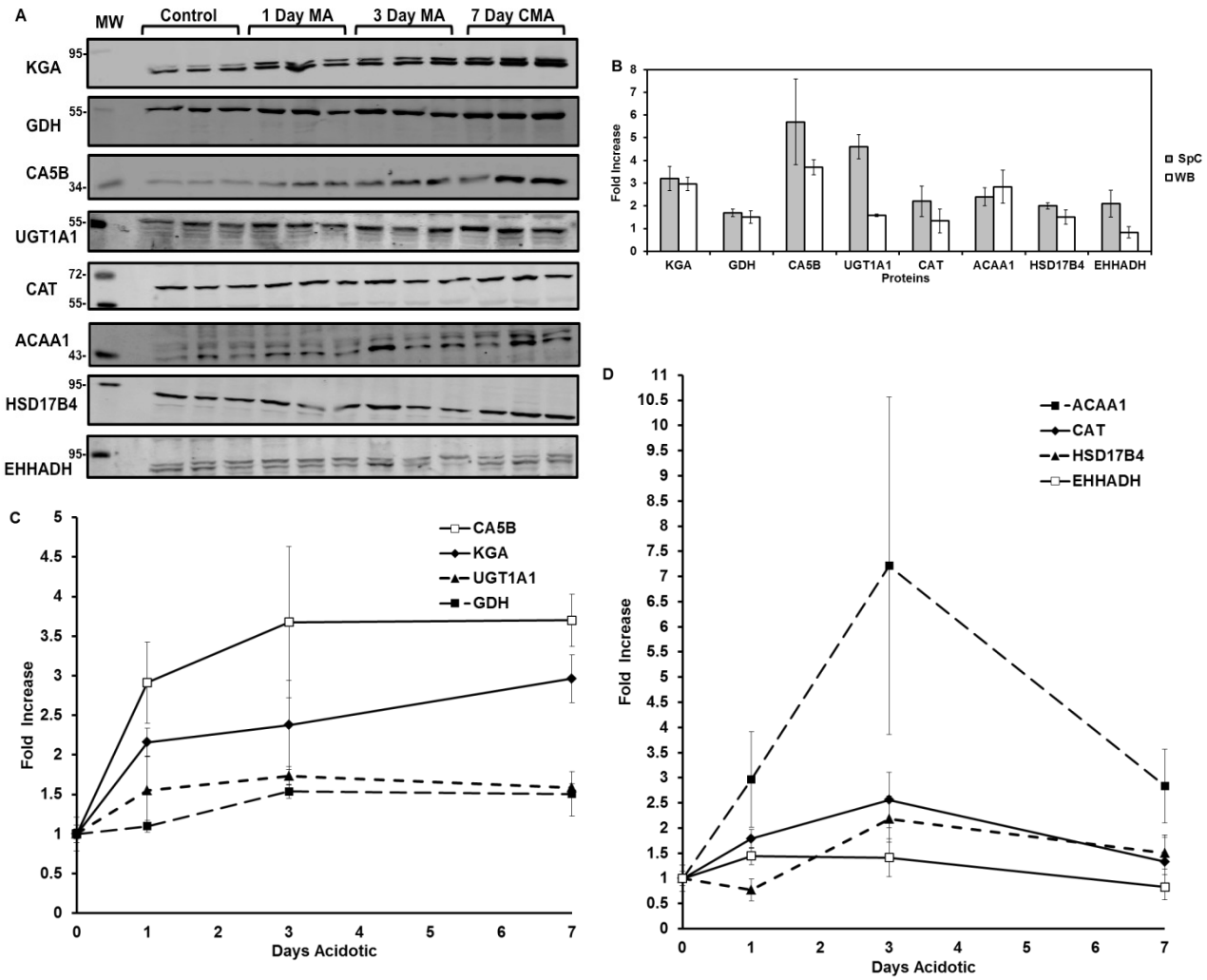

Fig. 2.7. Western blot analysis of the temporal changes in abundance of proteins identified by spectral count analysis. A. Separate mitochondrial (M) samples were isolated from proximal convoluted tubules of three control (Ctrl), three 1-d acidotic (MA), three 3-d acidotic (MA) and three 7-d chronic acidotic (CMA) rats. Western blot analysis was performed using 8 specific antibodies to validate the changes in protein abundance calculated by comparing the spectral counts of control and 7-d chronic acidotic samples (CMA). MW are molecular weight standards. Each blot was normalized to a mitochondrial protein that served as a loading control. The bands were imaged and quantified with an Odyssey Infrared Imager. B. Comparison of the fold changes calculated from Western blot analyses (open bars) and spectral counts (solid bars). The reported data are the mean ± S.E. of the fold increase of the triplicate 7-d acidotic samples normalized to the control samples. C & D. Time course of the fold changes in the 8 proteins during development of chronic acidosis derived from the Western blot analyses in Panel A. The reported data points are the mean ± S.E. of triplicate samples.

analysis. Overall, the results of the spectral counting analysis of relative protein abundance were largely validated by the data obtained from the Western blots.

2.4f Time course Western blot analysis

Additional mitochondrial fractions were obtained from triplicate control, 1-d acute, 3-d, and 7-day chronic acidotic rats to evaluate the temporal changes in expression of these proteins. The enrichment of the mitochondrial cytochrome c oxidase activity in all of the samples was 7-fold which is similar to that observed in the initial study (data not shown). Western blot analyses were used to quantify the relative abundance of the proteins in the temporal samples. The level of KGA is increased at 1 d and continues to increase for 7 d during the development of chronic acidosis (Fig. 2.7 C). GDH exhibits a more gradual adaptation, is not significantly increased until 3 d, and is expressed at a similar level in the 7-d chronic acidotic samples. The temporal profiles for KGA and GDH are similar to what was previously observed by proteomic analysis of whole cell lysates of isolated proximal convoluted tubules.[17] CA5B is increased 2.9-fold after 1 d and then plateaus at a 3.7-fold increase after 3 d. UGT1a1 is increased 1.6-fold after 1 d and then remains at that level through the 7-d period. Catalase was maximally induced by 3 d (2.6-fold increase) (Fig. 2.7 D). ACAA1 was induced rapidly and reached a maximum of 7.2-fold by 3 d but decreased to 2.8-fold by 7 d. EHHADH showed a 1.4-fold increase at 1 and 3 d but no change at 7 d. All of the proteins except for KGA appear to plateau or even decrease between 3 d and 7 d. This may be due to the fact that by 7 d the metabolic acidosis is partially compensated.[43]

2.4g Hypertrophy

During chronic metabolic acidosis the proximal convoluted tubule undergoes significant hypertrophy.[44] Thus, it was important to determine if the increase in protein expression was due to the hypertrophy and not an adaptation to metabolic acidosis. The loss of one kidney causes a more extensive hypertrophy of the proximal convoluted tubule in the remaining kidney.[45] Therefore, mitochondria were prepared from proximal convoluted tubules that were isolated from 3 sham-operated rats and 3 unilateral nephrectomized rats (UNX) 21-d post-surgery. The maximal compensatory hypertrophy of the proximal convoluted tubule occurs at 21-d post unilateral nephrectomy.[28] Unilateral nephrectomized rats maintain normal blood pH and HCO_3^- levels.[46] The wet weight of the remaining kidney was increased 36% compared to sham operated control kidney. The isolated mitochondrial fractions were analyzed by Western blotting to determine if the hyperacetylation and increased protein expression observed during acidosis was due, in part, to the hypertrophy (Fig. 2.8 A & B). There was no significant difference in total protein lysine acetylation between UNX and the sham-operated controls (Fig. 2.8 C). Therefore, increased mitochondrial protein lysine acetylation occurs in response to the changes in acid-base balance and not the hypertrophy that occurs during acidosis. The levels of all the analyzed proteins except for GDH were unchanged in the UNX samples compared to the sham operated controls (Fig. 2.8 C). GDH showed a significant 2-fold decrease in the mitochondria isolated from the UNX rats, indicating that the fold increase observed during metabolic acidosis is an over compensation for the decrease caused by hypertrophy alone. Overall, the Western blot analyses indicate that the increases in lysine acetylation and protein abundance observed during chronic metabolic acidosis are not merely a response to the associated hypertrophy.

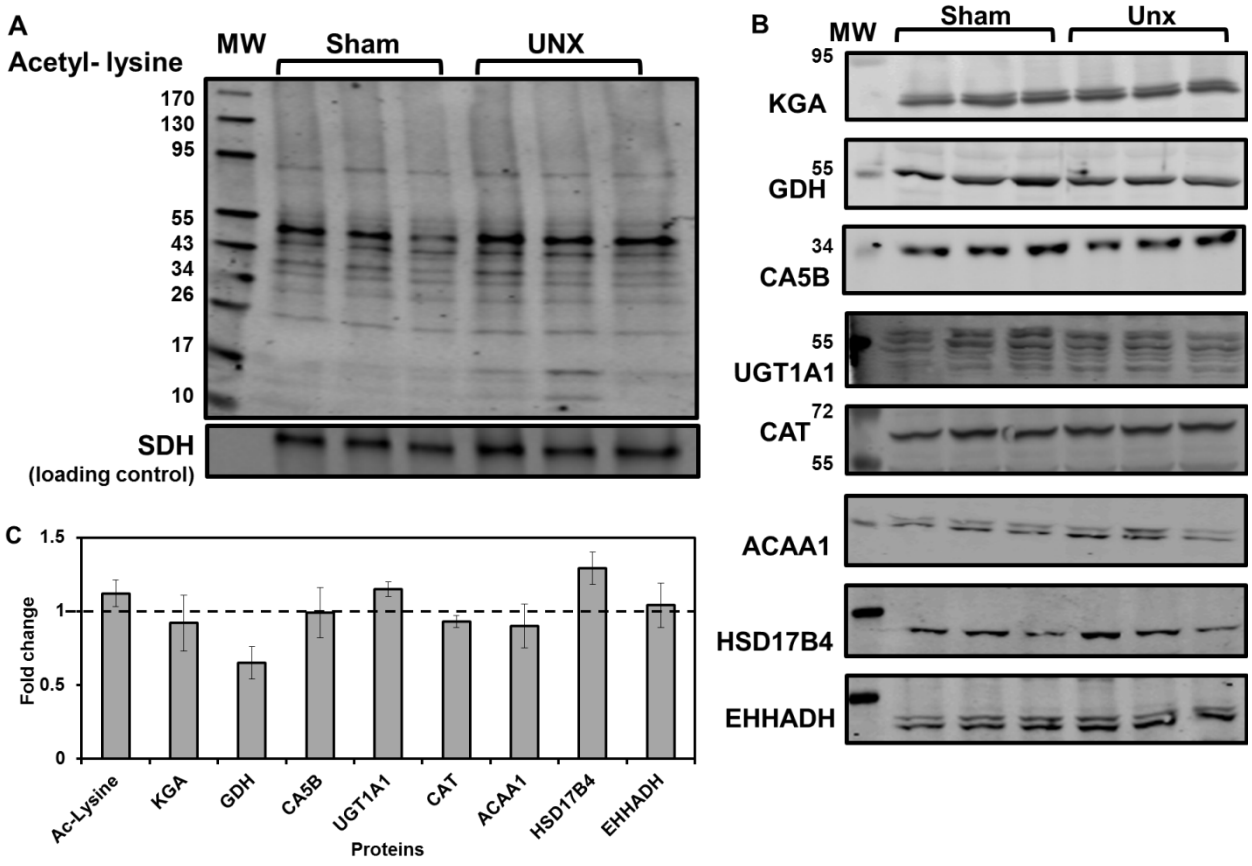

Fig. 2.8. Effect of unilateral nephrectomy on lysine acetylation and protein abundance of mitochondrial proteins. A. Western blot analysis of homogenates of mitochondria isolated from proximal convoluted tubules from 3 sham-operated and 3 uninephrectomized (UNX) rats was performed using an antibody specific for N-ε-acetyl-lysine. B. Western blot analysis was performed using antibodies that are specific for 8 of the proteins that were identified to increase significantly by spectral counting during 7-d chronic acidosis (CMA). Each blot was normalized to a mitochondrial protein that served as a loading control. MW are molecular weight standards. The bands in Panel B. were imaged and quantified with an Odyssey Infrared Imager. C. Comparison of fold-changes in protein expression in UNX rats. The reported data are the mean ± S.E. of the intensities of the triplicate UNX samples normalized to the sham-operated control samples. The dashed line indicates no change in abundance.

2.5 Discussion

Previous proteomic analyses have established that mitochondria isolated from rat muscle, heart and liver exhibit significant differences in protein content.[47] The various segments of the renal nephron contain mitochondria that differ in size, subcellular location, and function.[35] Therefore, it is very likely that the proteomes of the mitochondria contained in the various nephron segments also differ significantly. This study combined established procedures to isolate rat renal proximal convoluted tubules [17, 18] with a subcellular fractionation protocol to yield a highly enriched preparation of mitochondria specific to the proximal convoluted tubule. Thus, the proteomic analysis described in the present study represents the initial characterization of mitochondria from a specific segment of the renal nephron. This organelle constitutes the primary site of the increase in renal ammoniagenesis that occurs during metabolic acidosis.[3, 4] Therefore, proteomic profiling of the mitochondria isolated from control and chronic acidotic rats also provides insight into the alterations in mitochondrial metabolism that either accompany or support the increased catabolism of glutamine. In addition, the resulting data expand our knowledge of the proteome of the renal proximal convoluted tubule. [17, 18, 19]

Lysine acetylation and tri-methylation are both detected as an addition of 42 Da. We were unable to distinguish between the two modifications due to mass accuracy limitations and the inability to detect low mass fragment ions (1/3 cut off rule) of ion trap mass spectrometers. However, tri-methylation of non-nuclear proteins is uncommon, whereas lysine acetylation of numerous mitochondrial proteins has been characterized in non-renal tissues.[37, 48] Therefore, the identified modifications are likely to be acetylated lysines. Lysine acetylation has been shown to produce conformational changes that affect enzyme activities and protein/protein interactions. In addition, lysine acetylation frequently occurs at sites of or near other post-translational

modifications. Therefore, lysine acetylation may block or induce other regulatory modifications.[49] The resulting crosstalk between the post-translational modifications produces a complex set of signaling networks. The identified sites of acetylation in the mitochondrial proteins of the proximal convoluted tubule provide a basis for future mutational and functional analyses to determine their role in the regulation of mitochondrial metabolism and possibly, in the rapid activation of glutamine catabolism that occurs during acute onset of metabolic acidosis.

Using stringent criteria, the combined proteomic analyses confidently identified 901 proteins in the mitochondrial preparation isolated from proximal convoluted tubules. Approximately 70% of the identified proteins are previously characterized proteins that have defined Gene Ontology (GO) terms. The analysis of GO terms indicated that the majority of the characterized proteins were previously identified as mitochondrial proteins. Given the incomplete nature of the current assignment of GO terms, it is feasible that many more of the characterized and uncharacterized proteins are also localized in the mitochondria. Spectral counting identified 33 proteins that exhibit a significant adaptive response during chronic metabolic acidosis (Table 2.3). Only 6 of these proteins, including KGA and GDH, were previously shown to exhibit an adaptive response to acidosis by either microarray analysis[16] or difference in-gel electrophoresis.[17]

The increases in KGA[15] and GDH[50] expression result from selective stabilization of their respective mRNAs. In both cases, the mRNA stabilization is mediated by an 8-base AU-rich sequence within their 3'-UTR that functions as a pH-response element (pH-RE). Of the 29 proteins that are significantly increased in acidosis, only 26 have mRNAs for which the 3'-UTR has been annotated. Of the characterized mRNAs, 16 or more than 60% contain an AU-rich sequence in their 3'-UTR that is > 85% identical to either of the pH-REs in the KGA mRNA.

The latter group includes two UDP-glucuronosyltransferases (2B15 and 1A1), carbonic anhydrase 5B, Rab-21, catalase and an enoyl-CoA hydratase. This group constitutes most of the proteins that are increased more than 3-fold. Therefore, mRNA stabilization may be a common mechanism that mediates the adaptive increases in many proteins in addition to KGA and GDH within the proximal convoluted tubule.

Various isozymes of carbonic anhydrase play an important role in cellular acid-base balance. They catalyze the reversible hydration of carbon dioxide to produce carbonic acid, which spontaneously dissociates to form a bicarbonate ion and a H^+.[51] The observed increase in the mitochondrial isoform of carbonic anhydrase (CA5B) during chronic metabolic acidosis may support the associated increase in renal gluconeogenesis by providing bicarbonate ions for the mitochondrial pyruvate carboxylase.[51, 52] This enzyme catalyzes an essential reaction in the synthesis of glucose from lactate or pyruvate. Alternatively, the increased expression of this carbonic anhydrase may facilitate the transport of bicarbonate produced by α-ketoglutarate dehydrogenase from the mitochondria to the cytoplasm.[42] This translocation is necessary to ensure that bicarbonate ions generated in the mitochondria during acidosis contribute to the net synthesis of bicarbonate ions that is essential to partially restore acid-base balance.

UDP-glucuronosyltransferases (UGT) catalyze the transfer of glucuronic acid to endogenous and exogenous compounds to increase their solubility and facilitate their excretion in the urine.[53] The human genome encodes 15 separate UGTs that are categorized into two gene families, 1a and 2B.[54] The proteomic analysis identified two UGTs that are significantly increased in the proximal convoluted tubule during acidosis. The primary substrates of UGT1a1 are bilirubin, opioids, and various xenobiotics, whereas UGT2B15 primarily targets bilirubin.[53] UGTs are associated with endoplasmic reticulum membrane through a C-terminal

transmembrane domain, which anchors the catalytic domain to the cytoplasmic surface. A specialized portion of the endoplasmic reticulum is closely associated with the mitochondria.[34] This association of the two organelles may account for the recovery of the two UGTs in the isolated mitochondria.

Catalase is another highly abundant protein in the mitochondrial samples that is significantly increased (2.2 fold) during chronic acidosis. Catalase is typically considered to be a peroxisomal marker. However, a recent study detected catalase in the matrix of rat heart mitochondria and demonstrated that it plays a significant role in reducing oxidative stress.[55] Furthermore, the over expression of mitochondrial catalase reduced the production of reactive oxidative species.[50] Western blot analysis of proximal convoluted tubule homogenates using antibodies to 4-hydroxy-2-nonenal (4-HNE) and malondialdehyde (MDA) showed no increase of these markers of oxidative stress during chronic acidosis (data not shown). Therefore, the up-regulation of the mitochondrial catalase during acidosis may counteract the potential increase in reactive oxygen species that would otherwise accompany an increase in electron transport and ATP synthesis. An additional novel finding is the observation that 3 enzymes involved in both mitochondrial and peroxisomal fatty acid metabolism are increased in acidosis. The acetyl-CoA acyltransferase, acyl-CoA oxidase, and enoyl-CoA hydratase are all enzymes that contribute to the synthesis of long-chain saturated and unsaturated fatty acids. Their increased expression suggests that acidosis may promote a remodeling of the lipids of the mitochondrial membranes.

The primary functions of the mitochondria-associated ER membrane (MAM) are lipid transport, the control of apoptosis, and the efficient shuttling of Ca^{2+} ions from the endoplasmic reticulum to the mitochondria.[29] The mitochondrial influx of Ca^{2+} ions is known to regulate flux through the TCA cycle by activating the isocitrate and α-ketoglutarate dehydrogenases. Calnexin

is a Ca^{2+} -dependent transmembrane chaperone that is compartmentalized to the MAM.[51] The association of calnexin with the Ca^{2+} -ATPase may inhibit Ca^{2+} uptake into the endoplasmic reticulum.[52] The level of calnexin associated with the isolated mitochondria was observed to decrease by 0.4-fold during acidosis. This may reflect the dissociation of calnexin from the Ca^{2+} -ATPase and its translocation from the MAM to other regions of the endoplasmic reticulum or to the plasma membrane. Previous studies also established that the level of calmodulin is rapidly increased in proximal convoluted tubule cells during acute onset of acidosis.[14] These findings suggest that increased Ca^{2+} signaling may contribute to the enhanced mitochondrial catabolism of glutamine during metabolic acidosis.

The proximal convoluted tubule undergoes a significant hypertrophy during chronic metabolic acidosis.[38] A similar hypertrophy occurs in the remnant kidney following unilateral nephrectomy.[23] Unilateral nephrectomy also causes an increase in metabolism and O_2 consumption in the remnant kidney.[53] However, Western blot analysis established that the increase in lysine acetylation and the increases in various proteins, including the mitochondrial catalase, that occur during chronic acidosis are not due to the associated hypertrophy. Therefore, the reported remodeling of the mitochondrial proteome of the proximal convoluted tubule occurs in response to the changes in acid-base balance during metabolic acidosis.

REFERENCES

1. Halperin, M. L., Metabolic aspects of metabolic acidosis. Clin Invest Med 1993, 16 (4), 294-305;

2. Wagner, C. A., Metabolic acidosis: new insights from mouse models. Curr Opin Nephrol Hypertens 2007, 16 (5), 471-6.

3. Weiner, I. D.; Hamm, L. L., Molecular mechanisms of renal ammonia transport. Annu Rev Physiol 2007, 69, 317-40.

4. Curthoys, N. P., Renal ammonium ion production and excretion. 2007; Vol. 4th Edition, p 1601-1619.

5. Curthoys, N. P.; Gstraunthaler, G., Mechanism of increased renal gene expression during metabolic acidosis. Am J Physiol Renal Physiol 2001, 281 (3), F381-90.

6. Squires, E. J.; Hall, D. E.; Brosnan, J. T., Arteriovenous differences for amino acids and lactate across kidneys of normal and acidotic rats. Biochem J 1976, 160 (1), 125-8.

7. Lowry, M.; Ross, B. D., Activation of oxoglutarate dehydrogenase in the kidney in response to acute acidosis. Biochem J 1980, 190 (3), 771-80.

8. Taylor, L.; Curthoys, N. P., Glutamine Metabolism: Role in acid-base balance. Biochem. Molec Biol. Ed. 2004, 32, 291-304.

9. Preisig, P. A.; Alpern, R. J., Chronic metabolic acidosis causes an adaptation in the apical membrane Na/H antiporter and basolateral membrane Na(HCO3)3 symporter in the rat proximal convoluted tubule. J Clin Invest 1988, 82 (4), 1445-53.

10. Tannen, R. L.; Ross, B. D., Ammoniagenesis by the isolated perfused rat kidney: the critical role of urinary acidification. Clin Sci (Lond) 1979, 56 (4), 353-64.

11. Curthoys, N. P.; Lowry, O. H., The distribution of glutaminase isoenzymes in the various structures of the nephron in normal, acidotic, and alkalotic rat kidney. J Biol Chem 1973, 248 (1), 162-8;

12. Wright, P. A.; Knepper, M. A., Phosphate-dependent glutaminase activity in rat renal cortical and medullary tubule segments. Am J Physiol 1990, 259 (6 Pt 2), F961-70.

13. Hansen, W. R.; Barsic-Tress, N.; Taylor, L.; Curthoys, N. P., The 3'-nontranslated region of rat renal glutaminase mRNA contains a pH-responsive stability element. Am J Physiol 1996, 271 (1 Pt 2), F126-31;

14. Hwang, J. J.; Perera, S.; Shapiro, R. A.; Curthoys, N. P., Mechanism of altered renal glutaminase gene expression in response to chronic acidosis. Biochemistry 1991, 30 (30), 7522-6.

15. Laterza, O. F.; Curthoys, N. P., Specificity and functional analysis of the pH-responsive element within renal glutaminase mRNA. Am J Physiol Renal Physiol 2000, 278 (6), F970-7.

16. Nowik, M.; Lecca, M. R.; Velic, A.; Rehrauer, H.; Brandli, A. W.; Wagner, C. A., Genome-wide gene expression profiling reveals renal genes regulated during metabolic acidosis. Physiol Genomics 2008, 32 (3), 322-34.

17. Curthoys, N. P.; Taylor, L.; Hoffert, J. D.; Knepper, M. A., Proteomic analysis of the adaptive response of rat renal proximal tubules to metabolic acidosis. Am J Physiol Renal Physiol 2007, 292 (1), F140-7

18. Walmsley, S. J.; Freund, D. M.; Curthoys, N. P., Proteomic profiling of the effect of metabolic acidosis on the apical membrane of the proximal convoluted tubule. Am J Physiol Renal Physiol 2012, 302 (11), F1465-77.

19. Walmsley, S. J.; Broeckling, C.; Hess, A.; Prenni, J.; Curthoys, N. P., Proteomic analysis of brush-border membrane vesicles isolated from purified proximal convoluted tubules. Am J Physiol Renal Physiol 2010, 298 (6), F1323-31.

20. Cooperstein, S. J.; Lazarow, A., A microspectrophotometric method for the determination of cytochrome oxidase. J Biol Chem 1951, 189 (2), 665-70.

21. Bradford, M. M., A rapid and sensitive method for the quantitation of microgram quantities of protein utilizing the principle of protein-dye binding. Anal Biochem 1976, 72, 248-54.

22. Smith, P. K.; Krohn, R. I.; Hermanson, G. T.; Mallia, A. K.; Gartner, F. H.; Provenzano, M. D.; Fujimoto, E. K.; Goeke, N. M.; Olson, B. J.; Klenk, D. C., Measurement of protein using bicinchoninic acid. Anal Biochem 1985, 150 (1), 76-85.

23. Keller, A.; Nesvizhskii, A. I.; Kolker, E.; Aebersold, R., Empirical statistical model to estimate the accuracy of peptide identifications made by MS/MS and database search. Anal Chem 2002, 74 (20), 5383-92.

24. Nesvizhskii, A. I.; Keller, A.; Kolker, E.; Aebersold, R., A statistical model for identifying proteins by tandem mass spectrometry. Anal Chem 2003, 75 (17), 4646-58.

25. Elias, J. E.; Gygi, S. P., Target-decoy search strategy for increased confidence in large-scale protein identifications by mass spectrometry. Nat Methods 2007, 4 (3), 207-14.

26. Paoletti, A. C.; Washburn, M. P., Quantitation in proteomic experiments utilizing mass spectrometry. Biotechnol Genet Eng Rev 2006, 22, 1-19.

27. Curthoys, N. P.; Kuhlenschmidt, T.; Godfrey, S. S.; Weiss, R. F., Phosphate-dependent glutaminase from rat kidney. Cause of increased activity in response to acidosis and identity with glutaminase from other tissues. Arch Biochem Biophys 1976, 172 (1), 162-7.

28. Pfaller, W.; Seppi, T.; Ohno, A.; Giebisch, G.; Beck, F. X., Quantitative morphology of renal cortical structures during compensatory hypertrophy. Exp Nephrol 1998, 6 (4), 308-19.

29. Doctor, R. B.; Chen, J.; Peters, L. L.; Lux, S. E.; Mandel, L. J., Distribution of epithelial ankyrin (Ank3) spliceoforms in renal proximal and distal tubules. Am J Physiol 1998, 274 (1 Pt 2), F129-38.

30. Reifschneider, N. H.; Goto, S.; Nakamoto, H.; Takahashi, R.; Sugawa, M.; Dencher, N. A.; Krause, F., Defining the Mitochondrial Proteomes from Five Rat Organs in a Physiologically Significant Context Using 2D Blue-Native/SDS-PAGE. Journal of Proteome Research 2006, 5 (5), 1117-1132.

31. Ghaedi K., T. S., Okumoto K., Matsuzono Y., Fujiki Y., The peroxin pex3p initiates membrane assembly in peroxisome biogenesis. Mol. Biol. Cell 2000, 11, 2085-102.

32. Huling, J. C.; Pisitkun, T.; Song, J. H.; Yu, M. J.; Hoffert, J. D.; Knepper, M. A., Gene expression databases for kidney epithelial cells. Am J Physiol Renal Physiol 2012, 302 (4), F401-7.

33. Sonnhammer, E. L.; von Heijne, G.; Krogh, A., A hidden Markov model for predicting transmembrane helices in protein sequences. Proc Int Conf Intell Syst Mol Biol 1998, 6, 175-82.

34. Hayashi, T.; Rizzuto, R.; Hajnoczky, G.; Su, T. P., MAM: more than just a housekeeper. Trends in cell biology 2009, 19 (2), 81-8.

35. Kriz, W., Kaissling, B, Structural Organization of the Mammalian Kidney. The Kidney: Physiology and Pathophysiology 2008, 4th Ed (Chapter 29), 479-564.

36. Schlüter, A.; Real-Chicharro, A.; Gabaldón, T.; Sánchez-Jiménez, F.; Pujol, A., PeroxisomeDB 2.0: an integrative view of the global peroxisomal metabolome. Nucleic Acids Research 2010, 38 (suppl 1), D800-D805.

37. Zhao, S.; Xu, W.; Jiang, W.; Yu, W.; Lin, Y.; Zhang, T.; Yao, J.; Zhou, L.; Zeng, Y.; Li, H.; Li, Y.; Shi, J.; An, W.; Hancock, S. M.; He, F.; Qin, L.; Chin, J.; Yang, P.; Chen, X.; Lei, Q.; Xiong, Y.; Guan, K. L., Regulation of cellular metabolism by protein lysine acetylation. Science 2010, 327 (5968), 1000-4.

38. Glozak, M. A.; Sengupta, N.; Zhang, X.; Seto, E., Acetylation and deacetylation of non-histone proteins. Gene 2005, 363, 15-23.

39. Liu, H.; Sadygov, R. G.; Yates, J. R., 3rd, A model for random sampling and estimation of relative protein abundance in shotgun proteomics. Anal Chem 2004, 76 (14), 4193-201.

40. Wright, P. A.; Knepper, M. A., Glutamate dehydrogenase activities in microdissected rat nephron segments: effects of acid-base loading. Am J Physiol 1990, 259 (1 Pt 2), F53-9.

41. Fujikawa-Adachi, K.; Nishimori, I.; Taguchi, T.; Onishi, S., Human mitochondrial carbonic anhydrase VB. cDNA cloning, mRNA expression, subcellular localization, and mapping to chromosome x. J Biol Chem 1999, 274 (30), 21228-33.

42. Shah, G. N.; Hewett-Emmett, D.; Grubb, J. H.; Migas, M. C.; Fleming, R. E.; Waheed, A.; Sly, W. S., Mitochondrial carbonic anhydrase CA VB: differences in tissue distribution and pattern of evolution from those of CA VA suggest distinct physiological roles. Proc Natl Acad Sci U S A 2000, 97 (4), 1677-82.

43. Sleeper, R. S.; Vertuno, L. L.; Strauss, F.; Preuss, H. G., Effects of acid challenge on in vivo and in vitro rat renal ammoniagenesis. Life Sci 1978, 22 (18), 1561-71.

44. Lotspeich, W. D., Renal Hypertrophy in Metabolic Acidosis and Its Relation to Ammonia Excretion. Am J Physiol 1965, 208, 1135-42.

45. Shechter, P.; Shi, J. D.; Rabkin, R., Renal tubular cell protein breakdown in uninephrectomized and ammonium chloride-loaded rats. Journal of the American Society of Nephrology 1994, 5 (5), 1201-7.

46. Jaramillo-Juarez, F.; Rodriguez-Vazquez, M. L.; Namorado, M. C.; Martin, D.; Reyes, J. L., Acidosis and weight loss are induced by cyclosporin A in uninephrectomized rats. Pediatr Nephrol 2000, 14 (2), 122-7.

47. Forner, F.; Foster, L. J.; Campanaro, S.; Valle, G.; Mann, M., Quantitative proteomic comparison of rat mitochondria from muscle, heart, and liver. Mol Cell Proteomics 2006, 5 (4), 608-19.

48. Oliver, S. S.; Denu, J. M., Dynamic interplay between histone H3 modifications and protein interpreters: emerging evidence for a "histone language". Chembiochem : a European journal of chemical biology 2011, 12 (2), 299-307.

49. Yang, X. J.; Seto, E., Lysine acetylation: codified crosstalk with other posttranslational modifications. Mol Cell 2008, 31 (4), 449-61.

50. Schroeder, J. M.; Liu, W.; Curthoys, N. P., pH-responsive stabilization of glutamate dehydrogenase mRNA in LLC-PK1-F+ cells. Am J Physiol Renal Physiol 2003, 285 (2), F258-65.

51. Dodgson, S. J.; Cherian, K., Mitochondrial carbonic anhydrase is involved in rat renal glucose synthesis. Am J Physiol 1989, 257 (6 Pt 1), E791-6.

52. Henry, R. P., Multiple roles of carbonic anhydrase in cellular transport and metabolism. Annu Rev Physiol 1996, 58, 523-38.

53. King, C. D.; Rios, G. R.; Green, M. D.; Tephly, T. R., UDP-glucuronosyltransferases. Current drug metabolism 2000, 1 (2), 143-61.

54. Tukey, R. H.; Strassburg, C. P., Human UDP-glucuronosyltransferases: metabolism, expression, and disease. Annual review of pharmacology and toxicology 2000, 40, 581-616.

55. Bai, J.; Cederbaum, A. I., Mitochondrial catalase and oxidative injury. Biological signals and receptors 2001, 10 (3-4), 189-99.

56. Gurgul, E.; Lortz, S.; Tiedge, M.; Jorns, A.; Lenzen, S., Mitochondrial catalase overexpression protects insulin-producing cells against toxicity of reactive oxygen species and proinflammatory cytokines. Diabetes 2004, 53 (9), 2271-80.

57. Myhill, N.; Lynes, E. M.; Nanji, J. A.; Blagoveshchenskaya, A. D.; Fei, H.; Carmine Simmen, K.; Cooper, T. J.; Thomas, G.; Simmen, T., The subcellular distribution of calnexin is mediated by PACS-2. Mol Biol Cell 2008, 19 (7), 2777-88.

58. Roderick, H. L.; Lechleiter, J. D.; Camacho, P., Cytosolic phosphorylation of calnexin controls intracellular Ca(2+) oscillations via an interaction with SERCA2b. J Cell Biol 2000, 149 (6), 1235-48.

59. Benipal, B.; Lash, L. H., Influence of renal compensatory hypertrophy on mitochondrial energetics and redox status. Biochemical pharmacology 2011, 81 (2), 295-303.

CHAPTER 3

Improved Detection of Quantitative Differences Using a Combination of Spectral Counting and MS/MS Total Ion Current [2]

3.1 Summary

A workflow was developed to quantify relative protein abundance changes in rat kidney mitochondria in response to metabolic acidosis. Specifically, a combination of two label-free relative quantitative strategies were employed and compared; spectral counting (SpC) and average MS/MS total ion current (MS^2 TIC). Spectral counting is a measure of the sum of MS/MS spectra assigned to all peptides for a given protein. MS^2 TIC is the average total ion current of the MS/MS spectra assigned to all peptides for a given protein. In total, forty nine proteins were observed to be significantly altered in response to metabolic acidosis (p-value < 0.05). Of these, 32 proteins were uniquely observed as significantly changing by SpC, 14 by MS^2 TIC, and only 3 by both approaches. Western blot analysis was performed to validate the observed protein changes. Eight proteins were confirmed by Western blotting and displayed similar fold changes to the MS methods. The results of this study illustrate both the limitations and complementary nature of these label-free methods for determining relative protein quantitation in complex biological samples.

3.2 Introduction

Mass spectrometry based quantitative proteomic approaches enable the observation of differences in protein levels between disease states and have been extensively utilized for the

discovery of potential protein biomarkers.[1, 2, 3, 4] The ability to detect quantitative changes within complex biological systems is essential to further our understanding of cellular processes and disease progression.[5] The analytical approaches employed for relative protein quantitation can be grouped into two major categories, labeling and label-free.[6] Examples of labeling approaches include isotope coded affinity tags (ICAT)[7], stable isotope labeling by amino acids in cell culture (SILAC)[8], tandem mass tags (TMT)[9] and isobaric tag for relative and absolute quantitation (iTRAQ).[10] Labeling methods can be limiting because of the complexity of sample preparation, reduced sampling size, incomplete labeling, cost of reagents, and time consuming data analysis.[11] Moreover, cell culture specific methods, such as SILAC, cannot be employed for the analysis of primary tissues which are often important for biomarker investigation in clinical studies.[12]

Label-free approaches have become widely employed due to their ease of use and diverse applications.[13] Furthermore, label-free methods have been shown to enable quantitation over a larger dynamic range as compared to stable isotope labeling approaches.[13] Spectral counting (SpC) is a label-free approach that is frequently used to determine relative protein abundance in shotgun proteomic experiments.[14] Spectral counting is a measure of the number of MS/MS spectra identified for all the peptides assigned to a protein. Liu, et al. demonstrated that the spectral count value strongly correlates with protein abundance in a complex matrix.[14] Additionally, SpC analysis has been shown to be highly sensitive for the detection of subtle changes in protein abundance.[15] However, Old, et al. illustrated a major limitation of SpC analysis for low abundance proteins (≤ 4 spectral counts) where quantitative values were found to be inaccurate.[15] Another example of label-free quantitation is the use of ion intensity as a quantitative measure. Most approaches base the quantitative value on the intensity of the parent ion peak which requires high resolution measurements to ensure neighboring peaks are

distinguished.[16] An alternative strategy is instead based on the average total ion current of the MS/MS spectra (MS^2 TIC) assigned to all peptides for a given protein. Fragment ion intensity measurements have been used in targeted quantitative approaches such as multiple reaction monitoring [17] and non-targeted labeling approaches such as iTRAQ.[10] Recently, two studies have successfully used either sum or average MS/MS TIC measurements in shot-gun proteomics experiments to identify phosphotyrosine binding proteins as well as to explore protein differences between total lung homogenates and lung endothelial plasma membrane subfractions.[18, 19] Asara, et al. demonstrated that MS^2 TIC displayed an improved dynamic range for detecting relative protein abundance changes as compared to SILAC.[19] MS^2 TIC methods have also been shown to provide improved sensitivity (as compared with SpC) for the accurate detection of quantitative changes for low abundance proteins.[20] While MS^2 TIC is not as extensively represented in the literature, it shows promise as a valuable technique that would be complementary to the more widely employed SpC approach.

One of the primary advantages of label-free quantitation is that the data required for the analysis is collected as part of the standard analytical workflow and further experimentation or sample preparation is not required. Thus, both SpC and MS^2 TIC analysis can easily be performed within the same experiment. Here, we present a detailed comparison of these two label-free approaches applied to the same dataset. Our results indicate that they are truly complementary and the use of both approaches increases the number of proteins found to be significantly changed without additional experimentation. The analysis was performed in the context of a larger study focused on understanding proteome remodeling in the mitochondria of the proximal convoluted tubule during the renal response to metabolic acidosis.[21] Briefly, metabolic acidosis is a common clinical condition that is caused by a decrease in blood pH and

bicarbonate concentration.[22] Previous studies have established that expression of a few mitochondrial proteins, including key enzymes of glutamine metabolism such as kidney-type glutaminase (KGA)[23, 24] and glutamate dehydrogenase (GDH)[25], are increased during metabolic acidosis.[26] Thus, the relative abundance changes observed for KGA and GDH were used as positive controls for this study. The results presented here describe the comparison of mitochondrial proteins that exhibit significant differences in protein abundance between control and acidotic rat kidneys as determined by SpC and MS^2 TIC analyses.

3.3 Materials and methods

3.3a Proteomic sample preparation

The study compared mitochondrial fractions of proximal convoluted tubules isolated from kidneys of control rats (n=3) and 7 d acidotic rats (n=3). Control rats drank tap water and rats that were made acidotic for 7 d were provided with 0.28 M NH_4Cl as their sole source of drinking water. Proximal convoluted tubule isolation and mitochondria enrichment procedures were described in detail.[21] All of the procedures were approved by the Institutional Animal Care and Use Committee at Colorado State University. Both Bradford [27] and bicinchoninic acid (Pierce) protein assays [28] were performed to determine protein concentrations. Briefly, 50 μg of the mitochondrial proteins underwent acetone precipitation, were resuspended in 8 M urea and 0.2% ProteaseMAX surfactant (Promega), reduced with dithiothreitol, and alkylated with idoacetamide. The proteins underwent tryptic digestion for 3 h at 37°C and then stopped with 0.5% trifluoroacetic acid. Peptides were dried in a speed-vac and purified using a reverse phase C18 TopTip (Glygen). Purified peptides were dried and reconstituted in 50 μl of 0.1% formic acid/3% acetonitrile.

3.3b Mass spectrometry

Briefly, 10 µg aliquot of each sample was injected onto a strong cation exchange (SCX) column (ZORBAX BioSCX Series II, 300 µm × 35 mm, 3.5 µm column, Agilent) and peptides were eluted using 20 µl salt bumps of 10, 15, 25, 35, 50, 75, 150, and 500 mM NaCl. The peptides were further fractionated on a reverse phase column (1200 nanoHPLC, Zorbax C18, 5µm, 75 µm ID x 150mm column, Agilent) using a linear gradient from 25%-55% buffer B (buffer B = 90% acetonitrile and 0.1% formic acid) at a flow rate of 300 nl/min. Peptides were eluted directly into the mass spectrometer (LTQ linear ion trap, Thermo Scientific) and spectra were collected over a m/z range of 200-2000 Da using a dynamic exclusion limit of 3 MS/MS spectra of a given peptide mass for 30 sec and an exclusion duration of 90 sec. The compound lists from the resulting spectra were produced using Xcalibar 2.2 software (Thermo Scientific) with an intensity threshold of 5,000 and 1 scan/group. Duplicate 2D-LC analysis was performed for each biological sample and sample order was randomized before analysis. The addition of 2D-LC to a relative quantitation workflow has been shown to not effect quantitation and results in an overall increase in peptide identifications.[29]

3.3c Bioinformatics

The tandem mass spectra (MS/MS) were searched against the Uniprot-KB *Rattus norvegicus* protein sequence database (74,140 sequence entries) which was concatenated with a reverse database using both the Mascot (version 2.3.02, Matrix Science) and SEQUEST (version v.27, rev. 11, Sorcerer, Sage-N Research) database search engines. The following search parameters were used: average mass, peptide mass tolerance of 2.5 Da, fragment ion mass tolerance of 1.0 Da, complete tryptic digestion allowing two missed cleavages, variable modifications of

methionine oxidation and lysine acetylation, and a fixed modification of cysteine carbamidomethylation. Peptide identifications from both search engine results were combined in Scaffold 3 (Version 3.6.0, Proteome Software) using protein identification algorithms. Search results from all .raw files associated with a biological sample (i.e. all 2D-LC fractions and duplicate injections) were summed within the Scaffold 3 software. Peptide probability thresholds of 90% and protein of 99% were applied with Peptide and Protein Prophet algorithms in Scaffold 3.[30, 31] Proteins containing shared peptides were grouped by Scaffold 3, satisfying the laws of parsimony. Using a target decoy approach a peptide false discovery rate (FDR) of 0.2% was determined.[32] Proteins that were identified by a minimum of 2 unique peptides in at least 1 biological replicate were considered confidently identified. Using these criteria, 901 total proteins were identified in all the samples.[21]

3.3d Label free protein quantitation

Box plots were generated to assess data quality between technical and biological replicates. Variance in the biological replicates was assessed by determining the number of proteins identified per sample, the total spectra identified, and the total peptides identified. Correlation of biological and technical replicates was tested using Pearson's correlation test. The statistical analysis was performed using the R v2.15 statistics package (http://r-project.org) and DanteR v1.0.2 (http://omics.pnl.gov/software/DanteR.php). MS/MS data to be used for quantitation was normalized between samples in Scaffold 3 by using the sum of the unweighted spectral counts for each sample to determine a sample specific scaling factor that was then applied to all proteins in that sample. Spectral counting and MS^2 TIC were separately performed on the normalized data. The average MS/MS total ion current value was chosen because it has been shown to be

less biased by protein length than the sum.[19] For SpC analysis, a pseudo value of 1 was added to all normalized values to eliminate zero values. For MS^2 TIC a pseudo count of 2,753.8 was added to all normalized values. This number represents the lowest observed MS^2 TIC value in the dataset. To test for significant changes in protein abundance between treatments, the Student's t-test was performed on the normalized spectral count or MS^2 TIC values. For a protein to be included in the quantitative analysis the following requirements had to be met; there must have been at least two unique peptides in at least two out of three biological replicates and there must have been a sum of ≥ 10 spectra overall in the biological replicates. Manual validation of MS/MS spectra was performed for protein identifications that met these thresholds and showed significant ($p < 0.05$) change in abundance between treatments, but only had two unique peptide assignments. Criteria for manual spectral validation included the following: 1) a minimum of at least 3 theoretical y or b ions in consecutive order with intensities greater than 5% of the maximum intensity; 2) an absence of prominent unassigned peaks greater than 5% of the maximum intensity; and 3) indicative residue specific fragmentation, such as intense ions N-terminal to proline and immediately C-terminal to aspartate and glutamate. Fold changes were calculated as the ratio of the mean normalized SpC or MS^2 TIC for the three biological replicates for each condition.

3.3e Western blot analyses

Additional mitochondrial fractions isolated from renal proximal convoluted tubules were prepared to enable validation of the results observed by SpC and MS^2 TIC analysis. For Western blotting, control and acidotic samples containing 10 μg of protein were separated by 8 or 10% SDS-PAGE. Western blot analysis was carried out as described previously.[21] Additionally, the

rabbit polyclonal heat shock cognate 71 kDa protein (HSP7C) (Abcam) antibody was used to validate the change identified by MS^2 TIC.

3.4 Results and discussion

3.4a Protein identifications and data quality assurance

The experimental workflow beginning with mitochondrial isolation from three control and three acidotic rat kidneys is illustrated in Figure 3.1. Key to this workflow is the ability to utilize two label-free relative quantitative approaches (SpC & MS^2 TIC) from the same set of mass spectrometry data. Spectral counts, by definition, are assigned in whole number increments where the total spectral count value for a protein is the sum (total number) of all spectra assigned to peptides from that protein. Conversely, MS^2 TIC values are by definition much larger values where the summation of all the total ion current for the MS/MS spectra are averaged for the assigned peptides from a given protein. The use of this total ion current value for each tandem mass spectra allows for a more weighted value to be assigned to each spectrum. Both SpC & MS^2 TIC values can be easily extracted from any dataset without special or additional data acquisition.

Careful design of a label-free quantitative experiment is critical to accurately identify protein changes.[33, 34] One metric of quantitative data quality is that the number of proteins, peptides, and spectra identified in each sample are similar. Variance in the raw data was assessed by calculating the coefficient of variance between samples (CV). The following % CV were calculated for number of proteins identified per sample (% CV for control 4.7 and acidotic 1.4), the total spectra identified (% CV for control 15.7 and acidotic 2.5), and the total peptides identified (% CV for control 20.4 and acidotic 4.1) (Fig. 3.2). The number of identified proteins, peptides, and spectra were within 20% for all the samples, both control and acidotic. Pearson's

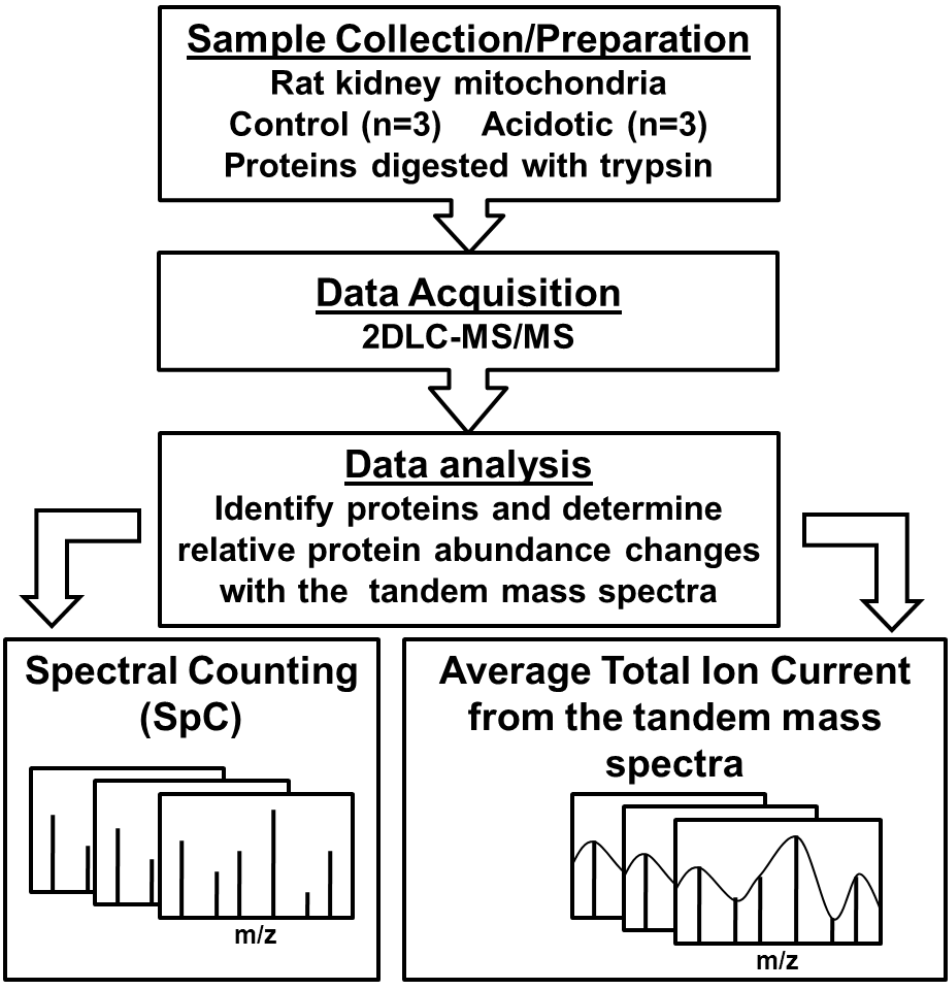

Fig. 3.1. The experimental workflow for proteomic analysis of rat renal mitochondrial proteins. Spectral counting (SpC) and average total ion current from the tandem mass spectra (MS^2 TIC) was used to determine changes in protein abundance occurring in response to metabolic acidosis.

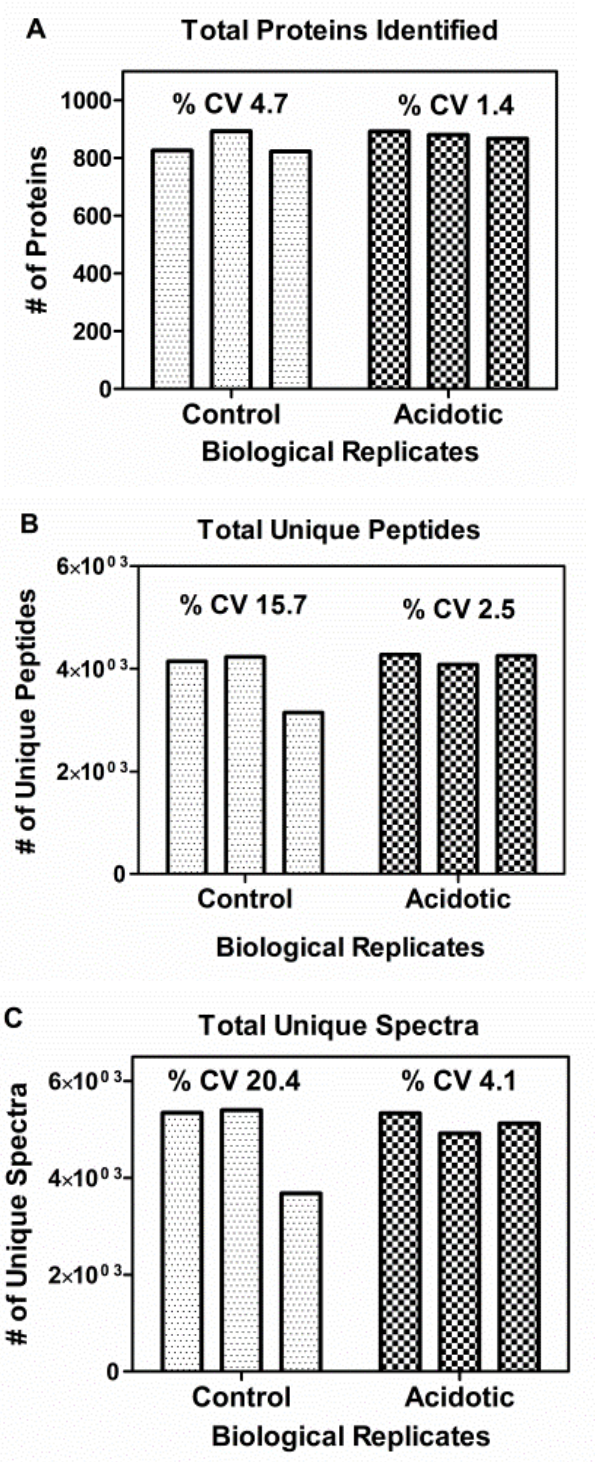

Fig. 3.2. Variance with in biological replicates represented as percent of the Coefficient of Variation (% CV) for total proteins (A), unique peptides (B), and spectra identified (C).

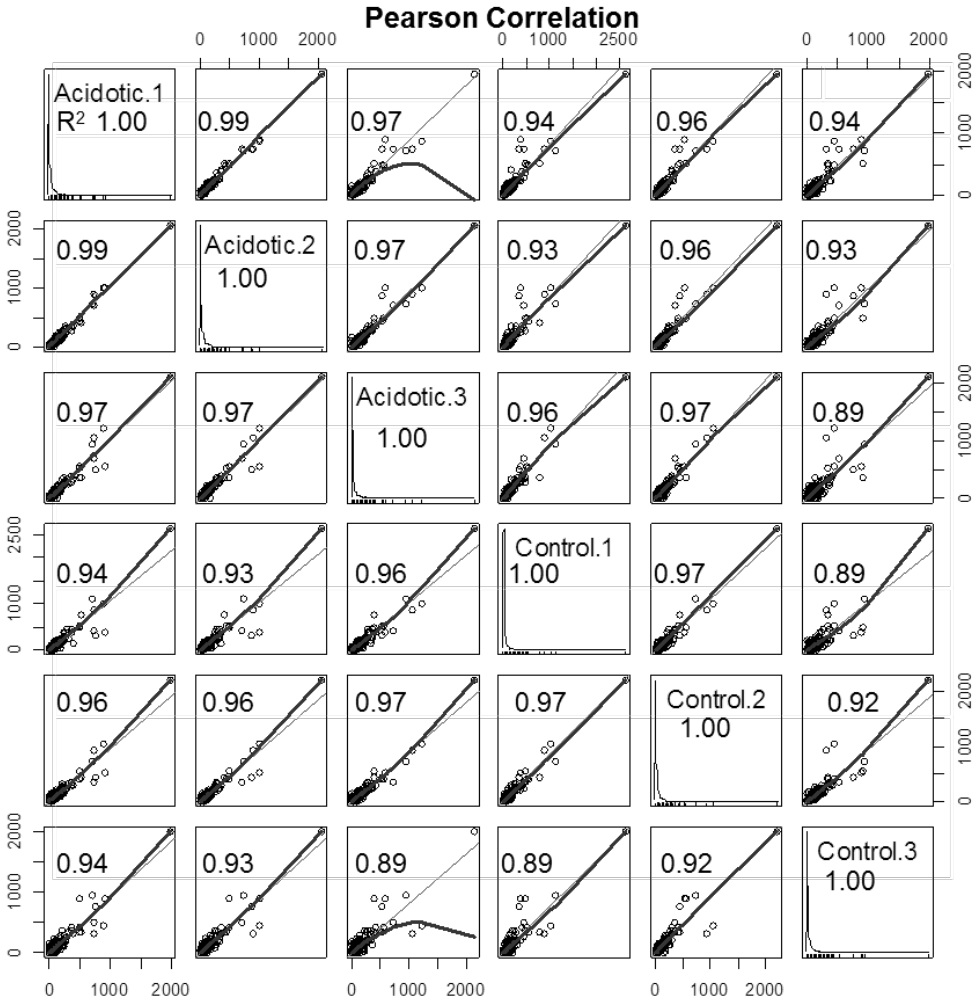

Fig. 3.3. Pearson correlation of normalized spectral counts from biological replicates control and acidotic. R^2 values for each correlation reported in each graph.

correlation calculations reported R^2 values ranging from 0.89-1.00 between all the samples (Fig. 3.3). Box plots for both pre and post-normalization of quantitative values from SpC and MS^2 TIC showed minimal variation and the effects of normalization (Fig. 3.4). Overall, the data showed acceptable qualitative features for quantitative analysis.

3.4b Label free protein quantitation

Normalization was performed on both the SpC and MS^2 TIC values to account for any analytical variations between samples. The Student's t-test was used to determine statistically significant changes in protein abundance (p-values ≤ 0.05). Each protein with a significant p-value had to meet the additional requirement of a sum of ≥ 10 spectra over the three biological replicates and have a minimum of two manually validated unique peptides in at least two biological replicates. Biological relevance is often assessed by calculating the fold change, although it relies solely on the ratio of the quantitative values, not the variance between samples. Therefore, fold changes were only calculated for those proteins meeting the above requirements and a fold change cut off was not applied.

Of the 901 proteins identified a total of 49 proteins were observed to be significantly altered (p-value < 0.05) in response to metabolic acidosis. Of these, 32 proteins were observed only in the SpC analysis (Table 3.1), 14 were observed only in the MS^2 TIC analysis (Table 3.2), and 3 were observed by both approaches (Fig. 3.5). The three common proteins, apolipoprotein A-IV, peroxisomal bifunctional enzyme (EHHADH), and glutamate dehydrogenase (GDH), are denoted in bold and italicized in the tables. Two proteins served as positive controls, KGA[23,24] and GDH [25], both of which are known to increase in abundance during acidosis.[26] In this analysis, both KGA and GDH were observed to be significantly increased upon acidosis by SpC. However, only GDH was observed to be under the significance cut off by MS^2 TIC.

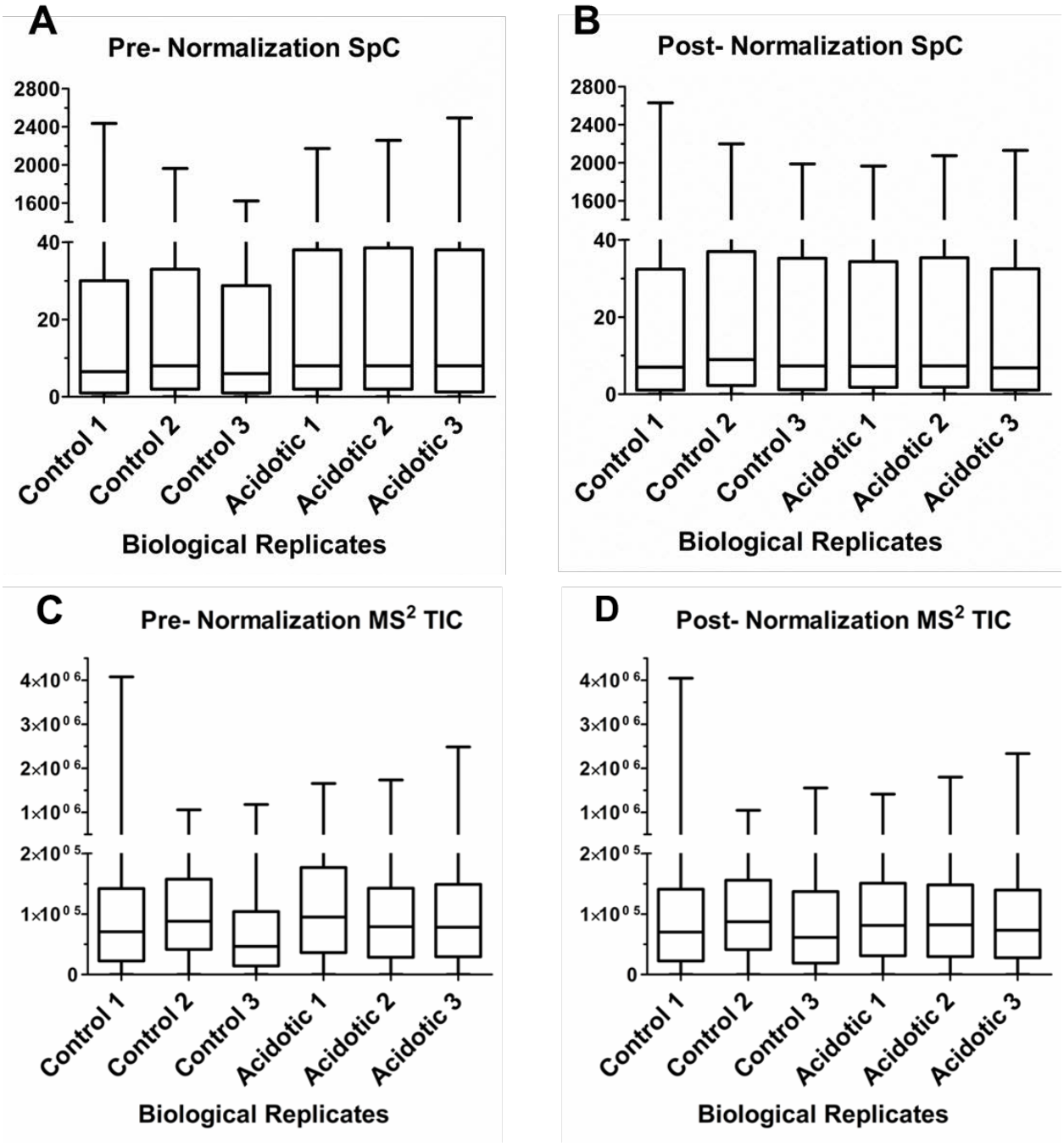

Fig. 3.4. Box plots showing dynamic range of pre and post-normalized spectral counts (SpC) or average total ion current (MS^2 TIC).

Table 3.1. Proteins Observed by SpC with Significant (p-value < 0.05) Abundance Changes in Response to Metabolic Acidosis

			Fold	Mean Normalized SpC Values			
Protein name	Accession #	P-value	Change	Control	S.E.	Acidotic	S.E.
UDP-glucuronosyltransferase 2B15	P36511	0.0002	6.4	1.8	1.0	17.0	0.7
UDP-glucuronosyltransferase 1-1 (UGT1A1)	Q64550	0.0009	4.6	11.0	1.8	54.1	4.5
Peroxisomal multifunctional enzyme type 2 (HSD17B4)	P97852	0.0018	2.0	48.1	3.6	95.3	5.3
Dimethylglycine dehydrogenase, mitochondrial	Q63342	0.0024	1.8	40.9	1.8	75.0	4.7
Glutamate dehydrogenase 1, mitochondrial (GDH)	P10860	0.0035	1.7	431.5	45.2	715.7	7.9
3-ketoacyl-CoA thiolase B, peroxisomal (ACAA1)	F1LPD6	0.0049	2.4	11.3	1.1	28.4	2.8
Enoyl-CoA hydratase domain-containing protein 3	Q3MIE0	0.0061	3.6	0.4	0.4	3.8	0.6
Vitamin D-binding protein	P04276	0.0062	2.6	15.0	4.4	40.2	1.9
Calnexin	P35565	0.0069	0.4	35.1	3.6	14.8	1.5
Catalase (CAT)	P04762	0.0095	2.2	55.1	12.0	123.1	8.3
Fumarylacetoacetate hydrolase domain-containing protein 2	B2RYW9	0.011	2.0	29.6	5.9	61.1	3.8
Ras-related protein Rab-21	Q6AXT5	0.011	4.1	1.5	0.8	9.5	1.6
Epoxide hydrolase 1	P07687	0.013	3.1	11.1	3.3	36.3	4.9
Cytochrome b5	P00173	0.014	1.7	37.5	5.8	64.7	2.8
Peroxisomal bifunctional enzyme (EHHADH)	P07896	0.014	2.1	14.3	3.5	31.5	2.0
Uncharacterized protein	D4A0Y1	0.014	4.0	1.2	0.7	7.7	1.4
Ectonucleoside triphosphate diphosphohydrolase 5	Q6P6S9	0.018	2.1	8.0	0.8	18.2	2.5
Kidney-type glutaminase (KGA)	P13264	0.019	3.2	17.7	2.1	59.3	10.7
4F2 cell-surface antigen heavy chain	Q794F9	0.02	0.5	105.6	13.0	50.5	6.8
Peroxisomal acyl-coenzyme A oxidase 1	P07872	0.021	1.9	26.2	6.8	51.4	0.5
Cytochrome P450 4A2	P20816	0.023	1.9	91.2	22.0	175.1	7.7
Filamin-B	D3ZD13	0.023	0.6	4.2	0.5	2.1	0.3
Protein AMBP	Q64240	0.024	5.0	2.0	0.9	13.8	3.2
ATP synthase-coupling factor 6, mitochondrial	P21571	0.027	0.8	115.6	4.4	96.9	3.3
Enoyl-CoA delta isomerase 1, mitochondrial	P23965	0.035	1.5	76.7	6.5	116.2	10.8
Protein FAM151A	Q642A7	0.036	0.4	32.8	6.3	11.7	2.5
ATP-binding cassette sub-family D member 3	P16970	0.037	1.8	29.3	6.3	52.5	4.0
Probable D-lactate dehydrogenase, mitochondrial	F1LVD7	0.037	1.7	27.0	4.0	45.7	4.5
GrpE protein homolog 1, mitochondrial	P97576	0.04	1.5	10.2	0.9	16.3	1.8
Apolipoprotein A-IV	P02651	0.041	1.8	46.3	10.0	83.6	7.6
All-trans-13,14-dihydroretinol saturase, isoform CRA_b	G3V7V6	0.043	4.9	0.7	0.4	7.5	2.3
NADPH--cytochrome P450 reductase	P00388	0.044	1.6	13.2	1.4	21.6	2.6
Ribonuclease 4	O55004	0.044	2.2	7.5	1.4	17.7	3.2
Electron transfer flavoprotein subunit beta	Q68FU3	0.046	1.3	93.0	9.3	125.5	6.5
Lon protease homolog, mitochondrial	Q924S5	0.049	0.7	86.5	10.1	57.5	2.7

Bold & itlaicized are common to both methods.

Table 3.2. Proteins Observed by MS^2 TIC with Significant (p-value < 0.05) Abundance Changes in Response to Metabolic Acidosis.

			Fold	Mean Normalized MS^2 TIC Values			
Protein name	Accession #	P-Value	Change	Control	S.E.	Acidotic	S.E.
Carbonic anhydrase 5B, mitochondrial (CA5B)	Q66HG6	9.9E-05	75.5	0.0E+00	0.0E+00	2.1E+05	1.3E+04
RCG41951, isoform CRA_a	D3ZCZ9	0.00073	2.2	6.2E+04	6.5E+03	1.4E+05	5.3E+03
Histone H4	P62804	0.0028	0.4	4.2E+05	2.6E+04	1.7E+05	2.9E+04
Tropomyosin alpha-3 chain	F1LRP5	0.004	0.2	5.8E+04	4.0E+03	7.5E+03	7.5E+03
Saccharopine dehydrogenase-like oxidoreductase	Q6AY30	0.0072	0.7	5.9E+04	2.0E+03	4.0E+04	3.1E+03
Uncharacterized protein	E9PT15	0.0086	1.4	2.2E+05	1.3E+04	3.1E+05	1.2E+04
Heat shock cognate 71 kDa protein (HSP7C)	P63018	0.016	0.7	2.0E+05	4.3E+03	1.4E+05	1.2E+04
EH domain-containing protein 1	Q641Z6	0.017	0.8	8.2E+04	3.7E+03	6.2E+04	3.7E+03
Peroxisomal bifunctional enzyme (EHHADH)	P07896	0.019	1.7	8.2E+04	1.7E+04	2.2E+05	1.7E+04
Glutamate dehydrogenase 1, mitochondrial (GDH)	P10860	0.022	0.9	2.0E+05	7.3E+03	1.7E+05	3.1E+03
Tubulin beta-5 chain	P69897	0.023	1.4	7.0E+04	5.8E+03	1.0E+05	5.9E+03
Apolipoprotein A-IV	P02651	0.026	1.3	1.5E+05	1.5E+03	2.0E+05	1.3E+04
Xaa-Pro aminopeptidase 1	O54975	0.028	2.1	6.2E+04	1.8E+04	1.3E+05	1.0E+04
Glutamyl aminopeptidase	P50123	0.035	0.6	1.4E+05	1.4E+04	8.8E+04	9.6E+03
Sulfate anion transporter 1	P45380	0.038	2.3	7.7E+04	1.1E+04	1.8E+05	3.1E+04
NADH dehydrogenase 1 alpha subcomplex, 8	D4A311	0.042	0.5	2.7E+05	4.7E+04	1.3E+05	9.1E+03
Triosephosphate isomerase	P48500	0.042	0.8	1.1E+05	6.4E+03	9.0E+04	3.3E+03

Bold & itlaicized are common to both methods.

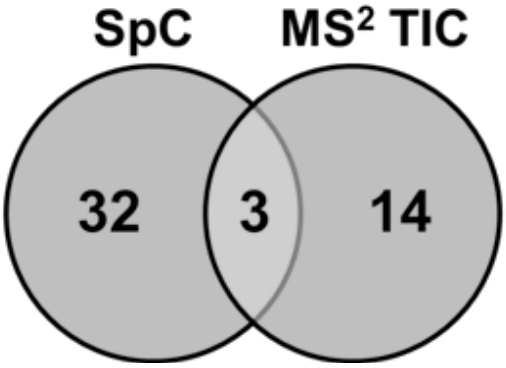

Fig. 3.5. Venn diagram of identified proteins observed to be significantly changing (p-values < 0.05) in response to metabolic acidosis using both spectral counting (SpC) and average MS/MS total ion current (MS^2 TIC).

Furthermore, the fold change observed for GDH by the MS^2 TIC method was actually a slight decrease (0.9). The significant p-value indicates that the MS^2 TIC values for GDH had very little variance among biological replicates. GDH is an extremely abundant protein in these samples (mean control MS^2 TIC = $2.0x10^5$), thus the lack of an applicable fold change is likely due to saturation of the MS^2 TIC signal (Table 3.2). While not within the significance threshold, KGA was observed to change by MS^2 TIC with a fold change of 1.3 (p-value = 0.08). Interestingly, if the significance threshold is raised to a p-value < 0.1 there are 92 proteins observed to be altered and only 9 proteins are observed to overlap between the two approaches.

Western blot analysis was performed as an independent method to validate several of the proteins observed to be significantly changing in abundance in response to metabolic acidosis. Western blotting was performed with control (n=3) and acidotic (n=3) rat renal mitochondria samples (Fig. 3.6). Blots were probed with specific antibodies to nine proteins and normalized by probing with an antibody to a mitochondrial protein that served as a loading control (Fig. 3.6 A). UDP-glucuronosyltransferase 1-1 (UGT1A1) was observed to be changing only by SpC (p-value = 0.0009, fold change = 4.6). However, Western blotting of UGT1A1 revealed a fold change of only 1.6. The larger fold change observed by SpC could be an artificial inflation due to the detection of shared peptides from other isoforms, whereas the antibody is specific only to the 1A1 isoform. Peroxisomal multifunctional enzyme type 2 (HSD17B4), 3-ketoacyl-CoA thiolase B (ACAA1), catalase (CAT), and kidney-type glutaminase (KGA) were all detected as significantly changing only by SpC. All four of these proteins yielded statistically equivalent fold changes by Western blotting with specific antibodies (Fig. 3.6 B). Two of the proteins uniquely observed by MS^2 TIC were also validated by Western blotting; carbonic anhydrase 5B (CA5B)

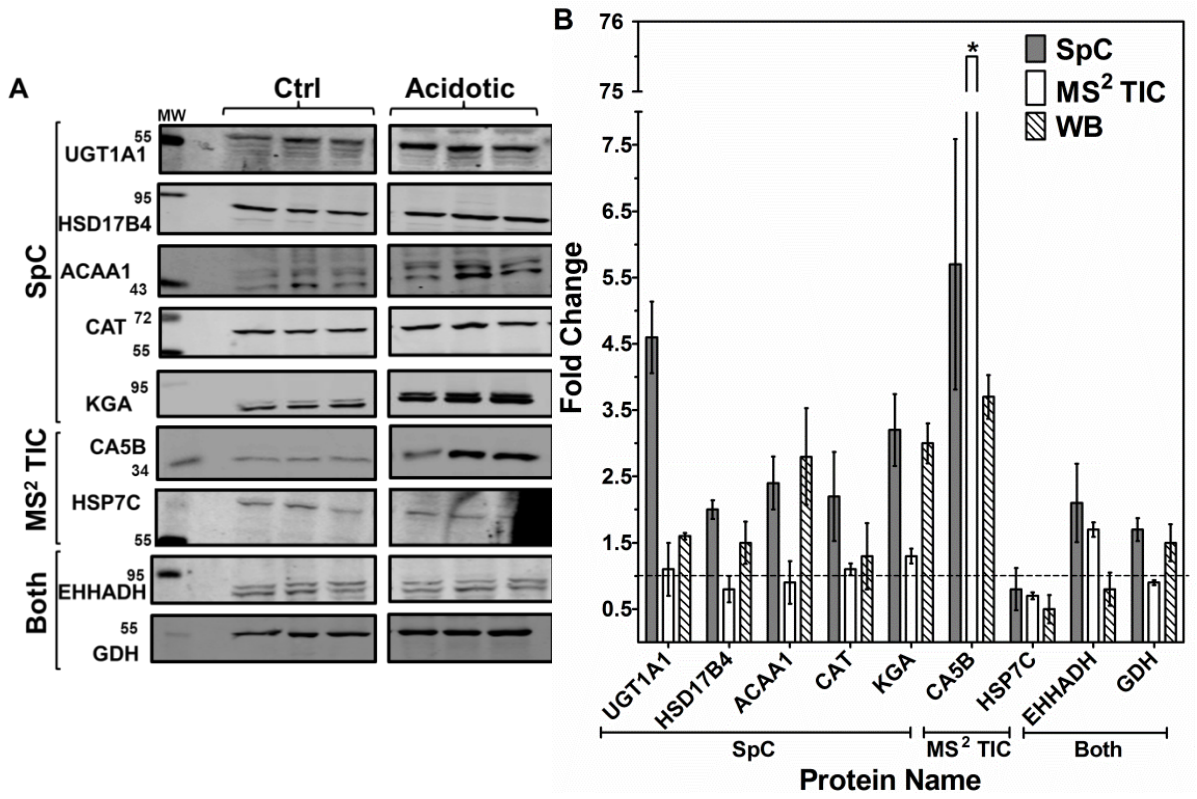

Fig. 3.6. Western blot analysis validating proteins found to be significantly changing in response to metabolic acidosis (p-values < 0.05) by either spectral counting (SpC), average total ion current (MS^2 TIC) or both. A: The control (ctrl) and acidotic samples protein bands were imaged and quantified and each blot was normalized to a loading control. The corresponding molecular weight marker is shown on left (MW). B: Fold changes from SpC, MS^2 TIC and Western blotting (WB). The reported data are the mean ± the S.E. of triplicate biological samples. The * indicates error not shown for CA5B MS^2 TIC, ± 4.8.

and heat shock cognate 71 kDa protein (HSP7C) (Fig 3.6 A). MS^2 TIC fold change for CA5B is exaggerated as this protein was not observed in control samples. CA5B narrowly fell outside the significant threshold in the SpC results, (p-value = 0.068). However, the fold change observed by SpC (5.7-fold) agrees well with the Western blotting results, (3.7-fold). CA5B had a mean spectral count value of only 4.7 in the acidotic samples and 0 in the control samples which illustrates the limitation of SpC for low abundance proteins. The decrease in HSP7C, identified uniquely by MS^2 TIC, was also confirmed by Western blotting. Of the three proteins observed by both approaches, two were further evaluated by Western blotting: peroxisomal bifunctional enzyme (EHHADH) and glutamate dehydrogenase (GDH). EHHADH did not show a significant fold change by Western blotting. This result may be due to the large amount of non-specific binding observed with this antibody. Statistically equivalent fold changes were observed by Western blot analysis and SpC for GDH.

3.4c Comparison of methods

Previous studies have shown that SpC is not accurate for proteins at low abundance (i.e. $\leq$ 4 spectral counts) and MS^2 TIC is not accurate for proteins with $\leq$ 5 identified MS/MS spectra.[15, 35, 19] To evaluate the trend within our dataset, the mean spectral counts of the triplicate acidotic samples were plotted against the calculated p-values (Fig. 3.7 A). The majority of the data is represented by proteins with < 100 spectral counts. As the spectral counts decrease the p-values tend to be less significant, illustrating the limitation of this method for proteins at low abundance. This is further represented in the inset of figure 3.7A which shows a clear shift in the distribution of proteins with p-values > 0.05, above which corresponds to proteins with very low SpC values. The range of the mean normalized SpC values for proteins with p-values < 0.05 is broad, ranging from 3.8 to 715.7. Conversely, the MS^2 TIC values do not exhibit this trend (Fig.

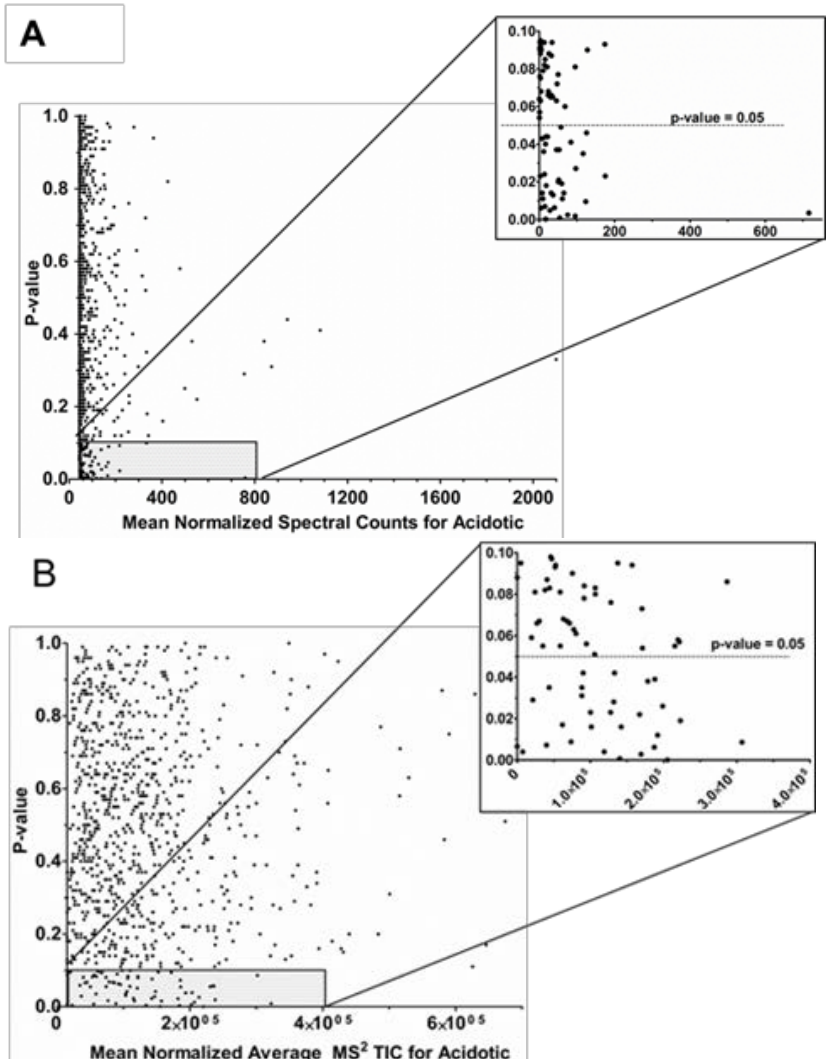

Fig. 3.7. Quantitative value vs. p-value. A: The mean SpC of triplicate acidotic samples (x-axis) vs. p-values B: The mean MS^2 TIC of triplicate acidotic samples (x-axis) vs. p-values. Both insets have only the data with p-values < 0.1 (y-axis).

3.7 B). The scale for the MS^2 TIC data is notably larger compared to the SpC data (x-axis of Fig. 3.7 A vs 3.7 B). As mentioned above, this is due to the fact that in SpC a value of 1 is assigned for each spectra whereas in MS^2 TIC the value for each protein corresponds the average ion signal of all the MS/MS spectra (a number much larger than 1). The difference in scale results in an increase of the quantifiable dynamic range of the MS^2 TIC approach.[20] The disadvantage of this larger scale is that saturation may occur at very high MS^2 TIC values. This is illustrated in Figure 3.7 B as there are no proteins with a p-value < 0.05 at MS^2 TIC mean values > $3.2x10^5$.

In this study, a significance level of p-value < 0.05 was used, but often fold changes are also useful and important in assessing biological relevance. Fold change calculations from SpC or MS^2 TIC analyses were compared to the corresponding p-values from each method (Fig. 3.8). For both approaches a convergence to a fold change of 1 was observed with increasing p-value, this trend is expected and adds confidence to the results. Additionally, the lack of data points present at a fold change of 1 with p-values < 0.05 is also encouraging. The notable difference in the data for the two approaches is that MS^2 TIC analysis results in much larger fold change values (Fig. 3.8 B is missing the top ten MS^2 TIC fold changes ranging from 20-140). The exaggerated fold changes are a result of the larger scale of MS^2 TIC values and thus the pseudo count approach is not as effective in dealing with zero values.

3.5 Conclusions

Label-free relative quantitation methods are extremely important in primary tissue experiments to further our understanding of disease states and enable biomarker discovery. Such samples are often very complex and the proteins of biological interest can be at low abundance within a high background. The ability to maximally mine proteomic data to improve our ability

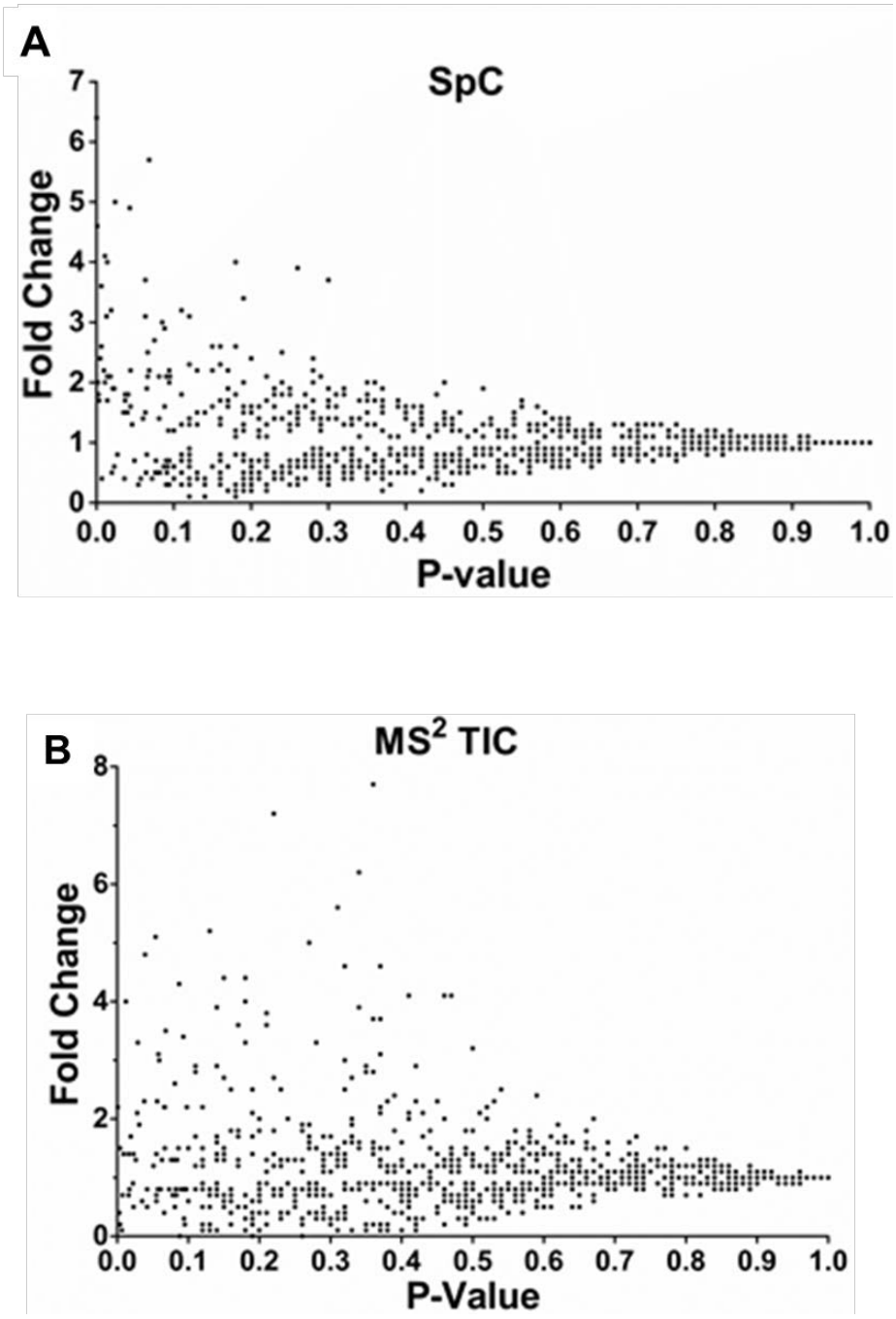

Fig. 3.8. P-value vs. fold change. A: The p-values from SpC analysis (x-axis) and the calculated fold changes (y-axis). B: The p-values from average MS^2 TIC (x-axis) and the calculated fold changes (y-axis). Ten values are not plotted here; largest fold change was 137 for MS^2 TIC.

to identify significant changes between disease states is essential. There is no current proteomic profiling strategy that is a capable of identifying the entire proteome or for determining all quantitative changes between disease states. Spectral counting is advantageous in its ease of use but can fail for proteins at low abundance. Conversely, MS^2 TIC measurements are accurate over a larger dynamic range but are subject to inaccuracies with signal saturation for highly abundant proteins. While each of these methods has specific advantages and disadvantages, together they enable a more comprehensive and accurate picture of quantitative protein changes over a wide dynamic range of protein concentrations. This study demonstrates that SpC and MS^2 TIC provide complementary information as there was little observed overlap in the results from each method. The dual approach is straightforward and requires minimal added effort to implement. Importantly, no additional samples or mass spectrometry analyses are needed to obtain both SpC and MS^2 TIC values. Therefore, the added value gained by employing a dual approach cost only the additional time for data analysis. In summary, the results of this study clearly illustrate the benefit of employing a dual label-free relative quantitative approach to enable a more comprehensive characterization of proteins in a complex biological matrix.

REFERENCES

1. Coombs, K. M., Quantitative proteomics of complex mixtures. Expert review of proteomics 2011, 8 (5), 659-77.

2. Filiou, M. D.; Turck, C. W.; Martins-de-Souza, D., Quantitative proteomics for investigating psychiatric disorders. Proteomics. Clinical applications 2011, 5 (1-2), 38-49.

3. Liang, S.; Xu, Z.; Xu, X.; Zhao, X.; Huang, C.; Wei, Y., Quantitative proteomics for cancer biomarker discovery. Comb Chem High Throughput Screen 2012, 15 (3), 221-31.

4. Zhang, Q.; Faca, V.; Hanash, S., Mining the plasma proteome for disease applications across seven logs of protein abundance. J Proteome Res 2011, 10 (1), 46-50.

5. Cravatt, B. F.; Simon, G. M.; Yates Iii, J. R., The biological impact of mass-spectrometry-based proteomics. Nature 2007, 450 (7172), 991-1000.

6. Xie, F.; Liu, T.; Qian, W. J.; Petyuk, V. A.; Smith, R. D., Liquid chromatography-mass spectrometry-based quantitative proteomics. The Journal of biological chemistry 2011, 286 (29), 25443-9.

7. Gygi, S. P.; Rist, B.; Gerber, S. A.; Turecek, F.; Gelb, M. H.; Aebersold, R., Quantitative analysis of complex protein mixtures using isotope-coded affinity tags. Nature biotechnology 1999, 17 (10), 994-9.

8. Ong, S. E.; Blagoev, B.; Kratchmarova, I.; Kristensen, D. B.; Steen, H.; Pandey, A.; Mann, M., Stable isotope labeling by amino acids in cell culture, SILAC, as a simple and accurate approach to expression proteomics. Mol Cell Proteomics 2002, 1 (5), 376-86.

9. Thompson, A.; Schäfer, J.; Kuhn, K.; Kienle, S.; Schwarz, J.; Schmidt, G.; Neumann, T.; Hamon, C., Tandem Mass Tags: A Novel Quantification Strategy for Comparative Analysis of Complex Protein Mixtures by MS/MS. Analytical Chemistry 2003, 75 (8), 1895-1904.

10. Ross, P. L.; Huang, Y. N.; Marchese, J. N.; Williamson, B.; Parker, K.; Hattan, S.; Khainovski, N.; Pillai, S.; Dey, S.; Daniels, S.; Purkayastha, S.; Juhasz, P.; Martin, S.; Bartlet-Jones, M.; He, F.; Jacobson, A.; Pappin, D. J., Multiplexed protein quantitation in Saccharomyces cerevisiae using amine-reactive isobaric tagging reagents. Mol Cell Proteomics 2004, 3 (12), 1154-69.

11. Panchaud, A.; Affolter, M.; Moreillon, P.; Kussmann, M., Experimental and computational approaches to quantitative proteomics: status quo and outlook. Journal of proteomics 2008, 71 (1), 19-33.

12. Nikolov, M.; Schmidt, C.; Urlaub, H., Quantitative mass spectrometry-based proteomics: an overview. Methods in molecular biology (Clifton, N.J.) 2012, 893, 85-100.

13. Bantscheff, M.; Schirle, M.; Sweetman, G.; Rick, J.; Kuster, B., Quantitative mass spectrometry in proteomics: a critical review. Analytical and bioanalytical chemistry 2007, 389 (4), 1017-31.

14. Liu, H.; Sadygov, R. G.; Yates, J. R., 3rd, A model for random sampling and estimation of relative protein abundance in shotgun proteomics. Anal Chem 2004, 76 (14), 4193-201.

15. Old, W. M.; Meyer-Arendt, K.; Aveline-Wolf, L.; Pierce, K. G.; Mendoza, A.; Sevinsky, J. R.; Resing, K. A.; Ahn, N. G., Comparison of label-free methods for quantifying human proteins by shotgun proteomics. Mol Cell Proteomics 2005, 4 (10), 1487-502.

16. Zhu, W.; Smith, J. W.; Huang, C. M., Mass spectrometry-based label-free quantitative proteomics. Journal of biomedicine & biotechnology 2010, 2010, 840518.

17. Wolf-Yadlin, A.; Hautaniemi, S.; Lauffenburger, D. A.; White, F. M., Multiple reaction monitoring for robust quantitative proteomic analysis of cellular signaling networks. Proc Natl Acad Sci U S A 2007, 104 (14), 5860-5.

18. Griffin, N. M.; Yu, J.; Long, F.; Oh, P.; Shore, S.; Li, Y.; Koziol, J. A.; Schnitzer, J. E., Label-free, normalized quantification of complex mass spectrometry data for proteomic analysis. Nat Biotech 2010, 28 (1), 83-89.

19. Asara, J. M.; Christofk, H. R.; Freimark, L. M.; Cantley, L. C., A label-free quantification method by MS/MS TIC compared to SILAC and spectral counting in a proteomics screen. PROTEOMICS 2008, 8 (5), 994-9.

20. Wu, Q.; Zhao, Q.; Liang, Z.; Qu, Y.; Zhang, L.; Zhang, Y., NSI and NSMT: usages of MS/MS fragment ion intensity for sensitive differential proteome detection and accurate protein fold change calculation in relative label-free proteome quantification. The Analyst 2012, 137 (13), 3146-53.

21. Freund, D. M., Prenni, J. E., Curthoys, N. P., Response of the Mitochondrial Proteome of Rat Renal Proximal Convoluted Tubules to Chronic Metabolic Acidosis. American Journal of Physiology - Renal Physiology 2013, 304(2) F145-F155.

22. Halperin, M. L., Metabolic aspects of metabolic acidosis. Clin Invest Med 1993, 16 (4), 294-305.

23. Curthoys, N. P.; Lowry, O. H., The distribution of glutaminase isoenzymes in the various structures of the nephron in normal, acidotic, and alkalotic rat kidney. J Biol Chem 1973, 248 (1), 162-8.

24. Wright, P. A.; Knepper, M. A., Phosphate-dependent glutaminase activity in rat renal cortical and medullary tubule segments. Am J Physiol 1990, 259 (6 Pt 2), F961-70.

25. Wright, P. A.; Knepper, M. A., Glutamate dehydrogenase activities in microdissected rat nephron segments: effects of acid-base loading. Am J Physiol 1990, 259 (1 Pt 2), F53-9.

26. Curthoys, N. P.; Taylor, L.; Hoffert, J. D.; Knepper, M. A., Proteomic analysis of the adaptive response of rat renal proximal tubules to metabolic acidosis. American Journal of Physiology - Renal Physiology 2007, 292 (1), F140-F147.

27. Bradford, M. M., A rapid and sensitive method for the quantitation of microgram quantities of protein utilizing the principle of protein-dye binding. Anal Biochem 1976, 72, 248-54.

28. Smith, P. K.; Krohn, R. I.; Hermanson, G. T.; Mallia, A. K.; Gartner, F. H.; Provenzano, M. D.; Fujimoto, E. K.; Goeke, N. M.; Olson, B. J.; Klenk, D. C., Measurement of protein using bicinchoninic acid. Anal Biochem 1985, 150 (1), 76-85.

29. Patel, N. A.; Crombie, A.; Slade, S. E.; Thalassinos, K.; Hughes, C.; Connolly, J. B.; Langridge, J.; Murrell, J. C.; Scrivens, J. H., Comparison of One- and Two-dimensional Liquid Chromatography Approaches in the Label-free Quantitative Analysis of Methylocella silvestris. J Proteome Res 2012, 11 (9), 4755-63.

30. Keller, A.; Nesvizhskii, A. I.; Kolker, E.; Aebersold, R., Empirical statistical model to estimate the accuracy of peptide identifications made by MS/MS and database search. Anal Chem 2002, 74 (20), 5383-92;

31. Nesvizhskii, A. I.; Keller, A.; Kolker, E.; Aebersold, R., A statistical model for identifying proteins by tandem mass spectrometry. Anal Chem 2003, 75 (17), 4646-58.

32. Elias, J. E.; Gygi, S. P., Target-decoy search strategy for increased confidence in large-scale protein identifications by mass spectrometry. Nat Methods 2007, 4 (3), 207-14.

33. Lundgren, D. H.; Hwang, S. I.; Wu, L.; Han, D. K., Role of spectral counting in quantitative proteomics. Expert review of proteomics 2010, 7 (1), 39-53.

34. Oberg, A. L.; Vitek, O., Statistical design of quantitative mass spectrometry-based proteomic experiments. J Proteome Res 2009, 8 (5), 2144-56.

35. Wong, J. W.; Sullivan, M. J.; Cagney, G., Computational methods for the comparative quantification of proteins in label-free LCn-MS experiments. Briefings in bioinformatics 2008, 9 (2), 156-65.

CHAPTER 4

Characterization of the Mitochondrial Inner Membrane Proteome of Renal Proximal Convoluted Tubules in Normal and Chronic Metabolic Acidosis Rats [3]

4.1 Summary

The renal proximal convoluted tubule responds to decreases in blood pH and bicarbonate concentration with pronounced alterations in protein expression. Previous studies have established that many of these adaptions occur in the mitochondria. To extend this study, a proteomic workflow was developed to characterize the mitochondrial inner membrane proteome of the proximal convoluted tubule in control and chronically acidotic rats. Analysis by liquid chromatography coupled with mass spectrometry confidently identified 215 proteins in the combined samples. Further proteomic analysis identified 18 peptides that contain an N-ε-acetyl-lysine of which 11 are novel sites. This study is the first proteomic characterization of the mitochondrial inner membrane proteome of the rat renal proximal convoluted tubule.

4.2 Introduction

Metabolic acidosis is a condition that is defined as a significant decrease in blood pH and bicarbonate ions.[1] During metabolic acidosis the extraction and catabolism of plasma glutamine within the renal proximal convoluted tubule increases substantially to produce ammonium and bicarbonate ions that partially restores blood pH.[2] The increased catabolism of glutamine is sustained by the remodeling of the renal proximal convoluted tubule (PCT) proteome.[3, 4, 5] Specifically, the mitochondrial matrix proteins, kidney-type glutaminase (KGA)[6, 7] and

glutamate dehydrogenase (GDH)[8] among others exhibit increased expression. Mitochondria are complex organelles comprised of an outer membrane, intermembrane space, inner membrane (MIM) and matrix. The inner membrane is the central location of the electron transport chain, ATP synthesis, and metabolite transport. Critical to glutamine catabolism is the import of glutamine into the mitochondrial matrix via an inner membrane carrier. It has been proposed that acidosis causes increased expression or activation of an unidentified mitochondrial inner membrane glutamine transporter.[9] Thus, we set out to characterize the mitochondrial inner membrane in both control and chronically acidotic rats to better characterize this mitochondrial compartment and to potentially identify the glutamine transporter. All mitochondrial inner membrane transporters belong to the SLC25 family of proteins.[10] In this study, eight SLC25 proteins were identified; however all of them have a previously identified function. Thus, while our results did not reveal a novel SLC25 protein that could be the glutamine transporter, we were able to characterize the overall proteome of the MIM. Specifically, we identified 215 MIM proteins and 18 acetylation sites in this enriched sub-fraction of mitochondria. These results represent the first comprehensive proteomic investigation of MIM in rat proximal convoluted tubules and are valuable as a resource for future studies

4.3 Materials and methods

4.3a Isolation mitochondrial inner membranes from proximal convoluted tubules

Proteomic analysis was performed on mitochondrial inner membranes (MIM) isolated from renal proximal convoluted tubules (PCT) of control rats (n=2) and 7 d acidotic rats (n=2). Control rats drank tap water and rats that were made chronically acidotic (CMA) were provided with 0.28 M NH_4Cl as their sole source of drinking water for 7 d. All of the procedures were

approved by the Institutional Animal Care and Use Committee at Colorado State University. The proximal convoluted tubule isolation and mitochondrial enrichment procedures were described in detail in Freund, *et al*.[5] Briefly, Percoll density gradient centrifugation was used to obtain the proximal convoluted tubules and differential and sucrose density centrifugation was performed to enrich for mitochondria. Once mitochondria were isolated, the pellet was resuspended in H_2O, incubated on ice for 20 min with gentle vortexing and then centrifuged at 12,000xg for 5 min.[11] The supernatant contains predominately mitochondrial intermembrane and outer membrane while the resulting pellet contains mitoplasts. The pellet and little remaining supernatant were centrifuged again at 12,000xg for 5 min to tighten the pellet and remove residual supernatant. The mitoplasts were subsequently treated with 0.1 M Na_2CO_3, pH 11.5, incubated on ice for 20 min and then centrifuged at 100,000xg for 30 min. The supernatant contains matrix proteins and the pellet is the enriched mitochondrial inner membrane fraction. The MIM fraction was resuspended in 6 M urea and stored in -80 $^{\circ}$C. Both Bradford [12] and bicinchoninic acid (Pierce) protein assays [13] were performed to determine protein concentrations subsequent to MIM fractionation. Samples containing 50 µg of protein were prepared and digested with trypsin as described previously. [5]

4.3b Mass spectrometry

The peptides were fractionated on a reverse phase column (1200 nanoHPLC, Zorbax C18, 5µm, 75 µm ID x 150mm column, Agilent) using a linear gradient from 25%-55% buffer B (buffer B = 90% acetonitrile and 0.1% formic acid) at a flow rate of 300 nl/min. Peptides were eluted directly into the mass spectrometer (LTQ linear ion trap, Thermo Scientific) and spectra were collected over a m/z range of 200-2000 Da using a dynamic exclusion limit of 3 MS/MS

spectra of a given peptide mass for 30 sec and an exclusion duration of 90 sec. The compound lists from the resulting spectra were produced using Xcalibar 2.2 software (Thermo Scientific) with an intensity threshold of 5,000 and 1 scan/group. Each biological sample was injected five times and sample order was randomized before analysis.

4.3c Bioinformatics

MS/MS spectra were searched against the Uniprot-KB *Rattus norvegicus* protein sequence database (74,140 sequence entries) concatenated with a reverse database using both the Mascot (version 2.3.02, Matrix Science) and SEQUEST (version v.27, rev. 11, Sorcerer, Sage-N Research) database search engines. The following search parameters were used: average mass, peptide mass tolerance of 2.5 Da, fragment ion mass tolerance of 1.0 Da, complete tryptic digestion allowing four missed cleavages, variable modifications of methionine oxidation and lysine acetylation, and a fixed modification of cysteine carbamidomethylation. Peptide identifications from both of the search engine results were combined using protein identification algorithms in Scaffold 3 (Version 3.6.0, Proteome Software). Peptide and protein probability thresholds of 90% and 99% were applied with Peptide and Protein Prophet algorithms in Scaffold 3.[14, 15] Proteins containing shared peptides were grouped by Scaffold 3 to satisfy the laws of parsimony. A peptide false discovery rate (FDR) of 0.2% was determined by the target decoy approach of searching the reversed database.[16] Only proteins that were identified by a minimum of 2 unique peptides in at least 1 biological replicate were considered confidently identified. Gene Ontology (GO) terms for cellular locations and processes were extracted from Scaffold 3. Additional functional information on the identified proteins was manually determined from Uniprot-KB database (www.uniprot.org). Manual validation of MS/MS spectra was

performed for protein identifications that met the initial thresholds that were based on two unique peptides for identified proteins and for all acetylated peptides. Criteria for manual validation included the following: 1) a minimum of at least 3 theoretical y or b ions in consecutive order that are peaks greater than 5% of the maximum intensity; 2) an absence of prominent unassigned peaks greater than 5% of the maximum intensity; and 3) indicative residue specific fragmentation, such as intense ions N-terminal to proline and immediately C-terminal to aspartate and glutamate

4.4d Western blot analysis

For Western blotting, mitochondrial inner membrane samples containing 10 μg of protein were separated by 4-20% gradient SDS-PAGE (BioRad). Proteins were transferred to polyvinylidenedifluoride membranes (Immobilon-FL, Millipore) and the blots were incubated overnight with a rabbit anti-acetylated-lysine (K-Ac^2-100) antibody (Cell Signaling) and a mouse monoclonal antibody to the 70 kDa subunit of mitochondrial succinate dehydrogenase (SDH) (MitoSciences) that was used as a loading control. Either 680 Dylight-conjugated goat anti-mouse IgG or 800 Dylight-conjugated goat anti-rabbit IgG (Pierce) was used as a secondary antibody. The resulting bands were visualized and quantified using an Odyssey Infrared Imager (LI-COR Biosciences).

4.4 Results and discussion

4.4a Proteomic profiling of mitochondrial inner membrane fractions from control and 7 d chronically acidotic rats

A large scale proteomic profiling of the mitochondrial inner membrane (MIM) of the renal proximal convoluted tubule from control (n=2) and 7 d chronic acidotic (n=2) rats was conducted. Figure 4.1 illustrates the experimental workflow which begins with isolating proximal convoluted tubules from renal cortex of control and chronically acidotic (CMA) rats by Percoll density centrifugation. Mitochondria were then isolated from the tubules by differential and sucrose density gradient centrifugation. Mitoplasts were obtained by mechanical disruption of the outer membrane and alkali treatment was used to isolate the inner membrane.[11] The MIM proteins were then digested with trypsin and analyzed by liquid chromatography coupled with tandem mass spectrometry (LC-MS/MS). The resulting tandem mass spectra were searched against Uniprot-KB Rat protein sequence database with Mascot and SEQUEST search engines. Protein identifications were compiled and validated in Scaffold 3. A total of 215 total proteins were identified in all samples with a peptide FDR of 0.2%. The number of predicted transmembrane domains was determined for each protein using TMHMM 2.0.[17] This analysis identified 66 proteins (31%) that have 1 to 15 predicted transmembrane helices. This percentage is greater than the 20% identified in the analysis of whole mitochondria isolated from proximal convoluted tubules.[5] Identifying a greater number of proteins with predicted transmembrane helices indicates that the MIM samples are enriched for membrane proteins to a greater extent than the whole mitochondria. Table 4.1 lists the identified proteins and the mean unweighted spectral counts identified in the samples from control and CMA rats. Of the 215 total proteins identified in the combined samples; 118 were common in both samples, while 89 and 8 were

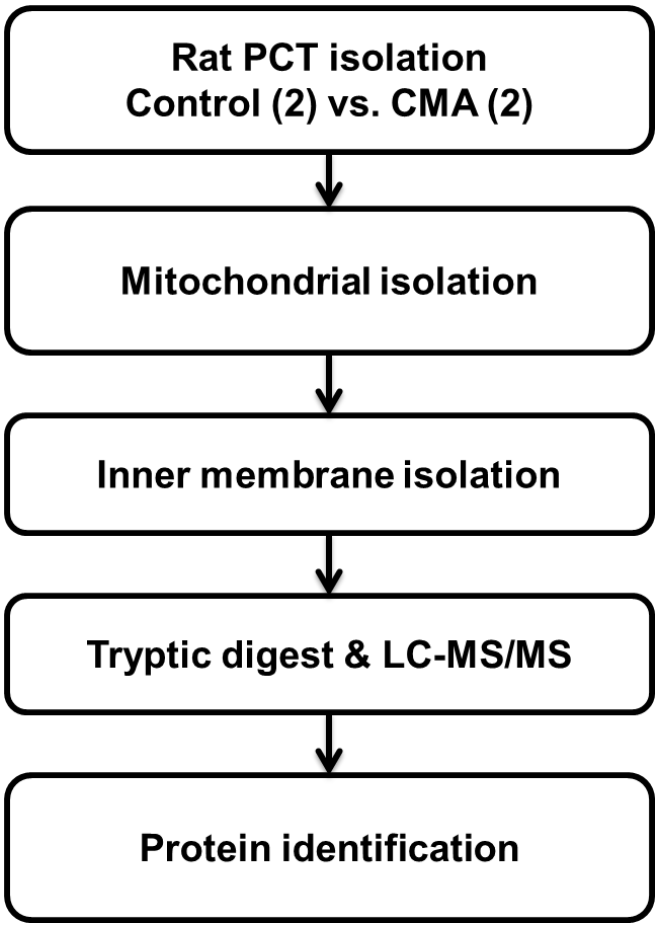

Fig. 4.1. Experimental workflow - Proximal convoluted tubules (PCT) were isolated from two control and two 7-d chronic acidotic rats (CMA). Mitochondria were isolated from the tubules by differential and sucrose gradient centrifugations. Mitochondrial inner membrane was enriched by hypotonic shock and subsequent alkaline treatment. Following tryptic digestion, the resulting peptides were analyzed by liquid chromatography (LC) coupled directly with tandem mass spectrometry (MS/MS). Proteins were identified by searching the mass spectra versus the Uniprot-KB Rat protein sequence database.

Table 4.1. Control and Acidotic Rat Mitochondrial Inner Membrane Proximal Convoluted Tubule Proteome

				Unweighted mean spectral counts				Predicted
Proteins identified (215)	**Gene Name**	**Accession #**	**Mass, kDa**	**Ctrl**	**Ctrl S.E.**	**CMA**	**CMA S.E.**	**TMD**
10 kDa heat shock protein, mitochondrial	Hspe1	P26772	11	4	4	3	3	
28S ribosomal protein S35, mitochondrial	Mrps35	D4A9Z6	36	1	1	0	0	
2-oxoglutarate dehydrogenase, mitochondrial	Ogdh	F8WGA5	118	27	4	32	13	
3-hydroxyacyl-CoA dehydrogenase type-2	Hsd17b10	F1LNT4	28	7	7	10	5	
3-hydroxyisobutyrate dehydrogenase, mitochondrial	Hibadh	P29266	35	5	5	0	0	
3-ketoacyl-CoA thiolase, mitochondrial	Acaa2	F1LWF9	42	52	2	17	2	
3-mercaptopyruvate sulfurtransferase	Mpst	P97532	33	38	4	34	7	
4-aminobutyrate aminotransferase, mitochondrial	Abat	D3ZL20	50	12	5	3	3	
4F2 cell-surface antigen heavy chain isoform 2	Slc3a2	Q794F9	58	12	9	4	4	1
4-nitrophenylphosphatase domain and non-neuronal SNAP25-like protein homolog 1	Nipsnap1	D4A867	37	5	0	0	0	
60 kDa heat shock protein, mitochondrial	Hspd1	P63039	61	86	9	37	21	
78 kDa glucose-regulated protein	Hspa5	P06761	72	2	2	0	0	
Acetyl-CoA acetyltransferase, mitochondrial	Acat1	P17764	45	54	8	43	2	
Aconitate hydratase, mitochondrial	Aco2	Q9ER34	85	79	20	97	40	
Actin, cytoplasmic 1	Actb	P60711	42	11	5	6	6	
Acyl-coenzyme A synthetase ACSM2, mitochondrial	Acsm2	O70490	64	45	14	37	6	
Acyl-coenzyme A thioesterase 2, mitochondrial	Acot2	O55171	50	9	5	0	0	
Acylpyruvase FAHD1, mitochondrial	Fahd1	F1M7U1	25	8	3	0	0	
Adenylate kinase isoenzyme 4, mitochondrial	Ak4	F8WG98	38	32	1	13	1	
ADP/ATP translocase 1	Slc25a4	Q05962	33	174	3	122	9	4
ADP/ATP translocase 2	Slc25a5	Q09073	33	313	6	177	10	2
Alanine--glyoxylate aminotransferase 2, mitochondrial	Agxt2	Q64565	57	41	21	18	7	
Alcohol dehydrogenase [NADP(+)]	Akr1a1	P51635	37	5	2	0	0	
Aldehyde dehydrogenase, mitochondrial	Aldh2	P11884	56	64	2	58	5	
Alpha-aminoadipic semialdehyde dehydrogenase	Aldh7a1	Q64057	59	21	2	16	8	
Alpha-aminoadipic semialdehyde synthase, mitochondrial	Aass	A2VCW9	103	0	0	23	16	
Alpha-enolase	Eno1	P04764	47	2	2	0	0	
Amine oxidase [flavin-containing] B	Maob	P19643	58	3	3	0	0	1
Aminopeptidase N	Anpep	P15684	109	49	11	13	1	1
Apoptosis-inducing factor 1, mitochondrial	Aifm1	Q9JM53	67	10	1	0	0	
Aquaporin-1	Aqp1	P29975	29	4	4	0	0	6
Aspartate aminotransferase, mitochondrial	Got2	P00507	47	17	1	6	1	
ATP synthase subunit alpha, mitochondrial	Atp5a1	P15999	60	219	29	195	52	
ATP synthase subunit b, mitochondrial	Atp5f1	P19511	29	55	19	37	3	
ATP synthase subunit beta, mitochondrial	Atp5b	P10719	56	247	77	129	16	
ATP synthase subunit d, mitochondrial	Atp5h	P31399	19	158	25	105	4	
ATP synthase subunit delta, mitochondrial	Atp5d	P35434	18	16	4	0	0	
ATP synthase subunit e, mitochondrial	Atp5i	P29419	8	14	1	4	4	
ATP synthase subunit f, mitochondrial	Atp5j2	D3ZAF6	10	41	11	9	9	1
ATP synthase subunit g, mitochondrial	Atp5l	Q6PDU7	11	23	4	4	4	
ATP synthase subunit gamma, mitochondrial	Atp5c1	P35435	30	38	11	8	0	
ATP synthase subunit O, mitochondrial	Atp5o	Q06647	23	37	1	22	4	
ATP synthase-coupling factor 6, mitochondrial	Atp5j	P21571	12	2	2	0	0	
ATPase family AAA domain-containing protein 3	Atad3	Q3KRE0	67	1	1	0	0	
ATP-binding cassette sub-family D member 3	Abcd3	P16970	75	9	2	4	2	3
Basigin isoform 1	Bsg	F1M6R2	30	14	10	0	0	1
Biphenyl hydrolase-like (Serine hydrolase)	Bphl	Q3B8N9	33	2	2	0	0	
Calnexin	Canx	P35565	67	15	3	0	0	1
Carnitine O-palmitoyltransferase 1, liver isoform	Cpt1a	P32198	88	2	2	0	0	1
Catechol O-methyltransferase domain-containing protein 1	Comtd1	D3ZM21	29	9	2	2	2	1
CDGSH iron-sulfur domain-containing protein 1	Cisd1	B0K020	12	17	2	0	0	1
Choline dehydrogenase, mitochondrial	Chdh	Q6UPE0	66	7	7	5	2	
Citrate synthase, mitochondrial	Cs	G3V936	52	1	1	0	0	
Coiled-coil-helix-coiled-coil-helix domain-containing protein 3, mitochondrial	Chchd3	D3ZUX5	26	15	4	10	3	
Collectrin	Tmem27	Q9ESG3	25	6	6	11	3	1
Cubilin	Cubn	O70244	399	3	3	0	0	
Cytochrome b5 type B	Cyb5b	P04166	16	14	2	0	0	1
Cytochrome b-c1 complex subunit 1, mitochondrial	COII	Q8SEZ5	26	72	19	20	3	2
Cytochrome b-c1 complex subunit 1, mitochondrial	Uqcrc1	Q68FY0	53	55	5	46	15	
Cytochrome b-c1 complex subunit 2, mitochondrial	Uqcrc2	P32551	48	84	19	63	21	
Cytochrome b-c1 complex subunit Rieske, mitochondrial	Uqcrfs1	P20788	29	5	5	2	2	
Cytochrome c oxidase subunit 4 isoform 1, mitochondrial	Cox4i1	P10888	20	54	10	44	1	1
Cytochrome c oxidase subunit 5A, mitochondrial	Cox5a	P11240	16	37	10	18	5	
Cytochrome c oxidase subunit 5B, mitochondrial	Cox5b	P12075	14	2	2	0	0	
Cytochrome c oxidase subunit 6C-2	Cox6c2	P11951	8	23	14	8	1	1
Cytochrome c-1	Cyc1	D3ZFQ8	35	23	1	18	3	
Cytochrome P450 2C23	Cyp2c23	P24470	56	14	2	5	5	1
Cytochrome P450 4A2	Cyp4a2	D3ZRJ1	58	3	3	6	2	2
Cytochrome P450 4A2	Cyp4a2	P20816	58	3	3	13	13	1
D-amino-acid oxidase	Dao	O35078	39	2	2	0	0	
Delta-1-pyrroline-5-carboxylate dehydrogenase, mitochondrial	Aldh4a1	P0C2X9	62	39	2	38	14	
Dihydrolipoamide S-succinyltransferase (E2 component of 2-oxo-glutarate complex), CRA_a	Dlst	G3V6P2	49	29	3	33	3	
Dihydrolipoyl dehydrogenase, mitochondrial	Dld	Q6P6R2	54	29	7	0	0	

Dihydrolipoyllysine-residue acetyltransferase component of pyruvate Dehydrogenase complex	Dlat	P08461	67	63	15	51	2	
Dimethylaniline monooxygenase [N-oxide-forming] 1	Fmo1	P36365	60	2	2	0	0	1
Dimethylglycine dehydrogenase, mitochondrial	Dmgdh	Q63342	96	1	1	0	0	
Dipeptidyl peptidase 4	Dpp4	P14740	88	13	13	6	1	1
DNA polymerase epsilon catalytic subunit A	Pole	D3Z8X4	262	0	0	1	1	
E3 ubiquitin-protein ligase SMURF1	Smurf1	D3ZCF5	83	0	0	2	2	
Electrogenic sodium bicarbonate cotransporter 1	Slc4a4	Q9JI66	116	6	6	0	0	9
Electron transfer flavoprotein subunit alpha, mitochondrial	Etfa	P13803	35	26	1	15	5	
Electron transfer flavoprotein subunit beta	Etfb	Q68FU3	28	2	2	0	0	
Electron transfer flavoprotein-ubiquinone oxidoreductase, mitochondrial	Etfdh	Q6UPE1	68	16	1	9	3	
Elongation factor Tu, mitochondrial	Tufm	P85834	50	20	2	6	6	
Enoyl-CoA delta isomerase 1, mitochondrial	Eci1	P23965	32	14	1	20	7	
Enoyl-CoA hydratase, mitochondrial	Echs1	P14604	32	15	15	17	17	
Ezrin	Ezr	P31977	69	5	5	0	0	
Fructose-bisphosphate aldolase B	Aldob	Q66HT1	40	10	4	0	0	
Fumarate hydratase, mitochondrial	Fh	P14408	50	12	0	0	0	
Fumarylacetoacetate hydrolase domain-containing protein 2	Fahd2	B2RYW9	35	2	2	0	0	
Gamma-glutamyltranspeptidase 1	Ggt1	P07314	62	10	10	19	5	1
Glutamate dehydrogenase 1, mitochondrial	Glud1	P10860	61	34	1	72	20	
Glutamyl aminopeptidase	Enpep	P50123	108	4	4	0	0	1
Glutathione peroxidase 1	Gpx1	P04041	22	6	6	7	7	
Glycine amidinotransferase, mitochondrial	Gatm	P50442	48	135	6	43	17	
Glycine dehydrogenase [decarboxylating], mitochondrial	Gldc	D3ZJJ9	114	0	0	7	7	
Glycine N-acyltransferase	Glyat	Q5PQT3	34	27	3	3	3	
Histidine triad nucleotide binding protein 2	Hint2	D4AB01	17	3	3	0	0	
Hydroxyacid oxidase 2	Hao2	Q07523	39	14	1	12	3	
Hydroxyacyl-coenzyme A dehydrogenase, mitochondrial	Hadh	Q9WVK7	34	31	13	19	1	
Isocitrate dehydrogenase [NAD] subunit alpha, mitochondrial	Idh3a	F1LNF7	40	3	3	5	5	
Isocitrate dehydrogenase [NAD] subunit beta, mitochondrial	Idh3B	Q68FX0	42	12	12	0	0	
Isocitrate dehydrogenase [NADP], mitochondrial	Idh2	P56574	51	68	9	55	20	
Kynurenine 3-monooxygenase	Kmo	D4A5K4	50	4	4	0	0	2
Kynurenine/alpha-aminoadipate aminotransferase, mitochondrial	Aadat	Q64602	48	8	6	0	0	
LETM1 and EF-hand domain-containing protein 1, mitochondrial	Letm1	Q5XIN6	83	27	13	3	3	1
Leucine-rich PPR motif-containing protein, mitochondrial	Lrpprc	Q5SGE0	157	1	1	0	0	
Liver carboxylesterase	NA	Q64573	62	4	4	0	0	
Long-chain specific acyl-CoA dehydrogenase, mitochondrial	Acadl	P15650	48	3	0	0	0	
Long-chain-fatty-acid--CoA ligase 1	Acsl1	P18163	78	4	1	0	0	1
Low-density lipoprotein receptor-related protein 2	Lrp2	P98158	519	129	41	76	2	1
Lysosome-associated membrane glycoprotein 1	Lamp1	F1MA33	44	3	3	0	0	1
Malate dehydrogenase, mitochondrial	Mdh2	P04636	36	66	13	37	9	
Medium-chain specific acyl-CoA dehydrogenase, mitochondrial	Acadm	P08503	47	1	1	3	3	
Membrane-associated progesterone receptor component 1	Pgrmc1	D3ZJS0	25	3	3	0	0	2
Methylcrotonoyl-CoA carboxylase beta chain, mitochondrial	Mccc2	Q5XIT9	62	1	1	7	7	
Methylmalonate-semialdehyde dehydrogenase [acylating], mitochondrial	Aldh6a1	G3V7J0	58	79	28	99	18	1
Microsomal glutathione S-transferase 3	Mgst3	D4ADS4	17	8	8	0	0	4
Mitochondrial 2-oxoglutarate/malate carrier protein	Slc25a11	G3V6H5	34	22	1	17	3	
Mitochondrial carrier homolog 2	Mtch2	B0BN52	34	8	5	4	4	
Mitochondrial dicarboxylate carrier	Slc25a10	O89035	31	41	7	44	9	
Mitochondrial import inner membrane translocase subunit TIM44	Timm44	G3V640	51	1	1	0	0	
Mitochondrial inner membrane protein	Immt	D3ZSD1	87	38	10	10	3	
Mitochondrial ornithine transporter 1	Slc25a15	D4A575	33	2	2	0	0	
MOSC domain-containing protein 2, mitochondrial	40970	O88994	38	17	5	0	0	1
Mucin and cadherin like, isoform CRA_c	Mucdhl	D3ZIC6	73	4	4	0	0	1
NAD(P) transhydrogenase, mitochondrial	Nnt	Q5BJZ3	114	57	17	28	5	12
NADH dehydrogenase (ubiquinone) 1 alpha subcomplex, 12	Ndufa12	F1LXA0	18	3	1	0	0	
NADH dehydrogenase [ubiquinone] 1 alpha subcomplex subunit 10, mitochondrial	Ndufa10	Q561S0	40	4	4	0	0	
NADH dehydrogenase [ubiquinone] 1 alpha subcomplex subunit 11	Ndufa11	Q80W89	15	1	1	0	0	2
NADH dehydrogenase [ubiquinone] 1 alpha subcomplex subunit 4	Ndufa4	B2RZD6	9	7	7	12	0	1
NADH dehydrogenase [ubiquinone] 1 alpha subcomplex subunit 8	Ndufa8	D4A311	20	10	3	11	1	
NADH dehydrogenase [ubiquinone] 1 alpha subcomplex subunit 9, mitochondrial	Ndufa9	Q5BK63	43	15	3	26	7	
NADH dehydrogenase [ubiquinone] 1 beta subcomplex subunit 10	Ndufb10	D4A0T0	21	72	25	71	7	
NADH dehydrogenase [ubiquinone] 1 beta subcomplex subunit 11, mitochondrial	Ndufb11	D4A7L4	18	2	2	0	0	1
NADH dehydrogenase [ubiquinone] 1 beta subcomplex subunit 5, mitochondrial	Ndufb5	D4A565	22	12	4	2	2	1
NADH dehydrogenase [ubiquinone] 1 beta subcomplex subunit 6	Ndufb6	D3ZDC3	12	14	8	0	0	
NADH dehydrogenase [ubiquinone] 1 beta subcomplex subunit 7	Ndufb7	D3ZLT1	17	4	4	0	0	
NADH dehydrogenase [ubiquinone] 1 beta subcomplex subunit 8, mitochondrial	Ndufb8	B2RYS8	22	6	6	0	0	
NADH dehydrogenase [ubiquinone] 1 subunit C2	Ndufc2	Q5PQZ9	14	15	10	14	14	1
NADH dehydrogenase [ubiquinone] flavoprotein 1, mitochondrial	Ndufv1	Q5XIH3	51	4	4	0	0	
NADH dehydrogenase [ubiquinone] flavoprotein 2, mitochondrial	Ndufv2	P19234	27	5	2	0	0	
NADH dehydrogenase [ubiquinone] iron-sulfur protein 3, mitochondrial	Ndufs3	D3ZG43	30	14	4	4	4	
NADH dehydrogenase [ubiquinone] iron-sulfur protein 7, mitochondrial	Ndufs7	Q5RJN0	24	4	4	0	0	
NADH-cytochrome b5 reductase 3	Cyb5r3	P20070	35	7	4	0	0	
NADH-ubiquinone oxidoreductase 75 kDa subunit, mitochondrial	Ndufs1	Q66HF1	79	15	2	7	2	
NADH-ubiquinone oxidoreductase chain 5	NADH5	Q8SEZ0	69	5	1	7	0	15
NADPH--cytochrome P450 reductase	Por	P00388	77	2	2	0	0	1

Neutral and basic amino acid transport protein rBAT	Slc3a1	Q64319	79	1	1	0	0	1
Omega-amidase NIT2	Nit2	Q497B0	31	2	2	0	0	
Ornithine aminotransferase, mitochondrial	Oat	P04182	48	16	3	16	8	
PDZK1-interacting protein 1	Pdzk1ip1	Q923S2	12	2	2	0	0	1
Phosphate carrier protein, mitochondrial isoform 2	Slc25a3	G3V741	40	92	18	57	18	2
PREDICTED: NADH dehydrogenase [ubiquinone] 1 beta subcomplex subunit 3-like	LOC100361144	D4A4P3	11	2	2	0	0	
PREDICTED: pyruvate dehydrogenase E1 component subunit alpha, mitochondrial-like	LOC685778	D4A5G8	43	1	1	0	0	
PREDICTED: tubulin alpha-1B chain	Tuba1b	D4A8I4	50	10	10	5	5	
Probable 4-hydroxy-2-oxoglutarate aldolase, mitochondrial	Hoga1	D4A2K1	34	34	5	28	1	
Prohibitin	Phb	P67779	30	86	25	93	6	
Prohibitin-2	Phb2	Q5XIH7	33	69	24	57	3	
Protein FAM151A	Fam151a	Q642A7	67	3	3	0	0	1
Pyridine nucleotide-disulfide oxidoreductase domain-containing protein 2	Pyroxd2	Q68FT3	63	43	2	56	17	
Pyruvate carboxylase, mitochondrial	Pc	P52873	130	94	7	70	3	
Pyruvate dehydrogenase E1 component subunit beta, mitochondrial	Pdhb	P49432	39	25	10	7	7	
Ras-related protein Rab-14	Rab14	B0BMW0	24	2	2	0	0	
Ras-related protein Rab-1A	Rab1	E9PU16	34	5	5	0	0	
Ras-related protein Rab-2A	Rab2a	F1LP82	24	1	1	1	1	
Ras-related protein Rab-5C	Rab5c	B0BNK1	23	9	3	0	0	
Ras-related protein Rab-7a	Rab7a	P09527	24	14	6	8	1	
Ras-related protein Rap-1A	Rap1a	P62836	21	0	0	5	3	
RCG20363, isoform CRA_a	Mosc1	G3V6I4	38	9	4	5	5	1
RCG38845, isoform CRA_b rCG_38845	rCG_38845	D3ZE15	17	35	11	8	2	1
Ribonuclease UK114	Hrsp12	F8WFW1	14	0	0	3	3	
Saccharopine dehydrogenase-like oxidoreductase	Sccpdh	Q6AY30	47	7	7	0	0	1
Serine hydroxymethyltransferase, mitochondrial	Shmt2	Q5U3Z7	56	0	0	2	2	
Sideroflexin 2	Sfxn2	G3V8N0	36	3	3	0	0	4
Sideroflexin-1	Sfxn1	Q63965	36	51	4	46	4	2
Sodium/glucose cotransporter 2	Slc5a2	F1LMI6	73	15	10	7	2	14
Sodium/potassium-transporting ATPase subunit alpha-1	Atp1a1	P06685	113	141	12	90	8	10
Sodium/potassium-transporting ATPase subunit alpha-4	Atp1a4	Q64541	114	4	4	0	0	10
Sodium/potassium-transporting ATPase subunit beta-1	Atp1b1	P07340	35	18	10	11	6	1
Sodium-dependent neutral amino acid transporter B(0)AT1	Slc6a19	D4A4Q0	57	2	2	0	0	10
Solute carrier family 22 member 1	Slc22a1	D4A656	62	2	2	0	0	12
Sorting and assembly machinery component 50 homolog	Samm50	Q6AXV4	52	20	0	18	1	
Stomatin-like protein 2	Stoml2	Q4FZT0	38	23	4	20	9	
Stress-70 protein, mitochondrial	Hspa9	P48721	74	26	2	10	5	
Succinate dehydrogenase [ubiquinone] flavoprotein subunit, mitochondrial	Sdha	Q920L2	72	20	4	21	7	
Succinate dehydrogenase [ubiquinone] iron-sulfur subunit, mitochondrial	Sdhb	P21913	32	2	2	0	0	
Succinyl-CoA ligase [GDP-forming] subunit beta, mitochondrial	Suclg2	F1LPV8	30	19	6	4	2	
Succinyl-CoA:3-ketoacid coenzyme A transferase 1, mitochondrial	Oxct1	B2GV06	56	20	4	8	8	
Sushi domain-containing protein 2	Susd2	D3ZEV8	90	11	11	11	0	
Synaptojanin-2-binding protein	Synj2bp	Q9WVJ4	16	2	2	0	0	1
Thioredoxin-dependent peroxide reductase, mitochondrial	Prdx3	G3V7I0	28	2	2	0	0	
Thiosulfate sulfurtransferase	Tst	P24329	33	22	2	14	10	
Transmembrane emp24 domain-containing protein 10	Tmed10	F1LYL3	17	2	2	0	0	1
Tricarboxylate transport protein, mitochondrial	Slc25a1	P32089	34	9	9	0	0	
Trifunctional enzyme subunit alpha, mitochondrial	Hadha	Q64428	83	24	1	27	7	
Tubulin beta-5 chain	Tubb5	P69897	50	6	6	0	0	
UDP-glucuronosyltransferase 1-1	Ugt1a1	Q64550	60	4	0	0	0	2
Uncharacterized protein	LOC100360985	F1LX07	26	5	5	0	0	
Uncharacterized protein	NA	D4A3J6	204	18	14	10	4	1
Uncharacterized protein	NA	D3ZE29	32	67	67	49	49	2
Uncharacterized protein	NA	D3ZEA8	920	0	0	2	2	
Uncharacterized protein	NA	F1LQZ1	36	8	8	0	0	
Uncharacterized protein	Slc25a13	F1LZW6	74	136	23	119	20	
Uncharacterized protein	Ubc	F1LML2	91	2	2	0	0	
Uncharacterized protein	NA	D4AD84	29	27	10	8	8	
Uncharacterized protein	NA	D4A0Q0	14	29	18	9	1	
Very long-chain acyl-CoA synthetase	Slc27a2	D3ZUP3	71	1	1	0	0	2
Very long-chain specific acyl-CoA dehydrogenase, mitochondrial	Acadvl	P45953	71	12	4	2	2	
Voltage-dependent anion-selective channel protein 1	Vdac1	Q9Z2L0	31	121	11	144	2	
Voltage-dependent anion-selective channel protein 2	Vdac2	F1LQJ3	32	21	0	21	5	
V-type proton ATPase 116 kDa subunit a isoform 4	Atp6v0a4	D3ZY90	95	7	7	0	0	6
V-type proton ATPase catalytic subunit A	Atp6v1a	D4A133	68	3	3	0	0	
V-type proton ATPase subunit B, brain isoform	Atp6v1b2	P62815	57	2	2	0	0	
Xaa-Pro aminopeptidase 2	Xpnpep2	Q99MA2	76	5	1	2	2	

Ctrl = Control, S.E. = Standard Error, CMA = Chronic Metabolic Acidosis, TMD= transmembrane domains

unique to the control and acidotic samples, respectively (Fig. 4.2 A). Gene Ontology (GO) terms were annotated by Scaffold 3 to acquire known cellular locations and functions for the identified proteins. Cellular locations are shown as a percent of the 176 proteins that had an annotated GO term (Fig. 4.2 B). The vast majority (132 proteins, or 78%) of the annotated proteins were identified as mitochondrial and all other organelles represented a very small proportion. Of the mitochondrial proteins, 52% were inner membrane proteins and 30% have no compartment assigned (Fig. 4.2 B). Altogether this confirms that the mitochondrial inner membrane was highly enriched by this protocol.

There are 165 proteins with a cellular process annotation and these included metabolic process (13%), electron transport chain (9%), and fatty acid beta-oxidation (6%) (Fig. 4.2 C). A large number of cellular processes contained less than 5 proteins and are categorized as other (36%). All of the cellular processes shown in Figure 4.2 C are recognized processes within mitochondria. In addition to mitochondrial location and processes being the most prominently represented, 127 of the proteins identified in this study (59%) are listed in the MitoProteome Database and have previously been established as mitochondrial by stringent criteria, (http://www.mitoproteome.org/data/proteome/index.html).

To further assess the inner membrane enrichment, the presence of known MIM markers; cytochrome c oxidase, prohibitin, and ADP/ATP translocase 1 were verified in the dataset. All three of these proteins were identified in the control and CMA samples with similar abundances based on calculated mean unweighted spectral counts (Fig. 4.3). ADP/ATP translocase 1 was identified as the fifth most abundant protein in these samples which is consistent with it being one of the most abundant proteins in the MIM.[18] However, ADP/ATP translocase 1 has fewer spectra in the CMA samples compared to the controls; this may be due to protein degradation of

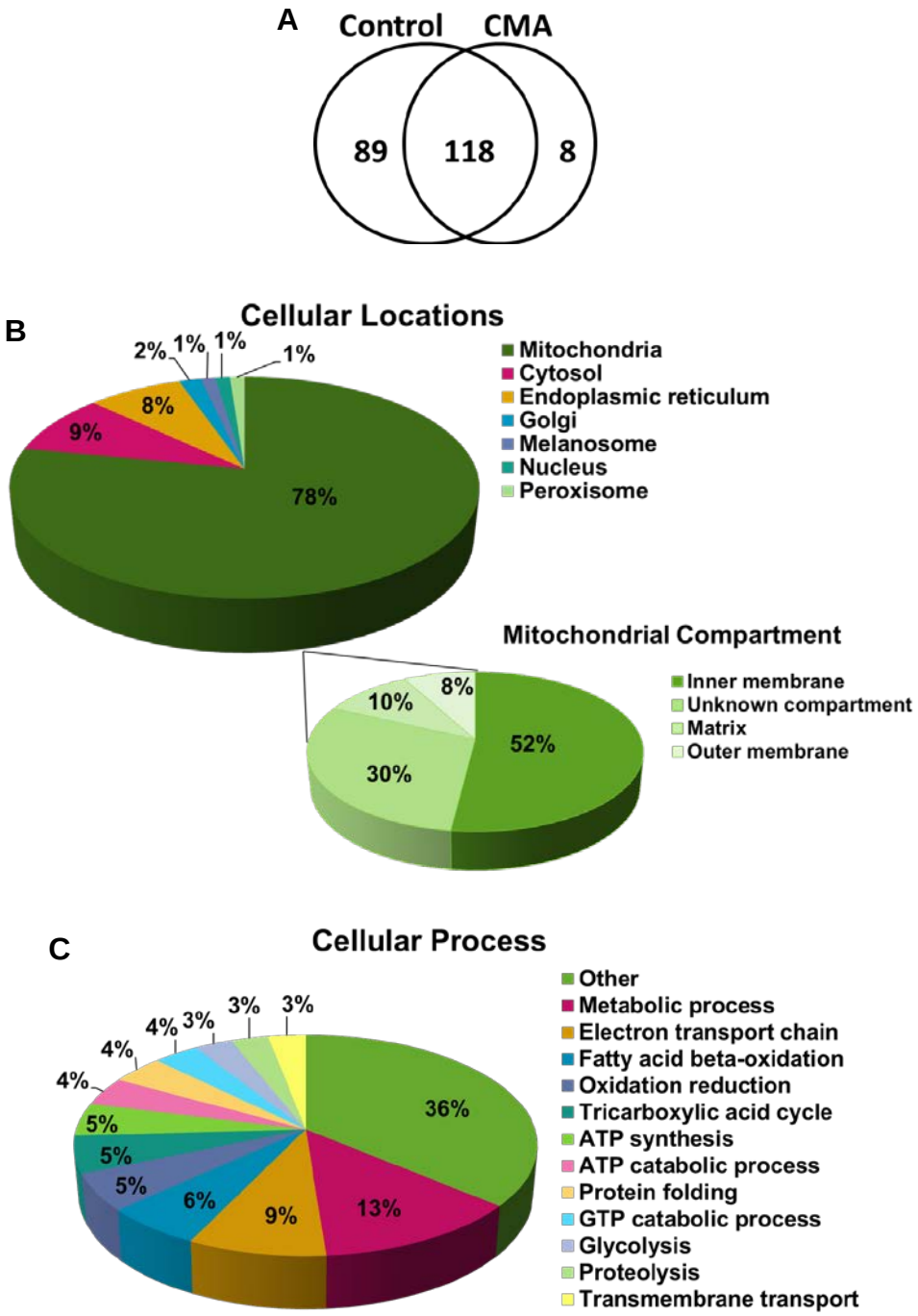

Fig. 4.2. Proteomic analysis- Venn diagram of total proteins identified in the mitochondria inner membranes isolated from control and 7-d chronic acidotic (CMA) rats (Panel A). Pie charts of the cellular locations and mitochondrial compartment (Panel B) and cellular processes (Panel C) as determined by Gene Ontology (GO) analysis of the identified proteins.

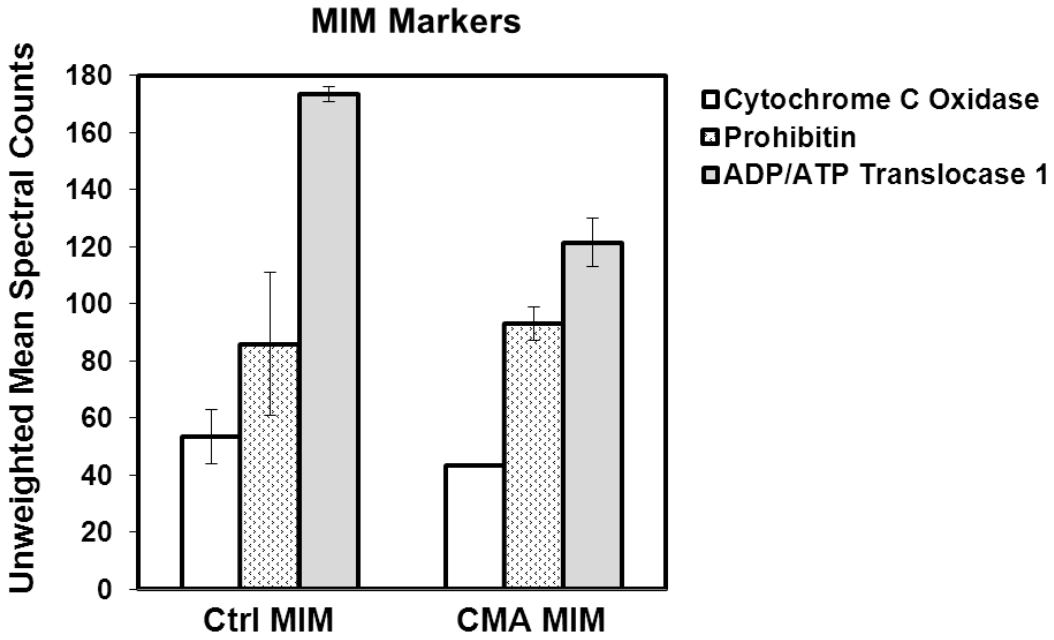

Fig. 4.3. Mitochondrial inner membrane markers identified by mass spectrometry. Mitochondrial inner membrane fractions (MIM) isolated from two control (Ctrl) and two 7-d chronic acidotic (CMA) underwent proteomic analysis. The reported data are the mean ± S.E. of the unweighted mean spectral counts of the identified MIM markers (Cytochrome c oxidase, Prohibitin, and ADP/ATP translocase 1).

the CMA samples. The CMA samples were stored for over a year prior to proteomic analysis while the control samples were stored for only 4 months.

4.4b Data quality assurance for label free quantitation

Spectral counting and average total ion current from the tandem mass spectra (MS^2 TIC) are label free quantitation methods that are frequently used to determine protein changes in large scale proteomics studies.[19] Prior to quantitative analysis it is imperative to critically assess the quality of a large scale proteomics dataset. To determine if the quantitative comparison will be accurate, the number of proteins, peptides, and spectra identified in each sample was comparedto insure they are similar (Figure 4.4). The coefficient of variance (CV) between biological duplicates was calculated and the % CV are all <20% which indicates very little variance. Unfortunately, an unacceptable amount of variance is present between the control and CMA samples. The calculated % CV for number of proteins identified per sample is 24.3%, the total spectra identified is 34.8%, and the total peptides is 32.4%. Overall, the CMA samples have fewer proteins, peptides, and spectra identified which again led us to suspect there was more protein degradation in the CMA then the controls. The CMA samples were stored for 8 months longer than the control samples and were assayed for protein immediately after harvest. The protein amounts injected for LC-MS/MS were based on the initial protein assays. Bradford assays that were performed on one control sample and one CMA sample after proteomic analysis showed a large difference. The assays confirmed there was a greater degree of protein loss in the CMA sample, 3.5 µg /ul (64%) less protein than the initial protein concentration, where the control was only 1.5 µg/ul (29%) less. The difference in protein degradation is a significant

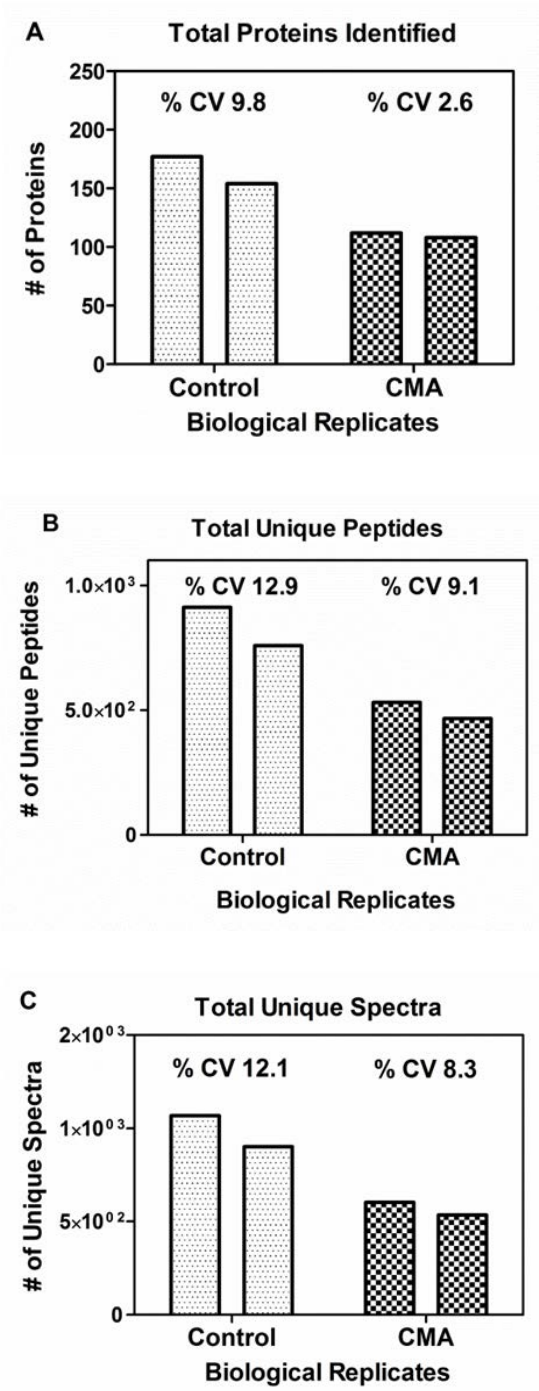

Fig. 4.4. Variance within biological replicates represented as percent of the Coefficient of Variation (% CV) for total proteins (A), unique peptides (B), and spectra identified (C). Mitochondrial inner membranes isolated from proximal convoluted tubules of control (n=2) and chronically acidotic (CMA) (n=2) rats.

problem. However, a quantitative analysis could be attempted if the datasets could be normalized to minimize this effect.

The MS/MS data was normalized between samples in Scaffold 3 by using the sum of spectral counts for each sample to determine a scaling factor that was then applied to each protein in the sample. Box plots were generated for the pre- and post- normalized spectral count (SpC) and average total ion current (MS^2 TIC) measurements (Fig. 4.5 A-D). Both quantitative measurements were not improved by the normalization because the median in the box plots are very different even after data was normalized (Fig. 4.5 B & D). Numerous other normalization methods were attempted, however similar box plots were generated (data not shown). Therefore, quantitative analysis was not carried out to assess difference between the control and chronically acidotic proximal convoluted tubule mitochondrial inner membrane proteomes.

4.4c Mitochondrial inner membrane protein lysine acetylation

Lysine acetylation has been proposed as an important mechanism that regulates cellular metabolism and is specifically prevalent in mitochondria.[20] Changes in mitochondrial lysine acetylation may play an important role in the cellular response to metabolic acidosis.[5] We have previously established the overall mitochondrial lysine acetylation increased 2.5-fold during CMA.[5] Therefore, lysine acetylation was measured in the MIM fractions from control and chronic acidotic rat proximal convoluted tubules. Western blot analysis using an anti-acetyl-lysine antibody indicated many proteins are acetylated, however no significant change in overall lysine acetylation was observed (Fig. 4.6 A & B). Thus, the MIM is not the site of increase in total mitochondrial protein acetylation during chronic metabolic acidosis. To further the investigation of protein acetylation all MS/MS spectra were searched with the variable

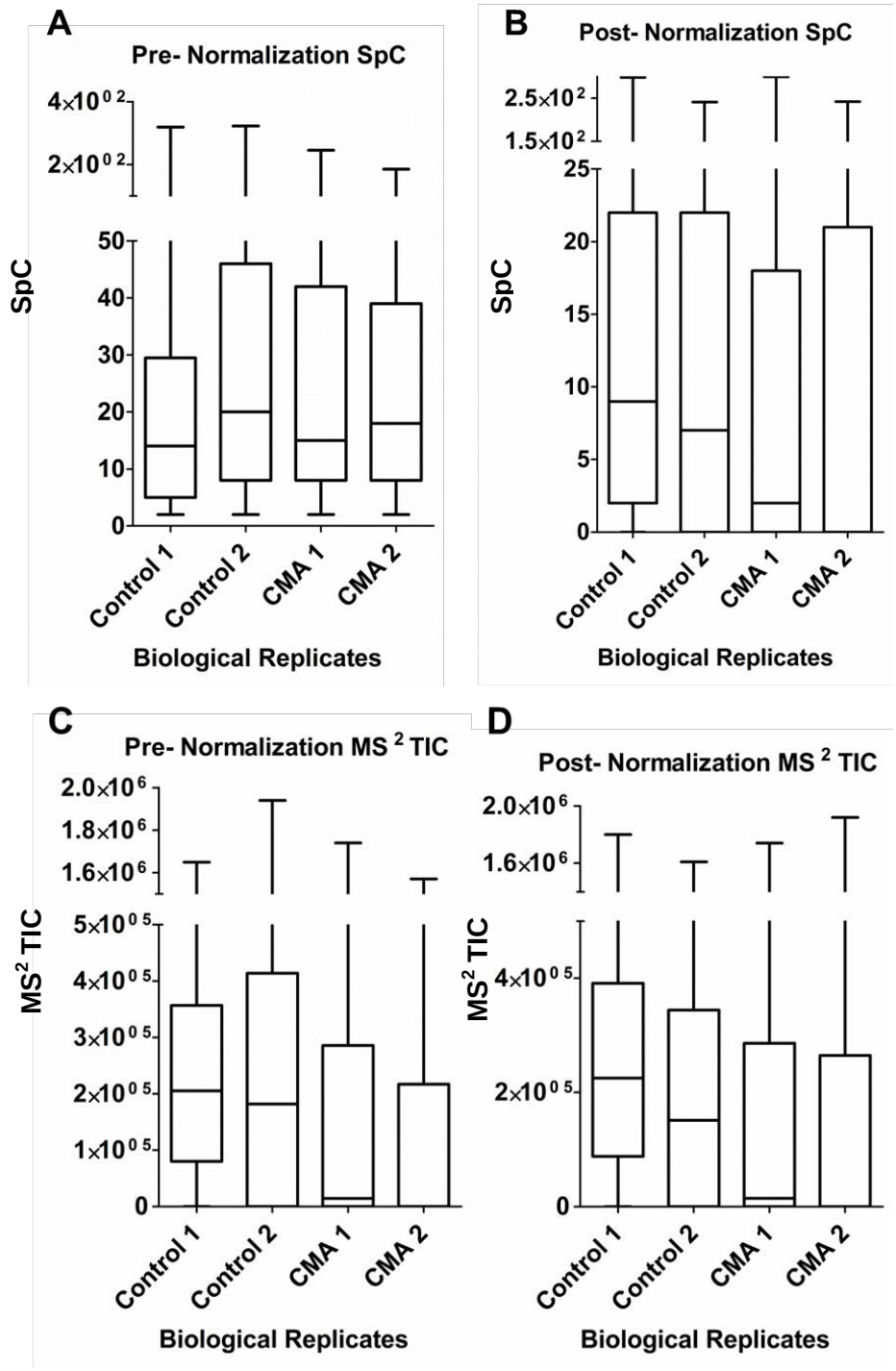

Fig. 4.5. Box plots showing dynamic range of pre and post-normalized spectral counts (SpC) (panel A & B) or average total ion current (MS^2 TIC) (panel C & D). Both biological duplicates are shown separately for control and chronically acidotic (CMA) samples. Normalized data retains the large amount of variance between biological replicates and conditions.

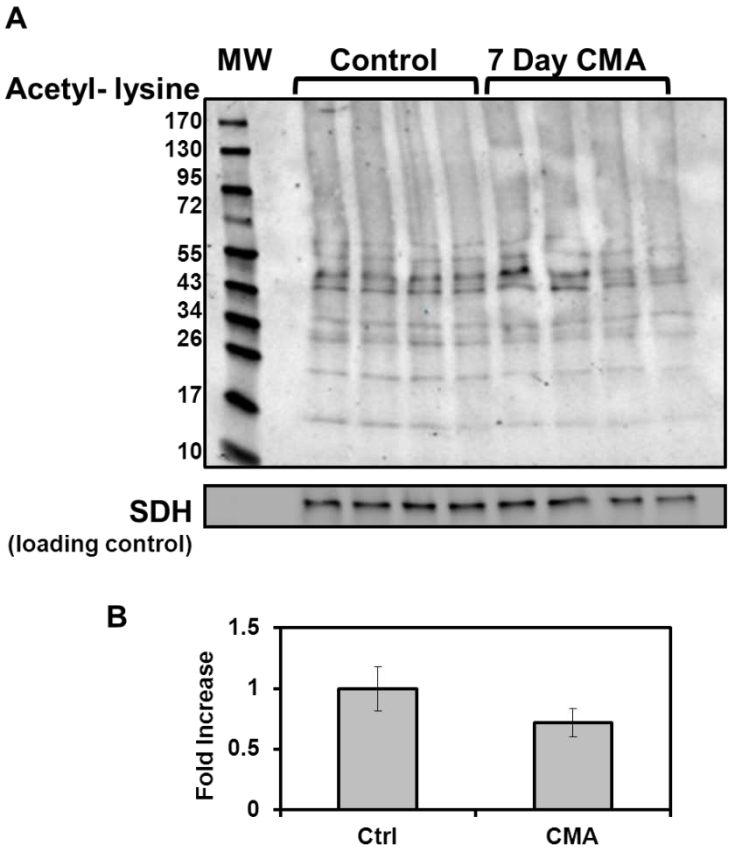

Fig. 4.6. Western blot analysis of lysine acetylation in mitochondrial inner membrane proteins. A. Mitochondrial inner membrane samples were isolated from proximal convoluted tubules of two control (Ctrl) and two 7-d chronic acidotic (CMA) rats. Western blot analysis of duplicate lanes of each sample was performed using an anti-N-ε-acetyl-lysine antibody. B. The acetylation of mitochondrial inner membrane proteins showed no significant change between control and CMA. The combined intensities of each lane in Panel A were normalized to the level of succinate dehydrogenase (SDH), which served as a loading control. The reported data are the mean ± the S.E. of all samples.

modification of lysine acetylation. After careful manual validation (described above) of each spectra this analysis resulted in identification of 18 acetylated peptides (Table 4.2). These acetylated peptides were assigned to 17 different proteins and 11 of the 18 sites were novel identifications compared to the sites previously curated on PhosphoSitePlus (www.phosphosite.org). Only 3 acetylation sites and 1 acetylated protein with a different site modified were identified in our previous study of whole mitochondria.[5] Acetylated proteins are involved in a wide range of biological activities including ATP synthesis, the citric acid cycle, transport, amino acid metabolism, and lipid metabolism. There are six acetylated proteins that are components of the oxidative phosphorylation pathway; two proteins are contained in complex I, one in complex IV, and three in complex V. Additionally, an acetylation site was identified on prohibitin and interestingly, this protein is known to regulate complex I activity. Lysine acetylation affects not only mitochondria but overall cellular function. Lysine acetylation has been proposed to block or induce other post-translational modifications on or near the modified amino acid.[38] The addition of an acetyl moiety on a lysine can prevent protein degradation by blocking this site from ubiquitination. Eight of the identified acetylation sites were also previously identified as sites of ubiquitination (www.phosphosite.org). Lysine acetylation and its role in acidosis have not been elucidated, but the profiling of acetylation sites may encourage further experimentation.

4.5 Conclusions

The increase in glutamine catabolism during metabolic acidosis occurs primarily in the miotchondria.[3, 4] Transport of glutamine across the mitochondrial inner membrane is specific and selective. Therefore this process may be an important site of regulation. Mitochondrial inner

Table 4.2. Identification of Mitochondrial Inner Membrane Acetylated Peptides

			# of Modified Spectra				
Protein name	**Accession #**	**Gene Symbol**	**Control**	**7 Day CMA**	**Peptide Sequence**	**Site ***	**Novel**
ADP/ATP translocase 2	Q09073	Slc25a5	34	26	TDAAVSFAKDFLAGGVAAAISK	K10 ●	No
			4	0	KGTDIMYTGTLDCWR	K245	Yes
ATP synthase subunit alpha, mitochondrial	P15999	Atp5a1	13	4	LKEIVTNFLAGFEP	K541●	No
ATP synthase subunit beta, mitochondrial †	P10719	Atp5b	17	1	VLDSGAPIKIPVGPETLGR	K133	No
Prohibitin	P67779	Phb	0	7	KLEAAEDIAYQLSR	K240	Yes
Aconitate hydratase, mitochondrial	Q9ER34	Aco2	8	7	FKLEAPDADELPR	K523	Yes
NADH dehydrogenase [ubiquinone] 1 beta subcomplex 10	D4A0T0	Ndufb10	13	16	DFKVDQEIINIIQER	K97	Yes
Acyl-coenzyme A synthetase ACSM2, mitochondrial	O70490	Acsm2	4	0	GIKDTEGYFHFMGR	K450	Yes
ADP/ATP translocase 1	Q05962	Slc25a4	29	22	GDQALSFLKDFLAGGIAAAVSK	K10 ●	No
RCG58449, isoform CRA_a	Q6PDU7	Atp5l	4	0	NLADKAPSMVAAAVTYSKPR	K11 or K24	K11-Yes, K24-No
Thiosulfate sulfurtransferase	P24329	Tst	0	4	KVDLSQPLIATCR	K237	Yes
Alpha-aminoadipic semialdehyde dehydrogenase	Q64057	Aldh7a1	2	3	FKNEEEVFEWNNEVK	K439	No
Sorting and assembly machinery component 50 homolog	Q6AXV4	Samm50	10	9	TKDDIIICEIGEVFK	K59	Yes
Cytochrome c oxidase subunit 6C-2	P11951	Cox6c2	7	0	NYDSMKDFEEMR	K61	No
Aspartate aminotransferase, mitochondrial	P00507	Got2	1	0	NLDKEYLPIGGLADFCK	K94	No
Uncharacterized protein	D3ZEA8	Unknown	0	2	CKSQLEGALSK	K3446	Yes
NADH dehydrogenase (Ubiquinone) 1 beta subcomplex 8	B2RYS8	Ndufb8	2	0	GGDPSKEPEPVVHYEI	K176	Yes
Uncharacterized protein	D3ZRJ1	Cyp4a2	0	1	KAQLQNEEELQK	K268	Yes

***** Site determining ion for acetyl- lysine was not always present and the acetyl peptide may have more than one possible lysine that could be modified.

● Acetylation site previously identified in Freund et al. 2012.

† Acetylated protein identified in Freund et al. 2012 but not the same site.

membranes were successfully isolated from renal proximal convoluted tubules of control and 7 d acidotic rats. A total of 215 proteins were identified in the combined samples. The vast majority of these proteins were annotated with a mitochondrial location. A total of 18 acetylated peptides were identified, 11 of which were novel. Lysine acetylation may participate in the rapid activation and regulation of glutamine catabolism that occurs during acute onset of metabolic acidosis. The data presented here represents the first comprehensive proteomic description of a specific compartment of mitochondria within this segment of the nephron.

REFERENCES

1. Halperin, M. L., Metabolic aspects of metabolic acidosis. Clin Invest Med 1993, 16 (4), 294-305.

2. Squires, E. J.; Hall, D. E.; Brosnan, J. T., Arteriovenous differences for amino acids and lactate across kidneys of normal and acidotic rats. Biochem J 1976, 160 (1), 125-8.

3. Curthoys, N. P.; Taylor, L.; Hoffert, J. D.; Knepper, M. A., Proteomic analysis of the adaptive response of rat renal proximal tubules to metabolic acidosis. Am J Physiol Renal Physiol 2007, 292 (1), F140-7.

4. Walmsley, S. J.; Freund, D. M.; Curthoys, N. P., Proteomic profiling of the effect of metabolic acidosis on the apical membrane of the proximal convoluted tubule. Am J Physiol Renal Physiol 2012, 302 (11), F1465-77.

5. Freund DM, P. J., Curthoys NP., Response of the Mitochondrial Proteome of Rat Renal Proximal Convoluted Tubules to Chronic Metabolic Acidosis. Am J Physiol Renal Physiol 2013, 304(2) F145-F155.

6. Curthoys, N. P.; Lowry, O. H., The distribution of glutaminase isoenzymes in the various structures of the nephron in normal, acidotic, and alkalotic rat kidney. J Biol Chem 1973, 248 (1), 162-8.

7. Wright, P. A.; Knepper, M. A., Phosphate-dependent glutaminase activity in rat renal cortical and medullary tubule segments. Am J Physiol 1990, 259 (6 Pt 2), F961-70.

8. Wright, P. A.; Knepper, M. A., Glutamate dehydrogenase activities in microdissected rat nephron segments: effects of acid-base loading. Am J Physiol 1990, 259 (1 Pt 2), F53-9.

9. Atlante, A.; Passarella, S.; Minervini, G. M.; Quagliariello, E., Glutamine transport in normal and acidotic rat kidney mitochondria. Arch Biochem Biophys 1994, 315 (2), 369-81.

10. Palmieri, F., The mitochondrial transporter family (SLC25): physiological and pathological implications. Pflugers Arch 2004, 447 (5), 689-709.

11. Da Cruz, S.; Xenarios, I.; Langridge, J.; Vilbois, F.; Parone, P. A.; Martinou, J. C., Proteomic analysis of the mouse liver mitochondrial inner membrane. J Biol Chem 2003, 278 (42), 41566-71.

12. Bradford, M. M., A rapid and sensitive method for the quantitation of microgram quantities of protein utilizing the principle of protein-dye binding. Anal Biochem 1976, 72, 248-54.

13. Smith, P. K.; Krohn, R. I.; Hermanson, G. T.; Mallia, A. K.; Gartner, F. H.; Provenzano, M. D.; Fujimoto, E. K.; Goeke, N. M.; Olson, B. J.; Klenk, D. C., Measurement of protein using bicinchoninic acid. Anal Biochem 1985, 150 (1), 76-85.

14. Keller, A.; Nesvizhskii, A. I.; Kolker, E.; Aebersold, R., Empirical statistical model to estimate the accuracy of peptide identifications made by MS/MS and database search. Anal Chem 2002, 74 (20), 5383-92.

15. Nesvizhskii, A. I.; Keller, A.; Kolker, E.; Aebersold, R., A statistical model for identifying proteins by tandem mass spectrometry. Analytical chemistry 2003, 75 (17), 4646-58.

16. Elias, J. E.; Gygi, S. P., Target-decoy search strategy for increased confidence in large-scale protein identifications by mass spectrometry. Nat Methods 2007, 4 (3), 207-14.

17. Sonnhammer, E. L.; von Heijne, G.; Krogh, A., A hidden Markov model for predicting transmembrane helices in protein sequences. Proc Int Conf Intell Syst Mol Biol 1998, 6, 175-82.

18. Taylor SW, W. D., Glenn GM, Zhang B, Fahy E, Gaucher SP, Capaldi RA, Gibson ; BW, G. S., An alternative strategy to determine the mitochondrial proteome using sucrose gradient fractionation and 1D PAGE on highly purified human heart mitochondria. J Proteome Res. 2002, 1 (5), 451-8.

19. Freund DM, P. J., Improved Detection of Quantitative Differences Using a Combination of Spectral Counting and MS/MS Total Ion Current. PROTEOMICS. In Press.

20. Zhao, S.; Xu, W.; Jiang, W.; Yu, W.; Lin, Y.; Zhang, T.; Yao, J.; Zhou, L.; Zeng, Y.; Li, H.; Li, Y.; Shi, J.; An, W.; Hancock, S. M.; He, F.; Qin, L.; Chin, J.; Yang, P.; Chen, X.; Lei, Q.; Xiong, Y.; Guan, K. L., Regulation of cellular metabolism by protein lysine acetylation. Science 2010, 327 (5968), 1000-4.

CHAPTER 5

Proteomic Profiling of the Effect of Metabolic Acidosis on the Apical Membrane of the Proximal Convoluted Tubule [4]

5.1 Summary

The physiological response to the onset of metabolic acidosis requires pronounced changes in renal gene expression. Adaptations within the proximal convoluted tubule support the increased extraction of plasma glutamine and the increased synthesis and transport of glucose and of NH_4^+ and HCO_3^- ions. Many of these adaptations involve proteins associated with the apical membrane. To quantify the temporal changes in these proteins, proteomic profiling was performed using brush-border membrane vesicles isolated from proximal convoluted tubules (BBMV PCT) that were purified from control and acidotic rats. This preparation is essentially free of contaminating apical membranes from other renal cortical cells. The analysis identified 298 proteins, 26% of which contained one or more transmembrane domains. Spectral counting analysis was used to assess changes in protein abundance between control and acidotic samples. The onset of acidosis produced a twofold, but transient, increase in the Na^+-dependent glucose transporter and a more gradual, but sustained, increase (3-fold) in the Na^+-dependent lactate transporter. These changes were associated with the loss of glycolytic and gluconeogenic enzymes that are contained in the BBMV PCT isolated from control rats. In addition, the levels of γ-glutamyltranspeptidase increased two-fold, while transporters that participate in the uptake of neutral amino acids, including glutamine, were decreased. These changes could facilitate the deamidation of glutamine within the tubular lumen. Finally, pronounced increases were also

observed in the levels of DAB2 (3-fold) and myosin 9 (7-fold), proteins that may participate in endocytosis of apical membrane proteins. Western blot analysis was used to validate the spectral counting results.

This chapter describes the work I contributed to the Walmsley S.J et al. publication.[1] Specifically, additional brush-border membrane vesicles were isolated from proximal convoluted tubules that were obtained from control, 1 d and 7 d acidotic rats. The fluid intake, blood pH and bicarbonate were determined for these rats. I also performed the optimization of specific antibodies for the validation of spectral counting by Western blot analysis.

5.2 Materials and methods

5.2a Animals and isolation of proximal convoluted tubule apical membranes

Male Sprague-Dawley rats weighing ~200 g (6-12 weeks old) were obtained from Charles River Laboratories (Kingston, NY). The proteomic study consisted of an n = 3 of each; control, 1-d acute acidotic, 3-d acidotic and 7-d chronic acidotic rats. The rats were allowed free access to a rodent chow (Harlan-Teklad, Madison, WI) and the control group was given tap water to drink. Acute metabolic acidosis (1 d) was induced by stomach loading rats with 20 mmol NH_4Cl/kg body weight and providing 0.28 M NH_4Cl solution for drinking water. Rats that were made acidotic for 3 d or 7 d were provided with 0.28 M NH_4Cl solution as the sole source of drinking water. Animals were observed daily to ensure consumption of 0.28 M NH_4Cl and all four groups of rats exhibited similar behavior. All procedures were approved by the Institutional Animal Care and Use Committee at Colorado State University.

All rats were sacrificed by decapitation at the end of treatment and the kidneys removed. The proximal convoluted tubules were isolated from renal cortex as described previously.[2] The

apical membranes were isolated by the preparation of brush-border membrane vesicles (BBMV) from isolated proximal convoluted tubules using the standard method of $MgCl_2$ precipitation.[3, 4, 1] Purified tubules were resuspended in 10 vol/wet wt of a solution containing (in mM) 300 mannitol, 5 EGTA, 1 PMSF, and 12 HEPES, pH 7.1. After polytron treatment (90 s, setting 5), the homogenate was diluted two-fold with H_2O, and then $MgCl_2$ was added to yield a final concentration of 12 mM. The mixture was incubated on ice for 15 min with intermittent and gentle mixing. Following centrifugation at 3,000 x g for 10 min at 4°C to remove mitochondria and cellular debris, the resultant supernatant was centrifuged at 30,000 x g for 40 min at 4°C to pellet the BBMV. The pellet was resuspended in 1 volume of (in mM) 150 mannitol, 2.5 EGTA, and 6 HEPES, pH 7.1 and homogenized with 15 passes of a glass Teflon homogenizer. The BBMV were precipitated again by the addition of 12 mM $MgCl_2$ and repetition of the incubation and centrifugation steps. The final pellet was resuspended in the previous mannitol buffer, and the BBMV were stored at -80°C.

5.2b Western blot analysis

Western blotting[2] analysis was used to validate some of the results obtained by spectral counting. Additional apical membranes were isolated from control, 1-d acute acidotic and 7-d chronic acidotic rat proximal convoluted tubules. Primary antibodies for Na^+/H^+ exchange regulatory cofactor 3, NHERF3 (Transduction Laboratories), aminopeptidase N, AN (Santa Cruz), fructose-bisphosphate aldolase B, FBA (Acris Antibodies), enolase (Abcam), sodium/glucose cotransporter 2, SGLT2 (Abcam) and glyceraldehyde 3-phosphate dehydrogenase, GAPDH (Imgenex) were obtained from the indicated suppliers. Dylight 680 conjugated goat anti-mouse or 800 goat anti-rabbit IgG (Pierce) was used as secondary antibody.

The resulting complexes were visualized and quantified using an Odyssey Infrared Imager (LI-COR Biosciences, Lincoln, NE). Proximal tubule whole cell lysates were used for NHERF3 Western blot analysis instead of apical membranes.

5.3 Results and discussion

5.3a Induction of metabolic acidosis in rats by NH_4Cl solution

To induce metabolic acidosis, rats were given 0.28 M NH_4Cl as the sole source of drinking water. This protocol has been well established to induce acidosis in animals. However another method includes 0.5-2% sucrose in the drinking water of control and acidotic animals.[5] With the addition of sucrose to the water the acidotic mice drank 20% less.[5, 6] We found it was not necessary to encourage the animals to drink by supplementing the water with sucrose. Fluid intake was measured daily. The 7-d acidotic rats consumed an average volume of the NH_4Cl solution (36.4 ± 2.5 ml/d) that was not significantly different from the amount of water consumed by the control rats (34.3 ± 1.9 ml/d) (Fig 5.1 A). Acute metabolic acidosis (1 d) was induced by stomach loading rats with 20 mmol NH_4Cl/kg body weight and providing 0.28 M NH_4Cl as drinking water. Acute acidotic rats consumed an average volume of the NH_4Cl solution (27.4 ± 2.5 ml/d) which is slightly less than the other rats likely due to the stomach loading and only one day of measured fluid intake. Overall the fluid intake data demonstrates the addition of sucrose to the NH_4Cl solution is unnecessary and the animals will drink an adequate amount of NH_4Cl without it.

Arterial blood pH and bicarbonate concentration were determined using an i-STAT 1 VetScan (Abaxis) (Fig. 5.1 B & C). The 1-d acute acidotic protocol produced a pronounced decrease in blood pH (7.11 ± 0.04) and HCO_3^- concentration (8.8 ± 1.1 mM). After 3 d, the

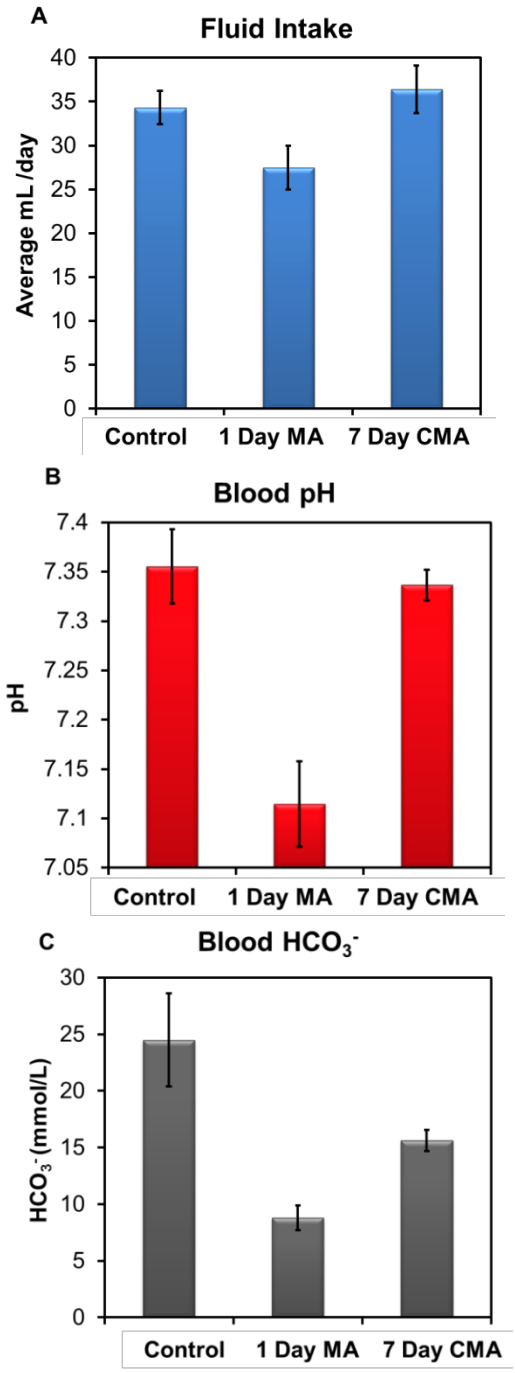

Fig. 5.1. Fluid intake, blood pH and HCO_3^- data from control and acidotic rats. Data collected from three control, three 1-d acidotic (MA) and three 7-d chronic acidotic rats (CMA). Control rats consumed water while acidotic rat were provided 0.28M NH_4Cl for 1 or 7 days, respectively (Panel A). Blood pH and HCO_3^- was measured with an iSTAT (Panel B). The reported data are the mean ± S.E. of the triplicate rats.

protocol without stomach loading produced a level of acidosis that is similar to the acute treatment[7], but by 7 d, the acidosis is partially compensated (pH = 7.34 ± 0.02, $[HCO_3^-]$ = 15.6 ± 0.9 mM). By contrast, the control rats had an arterial blood pH of 7.37 ± 0.04 and a HCO_3^- concentration of 23.9 ± 2.4 mM. Therefore the NH_4Cl treatment produced the anticipated induction of hypercholremic metabolic acidosis in these animals.

5.3b Apical membrane isolation and validation of proteins altered in metabolic acidosis by Western blotting

Spectral counting analysis (SpC) was used to determine relative abundance changes in 1-d and 7-d acidotic proximal convoluted tubule apical membranes.[1] Western blotting was performed to confirm some of the proteins that showed changes by SpC. Additional apical membranes were isolated from control (n=3), 1 d acute acidotic, and 7 d chronic acidotic (n=3) rat proximal convoluted tubules for Western blots (Fig. 5.2). The Western blotting indicated that the levels of SGLT2 were increased to a greater extent than suggested by SpC and that it remains elevated after 7 d of chronic acidosis. By contrast, Western blotting suggested that aminopeptidase N was decreased only in the 7-d acidotic rats. The Western blot data for NHERF3, fructose-bisphosphate aldolase B, enolase and GAPDH confirmed the observed changes from SpC. A comparison of the $\log_2$ relative fold changes in abundance determined by SpC and Western blotting analysis demonstrates that the results of the two analyses are highly correlated (Fig. 5.3 A & B).

Previous observations suggests that during normal acid-base balance enzymes of glucose metabolism may form a complex that is sequestered near or associated with the brush border membrane of the proximal convoluted tubule.[2] Previous immunofluorescence studies have

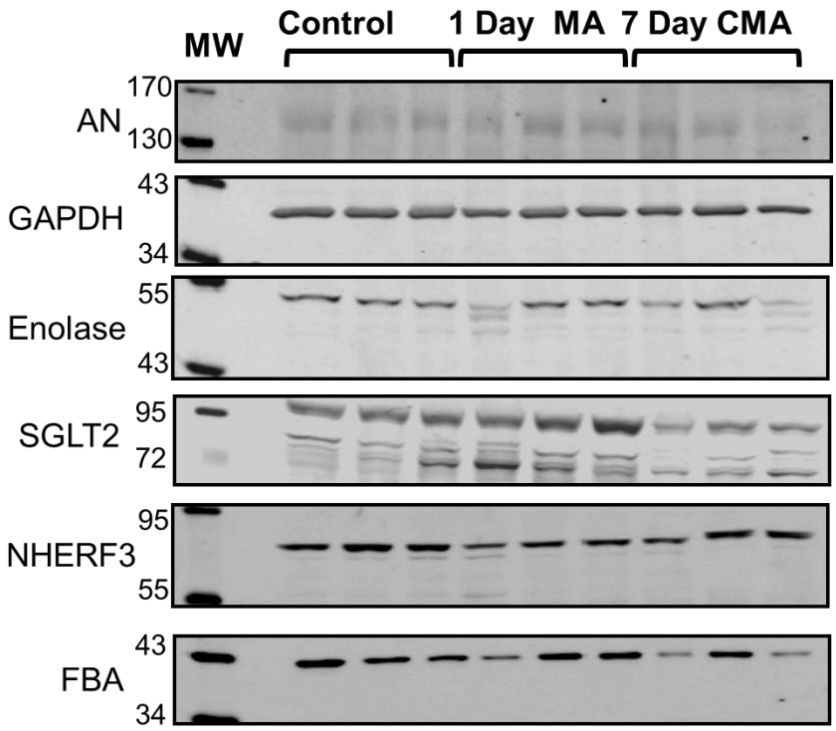

Fig. 5.2. Western blot analysis was performed on separate preparations of apical membrane from proximal convoluted tubules isolated from 3 control, 3-1day MA, and 3- 7 day CMA rats. Western blot analysis was performed using 6 specific antibodies to compare the relative levels of the proteins. The following antibodies were used; aminopeptidase N (AN), glyceraldehyde 3-phosphate dehydrogenase (GAPDH), enolase, sodium/glucose cotransporter 2 (SGLT2), Na^+/H^+ exchange regulatory cofactor 3 (NHERF3), and fructose-bisphosphate aldolase (FBA). The resulting bands were imaged and quantified using an Odyssey Infrared Imager. Proximal tubule whole cell lysates were used for NHERF3 Western blot analysis instead of apical membranes. The corresponding molecular weight marker is shown on left (MW).

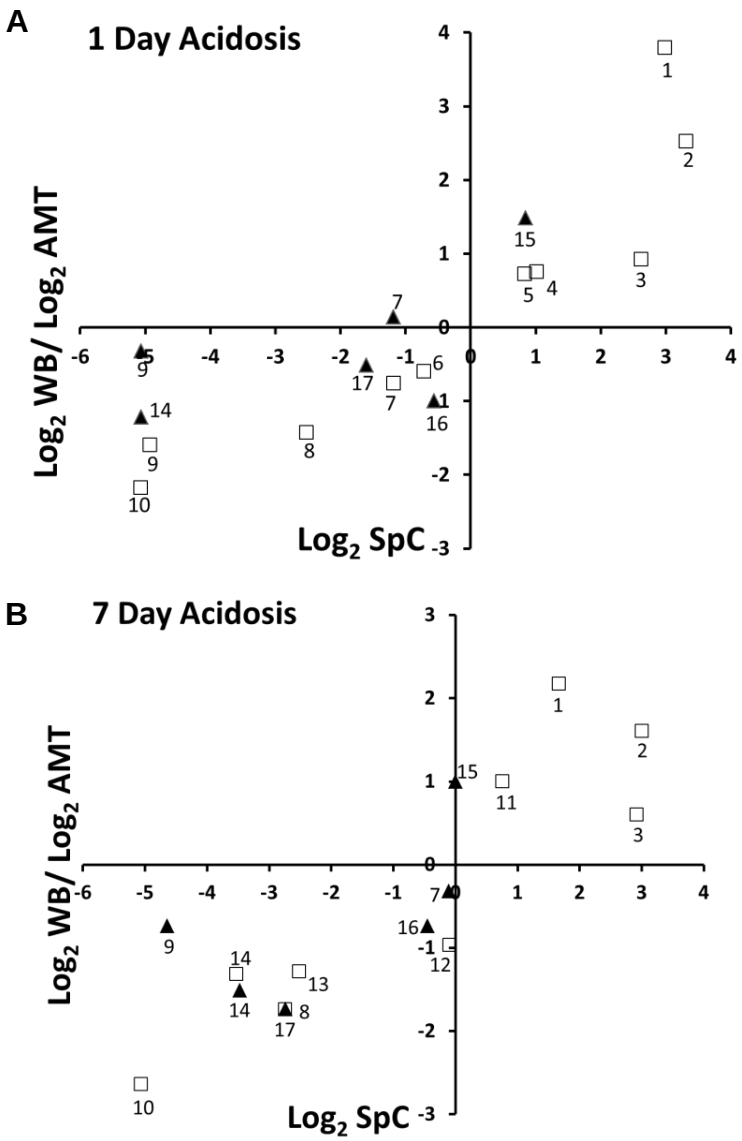

Fig. 5.3. The comparison of the $\log_2$ fold changes determined by spectral counting (SpC), accurate mass and time tags (AMT), and Western blot (WB) analysis. The fold change in LC/MS peak intensities of the identified peptides (AMT) are compared to the relative abundance of the corresponding protein determined by SpC (□). The AMT was done by Walmsley, S.J and is described in detail in the Walmsley S.J et al. publication.[1] Fold changes calculated by WB analysis compared to the fold differences for the proteins by SpC (▲). The illustrated proteins are: 1. beta subunit of ATP synthase; 2. voltage dependent anion channel-1; 3. myosin-9; 4. C1 subunit of V-type H^+-ATPase; 5. collectrin; 6. ezrin; 7. aminopeptidase N; 8. fructose 1,6-bisphosphatase-1; 9. glyceraldehyde 3-phosphate dehydrogenase; 10. fatty acid binding protein-1; 11. γ-glutamyl-transpeptidase; 12. B2 subunit of V-type H^+-ATPase; 13. transketolase; 14. enolase. 15. Sodium/glucose cotransporter 2; 16. Na+/H+ exchange regulatory cofactor 3, Pdzk1; 17. Fructose-bisphosphate aldolase. In this figure, I contributed the Western blot results.

clearly established that aldolase [8] and fructose 1,6-bisphosphatase [9] are normally localized to the apical membrane of the proximal convoluted tubule.[10] Similar observations in erythrocytes suggested that the association of the enzymes of glycolysis with the membrane may generate a higher localized concentration of ATP that is used to support active transport processes.[11] The finding that several proteins involved in the reversible steps of glycolysis and in gluconeogenesis are significantly decreased or no longer detectable in BBMV isolated from acidotic rats suggests that the sequestered complex may dissociate from the apical membrane during acidosis. The release of enzymes, including fructose-1,6-bisphosphatase and phospho*enol*pyruvate carboxykinase, may support the rapid increase in glucose synthesis.[12] The selective return of aldolase to the brush border membrane following 7 d of acidosis may be due to its functional association with the A, B, and E subunits of the V-type H^+-ATPase.[8] Previous studies have clearly established that aldolase co-localizes with the H^+-ATPase and that this interaction is essential for the membrane insertion and correct assembly of the H^+-ATPase.[13] Thus, the transient decrease in aldolase may contribute to the altered ratios of H^+-ATPase subunits that are observed during onset of acidosis.

The observed transient increase in the Na+-dependent glucose transporter (SGLT2) was confirmed by Western blot analysis. This finding suggests that a greater proportion of the filtered glucose may be reabsorbed within the early proximal convoluted tubule during onset of acidosis. The reabsorbed glucose could provide energy to support the pronounced remodeling of the cellular proteome that occurs during early onset of acidosis. However, given the rapid and pronounced shift towards gluconeogenesis, it is more likely that the reabsorbed glucose undergoes transepithelial transport and is returned to the blood.

REFERENCES

1. Walmsley, S. J.; Freund, D. M.; Curthoys, N. P., Proteomic profiling of the effect of metabolic acidosis on the apical membrane of the proximal convoluted tubule. Am J Physiol Renal Physiol 2012, 302 (11), F1465-77.

2. Walmsley, S. J.; Broeckling, C.; Hess, A.; Prenni, J.; Curthoys, N. P., Proteomic analysis of brush-border membrane vesicles isolated from purified proximal convoluted tubules. Am J Physiol Renal Physiol 2010, 298 (6), F1323-31.

3. Adam, W. R.; Koretsky, A. P.; Weiner, M. W., 31P-NMR in vivo measurement of renal intracellular pH: effects of acidosis and K+ depletion in rats. Am J Physiol 1986, 251 (5 Pt 2), F904-10.

4. Biber, J.; Stieger, B.; Stange, G.; Murer, H., Isolation of renal proximal tubular brush-border membranes. Nat Protoc 2007, 2 (6), 1356-9.

5. Nowik, M.; Lecca, M. R.; Velic, A.; Rehrauer, H.; Brandli, A. W.; Wagner, C. A., Genome-wide gene expression profiling reveals renal genes regulated during metabolic acidosis. Physiol Genomics 2008, 32 (3), 322-34.

6. Nowik, M.; Kampik, N. B.; Mihailova, M.; Eladari, D.; Wagner, C. A., Induction of metabolic acidosis with ammonium chloride (NH_4Cl) in mice and rats--species differences and technical considerations. Cell Physiol Biochem 2010, 26 (6), 1059-72.

7. Sleeper, R. S.; Vertuno, L. L.; Strauss, F.; Preuss, H. G., Effects of acid challenge on in vivo and in vitro rat renal ammoniagenesis. Life Sci 1978, 22 (18), 1561-71.

8. Lu, M.; Holliday, L. S.; Zhang, L.; Dunn, W. A., Jr.; Gluck, S. L., Interaction between aldolase and vacuolar H+-ATPase: evidence for direct coupling of glycolysis to the ATP-hydrolyzing proton pump. J Biol Chem 2001, 276 (32), 30407-13.

9. Yanez, A. J.; Bertinat, R.; Concha, II; Slebe, J. C., Nuclear localization of liver FBPase isoenzyme in kidney and liver. FEBS Lett 2003, 550 (1-3), 35-40.

10. Lu, M.; Ammar, D.; Ives, H.; Albrecht, F.; Gluck, S. L., Physical interaction between aldolase and vacuolar H+-ATPase is essential for the assembly and activity of the proton pump. J Biol Chem 2007, 282 (34), 24495-503.

11. Harris, S. J.; Winzor, D. J., Interactions of glycolytic enzymes with erythrocyte membranes. Biochimica et Biophysica Acta (BBA) - Protein Structure and Molecular Enzymology 1990, 1038 (3), 306-314.

12. Gerich, J. E.; Meyer, C.; Woerle, H. J.; Stumvoll, M., Renal gluconeogenesis: its importance in human glucose homeostasis. Diabetes Care 2001, 24 (2), 382-91.

13. Lu, M.; Sautin, Y. Y.; Holliday, L. S.; Gluck, S. L., The glycolytic enzyme aldolase mediates assembly, expression, and activity of vacuolar H+-ATPase. J Biol Chem 2004, 279 (10), 8732-9.

CHAPTER 6

Conclusions and Future Directions

6.1 Summary

The human kidneys contain more than one million glomeruli, which filter nearly 200 liters of plasma per day. The proximal tubule is the segment of the nephron that immediately follows the glomeruli. This portion of the nephron contributes to fluid, electrolyte and nutrient homeostasis by reabsorbing 60-70% of the filtered water and NaCl and an even greater proportion of the $NaHCO_3$. The initial or convoluted portion of the proximal tubule reabsorbs nearly all of the nutrients in the glomerular filtrate and is the site of active secretion and many of the metabolic functions of the kidney. For example, the proximal convoluted tubule is the primary site of renal ammoniagenesis and gluconeogenesis, processes that are significantly activated during metabolic acidosis. Three independent proteomic studies have characterized the apical membrane, mitochondrial and soluble cytosolic fractions of the proximal convoluted tubule at various stages of onset of metabolic acidosis. First, apical membranes were purified from proximal convoluted tubules isolated from control, 1-d acute acidotic, 3-d acidotic, and 7-d chronic acidotic rats.[1] Liquid chromatography coupled with mass spectrometry (LC-MS/MS) identified a total of 298 proteins in all of the apical membrane samples. Secondly, mitochondria isolated from the proximal convoluted tubule of control and 7-d chronic acidotic rats were analyzed by two-dimensional liquid chromatography coupled with mass spectrometry (2D-LC-MS/MS).[2] The mitochondrial study identified a total of 901 proteins. Finally, the corresponding soluble cytosolic fractions from control, 1-d acute acidotic and 7-d chronically acidotic rats were

also analyzed by 2D-LC-MS/MS (unpublished data of Schauer, K.L., Freund, D.M., Prenni, J.E. and Curthoys, N.P.). The latter study identified 461 proteins across all samples.

6.2 Combined proteomic analyses of the proximal convoluted tubule in chronic metabolic acidosis

The combined proteomic analyses provide a more comprehensive profile of the proteins expressed in the proximal convoluted tubule and may identify novel functions of this nephron segment. Each analysis contributed hundreds of protein identifications that can now be assigned to this segment of the nephron. There were 1239 non-redundant proteins that were identified in one or more of the fractions. The Automated Bioinformatics Extractor (ABE) http://helixweb.nih.gov/ESBL/ABE/ was used to obtain Gene Ontology (GO) terms for the apical membrane fractions. GO terms for the mitochondrial and soluble cytosolic proteins were extracted from Scaffold 3. Of the total identified proteins, 783 had annotated GO terms for cellular processes. Clustering of the GO terms from the three studies provides an assessment of the predominant cellular processes in the proximal convoluted tubule (Fig. 6.1). The various processes are represented as the percent of the 783 annotated proteins. Many of the proteins (34%) clustered into processes with <6 components. These were combined into the other category. The general annotation of metabolic process (12%) accounted for the second largest percentage of proteins. Other general cellular processes that were noteworthy in the dataset were transport (7%), oxidation/reduction (7%), translation (7%), proteolysis (5%) and the electron transport chain (3%). Overall, the larger clusters of cellular processes in the proximal convoluted tubule are significant processes in all cell types. Label free quantitative analyses were performed on the three-proteomic datasets to determine relative differences in protein abundance that

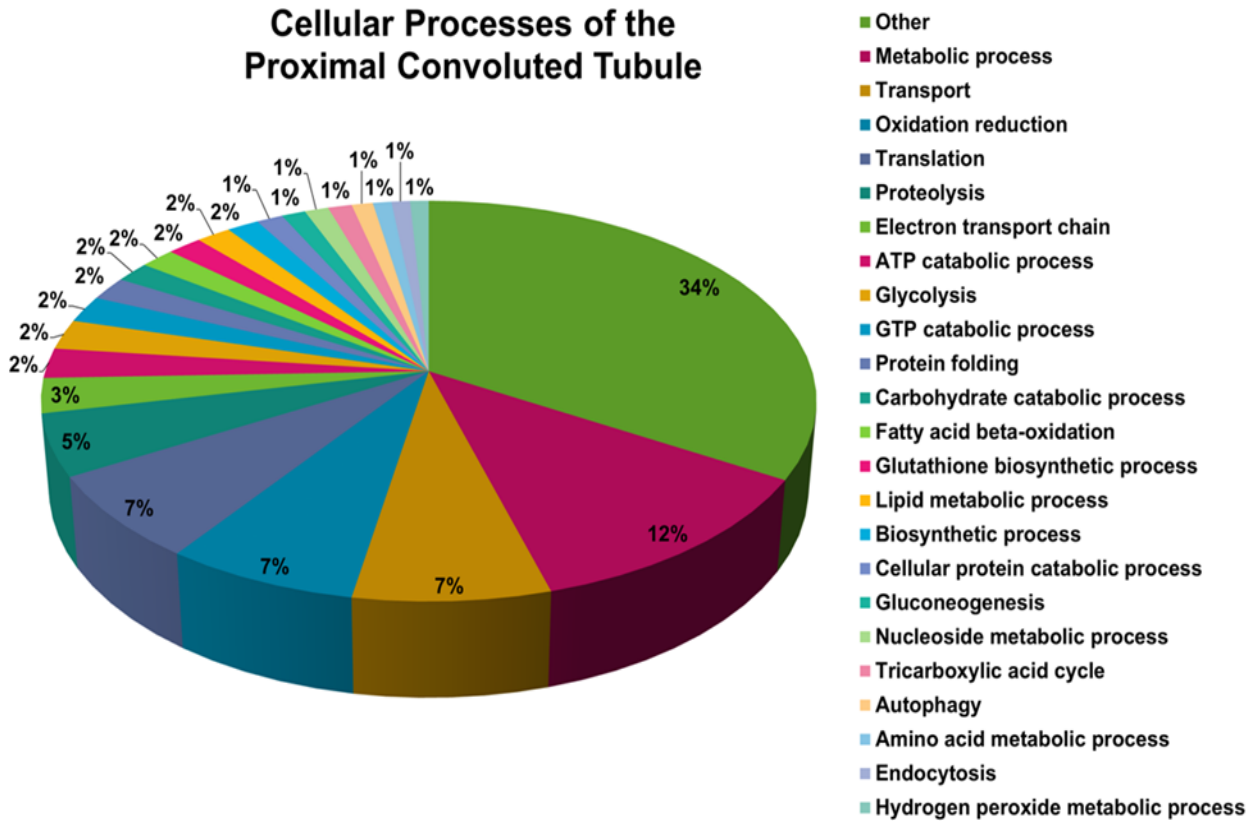

Fig. 6.1. Pie chart of the cellular processes as determined by Gene Ontology (GO) analysis of the identified proteins in the apical membrane, mitochondrial and soluble cytosolic fractions of the proximal convoluted tubule.

occur during metabolic acidosis. The analyses of control and 7-d chronic metabolic acidotic samples were common to the three studies. Spectral counting (SpC) and the student's T-test were used to identify proteins that are significantly altered in abundance between control and 7d acidotic samples in the apical membrane and mitochondrial fractions. However, both SpC and average MS/MS total ion current (MS^2 TIC) [3] were used for the soluble cytosolic data. The following cut-offs for significance were applied to the apical membrane dataset: a p-value ≤ 0.05 and a fold change ≥ 1.5. Using these criteria, there were 39 proteins that were significantly altered in the 7-d acidotic apical membrane samples. The same significance cut-offs were used in the mitochondrial study, resulting in 33 proteins that had altered abundances. Carbonic anhydrase 5B was included in this list even though it has a p-value of 0.07 because of its implicated role in mitochondrial HCO_3^-metabolism and/or transport. The soluble cytosolic study used a significance cut-off of p-value ≤ 0.1 and a fold change ≥ 1.5 to determine changes in relative protein abundance. In this experiment, using a combination of SpC and MS^2 TIC, 26 proteins were significantly altered after 7-d of acidosis in the soluble cytosolic fractions.

Proteomic profiling of subcellular fractions (as opposed to a whole cell lysate) can increase detection of low abundance proteins and allow for a more comprehensive analysis of the proteome. As expected, there were very few significantly altered proteins in common between the three subcellular fractions (Fig 6.2 A & B). Among the 98 proteins which exhibit a significant change in the three studies, only 2 were detected in more than one analysis. Glutamate dehydrogenase (GDH) was the only significantly increased protein that was detected in two separate fractions (Fig 6.2 A), both in the mitochondria, its known location, and in the apical membrane fraction. The mitochondria of the proximal convoluted tubule are positioned in very close proximity to the apical membrane.[1] Therefore, it is not surprising that this extremely

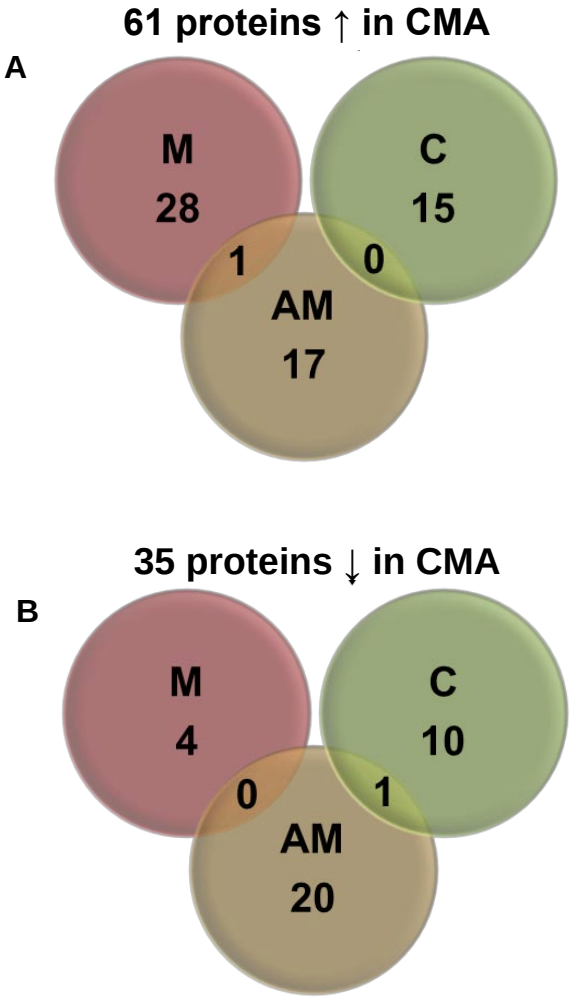

Fig. 6.2. Venn diagram of identified proteins observed to be significantly in response to chronic metabolic acidosis. Proteins were identified in apical membrane (AM), mitochondria (M), or soluble cytosolic (C) fractions prepared from proximal convoluted tubules isolated from control (Ctrl) and 7-d chronic acidotic (CMA) rats. Panel A are the proteins found increased (↑) in abundance and panel B are those decreased (↓) in abundance in CMA.

abundant protein was also incorporated inside the apical membrane vesicles that are formed during polytron homogenization. The cytosolic triosephosphate isomerase (TPI) was significantly decreased in both the apical membrane and soluble cytosolic fractions. Previous studies indicate that many of the enzymes of glycolysis are localized immediately under the apical membrane in control rats.[1] This association is apparently disrupted during onset of acidosis.[1] Thus, it is not surprising that TPI, an extremely abundant glycolytic enzyme, was also observed to decrease in the apical membrane fractions.

Overall, in the three studies there were 61 unique proteins which exhibit an increase after 7 d of chronic acidosis (Table 6.1). Only 12 (20%) of these proteins were shown previously to exhibit similar increases by either the preceding microarray or DIGE analysis (indicated by bold and italics type, respectively, in Table 6.1).[4, 5] Of these 61 proteins, 33 were also identified in the proteomic analysis of 1-d acute acidotic rats, of which 15 (45%) were also increased after 1 d (denoted by an asterisk in Table 6.1). There were 35 unique proteins in the three studies that exhibit a significant decrease in the 7-d chronic acidotic rats (Table 6.2). Only 6 (17%) of these proteins were previously shown to exhibit similar alterations by either microarray or DIGE studies (indicated by bold and italics type, respectively, in Table 6.2).[4, 5] Of the 35 proteins, 31 were also identified in the proteomic analysis of the 1-d acute acidotic rats and 19 (61%) were also decreased at 1 d (Table 6.2 denoted by an asterisk).

Bioinformatics analysis was performed to further our understanding of how the proximal convoluted tubule responds to the decrease in blood pH and HCO_3^- during metabolic acidosis. Gene names of the significantly increased or decreased proteins were submitted to Search Tool for the Retrieval of Interacting Genes (STRING) - Known and Predicted Protein-Protein Interactions available at http://string-db.org/ to identify potential associations. The STRING

Table 6.1. Proximal Convoluted Tubule Proteins Significantly Increased in Chronic Metabolic Acidosis

Protein name	Accession #	Gene	Fraction	p-value	Fold change	Metabolic Process
UDP-glucuronosyltransferase 2B15	P36511	Ugt2b15	M	0.0002	6.4	Xenobiotic glucuronidation
Histone H2A type 1-C	P0C169	HIST1H2AC	AM	0.0007*	10.3	Nucleosome assembly
UDP-glucuronosyltransferase 1-1	Q64550	Ugt1a1	M	0.0009	4.6	Xenobiotic glucuronidation
Gamma-glutamyltranspeptidase 1	P07314	Ggt1	AM	0.001*	1.6	Cellular response to oxidative stress
ATP synthase, H+ mitochondrial F0, subunit G	Q6PDU7	Atp5l	AM	0.001*	10.3	Electron transport chain
17-beta-hydroxysteroid dehydrogenase 4	P97852	Hsd17b4	M	0.002	2.0	Cholesterol metabolic process
Dimethylglycine dehydrogenase, mitochondrial	Q63342	Dmgdh	M	0.002	1.5	Betaine catabolic process
Glutamate dehydrogenase 1, mitochondrial	P10860	Glud1	M, AM	0.004, 0.04	1.7, 5.3	Glutamate catabolic process
Histone H4	P62804	Hist1h4b	AM	0.005*	10.7	Cell differentiation
Acetyl-Coenzyme A acyltransferase 1B	F1LPD6	Acaa1b	M	0.005	2.4	Fatty acid metabolic process
Enoyl-CoA hydratase domain-containing protein 3	Q3MIE0	Echdc3	M	0.006	3.6	NA
Vitamin D-binding protein	P04276	Gc	M	0.006	2.6	Vitamin D metabolic process
Cytochrome c oxidase subunit 2	Q8SEZ5	COII	AM	0.009*	12.2	Electron transport chain
Catalase	P04762	Cat	M	0.01	2.2	Hydrogen peroxide catabolic process
Ras-related protein Rab-21	Q6AXT5	Rab21	M	0.01	4.1	GTP catabolic process
Fumarylacetoacetate hydrolase domain-containing protein	B2RYW9	Fahd2	M	0.01	2.0	Metabolic process
ATP synthase subunit beta, mitochondrial	P10719	Atp5b	AM	0.01*	3.2	Lipid metabolic process
Phosphoenolpyruvate carboxykinase, cytosolic [GTP]	P07379	Pck1	C	0.01*	3.4	Gluconeogenesis
Epoxide hydrolase 1	P07687	Ephx1	M	0.01	3.1	Aromatic compound catabolic process
Cadherin 16	Q66H67	Cdh16	AM	0.01	1.5	Cell adhesion
Cytochrome P450 4A14	P20817	Cyp4a14	AM	0.01	6.0	Arachidonic acid metabolic process
Cytochrome c oxidase 6B1	D3ZD09	Cox6b1	AM	0.01	11.0	Electron transport chain
Uncharacterized protein	D4A0Y1	Cfb	M	0.01	4.0	Proteolysis
Enoyl-coenzyme A hydratase/3-hydroxyacyl-coenzyme A	P07896	Ehhadh	M	0.01	2.1	Internal protein amino acid acetylation
Cytochrome b5	P00173	Cyb5a	M	0.01	1.7	Electron transport chain
Ectonucleoside triphosphate diphosphohydrolase 5	Q6P6S9	Entpd5	M	0.02	2.1	Protein amino acid N-linked glycosylation
ATP synthase subunit alpha, mitochondrial	P15999	Atp5a1	AM	0.02*	4.8	Lipid metabolic process
Glutaminase kidney isoform, mitochondrial	P13264	Gls	M	0.02	3.2	Glutamate catabolic process
Peroxisomal acyl-coenzyme A oxidase 1	P07872	Acox1	M	0.02	1.9	Fatty acid metabolic process
Voltage-dependent anion-selective channel 1	Q9Z2L0	Vdac1	AM	0.02*	8.5	Mitochondrial calcium ion transport
Cytochrome P450 4A2	P20816	Cyp4a2	M	0.02	1.9	Icosanoid biosynthetic process
Protein AMBP	Q64240	Ambp	M	0.02	5.0	NA
Glutathione S-transferase P	P04906	Gstp1	C	0.03	3.1	Metabolic process
Sodium/potassium-ATPase subunit alpha-1	P06685	Atp1a1	AM	0.03*	1.7	ATP catabolic process
Cytochrome c oxidase subunit 5A, mitochondrial	P11240	Cox5a	AM	0.03*	11.7	Electron transport chain
D-dopachrome decarboxylase	P30046	Ddt	C	0.03	5.5	Melanin biosynthetic process
ATPase, H+ transporting, lysosomal 38kDa, V0 subunit d1	Q5M7T6	Atp6v0d1	AM	0.03*	2.0	Hydrogen ion transport
Enoyl-CoA delta isomerase 1, mitochondrial	P23965	Eci1	M	0.04	1.5	Fatty acid beta-oxidation
ATP-binding cassette sub-family D member 3	P16970	Abcd3	M	0.04	1.8	ATP catabolic process
Probable D-lactate dehydrogenase, mitochondrial	F1LVD7	Ldhd	M	0.04	1.7	Oxidation reduction
Ectonucleotide pyrophos.ase/phosphodiesterase fam 3	P97675	Enpp3	AM	0.04*	1.6	Nucleoside triphosphate catabolic process
Uncharacterized protein: Atp6v0a4	D3ZY90	Atp6v0a4	AM	0.04	2.4	Hydrogen ion transport
Prostaglandin E synthase 3	P83868	Ptges3	C	0.04	15.9	Fatty acid metabolism
Ketohexokinase	Q02974	Khk	C	0.04	2.1	Carbohydrate catabolic process
GrpE protein homolog 1, mitochondrial	P97576	Grpel1	M	0.04	1.5	Protein folding
Apolipoprotein A-IV	P02651	Apoa4	M	0.04	1.8	Lipoprotein metabolic process
Uncharacterized protein	D3ZPL5	RGD1562953	C	0.04	3.1	Ribosome biogenesis
All-trans-13,14-dihydroretinol saturase, isoform CRA_b	G3V7V6	Retsat	M	0.04	4.9	NA
Ribonuclease 4	O55004	Rnase4	M	0.04	2.2	Nucleic acid phosphodiester bond hydrolysis
NADPH--cytochrome P450 reductase	P00388	Por	M	0.04	1.6	Flavonoid metabolic process
Pyruvate carboxylase, mitochondrial	P52873	Pc	C	0.05*	2.1	Gluconeogenesis
Aquaporin-1	P29975	Aqp1	AM	0.05	1.5	Water transport
Retinol-binding protein 4	P04916	Rbp4	C	0.05	2.8	Gluconeogenesis
Eukaryotic translation initiation factor 4A1	Q6P3V8	Eif4a1	C	0.06*	3.1	Translational initiation
Heat shock protein HSP 90-alpha	P82995	Hsp90aa1	C	0.06	1.6	Protein folding
Xanthine dehydrogenase/oxidase	F1LQS6	Xdh	C	0.06	2.1	Oxidation reduction
Glycerol Kinase	Q63060	Gk	C	0.07	2.9	Glycerol catabolic process
Carbonic anhydrase 5B, mitochondrial	Q66HG6	Ca5b	M	0.07	5.7	Bicarbonate transport
Chloride intracellular channel protein 1	Q6MG61	Clic1	C	0.07	2.0	Ion transport
Acetyl-CoA acetyltransferase, mitochondrial	P17764	Acat1	C	0.07	1.9	Proximal convoluted tubule development
RCG34378, isoform CRA_h	G3V957	LOC100359960	C	0.10	1.8	Translation

Proteins in italics and bold were previously shown to be induced during acidosis. AM - apical membrane, M - mitochondria, C-cytosol

* Indicates protein is also signficant in 1d, acute acidosis

Table 6.2. Proximal Convoluted Tubule Proteins Significantly Decreased in Chronic Metabolic Acidosis

Protein name	Accession #	Gene	Fraction	p-value	Fold change	Metabolic process
Fructose-1,6-bisphosphatase 1	P19112	Fbp1	AM	0.0002*	0.1	Gluconeogenesis
Triosephosphate isomerase	P48500	Tpi1	AM, C	0.003*, 0.02	0.1, 0.5	Gluconeogenesis
Sodium/potassium-transporting ATPase subunit alpha-1	P06685	Atp1a1	C	0.003*	0.1	Metabolic process
GM2 ganglioside activator	D3ZR01	Gm2a	AM	0.003	0.5	Lipid metabolism
14-3-3 protein zeta/delta	P63102	Ywhaz	AM	0.006*	0.2	mRNA metabolic process
Calnexin	P35565	Canx	M	0.007	0.4	Protein folding
Cytosolic non-specific dipeptidase	Q6Q0N1	Cndp2	AM	0.008*	0.1	Proteolysis
Enolase	Q5EB49	Eno1	AM	0.008*	0.1	Glycolysis
Low-density lipoprotein receptor-related protein 2	P98158	Lrp2	C	0.01*	0.4	Vitamin metabolic process
Heat shock cognate 71 kDa protein	P63018	Hspa8	AM	0.01*	0.3	mRNA processing
Uncharacterized protein	D3ZNI1	NA	AM	0.01*	0.1	NA
Sorbitol dehydrogenase	P27867	Sord	AM	0.01*	0.1	Oxidation reduction
Malate dehydrogenase, cytoplasmic	O88989	Mdh1	AM	0.02*	0.1	Tricarboxylic acid cycle
Aromatic-L-amino-acid decarboxylase	P14173	Ddc	C	0.02	0.3	Amino acid metabolic process
Transporter	D4A4Q0	Slc6a19	AM	0.02	0.5	Transport
4F2 cell-surface antigen heavy chain	Q794F9	Slc3a2	M	0.02	0.5	Carbohydrate metabolic process
Brain acid soluble protein 1	Q05175	Basp1	AM	0.02	0.4	Negative regulation of transcription
Filamin-B	D3ZD13	Flnb	M	0.02	0.6	GTP catabolic process
Nucleoside diphosphate kinase B	P19804	Nme2	AM	0.03*	0.1	Positive regulation of epithelial cell proliferation
Transgelin-2	Q5XFX0	Tagln2	C	0.03	0.5	NA
Argininosuccinate synthase	P09034	Ass1	AM	0.03*	0.1	Urea cycle
L-lactate dehydrogenase B chain	P42123	Ldhb	AM	0.03*	0.1	Carbohydrate metabolic process
Ribonuclease UK114	P52759	Hrsp12	AM	0.03*	0.1	Regulation of translation termination
Membrane-bound carbonic anhydrase 12	A2IBE2	Car12	AM	0.03	0.2	One-carbon compound metabolic process
Protein FAM151A	Q642A7	Fam151a	M	0.04	0.4	NA
Heat shock protein HSP 90-beta	P34058	Hsp90ab1	AM	0.04*	0.2	Response to salt stress
Aldehyde_dehydrogenase 8a1	D3ZXY4	Aldh8a1	AM	0.04	0.3	Retinal metabolic process
Isocitrate dehydrogenase [NADP] cytoplasmic	P41562	Idh1	AM	0.04*	0.1	Tricarboxylic acid cycle
Alcohol dehydrogenase [NADP+]	P51635	Akr1a1	AM	0.05*	0.1	Glucose metabolic process
N-acylglucosamine 2-epimerase	P51607	Renbp	C	0.05	0.2	Mannose metabolic process
Acyl-coenzyme A thioesterase 1	O88267	Acot1	C	0.05*	0.5	Lipid metabolic process
ATPase, H+ transporting, V1 subunit E 1, CRA_a	G3V7L8	Atp6v1e1	C	0.06	0.3	ATP hydrolysis coupled proton transport
4-hydroxyphenylpyruvate dioxygenase (Fragment)	F1LNW9	Hpd	C	0.07	0.5	Amino acid metabolic process
Purine nucleoside phosphorylase	P85973	Pnp	C	0.08	0.2	Purine nucleoside metabolic process
Adenylyl cyclase-associated protein 1	Q08163	Cap1	C	0.10	0.2	Receptor-mediated endocytosis

Proteins in italics and bold were previously shown to be induced during acidosis. AM - apical membrane, M - mitochondria, C-cytosol

* Indicates protein is also signficant in 1d, acute acidosis

database provides information on known and predicted protein interactions. The interactions include direct (physical) and indirect (functional) gene associations that are derived from multiple sources.[6] The proteins that are increased or decreased in 7-d chronic acidotic rats were submitted separately for analysis by STRING. A total of 58 of the 61 increased proteins are annotated in STRING but only 33 proteins had at least one interaction (Fig. 6.3). Visually there are at least five main groupings of proteins, which represent processes or pathways that are increased during chronic metabolic acidosis. These include oxidative phosphorylation, pyruvate, glutamine and glutamate, fatty acid, and xenobiotics metabolism. STRING analysis annotated 34 of 35 decreased proteins, but only 12 proteins had at least one interaction (Fig. 6.4). Enzymes of glucose metabolism are the one grouping of a process or pathway that is decreased during chronic acidosis. Further bioinformatics analyses were performed to elucidate the processes and pathways to which these genes are associated.

The cellular processes for 59 of the 61 proteins that are significantly increased during chronic acidosis were obtained from their GO terms (Fig. 6.5A). The electron transport chain accounted for 9% of the increased proteins, while 7% contributed to fatty acid metabolism. An additional 5% of the increased proteins clustered as gluconeogenesis, a process previously known to increase during chronic acidosis. Additional increased processes include: glutamate catabolism (4%), ATP catabolism (4%), hydrogen ion transport (3%), lipid metabolism (3%), protein folding (3%), xenobiotic glucuronidation (3%), translation (3%), and oxidation/reduction (3%). Processes represented by only one protein were grouped together as other (53%).

The list of significantly altered gene names was also submitted to Database for Annotation, Visualization and Integrated Discovery (DAVID) Bioinformatics Resources 6.7 available at http://david.abcc.ncifcrf.gov/. Information was then obtained from the Kyoto

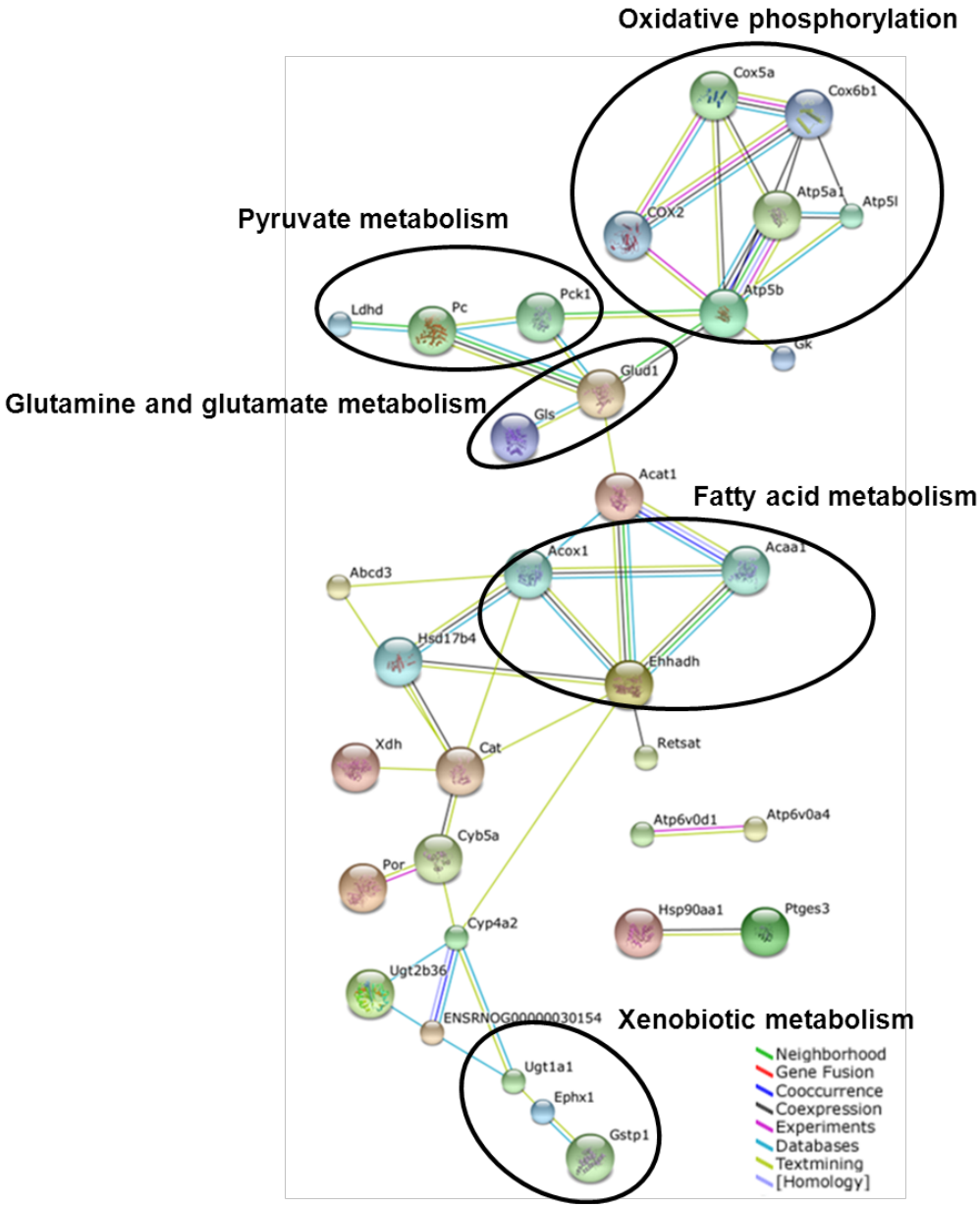

Fig. 6.3. STRING association analysis of the proteins with a significant increase in abundance during chronic metabolic acidosis. Circles represent various gene names and the lines correspond to a connection via any of the eight represented.

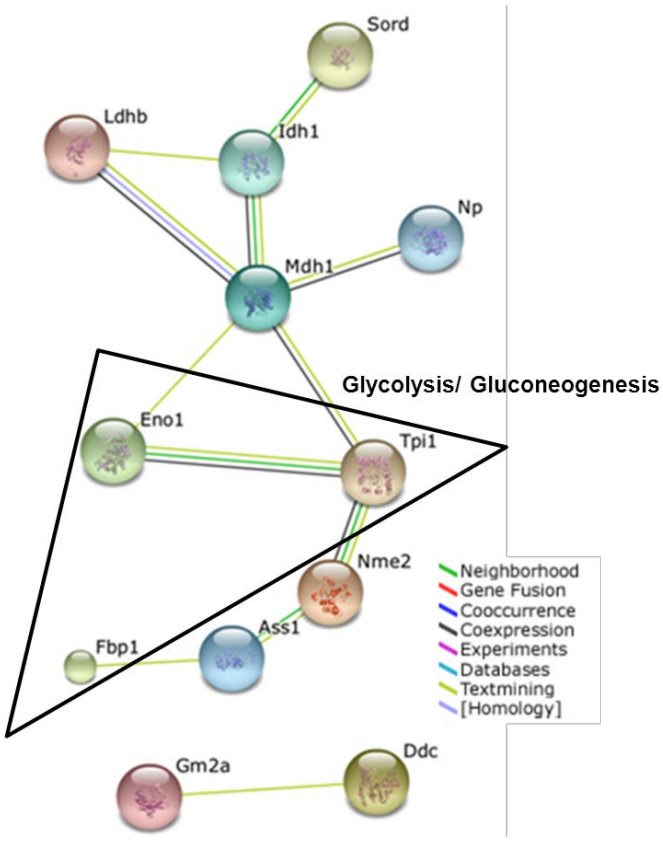

Fig. 6.4. STRING association analysis of the proteins with a significant decrease in abundance during chronic metabolic acidosis. Circles represent various gene names and the lines correspond to a connection via any of the eight represented.

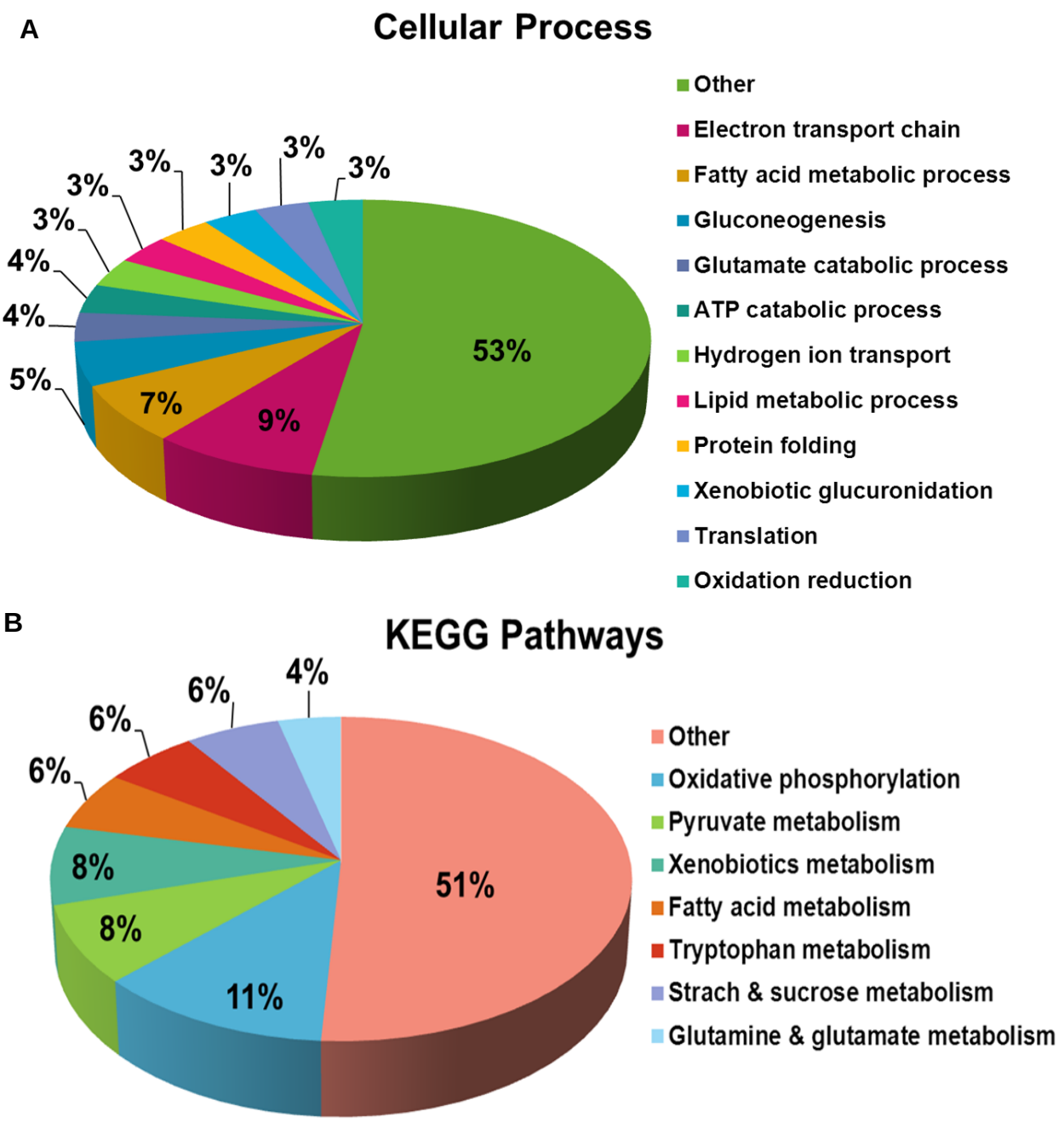

Fig. 6.5. Pie charts of the proteins significantly increased in chronic metabolic acidosis. Cellular processes (Panel A) as determined by Gene Ontology (GO) analysis and Kyoto Encylopedia of Genes and Genomes (KEGG) pathways obtained from DAVID Bioinformatics Resources (Panel B).

Encylopedia of Genes and Genomes (KEGG) database by DAVID.[7, 8] Functional annotation and grouping into KEGG pathways was available for 51 of the 61 increased proteins and pathways are shown as a percent of those annotated (Fig. 6.5 B). The pathways that were represented by only one protein were grouped in the other category (51%). There were a few proteins that are associated with one or more pathway and are listed more than once. Oxidative phosphorylation accounted for 11% and included the following gene names COX5A from complex IV and ATP51, ATP5A1, ATP5B, ATP6V0D1, and ATP6V0A4 from complex V. Pyruvate metabolism (8%) grouped the genes PCK1, LDHD, PC, and ACAT1. The additional pathways and corresponding genes were the following: (8%) xenobiotics metabolism, GSTP1, UGT1A1, UGT2B15, and EPHX1; (6%) fatty acid metabolism, ACAA1, ACOX1, EHHADH; (6%) tryptophan metabolism, CAT, EHHADH, and ACAT1; (6%) starch and sucrose metabolism, ENPP3, UGT1A1, UGT2B15; and (4%) glutamine and glutamate metabolism, GLS and GLUD1. The five groupings of genes shown interacting in the STRING analysis were assigned to the following KEGG pathways; oxidative phosphorylation, pyruvate, glutamine and glutamate, fatty acid, and xenobiotics metabolism (Fig. 6.3).

The cellular processes for 33 of the 35 decreased proteins were then obtained from their GO terms (Fig. 6.6 A). Each of the following cellular processes accounted for 6% of the annotated proteins: amino acid and carbohydrate metabolism, gluconeogenesis, lipid metabolism, mRNA processing, and the TCA cycle. The remaining processes were represented by only one protein and were grouped together as other (64%). The functional annotation by DAVID that grouped proteins into KEGG pathways was available for 34 of the 35 decreased proteins and pathways are shown as a percent of those annotated (Fig. 6.6 B). The pathways and respective genes for the proteins that are decreased in 7-d chronic acidotic rats are the following: (12%)

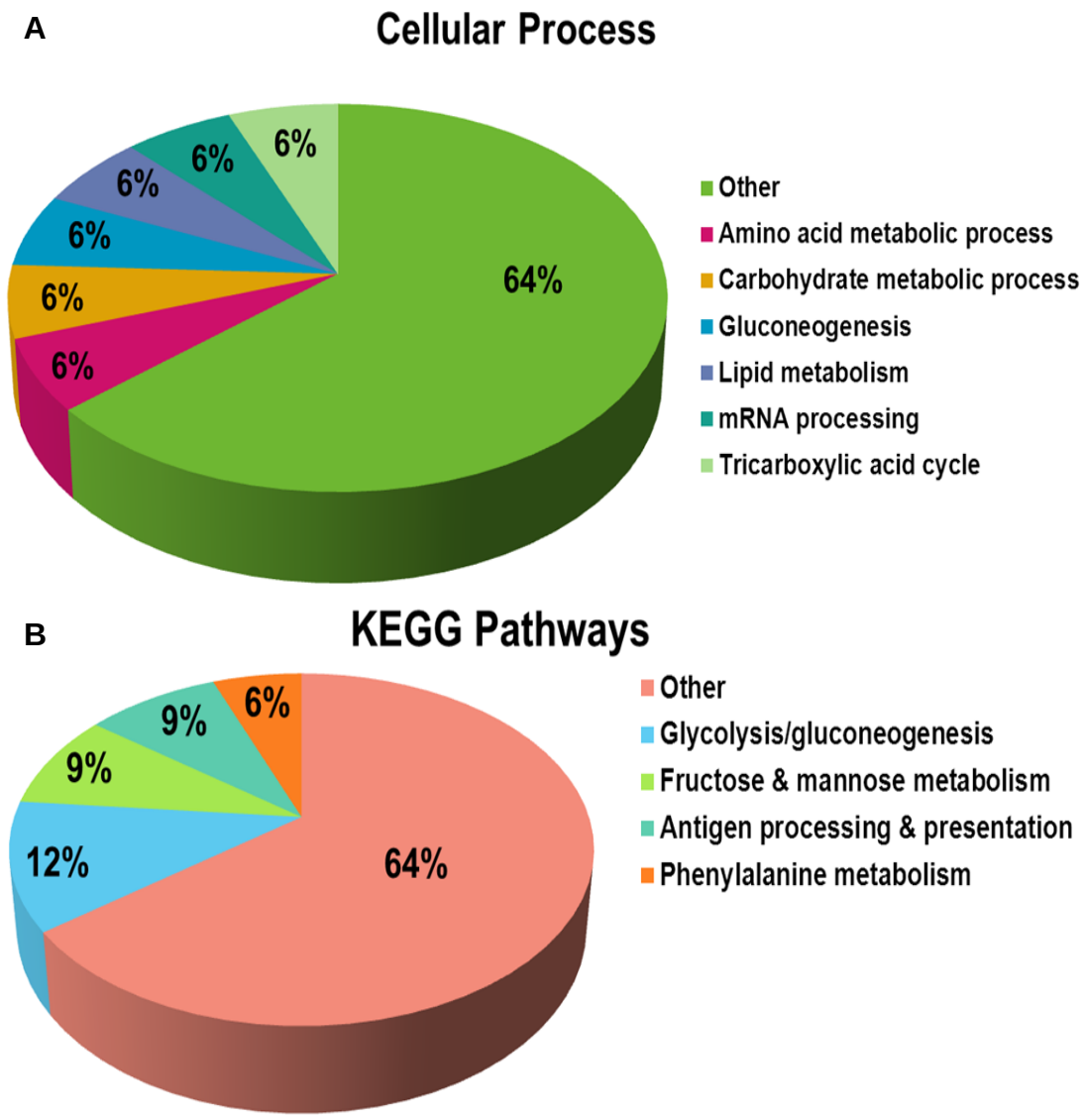

Fig. 6.6. Pie charts of the proteins significantly decreased in chronic metabolic acidosis. Cellular processes (Panel A) as determined by Gene Ontology (GO) analysis and Kyoto Encylopedia of Genes and Genomes (KEGG) pathways obtained from DAVID Bioinformatics Resources (Panel B)

glycolysis/gluconeogenesis, FBP1, TPI1, AKR1A1, ENO1; (9%) fructose and mannose metabolism, FBP1, SORD, TPI1; (9%) antigen processing and presentation, HSPA8, HSP90, CANX; and (6%) phenylalanine metabolism, DDC and HPD. The one group of genes shown interacting in the STRING analysis was assigned to the KEGG pathway of glycolysis/gluconeogenesis (Fig. 6.4). Altogether the bioinformatics analysis performed here suggested overall processes and pathways in the proximal convoluted tubule that are increased or decreased upon chronic metabolic acidosis.

6.3 Future directions

This dissertation describes the application of MS-based proteomics to analyze the response of the rat renal proximal convoluted tubule to metabolic acidosis. Chronic metabolic acidosis (CMA), where the decrease in blood pH and bicarbonate last for 7 days, was the main focus of these studies. Differences in protein abundance were described for chronic metabolic acidosis which suggests alterations in the cellular state. A mitochondrial isolation protocol was developed to enrich for mitochondria by 8-fold compared to whole cell lysate. Western blot analysis was performed to validate protein changes found by spectral counting analysis in the mitochondria. There were seven proteins identified in chapter 2 as increased in CMA by spectral counting and then validated by Western blotting. Two of these seven were the previously characterized mitochondrial protein kidney-type glutaminase (KGA) and glutamate dehydrogenase (GDH) known to be increased in CMA. The increase in KGA[9] and GDH[10] protein abundance results from selective stabilization of their respective mRNAs. In both cases, the mRNA stabilization is mediated by an 8-base AU-rich sequence within their 3'-UTR that functions as a pH-response element (pH-RE). Of the 29 proteins that were found significantly

increased in CMA by spectral counting, only 26 have mRNAs for which the 3'-UTR has been annotated. Of the characterized mRNAs, 16 or more than 60% contain an AU-rich sequence in their 3'-UTR that is > 85% identical to either of the pH-REs in the KGA mRNA. The latter group includes three proteins that were validated by Western blotting; UDP-glucuronosyltransferase 1A1 (UGT1A1), carbonic anhydrase 5B (CA5B), and catalase (CAT). Therefore, mRNA stabilization may be a common mechanism that mediates the adaptive increases in many proteins in addition to KGA and GDH within the proximal convoluted tubule. To test this hypothesis, initial experiments will be performed to determine if the latter proteins exhibit a similar response in LLC-PK_1-F^+-9C cells. If so, quantitative real time reverse transcription polymerase chain reaction (qRT-PCR) can be performed to measure the level of UGT1A1, CA5B and CAT mRNAs in control cells versus cells treated with acidic medium. Similarly, time course analysis of cells treated with actinomycin D will be assayed by qRT-PCR to determine half-lives of the respective transcripts.

The cytosolic phospho*enol*pyruvate carboxykinase (PEPCK) is up-regulated in response to metabolic acidosis within the proximal convoluted tubule.[11] The initial increase in PEPCK results from increased transcription of the respective gene, which has numerous regulatory promoter elements that control its expression.[12] The sustained increase in PEPCK during CMA is due, in part, to mRNA stabilization.[13] Therefore, the increased proteins found in this study could also result from increases in transcription. In order to test this hypothesis, luciferase reporter constructs can be made for the proteins that were validated by Western blotting. Even though UGT1A1, CA5B, and CAT have potential pH-REs the increased protein in CMA could also be due to increased transcription. Luciferase assays can be conducted in cells treated with control and acidic medium to determine if the promoter and/ or portions of the 3'UTR contribute

to the pH response seen at the protein level. The qRT-PCR and luciferase assays can also be done for acetyl coenzyme A acyltransferase 1B (ACAA1) and 17-beta-hydroxysteroid dehydrogenase 4 (HSD17B4). Neither of these proteins have potential pH-REs in their mRNAs. However, the above mentioned assays can elucidate the mechanism by which their protein levels are increased in CMA. Specifically, ACAA1 like PEPCK, exhibits a large induction during the initial onset of acidosis. Therefore, ACAA1 up-regulation in response to metabolic acidosis may also result from increased transcription.

Three enzymes involved in both mitochondrial and peroxisomal fatty acid metabolism are increased in metabolic acidosis. ACAA1, acyl-CoA oxidase, and enoyl-CoA hydratase are all enzymes that contribute to the synthesis of long-chain saturated and unsaturated fatty acids. The increased expression of these enzymes suggests that acidosis may promote a remodeling of the lipids in the mitochondrial membranes. Therefore, lipidomics could be performed to determine if there is a remodeling of the lipids in the mitochondrial membranes. Chapter 4 used a mitochondrial inner membrane isolation protocol that could be used to separate the compartments of the mitochondria prior to analysis to determine lipid changes specific to the outer and inner membranes of the mitochondria.

Lysine acetylation sites were identified in the mitochondria and mitochondrial inner membrane of both control and CMA samples. The identified sites of acetylation in the mitochondrial proteins of the proximal convoluted tubule provide a basis for future mutational and functional analyses to determine their role in the regulation of mitochondrial metabolism during metabolic acidosis. In the 7-d chronic acidotic mitochondrial samples, Western blotting showed lysine acetylation was increased 2.5-fold relative to the control. However, later analysis showed the mitochondrial inner membrane had no change in lysine acetylation in CMA. Further

analysis could determine specifically which proteins and lysine residues are acetylated that contributes to the increase in overall mitochondrial acetylation in CMA. To accurately determine that the sites we found are acetyl and not tri-methylation, a high resolution and high mass accuracy instrument such as an Orbitrap mass spectrometer must be used. Moreover, to properly interrogate as many sites as possible of this modification, an antibody-based lysine acetyl peptide enrichment should be performed to reduce the background. Lastly, to obtain accurate quantitative measurements of changes in specific lysine acetylation sites, an isobaric labeling method must be performed. Much work remains to be done in the field of regulation of mitochondrial metabolism by lysine acetylation. However, the profiling of sites in various cell types and diseases are essential to identify potential sites of cellular regulation by lysine acetylation.

The use of 2D-LC and multiple injections was shown to be the ideal method for increased protein identifications and quantitative measurements. We identified significantly fewer proteins with the 1D-LC-MS/MS approach used in chapter 4. Therefore, any future experiments with the goal of identifying as many proteins as possible and/or using label free quantitative analysis should be done with 2D-LC. Chapter 4 concentrated on the mitochondrial inner membrane of the proximal convoluted tubule. The procedure we used produced mitochondrial inner membranes that were highly enriched. This same protocol could be repeated with a sufficient number of rats and with 2D-LC. Then label free quantitative analysis could be performed to determine proteins changed during metabolic acidosis within the inner membrane. This study may reveal a transporter that is significantly increased in CMA that may be the glutamine transporter. However, it is possible that there is no change in abundance of the glutamine transporter during CMA but instead its activation is triggered by a post-translational modification.

This dissertation demonstrated quantitative proteomics is a useful technique to characterize the proximal convoluted tubule response to metabolic acidosis. However, to completely understand the cellular state, a systems view should be taken of all cellular processes. A system biology approach with information derived from the genome, transcriptome, proteome, and metabolome levels will better explain the cellular status of the proximal convoluted tubule and how it changes in CMA. Changes in transcript levels do not necessarily parallel changes in the protein and changes in the level of protein do not necessarily result in an immediate change in enzymatic activity. Therefore, it is important to investigate the changes in gene transcripts, proteins, and metabolites to fully understand the regulation of cellular processes at a systems level. The missing component of a systems understanding of the proximal convoluted tubule response to chronic metabolic acidosis is metabolomics studies.

REFERENCES

1. Walmsley, S. J.; Freund, D. M.; Curthoys, N. P., Proteomic profiling of the effect of metabolic acidosis on the apical membrane of the proximal convoluted tubule. Am J Physiol Renal Physiol 2012, 302 (11), F1465-77.

2. Freund D.M., P. J. E., Curthoys N.P., Response of the Mitochondrial Proteome of Rat Renal Proximal Convoluted Tubules to Chronic Metabolic Acidosis. Am J Physiol Renal Physiol 2013, 304(2) F145-F155.

3. Freund DM, P. J., Improved Detection of Quantitative Differences Using a Combination of Spectral Counting and MS/MS Total Ion Current. In Press.

4. Nowik, M.; Lecca, M. R.; Velic, A.; Rehrauer, H.; Brandli, A. W.; Wagner, C. A., Genome-wide gene expression profiling reveals renal genes regulated during metabolic acidosis. Physiol Genomics 2008, 32 (3), 322-34.

5. Curthoys, N. P.; Taylor, L.; Hoffert, J. D.; Knepper, M. A., Proteomic analysis of the adaptive response of rat renal proximal tubules to metabolic acidosis. Am J Physiol Renal Physiol 2007, 292 (1), F140-7.

6. Szklarczyk, D.; Franceschini, A.; Kuhn, M.; Simonovic, M.; Roth, A.; Minguez, P.; Doerks, T.; Stark, M.; Muller, J.; Bork, P.; Jensen, L. J.; von Mering, C., The STRING database in 2011: functional interaction networks of proteins, globally integrated and scored. Nucleic Acids Res 2011, 39 (Database issue), D561-8.

7. Huang da, W.; Sherman, B. T.; Lempicki, R. A., Systematic and integrative analysis of large gene lists using DAVID bioinformatics resources. Nat Protoc 2009, 4 (1), 44-57.

8. Huang da, W.; Sherman, B. T.; Lempicki, R. A., Bioinformatics enrichment tools: paths toward the comprehensive functional analysis of large gene lists. Nucleic Acids Res 2009, 37 (1), 1-13.

9. Laterza, O. F.; Curthoys, N. P., Specificity and functional analysis of the pH-responsive element within renal glutaminase mRNA. Am J Physiol Renal Physiol 2000, 278 (6), F970-7.

10. Schroeder, J. M.; Liu, W.; Curthoys, N. P., pH-responsive stabilization of glutamate dehydrogenase mRNA in LLC-PK1-F+ cells. Am J Physiol Renal Physiol 2003, 285 (2), F258-65. Epub 2003 Apr 08.

11. Drenowska, K.; Craig, M.; Digiovanni, S.; McCarty, J.; Moorman, A.; Lamars, W.; Schoolwerth, A. C., PEPCK mRNA localization in proximal tubule and gene regulation during metabolic acidosis. J. Physiol. Phram. 2002, 53, 3-20.

12. Hanson, R. W.; Reshef, L., Regulation of phosphoenolpyruvate carboxykinase (GTP) gene expression. Annu Rev Biochem 1997, 66, 581-611.

13. Hajarnis, S.; Schroeder, J. M.; Curthoys, N. P., 3'-Untranslated region of phosphoenolpyruvate carboxykinase mRNA contains multiple instability elements that bind AUF1. J Biol Chem 2005, 280 (31), 28272-80.

ENDNOTES

[1] Chapter 2 describes work published in American Journal of Physiology - Renal Physiology. Freund, D. M., Prenni, J. E., Curthoys, N. P., Response of the Mitochondrial Proteome of Rat Renal Proximal Convoluted Tubules to Chronic Metabolic Acidosis. American Journal of Physiology - Renal Physiology 2013, 304(2) F145-F155

[2] Chapter 3 describes work that is in press in the Journal of Proteome Research. Freund, D.M. and Prenni, J.E, Improved Detection of Quantitative Differences Using a Combination of Spectral Counting and MS/MS Total Ion Current.

[3] Chapter 4 describes work that is under review for publication in PROTEOMICS. Freund, D. M., Prenni, J. E., Curthoys, N. P., Proteomic Profiling of the Mitochondrial Inner Membrane of Rat Renal Proximal Convoluted Tubules.

[4] Chapter 5 describes work that I contributed to the following manuscript: Walmsley S.J., Freund D.M., Curthoys N.P. Proteomic profiling of the effect of metabolic acidosis on the apical membrane of the proximal convoluted tubule. American Journal of Physiology - Renal Physiology 302: F1465–F1477, 2012